ELECTRONIC SPECTROSCOPY BY THE ELECTRON IMPACT METHOD

Thesis by

Oren Allen Mosher

In Partial Fulfillment of the Requirements

for the Degree of

Doctor of Philosophy

California Institute of Technology

Pasadena, California

1975

(Submitted September 12, 1974)

Acknowledgments

Professor Aron Kuppermann has been an unfailing source of support and encouragement during the course of these experiments. He not only provided sound scientific advice but also continued to expect the eventual success of the project even at times when it seemed doubtful to me.

Many members of the Kuppermann research group have also assisted me in these studies. Foremost among these is Wayne Flicker with whom I have worked closely for four years. He helped in putting the machine into operation, taking data, and also wrote the computer programs which were used to analyze the data. It has been a great personal pleasure to work with him and also to be a coauthor with him on several publications. Mike Coggiola has also helped take data on the machine and written two joint papers. In addition, Wayne and Mike have written the DCS, ratio, and spectral display programs used to make the figures in this thesis. Other members of the group who have assisted in taking the data are Tony Barre, Dave Mikkelsen, and Bob Frueholz. Jon Burke has been a source of help in solving problems in the data handling and analysis programs. Doug Mason taught me a great deal about high vacuum technology and electronics in general. The pulse amplifier used in these studies was

a product of our joint efforts. In addition, Doug developed the suspended mounting scheme used for the electron multiplier.

Sandor Trajmar of the Jet Propulsion Laboratory was a source of valuable advice about the instrument. He was kind enough to loan the electron gun employed in these studies and also provided the results of his scattering volume correction calculations.

Mike Foster of the Caltech Chemistry Department provided the azomethane sample and encouraged the azo compound study. I also thank him for his cooperation in combining the results of his trapped electron study with our results in two joint papers on this molecule.

After more than five years as an experimental chemical physicist I am convinced that a good electronics shop, instrument shop, and draftsmen are critically important for successful work in this field. Bill Schuelke as supervisor and both Tony Stark and Villy Jorgenson of the instrument shop were all very helpful in avoiding numerous pitfalls during the construction of the instrument, and in solving problems which later became apparent. Dick Ehrich made a superb set of drawings of the machine. These drawings formed the basis for some of the figures in this thesis for which I thank him. John Henigman provided a great deal of help in various electronics problems in his role as supervisor of the electronics shop.

I also wish to thank both the Atomic Energy Commission and the National Science Foundation for financial support. My parents were also a source of emotional and financial support during the course of these studies for which I am grateful.

Abstract

A previously constructed variable angle electron-impact spectrometer has been rebuilt and used to study electronic excitation spectra in the energy-loss range from 0 eV to beyond 15 eV for 13 molecules. Spectra were obtained in the impact energy range from 20 eV to 70 eV and for scattering angles from 0° to 80°. The differential scattering cross sections were obtained for several low-lying electronic transitions and used to determine whether a transition was spin-allowed or spin-forbidden. Further assignments of some transitions were made by comparison of the present results with earlier theoretical and experimental studies.

In the 1,3-conjugated polyenes the three lowest energy excited states are the $1\,^3B_u$, the $1\,^3A_g$ and the $1\,^1B_u$. These states have been studied here and produce peaks in the energy-loss spectrum at 3.22 eV, 4.91 eV, and 5.92 eV in s-trans-1,3-butadiene, at 3.14 eV, 4.87 eV, and 5.80 eV in 1-trans-3-pentadiene, at 3.20 eV, 4.93 eV, and 5.77 eV in 1,3-hexadiene, and at 3.11 eV, 4.85 eV, and 5.69 eV in cis-2-trans-4-hexadiene. The energies of the low-lying transitions in the 1,3 and 2,4 non-cyclic dienes are nearly invariant with respect to alkyl substitution. This indicates that these are $\pi \rightarrow \pi^*$ transitions and that the σ, π separability approximation is applicable to these

molecules. In 1,3-cyclohexadiene the state which is equivalent to the $1\,^3A_g$ is not seen but transitions to the states which are equivalent to the $1\,^3B_u$ and the $1\,^1B_u$ states produce peaks at 2.94 eV and 4.94 eV, respectively. The shifts in the transition energies from the non-cyclic diene values are probably associated with the increased closeness of the two π bonds. In 1,3,5-hexatriene the energies of the transitions to the $1\,^3B_u$, $1\,^3A_g$, and $1\,^1B_u$ states are 2.61 eV, 4.11 eV, and 5.13 eV, respectively. There was no evidence for a weak singlet $\rightarrow$ singlet transition below the $\tilde{X}^1A_g \rightarrow 1\,^1B_u$ transition in contrast to the results of recent studies on larger substituted polyenes.

Some non 1,3-conjugated polyenes were studied. The $\pi \rightarrow \pi^*$, singlet $\rightarrow$ triplet transition produced a peak at 4.25 eV in 1,4-hexadiene, 4.25 eV in 1,5-hexadiene and 4.29 eV in 1,4-cyclohexadiene. The strong $\pi \rightarrow \pi^*$, singlet $\rightarrow$ singlet transition peaks at 6.84 eV, 7.00 eV, and 7.95 eV in these molecules. The results for the non-cyclic dienes were quite similar to the results in the alkyl substituted ethylenes and again suggest that the σ, π separation is valid. For 1,4-cyclohexadiene, however, the upward shift in the singlet $\rightarrow$ singlet transition energy may reflect the interaction of the two π orbitals by hyperconjugation with the σ_{CH} orbitals. Such an interaction implies a breakdown of the σ, π separability approximation.

Two azo compounds (R–N=N–R) have been studied. The first three excited states are the $1\,^3B_g$, the $1\,^1B_g$, and a second triplet state. In azomethane transitions to these states produce maxima at 2.75 eV, 3.50 eV, and 4.8_4 eV. The corresponding values in azo-t-butane are 2.67 eV, 3.37 eV, and 4.9 eV. The near equality of the three lowest transition energies of these two azo compounds suggests that these excitations are primarily due to the azo group electrons.

In propadiene (allene) the 1, 2 interaction of the double bonds produces two singlet→triplet transitions with maxima at 4.28 eV and 4.89 eV. The separation of 0.61 eV between these triplet states is substantially smaller than the corresponding splitting of 1.69 eV in 1, 3-butadiene indicating a much smaller π - π interaction due to the perpendicularity of the π molecular orbitals.

In thiophosgene (Cl_2CS) a previously unreported singlet→triplet transition was seen at 3.1 eV.

These results illustrate the power of low energy variable angle electron-impact spectroscopy in the elucidation of the electronic structure of π-electron molecules.

Table of Contents

1. Introduction

The technique of low energy electron scattering has been shown to be a powerful method for observing electronic transitions in atoms and molecules which are forbidden by electric dipole-radiation selection rules (see discussion in Section 2). The studies reported here are concerned with two kinds of optically forbidden transitions. Transitions which violate the spin selection rule ($\Delta S = 0$)[1] are easily produced by exchange of the incoming electron with one of the molecular electrons. The importance of this mechanism was originally pointed out by Oppenheimer.[2] The overall spin of the electron plus molecule system is conserved but the exchange of electrons permits the change in the spin multiplicity of the molecule. In an optical absorption spectrum, spin forbidden transitions have oscillator strengths which are usually 5 to 8 orders of magnitude weaker than those of optically allowed transitions.[3] In the electron-impact spectrum, however, spin forbidden transitions are typically (see Section 6) 5% to 10% as strong as the optically allowed transitions at scattering angles of 40° and above in the 20 eV to 60 eV impact energy range. A second type of forbidden transition which has been studied are spin allowed but symmetry forbidden transitions. In the electron-impact spectrum these transitions are 5% to 25% as strong

(see Section 6) as an optically allowed transition. This represents an increase of from 1 to 3 orders of magnitude in the corresponding intensity ratio in the optical spectrum.[3] Thus many transitions which are difficult to observe by optical absorption spectroscopy are easily seen by electron-impact spectroscopy.

The usefulness of the electron-impact method is not limited to a determination of transition energies. In many cases one can also determine the type of transition which has occurred in the molecule, if the electron-impact spectrum is studied at different scattering angles and impact energies. The quantity $\sigma_n(E_0, \theta, \phi)d\Omega$ measures the probability that an electron of incident energy E_0 will excite the n^{th} molecular state and then be scattered into the solid angle $d\Omega$ where $d\Omega = \sin\theta \, d\theta \, d\phi$. $\sigma_n(E_0, \theta, \phi)$ is known as the differential cross section (DCS) and has units of cm^2/sr. The angles θ and ϕ are measured with respect to the incident electron beam direction. θ measures the polar angle of the outgoing electron with respect to the incident beam while ϕ is the azimuthal angle about the incident beam. This is shown schematically as follows.

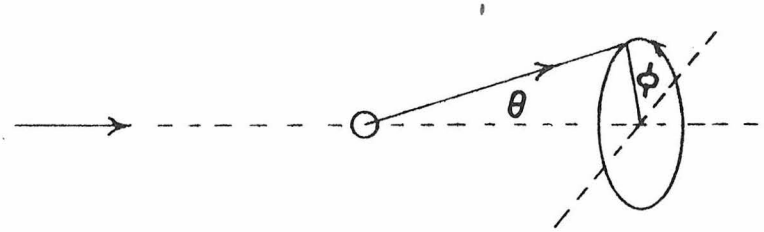

For randomly oriented target molecules, as used in this study, there is no unique way to define ϕ and thus the DCS does not depend on ϕ.

The following characteristics have been observed [4, 5] for the DCS's associated with each of three types of transitions in molecules. For spin forbidden transitions $\sigma_n(E_0, \theta)$ is usually constant within a factor of 2 or 3 over the angular range from 10° to 80°. This is a simple consequence of the exchange mechanism for excitation of these states. The outgoing electron "forgets" which direction the incident electron came from and thus the DCS is relatively isotropic (see discussion in Section 3). In the case of optically allowed transitions the DCS is strongly peaked at $\theta = 0°$ because excitation occurs via long-range coulombic interaction. Energy transfer occurs most often with a very small deflection of the incident electron and this produces a strongly forward peaked DCS. A spin allowed but symmetry forbidden transition usually shows an intermediate type of behavior. Its DCS is still forward peaked but not quite as strongly as the DCS of an optically allowed transition. Thus a measurement of the DCS of a transition can aid in identifying the type of transition which is occurring.

The aim of the present research was to modify the previous version of the spectrometer [4, 5] so that it could be operated with higher reliability and could also be serviced more readily. These

goals were accomplished by completely rebuilding the internal support frame and modifying the way the lenses and spheres are mounted. More versatile electron lenses were installed in each stage, the spheres were increased in size and the previous discrete dynode multiplier was replaced by a Spiraltron continous dynode multiplier. A new pulse amplifier and discriminator, which was faster and more reliable than the previous detector electronics, was also designed.

After completing the rebuilding process described in the previous paragraph, the machine was placed in operation and has remained in operation about 97% of the time over a ten-month time interval. A systematic program of DCS measurements for many of the low-lying transitions in more than 34 molecules has been completed. These studies had two goals. The first was a determination of transition energy values and the types of transitions occurring in these molecules. The second was a study of the effects of substitution of different groups among a family of molecules. Much of this information was known for optically allowed transitions but very few such comparisons are available for optically forbidden transitions. Thus, the results for six different conjugated dienes are reported and compared. Two different alkyl substituted azo compounds (R–N=N–R) as well as a number of nonconjugated dienes were also studied and reported here. In addition, the fluorine substituted ethylenes, the

methyl substituted ethylenes, some alkynes, some fluorobenzenes, some five-membered heterocyclic compounds, and finally CO_2 and its sulfur substituted analogs have been studied in collaboration with M. J. Coggiola (the fluoroethylenes), R. P. Frueholz (benzene and fluorobenzenes) and W. M. Flicker (the other families of molecules listed). These individuals will report these results elsewhere.

The remainder of this thesis is divided into sections as follows; Section 2 summarizes the historical development of electron-scattering experiments; Section 3 discusses electron-molecule scattering theory in the intermediate energy range (E_0 from 10 eV to 100 eV); Section 4 shows the spectrometer layout and construction details; Section 5 indicates how the spectrometer was operated and discusses data handling techniques; Section 6 reports the observed results for each molecule.

References

1. G. Herzberg, Electronic Spectra of Polyatomic Molecules (D. Van Nostrand, Inc., 1966), pp. 128-142.

2. J. R. Oppenheimer, Phys. Rev., 32, 361 (1928).

3. S. P. McGlynn, T. Azumi, and M. Kinoshita, Molecular Spectroscopy of the Triplet State (Prentice-Hall, Inc., New Jersey, 1969), pp. 19-20.

4. J. K. Rice, Ph.D. Thesis, California Institute of Technology, 1969.

5. S. Trajmar, J. K. Rice, and A. Kuppermann, Adv. Chem. Phys., 18, 15 (1970).

2. Historical Survey

2.1 Experiments Prior to 1940

The study of inelastic collisions of electrons with atoms was reported as early as 1902 by Lenard.[1] Similar more extensive studies were performed by Franck and Hertz in 1914.[2,3] Both of these were fixed angle studies and thus did not measure a DCS.

The first study of the angular distribution of inelastically scattered electrons off an atom was by Dymond[4] in 1927, who measured the angular distribution from 0° to 90° of electrons which had excited He to its 2^1P state. Mohr and Nicoll[5-8] were two of the earliest investigators of angular distributions of inelastically scattered electrons off molecules. Their apparatus could observe scattering in the angular range of 10° to 155°, and was used to study both atoms (He, Ne, A, Hg) and molecules (H_2, CH_4).

The early experiments had three major limitations. The energy resolution of the experiments was low because the energy spread of the incident beam was that of a thermal distribution at the temperature of the electron source. Electrostatic deflection energy analyzers were used[5-8] to discriminate against elastically scattered electrons but no analyzer was used to make the incident beam more monochromatic. A second problem was the fact that the scattered

current was detected by a Faraday cylinder and current measuring equipment. The electron multipliers which are in use today permit single electron detection and are 2 to 3 orders of magnitude more sensitive than even the best currently available current measuring device (the vibrating reed electrometer). Finally, the vacuum pumps and systems (feed throughs, vacuum chamber materials, etc.) were much less sophisticated than those currently in use. An appreciation of the many experimental problems makes the results of the early experimentalists seem very impressive.

2.2 Experiments After 1945

2.2.1 Exciation by Electrons with at least 2 eV of Excess Energy

The earliest modern work appears to be that of Lassettre and co-workers which began during the late 1940's. These experiments[9-12] did not use a monochromatic incident beam, but the improved instrument[9,10] did use an electron multiplier as a detector.

Marmet and Kerwin[13] reported the successful development of a monochromatic electron source using a 127° electrostatic analyzer in 1960. This appears to have stimulated development of several electron-impact spectrometers using monochromatic electron sources. Skerbele and Lassettre[14] reported an instrument using

two 180° electrostatic analyzers in 1964. Higher resolution spectrometers [15-17] were reported in the years from 1965 to 1968. The spectrometer in Reference 17 was capable of studying scattering from -16° to +16° while the earlier instruments were limited to smaller angles around 0°. The work of Lassettre and associates has been particularly concerned with the accurate measurement of excitation cross sections and generalized oscillator strengths. They have shown the connection of the generalized oscillator strength with optical oscillator strengths in a number of molecules.[18] This has required careful study of the cross sections near 0° scattering angles and impact energies above 100 eV, although some of their work has gone down to 35 eV impact energies.

Kuppermann and Raff [19, 20] were the first to observe spin forbidden transitions in electron-impact energy loss spectra in 1962. No monochromator was used on the incident beam. The energy loss was measured by the retarding potential difference method and electrons were collected at scattering angles from 22° to 112°. An improved version of this instrument which collected electrons in a small range of angles about 90° was developed by Wei and Kuppermann.[21, 22] Both instruments were designed for the 30 eV to 60 eV impact energy range and used current measuring detectors.

G. J. Schulz reported [23] the first inelastic scattering study using both a monochromator and an energy loss analyzer in 1962. He studied vibrational excitation of N_2 at 0° using two 127° analyzers and a nitrogen molecular beam target. This study was done, however, in the 1.5 eV to 4 eV impact energy range and was concerned with temporary negative ion formation so it might also be classified as a threshold excitation study (see Section 2.2.2).

Simpson and his co-workers [24, 25] were also developing a spectrometer based on two 180° analyzers at about the same time as Lassettre. The first instrument [25] was limited to 0° scattering but a later model [26, 27] could study scattering from -20° to +90°. These instruments employed a scattering chamber holding the gaseous target and were designed for optimal operation in the 10 eV to 100 eV impact energy range. Simpson and co-workers have been very interested in the design of high-resolution machines with detailed attention to electron optics and optimum operation of the energy analyzers.

Rice, Kuppermann, and Trajmar [28, 29] developed a machine similar to the variable angle machine of Simpson. They used this machine for extensive studies [28, 29] of the DCSs for excitation of He, N_2, CO, C_2H_2, C_2H_4, H_2 and developed and verified many of the generalizations about DCS behavior for the different types of

transitions which were discussed in Section 1. This instrument used a scattering chamber to hold the target gas. In later work, Trajmar and Chutjian[30] developed a higher resolution instrument which used a molecular beam target, dual 180° analyzers and scanned scattering angles from -30° to 138°.

The years from 1960 to 1974 have seen a rapid increase in the number of high-resolution electron spectrometers. Many of these instruments can operate routinely with energy resolution of 0.02 eV to 0.05 eV. Williams and Doering have reported[31] a machine similar to the variable angle Simpson spectrometer.[27] Comer and Read's instrument[32] used dual 180° analyzers and a molecular beam target and could observe scattering angles from -5° to 85°. Hasted and co-workers[33,34] built a fixed angle (θ = 0°) spectrometer employing dual 127° analyzers which was used to study inelastic scattering in the 1 to 4 eV impact energy range. Tam and Brion[35] also used dual 127° analyzers and could study scattering angles from -30° to +100° while a similar instrument by Roy et al.[36] includes the range from -20° to +100°. McConkey and co-workers[37] have also developed a spectrometer similar to the variable angle Simpson-type spectrometer.[27]

A spectrometer developed by Joyez, Hall, Reinhardt, and Mazeau[38] is worthy of special mention. It uses dual 127° analyzers and utilizes a molecular beam target. The instrument scans

scattering angles from -30° to +125° and achieves a resolution of 0.02 eV (full width at half maximum of the elastic peak). The unique feature is the instrument's ability to operate down to 0.02 eV above an excitation threshold. It appears to be the first combination of an intermediate range energy loss instrument with a differential threshold excitation spectrometer (see discussion of threshold excitation instruments in Section 2.2.2).

2.2.2. Excitation at or Near Threshold

Excitation of an atom or molecule within 1 eV or 2 eV of the excitation threshold often leads to a spectrum whose relative peak intensities for different inelastic processes are very different from those seen optically or by intermediate impact energy excitation spectra (see discussion in part D of paper in Appendix I). In many cases spin-forbidden transitions are seen as the most prominent features. Three methods have been used to study threshold excitation. The "trapped electron" method and the SF_6 scavenger method both measure an integral (with respect to θ) cross section in the energy region just above threshold. The instrument of Joyez et al.,[38] in contrast, measures the differential excitation cross section at or near threshold.

Schulz was the developer of the trapped electron method[39, 40] about 1958. A retarding potential difference (RPD) gun was used to

provide the low energy electron beam. If an electron undergoes a collision with an atom or molecule and ends up with less than W eV of kinetic energy where W is the trapping potential in the collision chamber, it cannot escape from the scattering chamber. The electron will slowly diffuse to a cylindrical collector near the outside of the scattering chamber. Thus the current to this collector is proportional to the slope of the integral excitation cross section near threshold. The well depth or trapping potential was adjustable up to 3 eV but the best results were obtained below 1 eV. Bowman and Miller [41] modified the Schulz-type apparatus by adding a periodic rectangular voltage pulse to the RPD gun and then employing phase sensitive detection of the collector current.

Brongersma and Oosterhoff [42] built a machine similar to that of Bowman and Miller but were able to achieve higher energy resolution by modification of certain details of construction. The well depth was still limited to 1 to 3 eV. In a later apparatus Knoop, Brongersma and Boerboom [43] developed a double RPD method which permitted observation at well depths of up to 10 eV. This was accomplished by putting a modulation voltage on the potential well itself and using phase sensitive detection techniques. Dance and Walker [44] have recently achieved a significant improvement in energy resolution by incorporating a trochoidal electron monochromator [45] instead of a modulated

RPD-type electron gun. This instrument has achieved an energy resolution of 0.06 eV in favorable cases.

An integral-type threshold excitation spectrometer with a novel detector system was reported by Curran [46] and by Christophorou and co-workers. [47, 48] SF_6 has a strong resonant electron-capture process which it undergoes with thermal electrons to produce SF_6^- for electrons of energy up to about 0.5 eV. There is also a strong dissociative attachment process leading to SF_5^- + F. Thus if SF_6 is introduced into a trapped electron chamber along with the atom or molecule to be studied and the SF_6^- or SF_5^- current is monitored, it gives the threshold excitation spectrum of the atom or molecule. Other authors have used different electron attaching species such as CCl_4 (to give Cl^-) [49] in place of SF_6.

References

1. P. Lenard, Ann. Physik., 8, 149 (1902).

2. J. Franck and G. Hertz, Verh der Phys. Ges., 16, 457 (1914).

3. J. Franck and G. Hertz, Z. Physik, 17, 409 (1916).

4. E. G. Dymond, Phys. Rev., 29, 433 (1927).

5. C. B. O. Mohr and F. H. Nicoll, Proc. Roy. Soc., A138, 229 (1932).

6. C. B. O. Mohr and F. H. Nicoll, Proc. Roy. Soc., A138, 469 (1932).

7. C. B. O. Mohr and F. H. Nicoll, Proc. Roy. Soc., A142, 320 (1933).

8. C. B. O. Mohr and F. H. Nicoll, Proc. Roy. Soc., A142, 647 (1933).

9. E. N. Lassettre, A. S. Berman, S. Silverman, and M. E. Krasnow, Phys. Rev., 95, 635 (1954).

10. E. N. Lassettre, Rad. Res. Suppl., 530 (1959).

11. E. N. Lassettre and S. A. Francis, J. Chem. Phys., 40, 1208 (1964).

12. E. N. Lassettre and E. A. Jones, J. Chem. Phys., 40, 1222 (1964).

13. P. Marmet and L. Kerwin, Can. J. Phys., 38, 787 (1960).

14. A. M. Skerbele and E. N. Lassettre, J. Chem. Phys., 40, 1271 (1964).

15. V. D. Meyer, A. Skerbele, and E. N. Lassettre, J. Chem. Phys., 43, 805 (1965).

16. E. Lassettre, A. Skerbele, and V. D. Meyer, J. Chem. Phys., 45, 3214 (1966).

17. E. N. Lassettre, A. Skerbele, M. A. Dillon, and K. J. Ross, J. Chem. Phys., 48, 5066 (1968).

18. E. N. Lassettre, Can. J. Chem., 47, 1733 (1969).

19. A. Kuppermann and L. M. Raff, J. Chem. Phys., 37, 2497 (1962).

20. A. Kuppermann and L. M. Raff, Disc. Faraday So., 35, 30 (1963).

21. P. S. P. Wei, Ph.D. Thesis, California Institute of Technology, 1968.

22. P. S. P. Wei and A. Kuppermann, Rev. Sci. Inst., 40, 783 (1969).

23. G. J. Schulz, Phys. Rev., 125, 229 (1962).

24. J. A. Simpson and S. R. Mielczarek, J. Chem. Phys., 39, 1606 (1963).

25. J. A. Simpson, Rev. Sci. Inst., 35, 1698 (1964).

26. J. A. Simpson, M. G. Menendez, and S. R. Mielczarek, Phys. Rev., 150, 76 (1966).

27. J. A. Simpson and C. E. Kuyatt, Rev. Sci. Inst., 38, 103 (1968).

28. (a) J. K. Rice, A. Kuppermann, and S. Trajmar, J. Chem. Phys., 48, 945 (1968); (b) A. Kuppermann, J. K. Rice, and S. Trajmar, J. Phys. Chem., 72, 3894 (1968).

29. (a) S. Trajmar, J. K. Rice, and A. Kuppermann, Adv. Chem. Phys., 18, 15 (1970); (b) J. K. Rice, Ph.D. Thesis, California Institute of Technology, 1969.

30. A. Chutjian, D. C. Cartwright, and S. Trajmar, Phys. Rev. Lett., 30, 195 (1973).

31. A. J. Williams III and J. P. Doering, J. Chem. Phys., 51, 2859 (1969).

32. J. Comer and F. H. Read, J. Phys. B, 4, 368 (1971).

33. J. B. Hasted and A. M. Awan, J. Phys. B, 2, 367 (1969).

34. I. W. Larkin and J. B. Hasted, J. Phys. B, 5, 95 (1972).

35. W. C. Tam and C. E. Brion, J. Elect. Spect., 2, 111 (1973).

36. D. Roy, A. Delâge, and J. D. Carette, Can. J. Phys., 51, 1597 (1973).

37. J. A. Preston, M. A. Hender, and J. W. McConkey, J. Phys. E, 6, 661 (1973).

38. G. Joyez, R. I. Hall, J. Reinhardt, and J. Mazeau, J. Elect. Spect., 2, 183 (1973).

39. G. J. Schulz, Phys. Rev., 112, 150 (1958).

40. G. J. Schulz, Phys. Rev., 116, 1141 (1959).

41. C. R. Bowman and W. D. Miller, J. Chem. Phys., 42, 681 (1965).

42. H. H. Brongersma and L. J. Oosterhoff, Chem. Phys. Lett., 1, 169 (1967).

43. F. W. E. Knoop, H. H. Brongersma, and A. J. H. Boerboom, Chem. Phys. Lett., 5, 450 (1970).

44. D. F. Dance and I. C. Walker, Chem. Phys. Lett., 18, 601 (1973).

45. A. Stamatovic and G. J. Schulz, Rev. Sci. Inst., 41, 423 (1970).

46. R. K. Curran, J. Chem. Phys., 38, 780 (1963).

47. R. N. Compton, L. G. Christophorou, and R. H. Heubner, Phys. Lett., 23, 656 (1966).

48. R. N. Compton, R. H. Heubner, P. W. Reinhardt, and L. G. Christophorou, J. Chem. Phys., 48, 901 (1968).

49. D. P. Ridge and J. L. Beauchamp, J. Chem. Phys., 51, 470 (1969).

3. Electron-Molecule Scattering Theory

3.1 Introduction

The formal theory of electron-molecule scattering can be written down using the Schrödinger equation. The computational techniques are so difficult for the electron-molecule problem, however, that only the simplest approximations have been used to solve for inelastic differential cross sections (DCS). Rice [1] has given a derivation of the coupled equations and shown how the various approximations come from neglecting various terms in the equations. These results will be summarized here and used as a background for discussing some of the available electron-molecule theoretical calculations.

3.2 Derivation of the Coupled Equations

The time independent Schrödinger equation can be written as $H\Psi = E\Psi$ where Ψ is the wavefunction, H is the Hamiltonian and E is the total energy. For the collision of an electron with a molecule containing N-1 electrons and N′ nuclei the Hamiltonian can be written as

$$H = -\frac{\hbar^2}{2}\left[\sum_{k=1}^{N}\frac{\nabla_k^2}{m} + \sum_{j=1}^{N'}\frac{\nabla_j^2}{m_j}\right] + e^2\left[\sum_{\ell>k}^{N}\sum_{k=1}^{N-1}\frac{1}{r_{\ell k}} - \sum_{k=1}^{N}\sum_{j=1}^{N'}\frac{Z_j}{|\vec{r}_k - \vec{R}_j|} + \sum_{j>i}^{N'}\sum_{i=1}^{N'-1}\frac{Z_j Z_i}{R_{ji}}\right] \quad (3\text{-}1)$$

The first term is the electron kinetic energy (KE), the second term is the nuclear KE, the third term is the electron-electron repulsion potential, the fourth term is the electron-nucleus attraction potential, and the fifth term is the nuclear repulsion potential.

The total Hamiltonian can now be arbitrarily separated into two parts. The first is the Hamiltonian for the molecule itself (H_{mol}) while the second is that of the free electron plus its electrostatic interaction with the molecule. We will assume that the eigenfunctions Φ_n of H_{mol} are known and that they can be factored into products of spatial (ψ_n) and spin functions (χ_{S,S_z}) with the following properties:

$$H_{mol}\,\Phi_n = \epsilon_n \Phi_n \tag{3-2}$$

$$\Phi_n = \psi_n \chi_{S,S_z} \tag{3-3}$$

$$\hat{S}^2 \chi_{S,S_z} = \hbar^2 S(S+1)\,\chi_{S,S_z} \tag{3-4}$$

$$\hat{S}_z \chi_{S,S_z} = \hbar S_z \chi_{S,S_z} \tag{3-5}$$

$$\langle \psi_n | \psi_m \rangle = \delta_{nm} \tag{3-6}$$

$$H_{mol}\,\psi_n = E_n \psi_n \tag{3-7}$$

The desired asymptotic form of Ψ is that of an incoming plane wave representing the incoming electron plus an outgoing spherical scattering wave with the molecule left in its n^{th} excited state. Of course the asymptotic form must reflect the indistinguishability of the electrons so a permutation operator P_{1N} is defined which will permute the coordinates of electron "one" in a pairwise manner with each of the other electrons. In addition, the asymptotic form will also be written as a sum over all possible bound excited states and an integral over molecular continuum states (unionized states above the first ionization potential) with a corresponding scattering amplitude (f_{on}) for each inelastic scattering channel. Thus

$$\Psi \underset{r \to \infty}{\sim} \sum_{n=0}^{\infty\prime} (1 - P_{1N}) \left[\left\{ e^{i\vec{k}_0 \cdot \vec{r}_1} \delta_{on} + \frac{f_{on}\, e^{i k_n r_1}}{r_1} \right\} \quad s_n \psi_n \right] \tag{3-8}$$

where $\sum'$ also includes the integration over the continuum states and s_n is a single electron spin function. It can also be shown[2] that the DCS for excitation of the molecule to its n^{th} state is

$$\sigma_{on}(k_0, \theta, \varphi) = \frac{k_n}{k_0} |f_{on}|^2 \tag{3-9}$$

and the corresponding total (integral) cross section is

$$Q_n(k_0) = \frac{k_n}{k_0} \int_0^{2\pi} d\varphi \int_0^{\pi} \sin\theta \, |f_{on}|^2 \, d\theta \tag{3-10}$$

To obtain a solution of Ψ which is valid in all regions of space we will expand again in products of the ψ_n and new functions G_n which depend on the space and spin coordinates of a single electron.

$$\Psi = \sum_{n=0}^{\infty}{}' (1 - P_{1N}) G_n \psi_n \tag{3-11}$$

This expansion is inserted into the Hamiltonian, the resulting expression is multiplied by ψ_m^* and integrated over all space and spin coordinates except those of electron one to yield

$$(\nabla_1^2 + k_m^2) G_m = \sum_{n=0}^{\infty}{}' \frac{2m}{\hbar^2} \langle \psi_m^* | V_{1\text{-mol}} | \psi_n \rangle$$

$$+ N-1 \sum_{n=0}^{\infty}{}' \langle \psi_m^* | \psi_n (\nabla_2^2 + k_n^2 - \frac{2m}{\hbar^2} V_{2\text{-mol}}) G_n \rangle \tag{3-12}$$

where

$$V_{i\text{-mol}} = e^2 \left[\sum_{\substack{k=1 \\ i \neq k}}^{N} \frac{1}{r_{ik}} - \sum_{j=1}^{N'} \frac{Z_j}{|\vec{r}_i - \vec{R}_k|} \right] \tag{3-13}$$

If these equations can be solved with the G_n having the following boundary conditions

$$G_n \underset{r\to\infty}{\sim} e^{i\vec{k}_0\cdot\vec{r}}\,\delta_{on}s_o + f_{on}\frac{e^{ik_n r}}{r}s_n \qquad (3\text{-}14)$$

then all aspects of the scattering problem will have been solved. Unfortunately this is not possible to achieve without approximations which will be discussed in the next section.

3.3 Approximations

3.3.1 Close-Coupling

The problem cannot be solved with the infinite expansion shown in (3-11) but if the expansion is truncated after a finite number of terms the remaining terms in equation 3-12 can be solved numerically. This approximation, known as close-coupling is still a very costly process because the equations in 3-12 are actually coupled integro-differential equations. The only apparent applications of this technique to molecules involve calculations of elastic, rotational or vibrational excitation of the ground electronic state. The earliest studies of elastic or rotational cross sections (both differential and total) appear to be those of Lane and Geltman on the hydrogen molecule.[3,4] These studies assumed that the wavefunction could be written as a product of electronic, nuclear vibration, and nuclear rotation functions and that only elastic or rotational excitation was considered. The results were shown to depend strongly on the value of a cutoff parameter in the

polarization part of the electron-molecule potential. If the parameter was chosen properly the theoretical results in the 0 eV to 10 eV impact energy region looked similar to those of experiments. A review article is available [5] which treats rotational close-coupling for H_2. Henry [6] has recently extended the close-coupling calculations to include both pure vibrational excitation of the ground electronic state and simultaneous vibrational rotational excitation. The results do not appear to be as good as those obtained for elastic scattering.

The close-coupling approximation appears to be even more difficult to use for larger systems. Burke and Sinfailam [7] have obtained the total cross section from .05 to 2 Rydbergs for electron scattering from N_2. The convergence of the expansion was very slow and even with 14 terms the eigenphase sum still appeared to be changing. The total cross section did exhibit the resonance corresponding to formation of N_2^- in the $^2\Pi_g$ state but the peak location was shifted from the peak location in the experiment. Burke and Chandra [8] suggested in a later paper that this approach would not be useful for electron collisions with larger diatomic and polyatomic molecules and his later papers have treated electron molecule scattering with pseudo-potential methods.

3.3.2 Distorted Wave

The distorted wave approximation results when only two terms are retained in the expansion (the initial and final state) and back coupling terms from n to 0 are also ignored. The theory has been developed in detail[9-13] for rotational or elastic scattering off of N_2 or H_2. Various empirical forms of the interaction potential of the electron with the molecule were used in these studies.

3.3.3 First-Order Approximations

Because of the problems inherent in calculations most of the available results use the first-order approximations. The Born-Oppenheimer approximation results if f_{oo} and f_{on} in (3-14) are assumed to be very small and thus G_0 or G_n is replaced by an undistorted plane wave. For a diatomic molecule where separability of ψ_n and ψ_0 into products of electronic, vibrational, and rotational functions is assumed the resulting expressions for the Born direct amplitude and the Ochkur form of the Born-Oppenheimer exchange amplitude are

$$f_{on}^{B} = \frac{-2me^2(N-1)}{\hbar^2 |k_0 - k_n|^2} \langle \varphi_n^* | e^{i(\vec{k}_0 - \vec{k}_n)\cdot\vec{r}} | \varphi_0 \rangle \qquad (3\text{-}15)$$

$$g_{on}^{O} = \frac{-2me^2}{\hbar^2 k_0^2} \langle \varphi_n^* | e^{i(\vec{k}_0 - \vec{k}_n)\cdot\vec{r}} | \varphi_0 \rangle \qquad (3\text{-}16)$$

where φ_0 and φ_n are the initial and final electronic states of the molecule. The way in which the terms for f and g are combined to give the scattering amplitude is given by

$$f_{0n}^{S,S_Z} = \left\langle \chi^{\text{init.}}_{S,S_Z}(1\ldots N) \,\middle|\, \chi^{\text{final}}_{S,S_Z}(1\ldots N) \right\rangle_{\text{spin}} f_{on}^{B} -$$

$$(N-1)\left\langle \chi^{\text{init.}}_{S,S_Z}(2,1,..N) \,\middle|\, \chi^{\text{final}}_{S,S_Z}(2,1,..N) \right\rangle g_{on}^{O} \qquad (3\text{-}17)$$

where S and S_Z are the total spin and its projection on an arbitrary axis.

Many first-order calculations are available for elastic, rotational, or vibrational excitation. Khare and co-workers[14,15] studied elastic scattering off H_2 from 10 eV to 900 eV using the plane wave approximation with the Ochkur approximation to handle exchange. Below 100 eV the results indicate that it is important to include both exchange scattering and the polarization of the molecular electron charge cloud to get good DCS shapes. Truhlar and co-workers[16-21] in a series of papers have made a systematic study of the effects of the potential used to represent the electron-molecule interaction and the type of approximation employed for elastic and vibrational excitation of H_2, N_2, and CO. Exchange is shown to be important in the impact energy range below 80 eV. Truhlar's elastic differential

cross sections have shapes which are fairly close to experiment in the 10° to 80° scattering angle range. The agreement for vibrational DCS curves is somewhat less than for the elastic process.

Electron excitation cross sections of molecules have been calculated using the Born-Oppenheimer approximation since the 1930s. In 1932 Massey and Mohr [22] used this approximation to calculate total cross sections for excitation of the $B^1\Sigma_u^+$ and $b^3\Sigma_u^+$ states in H_2. The DCS for the B state was also obtained and predicted to peak away from 0°. Roscoe [23] in a study in 1941 also used the Born approximation to calculate DCS curves for the $B^1\Sigma_u^+$, $C^1\Pi$, and $D^1\Pi$ state of H_2. His results predicted that all DCS curves were forward peaked which is consistent with the experimental results. In more recent studies Khare [24, 25] has also studied the B, C, and D states of H_2 obtaining both integral and differential cross sections from threshold to 300 eV. Miller and co-workers have also applied the first Born approximation at energies above 300 eV to H_2 Rydberg states, [26] H_2O Rydberg states [27] and seven low-lying singlets in ethylene. [28] The results are presented in terms of generalized oscillator strengths f_n which are related to the differential cross section by

$$f_n = \frac{W}{2} |k_0 - k_n|^2 \frac{k_0}{k_n} \sigma_n \qquad (3\text{-}18)$$

Miller's calculations show that Rydberg states have generalized oscillator strengths which have minima in f(K) vs. K^2 plots while valence states do not. Thus a determination of the generalized oscillator strength by electron impact methods may provide further information about the nature of the excited state.

In addition to the Massey and Mohr calculation[22] on the $b^3\Sigma_u^+$ of H_2 there are only scattered reports of studies of spin forbidden DCS calculations. Khare and Moiseiwitsch[29] studied the b state of H_2 using the first-order exchange approximation while Khare[30] later extended the study to the $a^3\Sigma_g^+$ and the $c^3\Pi_u$ states of H_2. Cartwright and Kuppermann[31,32] and co-workers used the Ochkur-Rudge approximation to calculate both integral and differential cross sections for the a and b states of H_2 from 10 eV to 85 eV. The first-order approximation was shown to give surprisingly good results above 40 eV for the DCS curves from 10° to 80°. Below 40 eV the agreement with experiment was much poorer. Cartwright[33] later used the same method to calculate total cross sections for the seven lowest triplet states in N_2.

Some generalizations which may be drawn from the studies mentioned above are as follows:

1. The cross sections are often very sensitive to the molecular wavefunctions.
2. The cross sections also depend on the type of potential used to represent the electron-molecule interaction. Polarization potentials should be included below 100 eV and the short range potentials are also important.
3. With the proper choices for wavefunctions and potentials good DCS curves can be obtained from 10° to 80° at impact energies above 25 eV to 50 eV. Below 25 eV the first-order methods fail rather badly.
4. Outside the range of 10° to 80° the results are often incorrect even for high incident energies. Below 10° the method fails because it is very difficult to treat long-range polarization potentials while above 80° distortion of the plane wave becomes very significant.

3.4 Alternate Approaches to the Problem

Two recent methods have appeared which use a somewhat different approach to the scattering problem. Rescigno, McCurdy, and McKoy[34-35] have developed a method which starts from the Lippmann-Schwinger equation for the transition operator T where

$$T(E) = V + V\, G_0^+(E)\, T(E) \qquad (3\text{-}19)$$

where $G_0^+(E)$ is the free particle Green's function. A truncated expansion of the exact potential V is made in a gaussian basis set. The choice of a square-integrable basis set makes evaluation of a number of matrix elements of $G_0^+(E)$ quite simple. In addition, the transformation of the T matrix from the expansion representation back to the scattering amplitude form also involves simple integrals. Their analysis has been limited to cylindrically symmetric potentials which have inversion symmetry. An application has been made[36] to calculate electron-H_2 elastic DCS values for incident energies below 0.7 a.u. in the static exchange approximation. The results were in excellent agreement with previous studies which used costly numerical integration techniques.

In a series of papers Taylor and co-workers[37-39] have used Green's function techniques to derive expressions for the S matrix for both elastic and inelastic electron-atom (molecule) scattering. The method has the advantage of decoupling the various scattering channels and results in a channel to channel formula which is exact. The transition potential between two channels is energy dependent in this formalism. Various approximations to the exact equations are discussed and an application has been made[40] to the calculation of elastic s, p, and d wave phase shifts for electron-helium scattering. The s and p wave phase shifts are in excellent agreement with the phase shifts from an

analysis of experimental results. The method has not yet been applied to electron-molecule scattering.

References

1. J. K. Rice, Ph.D. Thesis, California Institute of Technology, 1969, pp. 13-44.

2. A. Messiah, Quantum Mechanics, II, John Wiley and Sons, Inc., New York, 1961, p. 836.

3. N. F. Lane and S. Geltman, Phys. Rev., 160, 53 (1967).

4. N. F. Lane and S. Geltman, Phys. Rev., 184, 46 (1969).

5. D. E. Golden, N. F. Lane, A. Temkin, and E. Gerjuoy, Rev. Mod. Phys., 43, 642 (1971).

6. R. J. W. Henry, Phys. Rev. A, 2, 1349 (1970).

7. P. G. Burke and A. L. Sinfailam, J. Phys. B, 3, 641 (1970).

8. P. G. Burke and N. Chandra, J. Phys. B, 5, 1696 (1972).

9. R. C. Mjolsness and D. H. Sampson, Phys. Rev. Lett., 13, 812 (1964).

10. D. H. Sampson and R. C. Mjolsness, Phys. Rev., 140, A1466 (1965).

11. K. Takayanagi and S. Geltman, Phys. Lett., 13, 135 (1964).

12. K. Takayanagi and S. Geltman, Phys. Rev., 138, A1003 (1965).

13. S. Geltman and K. Takayanagi, Phys. Rev., 143, 25 (1966).

14. S. P. Khare and B. L. Moiseiwitsch, Proc. Phys. Soc., 85, 821 (1965).

15. S. P. Khare and P. Shobha, J. Phys. B, 5, 1938 (1972).

16. D. G. Truhlar and J. K. Rice, J. Chem. Phys., 52, 4480 (1970).

17. S. Trajmar, D. G. Truhlar, and J. K. Rice, J. Chem. Phys., 52, 4502 (1970).

18. S. Trajmar, D. G. Truhlar, J. K. Rice, and A. Kuppermann, J. Chem. Phys., 52, 4516 (1970).

19. D. G. Truhlar, S. Trajmar, and W. Williams, J. Chem. Phys., 57, 3250 (1972).

20. D. G. Truhlar, J. Chem. Phys., 57, 3260 (1972).

21. D. G. Truhlar, W. Williams, and S. Trajmar, J. Chem. Phys., 57, 4307 (1972).

22. H. S. W. Massey and C. B. O. Mohr, Proc. Roy. Soc. A, 135, 258 (1932).

23. R. Roscoe, Phil. Magazine, 31, 349 (1941).

24. S. P. Khare, Phys. Rev., 149, 33 (1966).

25. S. P. Khare, Phys. Rev., 152, 74 (1966).

26. K. J. Miller and M. Krauss, J. Chem. Phys., 47, 3754 (1967).

27. K. J. Miller, S. R. Mielczarek, and M. Krauss, J. Chem. Phys., 51, 26 (1969).

28. K. J. Miller, J. Chem. Phys., 51, 5235 (1969).

29. S. P. Khare and B. L. Moiseiwitsch, Proc. Phys. Soc. (London), 88, 605 (1966).

30. S. P. Khare, Phys. Rev., 157, 107 (1967).

31. D. C. Cartwright and A. Kuppermann, Phys. Rev., 163, 86 (1967).

32. S. Trajmar, D. C. Cartwright, J. K. Rice, R. T. Brinkman, and A. Kuppermann, J. Chem. Phys., 49, 5464 (1968).

33. D. C. Cartwright, Phys. Rev. A, 3, 1331 (1970).

34. T. N. Rescigno, C. W. McCurdy, and V. McKoy, to be published in Chem. Phys. Lett.

35. T. N. Rescigno, C. W. McCurdy, and V. McKoy, to be published in Phys. Rev. A.

36. T. N. Rescigno, C. W. McCurdy, and V. McKoy, unpublished results.

37. G. Csanak, H. S. Taylor, and R. Yaris, Phys. Rev. A, 3, 1322 (1971).

38. G. Csanak, H. S. Taylor, and R. Yaris, Adv. in Atomic and Mol. Physics, 7, 288 (1971).

39. G. Csanak, H. S. Taylor, and D. N. Tripathy, J. Phys. B, 6, 2040 (1973).

40. B. S. Yarlagadda, G. Csanak, H. S. Taylor, B. Schneider, and R. Yaris, Phys. Rev. A, 7, 146 (1973).

4. Components of the Spectrometer

4.1. Introduction

Figure 1 is a 1/2 scale schematic representation of the spectrometer. The gun lenses extract an electron beam from a directly heated filament and focus the beam at the entrance of the monochromator. The monochromator transmits a narrow energy slice out of the thermal energy distribution of these electrons. The entrance lenses refocus the beam at the scattering center.

After collision with the target molecules, the scattered electrons pass through two scattering angle defining apertures and are focused onto the entrance of the second 180° hemisphere, the energy loss analyzer or selector. The second sphere transmits only those electrons which have lost a specified amount of energy to the detector lenses which then focus these electrons onto the entrance cone of a Spiraltron multiplier.

The gun lenses, monochromator, entrance lenses, and the entrance side of the scattering are mounted on a gear wheel and can be rotated a total of 110° around the scattering center. This rotation moves the first half into or out of the plane of the paper in Figure 1. The scattering chamber is not bent at a scattering angle of 30°, so the rotation permits observation of electrons which have scattered at

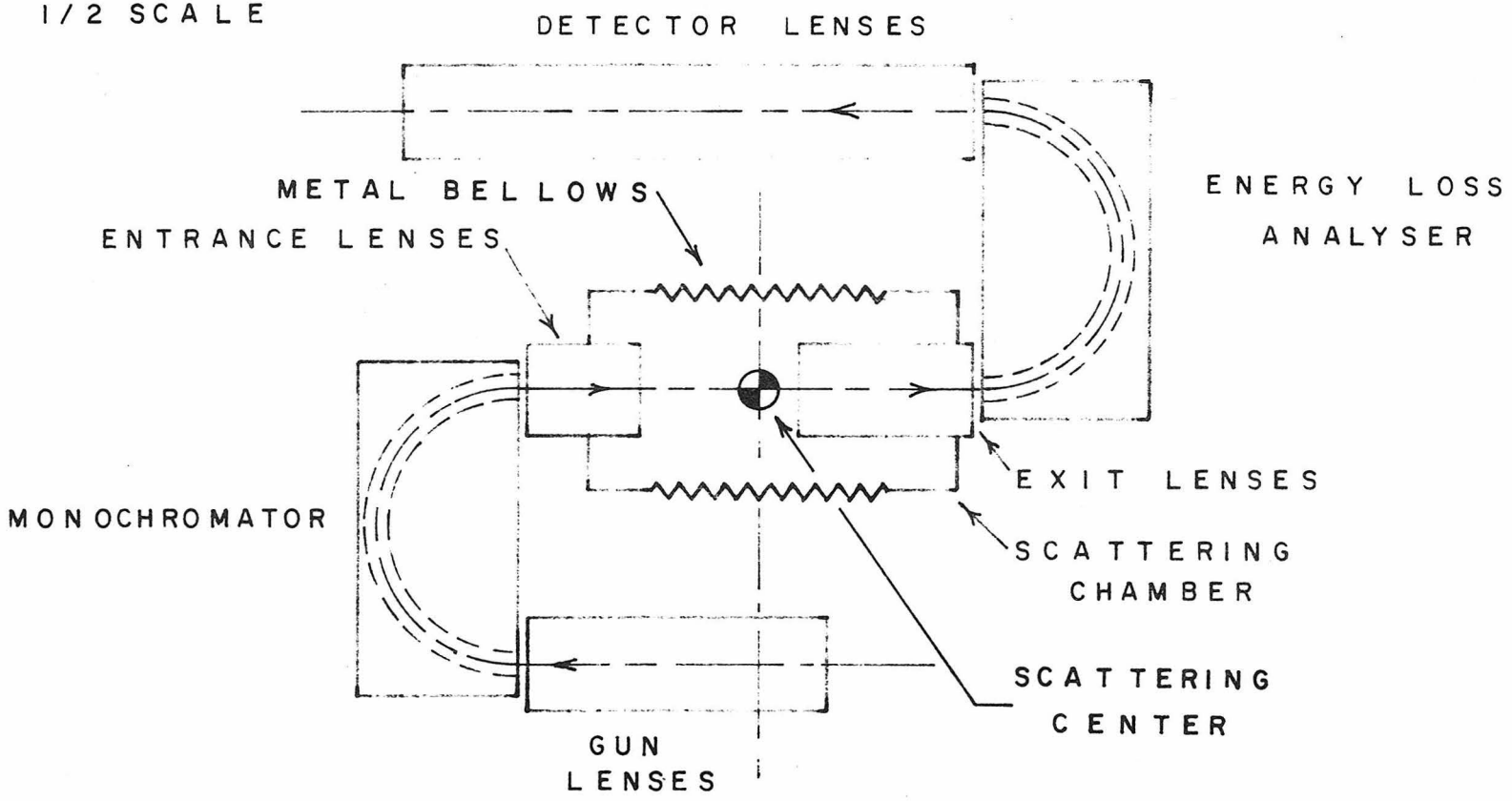

FIGURE 1 SPECTROMETER BLOCK DIAGRAM

angles ranging from -25° to +85°.

4.2. The Filament and Gun Lenses

Figure 2 shows a cross sectional view of the electron gun. The electron gun was designed by Sandor Trajmar (see acknowledgements). The filament holder is made out of boron nitride as are the interelectrode spacer-insulators and the insulators for the six deflector plates. The cathode itself is made of 316 stainless steel (SS) because it is heated by radiation from the filament which operates between 1850 and 2200°C. (This temperature range was actually measured by placing the filament and the lense following it in a glass vacuum jar and determining the temperature during operation with an optical pyrometer--see Section 4.17.1). The filament alignment ring is also made of 316 SS for the same reason. The remaining lenses and the deflector plates are made of oxygen-free high-conductivity (OFHC) copper. The apertures (A1 - A4) are .005" thick molybdenum and have the following hole diameters; A1 = 0.03", A2 = A3 = 0.02", A4 = 0.08". It should be noted that the original gun design called for A2 = 0.016". A 0.005" diameter tungsten filament (AEI Inc., Cat. #80-3236) is the electron source. The filament, the cathode and A1 form a Pierce diode extraction system. The gun utilizes a multistage accelerating system as discussed by Simpson and Kuyatt [1] to overcome

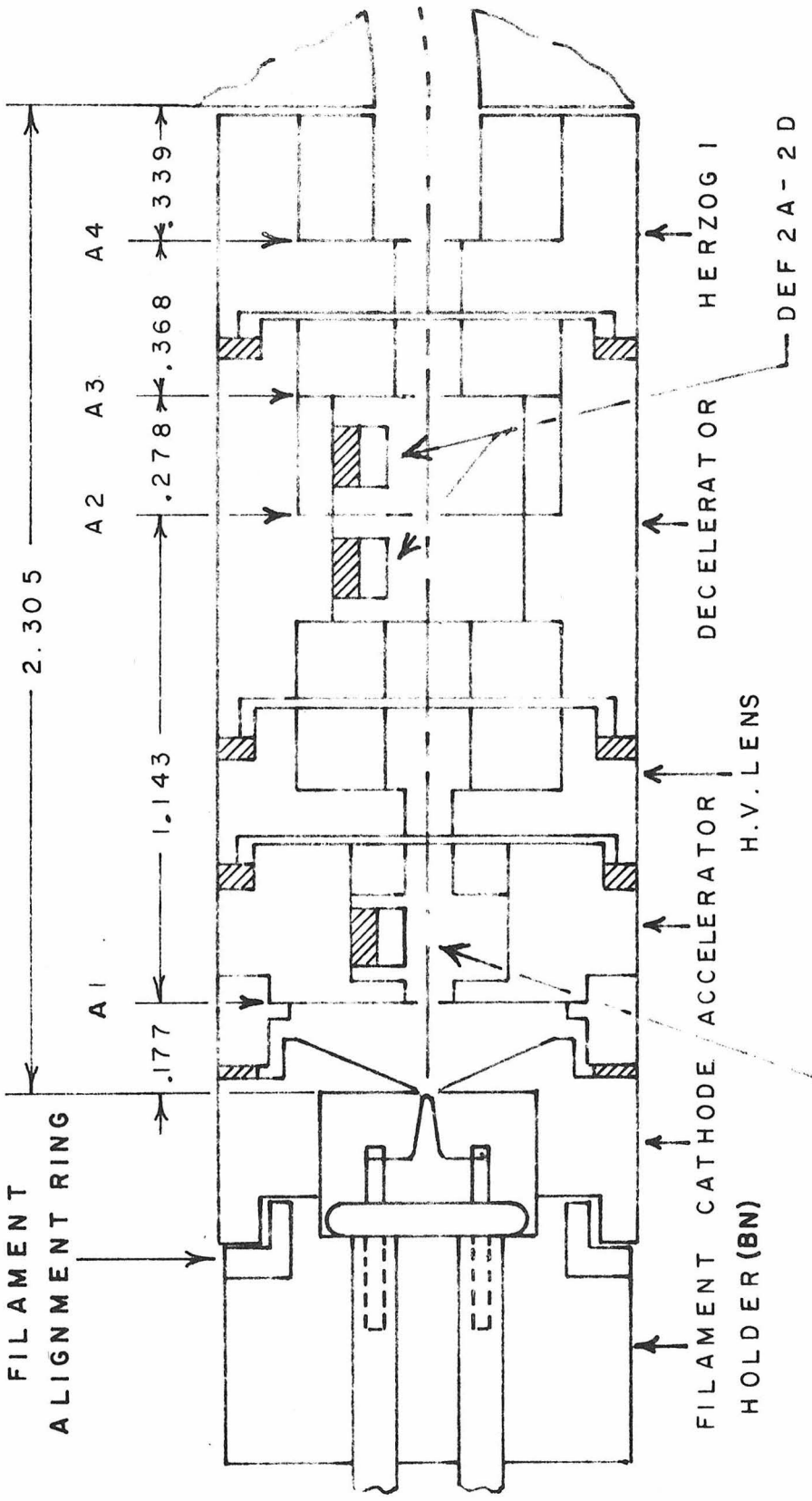

FIGURE 2 GUN LENSES

the space charge in front of the cathode. A unipotential gun could not achieve the desired space charge limited currents at the desired analyzer energy (~ 2 to 4 eV) and the desired beam divergence (~ 0.1 radians maximum). The two stage acceleration system (Cathode-Accelerator and Accelerator-High voltage lens) is then followed by a two-stage deceleration system (H. V. Lens-Decelerator and Decelerator-Herzog 1) which forms an image on the monochromator entrance plane whose object is A2 (the entrance window). This method, which has been discussed by Kuyatt and Simpson [2] means that no physical aperture is required in the monochromator entrance plane. This is advantageous because it is difficult to get 2 to 4 eV energy electron beams through small apertures. Both space charge and aperture edge effects distort the beam. The production of secondary electrons is also a problem for apertured beams in this energy range. A3 (the pupil) serves to limit the angular divergence of the beam by stripping away electrons which are more than 0.01" off axis at that point. A4 is a spatter aperture which is designed to stop stray secondary electrons and also electrons which have been reflected from lens surfaces in the earlier stages of the gun. The three pairs of deflector plates were included to correct for angular misalignment of the beam.

The filament holder and filament alignment ring were designed to permit the accurate positioning of the filament in the center of the cathode. The filaments exact position on the filament pins varied and the tips were often off center. The tubes which hold the filament pins can be moved back and forth in the filament holder and then secured with set screws to adjust for filament length variations. Centering is then accomplished by making the filament alignment ring outside diameter smaller than the cathode inside diameter. Three set screws, which are equally spaced around the cathode, can then be adjusted in or out to vary the position of the alignment ring and thus the filament tip relative to the cathode hole.

All lenses were cleaned in an ultrasonic cleaner before assembly. In addition, special care is required with the apertures. After machining and cleaning they were inspected under a 7X magnifying glass for any burrs or dirt around the aperture. The hole itself must be close to perfectly round and the aperture disk should not be distorted from the pressure of drilling. Cotton tipped applicators were of use in removing any residual dirt. The hole should then be reinspected for pieces of cotton. At all times after cleaning, the lenses and apertures were handled with surgical gloves to preserve surface cleanliness.

The cathode, which is made of stainless steel, has a tendency to become magnetic. This can badly distort slow moving electron beams. Its magnetism was measured after construction and lowered to < 0.01 gauss using an Electromatic A1-6-2 degausser. After operation it is also useful to degauss the cathode whenever it is removed to replace a burnt out filament.

For all lenses in this machine, Burndy pin connectors are attached to the lens so that leads can be quickly removed or attached during assembly operations.

4.3. Monochromator and Analyzer

Figure 3 shows the hemispheres which were used in this work. The mean electron path radius is 1.50". The inner sphere radius is 1.375" while the outer sphere radius is 1.625". The inner and outer spheres are of OFHC copper, the bracket insulators and the base support are boron nitride and the bracket itself is aluminum. The close fit between the bracket, the bracket insulator, and the inner sphere accurately positions the inner sphere relative to the bracket. The bracket then slides over the edge of the outer sphere and thus the inner and outer spheres are located to within ± 0.001" of their desired concentric positions.

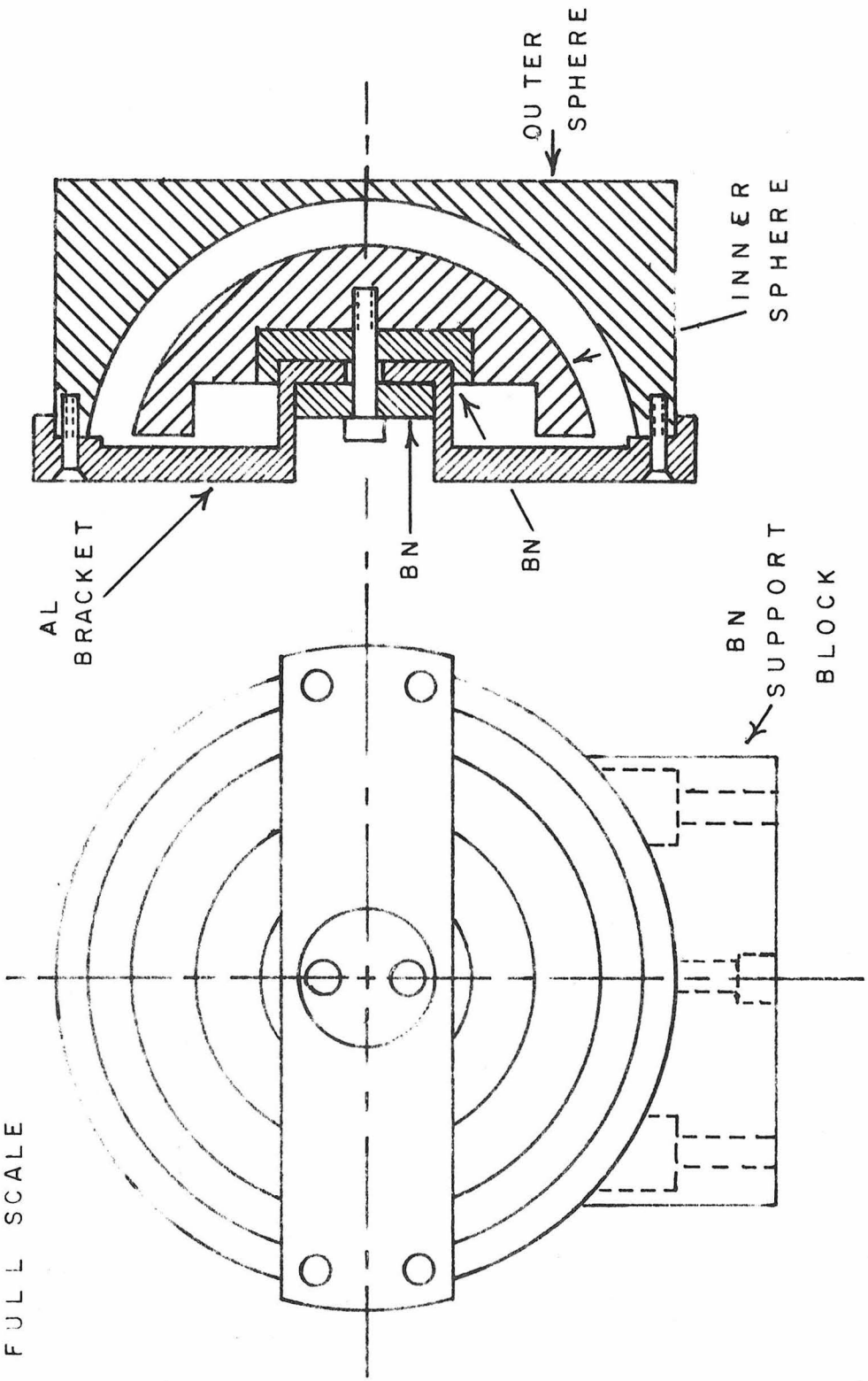

FIGURE 3 HEMISPHERE ASSEMBLY

The outer sphere is located relative to the BN support base by metal pins which extend into both pieces. The outer sphere and the support base are then hold together by screws which come up from the bottom of the support block.

4.4. Entrance Lenses

The entrance lenses, shown in Figure 4, are designed to accelerate the energy analyzed beam leaving the monochromator and focus it through the entrance aperture (A5) of the scattering chamber. Herzog 2 (H2) is a field matching lens which is included to minimize distortion of the field between the spheres. L2A and L2B form a double aperture lens[3] when L2B is held at the scattering chamber potential. L2B can actually be varied in order to focus the beam closer to the scattering center rather than at A5. This tends to decrease the angular divergence of the beam at the scattering center. Two perpendicular pairs of deflector plates are included to correct the beam alignment although it was found that these were not necessary. The gun stage deflectors could be used to adjust the beam position so that it passed through A5.

All insulators are of boron nitride while all lenses (H2, L2A, L2B) and the deflector plates (DEF3A-3D) are made of OFHC copper. The aperture (A5) has a hole diameter of 0.03" and is made of 0.05"

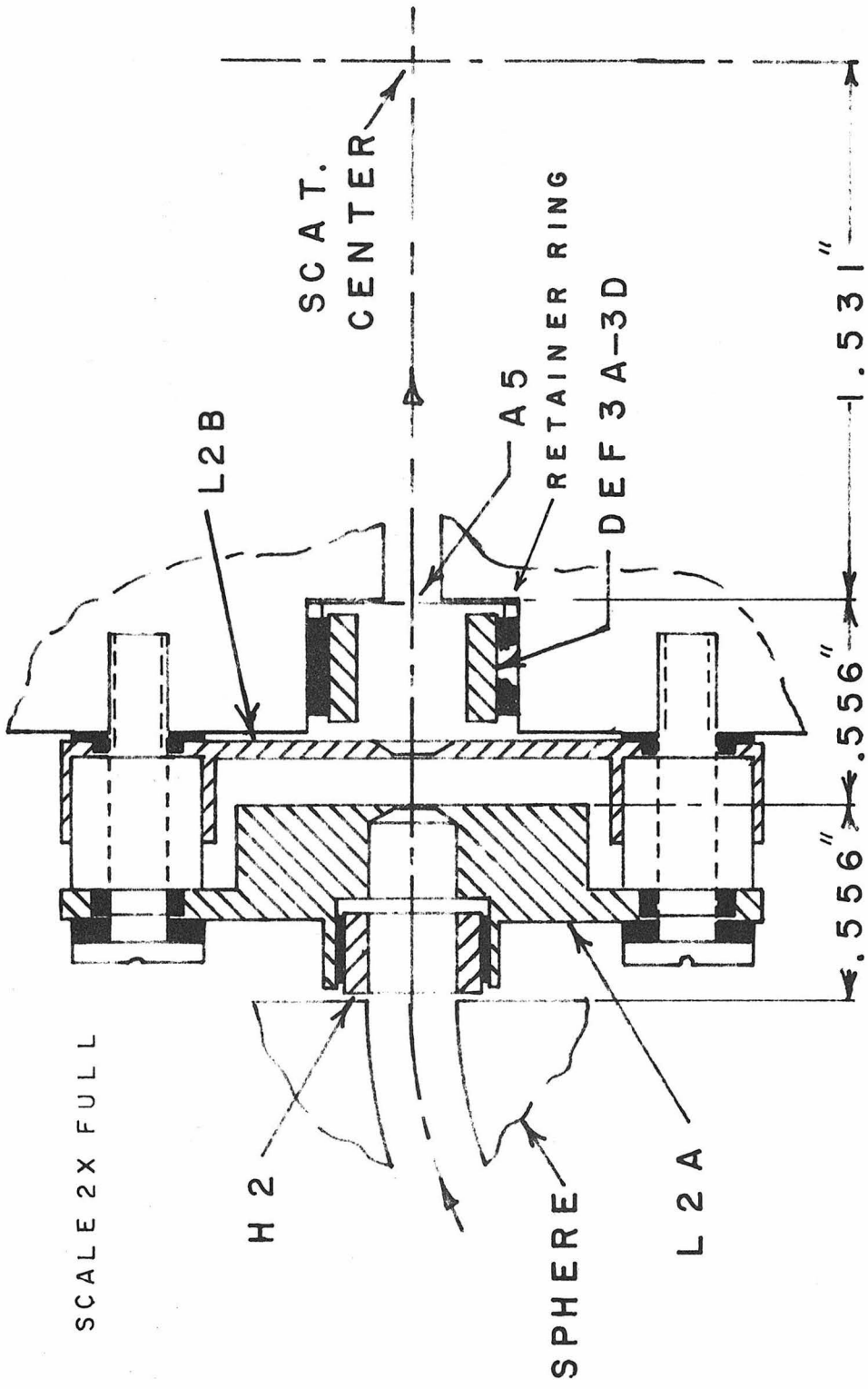

FIGURE 4 ENTRANCE LENSES

thick molybdenum. The aperture is retained by a small copper ring which fits behind the deflector plate insulators. The lenses are accurately positioned by the mounting screws because they are actually modified shoulder screws. The screws have an unthreaded portion above the threads which fits tightly into the unthreaded top portion of each angle plate hole. In addition, the BN insulating rings around the screws in L2A and L2B fit tightly on the unthreaded screw body and thus position the lenses within ±0.002" of the true center position.

The drawing in Figure 4 is made at twice full scale and the important dimensions are indicated on the drawing.

4.5. Exit Lenses

The exit lenses define the scattering geometry (i.e., the physical region of space inside the scattering chamber from which electrons are accepted) and then focus these electrons on the entrance of the energy loss analyzer. A twice full scale drawing of these lenses is shown in Figure 5. The combination of the nose cone aperture A6 and aperture A7 serve to define the detector acceptance angle (0.033 radians) and the solid angle (0.014 steradians) which the detector system subtends. These values apply strictly only to the scattering center itself rather than other points in the scattering

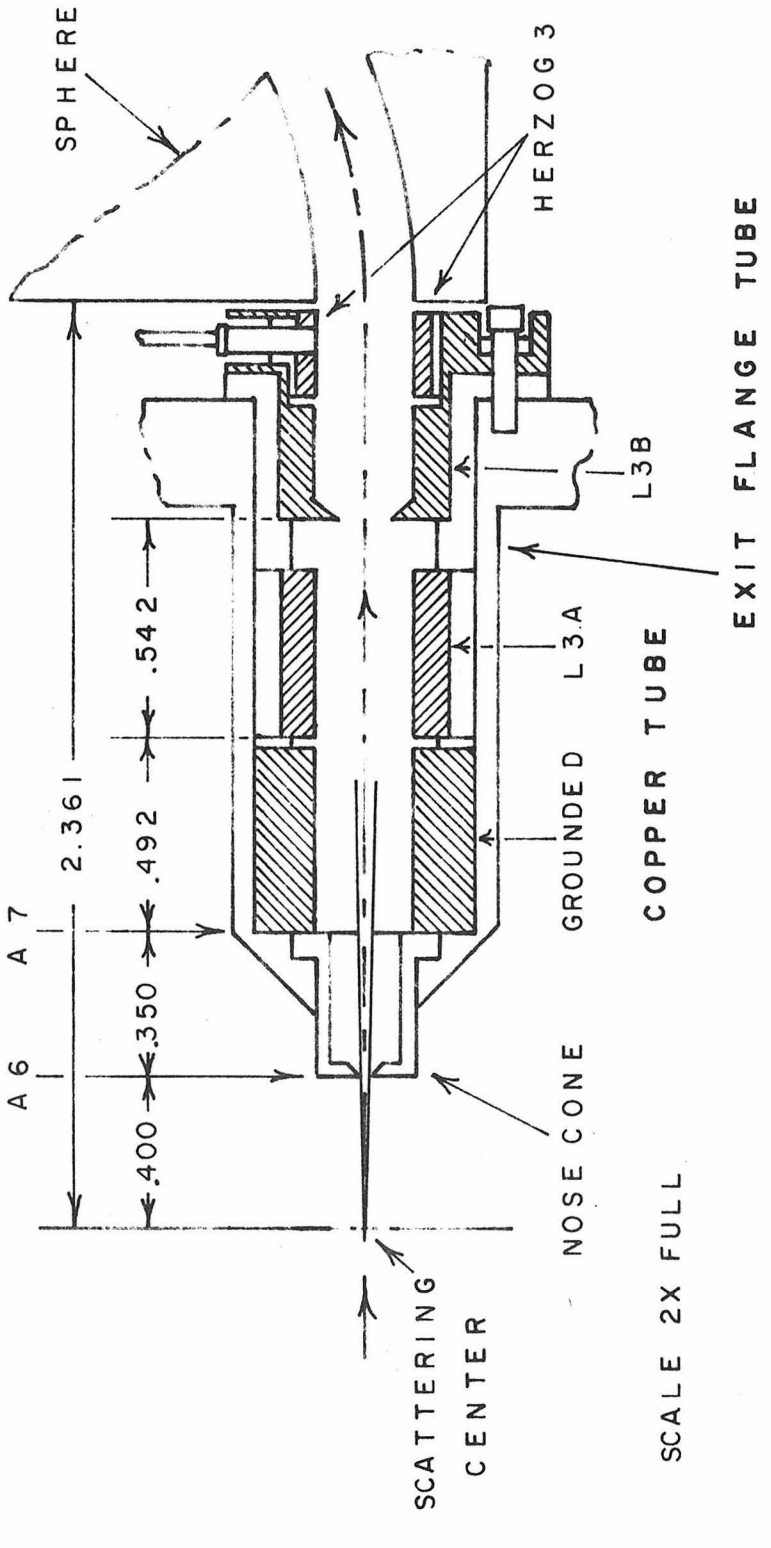

FIGURE 5 EXIT LENSES

volume. Both A6 and A7 have a 0.03" hole diameter. The nose cone and all lenses (L3A, L3B, and Herzog 3) are made of OFHC copper. The insulators are made of boron nitride. Slots are cut in the insulator surrounding L3B to permit the L3A lead to come out of the exit flange tube. Aperture A7 is made of 0.005" thick molybdenum. Two screws which attach L3B to the bellows flange serve to hold all the lens elements in position inside the bellows flange tube. The important physical dimensions are shown in Figure 5.

4.6. Detector Lenses

After the electrons have been energy loss analyzed in the selector, they enter the detector lenses shown in Figure 6. These lenses accelerate the beam and focus it on the entrance cone of the electron multiplier. The lenses (Herzog 4 (H4), L4 and the Faraday Cup Housing lens (FCH)) are made of OFHC copper as are the deflector plates (DEF 4A and 4B). Boron nitride insulators are used around H4, between L4 and FCH, and between FCH and the deflector plates. Aperture 8 (A8) is 0.005" thick molybdenum with a 0.03" hole diameter. A8 rejects electrons that are significantly off axis. This helps determine the energy resolution of the energy loss analyzer.

The Faraday cup (FC) is made of OFHC copper and is held in position by synthetic sapphire insulators which were custom made by INSACO Inc. The purpose of these insulators was to provide high resistance between the Faraday cup and the FCH lens so that very low level current mode measurements could be made. The resistance achieved was measured to be $> 1 \times 10^{15}$ ohms. No current mode measurements were actually made for the molecules reported in this thesis. A separately adjustable voltage was applied to FC so that it could be brought to the same voltage as FCH and thus would have no electron optical effect during pulse counting experiments.

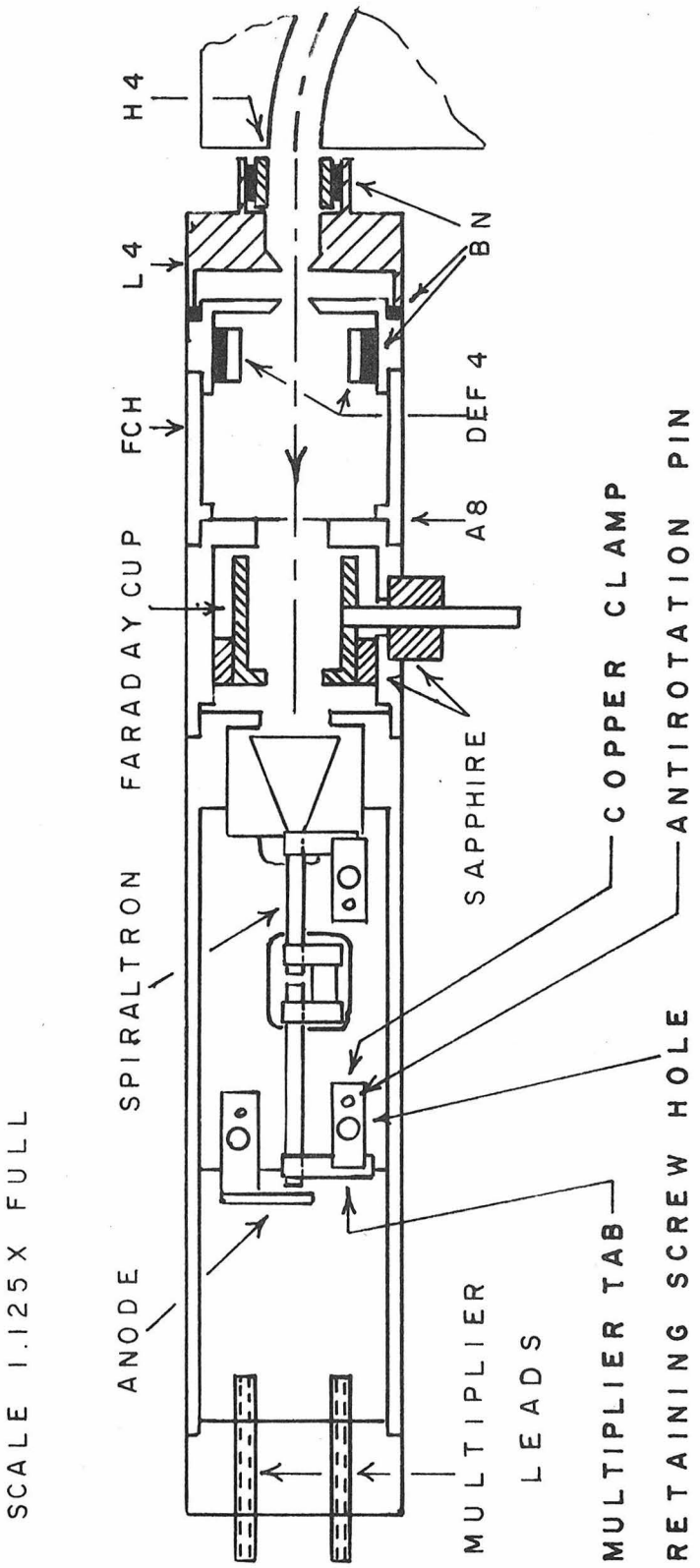

FIGURE 6 DETECTOR LENSES

The electron multiplier (Spiraltron 4219X by Bendix Corp.) was mounted on a vespel (a high vacuum insulator material by DuPont) half cylinder which slid into the end of the FCH tube. The mount was designed so that the multiplier was held only by its tabs. The vespel was cut away, as shown in Figure 6 so that it did not contact the very fragile glass multiplier tube. The copper clamps which hold each tab down on the vespel surface had a pin which located them in the vespel and then a screw which actually tightened down on the copper clamp. The pin prevented rotation of the copper clamp while the retaining screw was being tightened. If the copper clamp were allowed to rotate, this would cause rotation of the multiplier tab (made of stainless steel) and thus break the multiplier itself. Before a new multiplier was mounted it was usually necessary to bend the tabs so that they were in the same plane and could thus be tightened on the vespel mounting plane without twisting the multiplier tube around its long axis.

The leads to the multiplier came through the vespel at the rear of the lens system. Three feed through pins were used. The wire attached to one pin went to the anode which was a copper tab positioned about 0.04" behind the multiplier tube. A second lead went directly to the rear copper clamp and provided the voltage to the back end of the multiplier tube. A third lead went to a glass encapsulated,

bakeable, 100 MΩ resistor (Pyrofilm Model PVC70) which was attached to the copper clamp at the cone end of the tube. The feedthrough pins were threaded pieces of copper rod which were held in position by a nut on each side of the vespel block. A second nut was then attached to each on the inside end to hold lead wires. Burndy pins were threaded and screwed directly onto the pins on the outside. This permitted easy attachment of leads to the main flange high voltage feedthrough.

One possible improvement of the multiplier mounting system would be to put the vespel mounting plate into an insulating cylinder rather than the present copper FCH lens cylinder. Because of the physical distances (as small as 0.05") between the multiplier tabs or the feedthrough pins and the FCH wall, small discharges occur along the insulator surfaces. These discharges which can occur as often as one or two per hour lead to noise spikes in the spectrum. The discharge frequency is a function of multiplier voltage. Very few were observed during initial multiplier operation at 2200 volts (see Section 5.6.1) but the rate is higher at the present 3300 volt level. The discharge frequency also depends on surface conditions and the frequency is often much greater following the change from one target gas to another in the instrument. By increasing the insulator distance between high voltage leads and any low voltage conductor, the noise spike frequency could be significantly decreased.

4.6.1. The Electron Multiplier

A Spiraltron electron multiplier was used to detect the electrons coming through A8 in the detector stage. The electrical configuration used is shown in Figure 7. A Fluke 408B high voltage power supply provides the necessary voltage for the Spiraltron. The 1.3×10^4 ohm resistor forces the narrow charge pulses which strike the anode to appear across the 1 μf blocking capacitor and go to the pulse amplifier rather than returning to the power supply. The pulses have a total duration of about 2 to 3 μsec and a full width at half maximum of < 1 μsec. The pulses have Fourier transform components in the 1 to 2 megahertz region. The impedance of the blocking capacitor is then about 150 ohms for these frequencies which is much less than the 1.3×10^4 ohm resistor.

The 1×10^8 ohm resistor is put in to eliminate the use of a second bias supply for the anode. The tube resistance is about 1.5×10^9 Ω so about 7% of the high voltage applied (V_{total}) appears across the 10^8 ohm resistor. The rear of the tube is then 0.07 V_{total} volts below the anode and the electrons emerging from the tube are accelerated and collected on the anode by this potential.

A resistor (5×10^7 ohms) is also connected between the cone end of the multiplier and ground to bias the cone above ground by 0.03 V_{total} volts. This bias serves to accelerate electrons into the

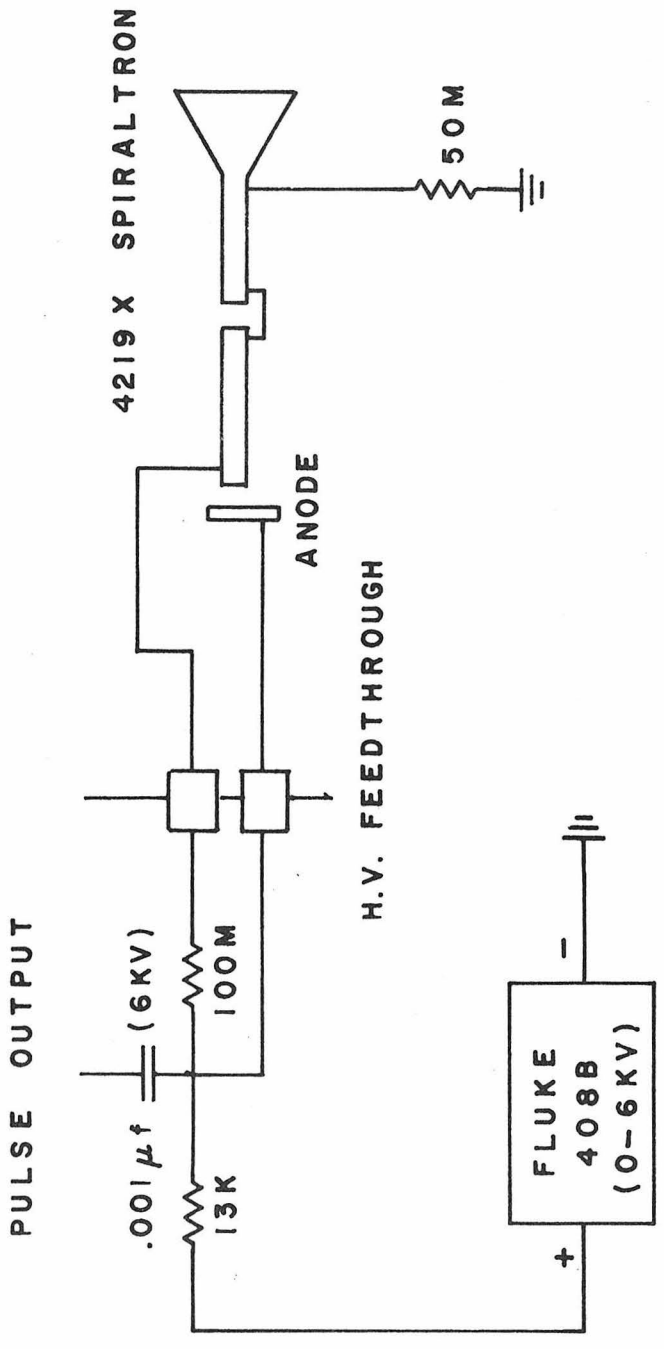

FIGURE 7 ELECTRON MULTIPLIER CIRCUIT

cone surface and thus facilitates the production of secondary electrons.

When the tube was first installed it gave pulses with an average height of about 0.015 volts with a multiplier voltage of around 2200 volts. In the subsequent months of operation the gain slowly deteriorated and required a slow increase in the multiplier voltage to obtain the same average pulse heights. At the present time after between 5×10^9 and 1×10^{10} total electron counts the multiplier is being operated at 3300 volts. A tabulation of count rate as a function of multiplier voltage is given in Table 4.6.1-1.

The pulse amplifier threshold was set to single count any pulse with a height exceeding about 0.002 volts. The elastic count rate was stable as indicated by the fact that it was the same at 3300 volts both before and after the measurements. One important fact was observed during this experiment. The Spiraltron does not respond immediately to changes in the tube voltage. There is a 15 to 20 second induction period following voltage changes, during which the count rate was not steady. This was particularly apparent when the voltage was lowered from 3300 to 3100 volts. The immediate response might be a drop in the count rate of 90% followed by a slow (10 to 15 second) return to the steady state value of only 60% drop. At the present time the gain is still relatively flat in the multiplier voltage region beyond 3300 or 3400 volts as seen in Table 4.6.1-1.

Table 4.6.1-1

Count Rate as a Function of Multiplier Voltage

Multiplier Voltage (volts)	Count Rate (10^3 counts/sec)
3000	12.9
3200	27.8
3300	32.9
3400	36.4
3500	39.3
3600	41.0
3900	44.2

4.7. Frame and Component Assembly

Figure 8 shows a side view of the assembled spectrometer. The frame itself is constructed of pieces of 1/2" thick electropolished 304 stainless steel. The overall configuration is roughly that of a rectangular box. The frame pieces are held together with screws but are accurately positioned by tapered pins. The frame pieces were ground to less than 0.001" variation in the thickness of each piece. They thus provide very accurate reference and locating surfaces. The bottom piece of the frame is a piece of 304 stainless steel channel which was bent, stress relieved, precision ground on top and side surfaces and then electropolished. The vertical frame members are screwed onto the sides of the channel. Rods are attached between the vertical frame pieces at the top on both ends to close the box-like structure. The bearing housing is mounted in a hole in the center of the channel. The gear wheel is mounted on a shaft extending upwards from the bearing housing. The first half spectrometer components are attached to the gear wheel. By rotating the gear wheel the incident electron direction can be changed relative to the fixed detector. This permits studies of angular variation of scattering processes.

The gun lenses are mounted on the gun lens mount and it is in turn screwed onto the gear wheel. Two pins on the gun mount enter holes in the gear wheel for accurate location. The monochromator

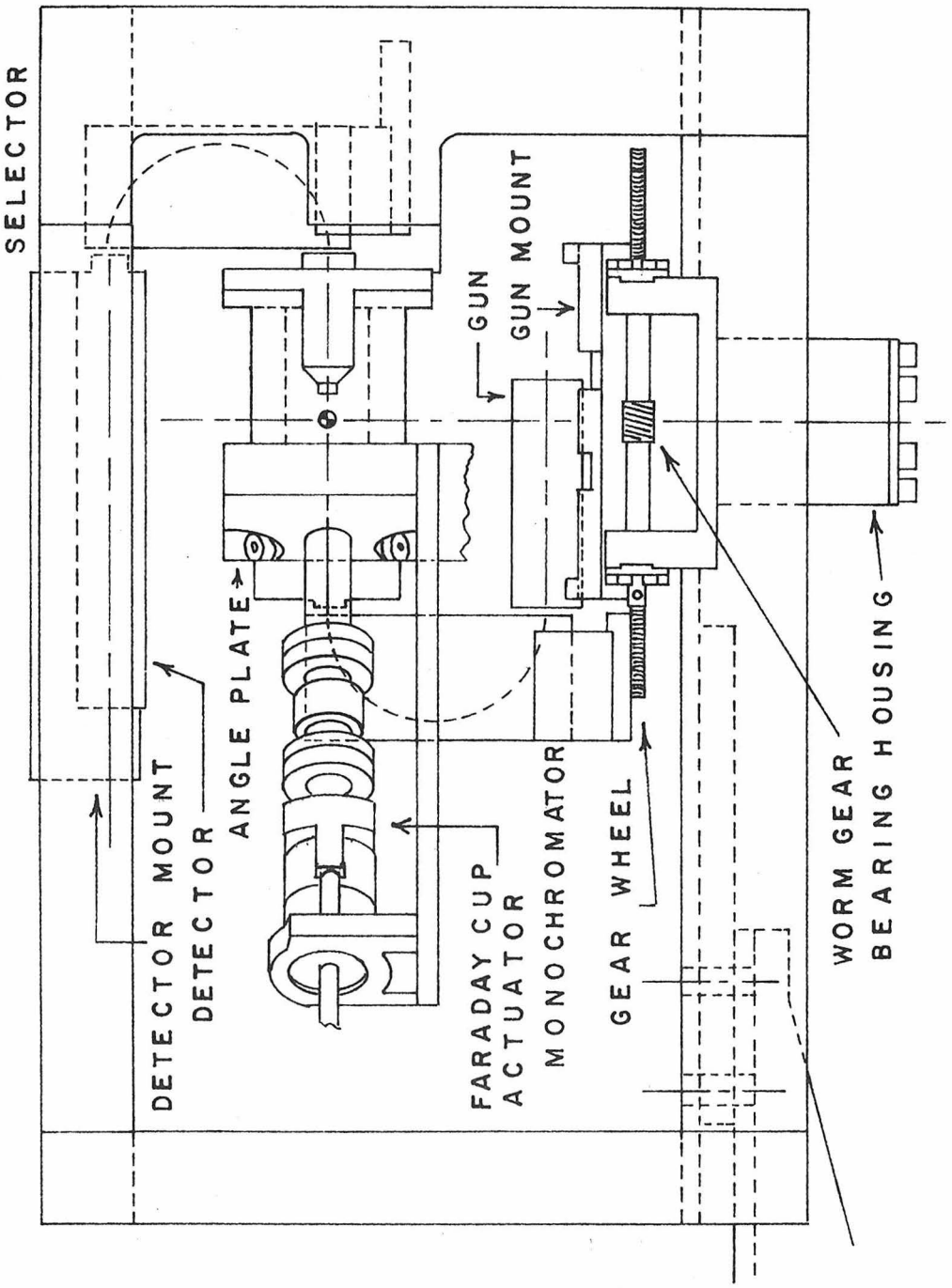

FIGURE 8 SPECTROMETER SIDE VIEW

BN support plate (see Figure 3) screws onto a metal plate which is then attached to the gear wheel and positioned by locating pins. The angle plate, which is shown broken away in Figure 8, also attaches to the gear wheel. The angle plate supports the entrance lenses, the entrance deflectors, and has the rotating end of the scattering chamber bolted to it. One end of the Faraday cup actuator attaches to the angle plate. The other end is mounted on a separate support plate coming out from the gear wheel.

The components after the scattering chamber are all rigidly attached to the upper part of the framework. The scattering chamber exit flange is mounted on a 1/2" thick plate which mounts between the vertical frame members. The exit flange provides a mount for the exit apertures and the exit lenses and has both the inner and outer bellows flanges bolted to it. The selector BN support block mounts on a metal plate which is mounted in slots on the inside of the vertical frame members. Finally, the detector lenses are attached to the detector mount which is then bolted to the upper horizontal frame piece. Certain important components mentioned above are discussed in more detail in the following sections.

4.8. The Scattering Chamber

Figure 9 shows a full scale drawing of the angle plate, the double bellows scattering chamber, and the exit flange in an assembled configuration. The inner and outer bellows are not bent when observing scattering at 30°. To vary the scattering angle, the angle plate and left end of the double bellows assembly is rotated around the scattering center. The exit lenses and the exit apertures (A6 and A7) slide into the tube-like extension of the exit flange. The angle plate holds the entrance optics, the entrance deflectors, one end of the Faraday cup actuator, and the left bellows flange.

The target gas enters the middle of the inner bellows through a hole in the exit flange. It leaks out continually through the entrance and exit apertures. The pumping speed of the diffusion pump (measured at 400 ± 50 ℓ/sec) is sufficiently high to keep the pressure around most spectrometer components at 1×10^{-6} torr while the scattering chamber pressure is as high as 1×10^{-2} torr.

The scattering chamber assembly is leak tight with the exception of these entrance and exit apertures. The bellows flanges are sealed on the angle plate or the exit flange with hollow tubular silver plated inconel O-rings (United Aircraft Products, Inc.). The nominal O-ring diameter is .033" with a 0.005" thick wall. Spacer rings of 0.020" thickness stainless steel are placed between the flanges on

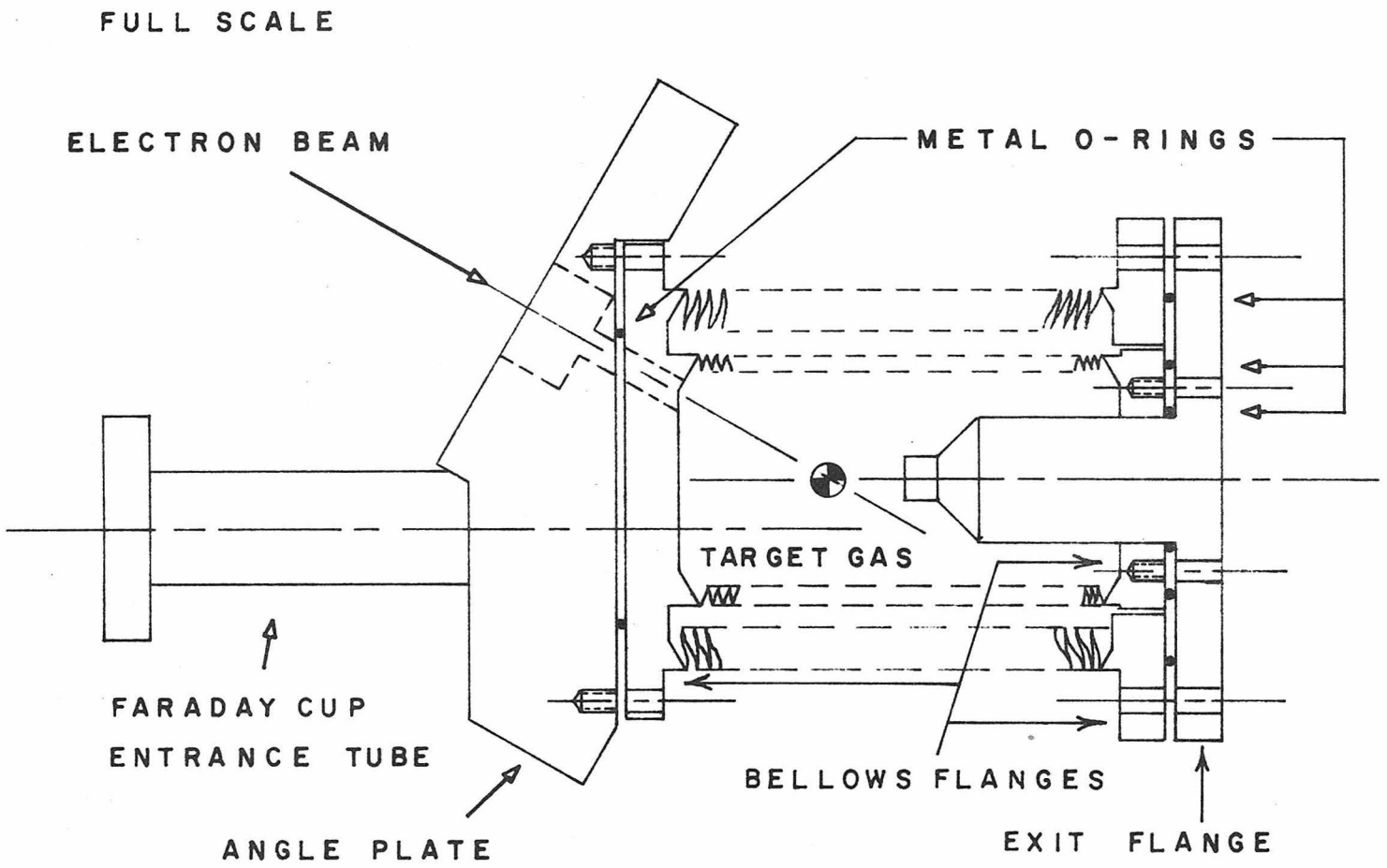

FIGURE 9 SCATTERING CHAMBER

either end to help hold the O-rings in place and also permit even compression of all sections of each O-ring. The function of each O-ring show in Figure 9 is as follows: The O-ring between the angle plate and the left bellows flange keeps the target gas from leaking out through this gap; the smallest diameter O-ring on the right stops the target gas from escaping between the inner bellows flange and the exit flange and subsequently out through the inner mounting screws. The intermediate diameter O-ring prevents the heating gas or fluid from escaping through the inner mounting screws. The large diameter O-ring prevents the heating gas or fluid from escaping through the gap between the outer bellows flange and the exit flange. It should be pointed out that no use was made of the heating gas capability of the instrument in this study. All the target gases had room temperature vapor pressures of at least 0.5 torr so raising the scattering chamber temperature was not required. The target gas was also kept from escaping out the Faraday cup assembly by O-ring seals discussed further in 4.10.

The double-bellows assembly was custom made by Metal Bellows Corp. The convolutions, which are approximately "S" shaped are welded together and then welded to the bellows end flanges. The material used in this assembly was 347 stainless steel. The flexibility of the structure thus obtained permits rotation of one end

relative to the other by +60°. By making the electron beam enter at 30° relative to the relaxed bellows axis, scattering angles of from -30° to +90° could be studied. In actual practice, interference of the angle plate with other spectrometer components limited this range to -25° to +85°.

4.9. The Angle Plate

Figure 10 shows both an end and a top view of the angle plate. The angle plate holds the entrance lenses. They are mounted with shoulder screws in the four lens mounting holes. Deflectors 3A, 3B, 3C, and 3D mount directly inside the angle plate. BN insulator segments are used between the deflector plates and the angle plate. The long-threaded copper rods, which pass through holes in the angle plate and holes in the BN segments, are screwed into the deflector plate segments to retain them. The copper mounting rods are also surrounded by insulators to prevent electrical contact with the angle plate. Voltages are applied to the deflector plates by inserting leads with Burndy pins attached directly into holes drilled in the top end of each copper mounting rod. The bellows flange attaches to the angle plate on the right side as shown in Figure 10. The Faraday cup actuator assembly mounts as shown in Figure 10 and the Faraday cup enters the scattering chamber through the Faraday cup entrance tube.

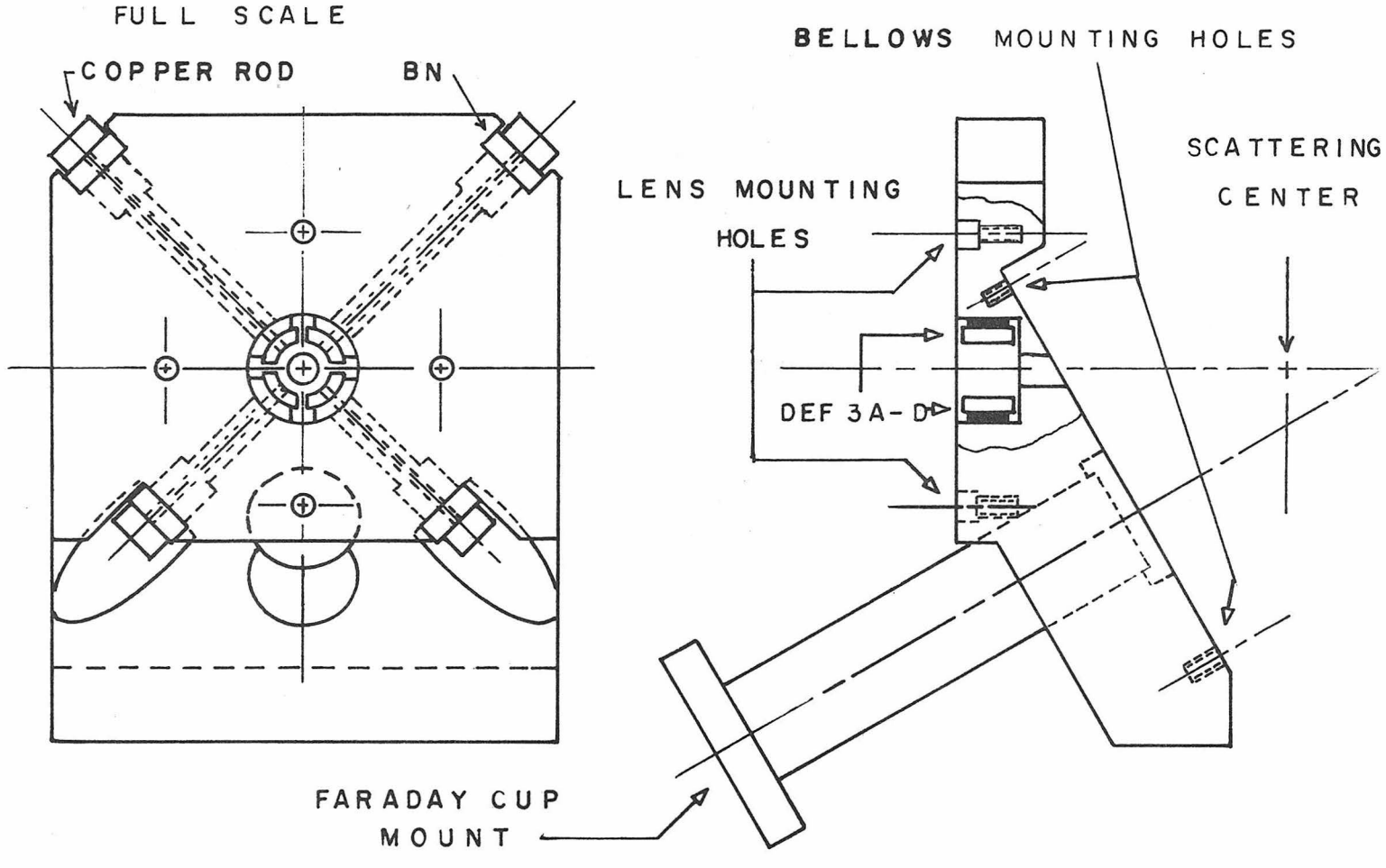

FIGURE 10 ENTRANCE ANGLE PLATE

4.10. Faraday Cup Actuator

Figure 11 shows the Faraday cup insertion mechanism. It is shown in the inserted position. The retracted Faraday cup position is also shown by the dotted outline. The purpose of this device is to insert the Faraday cup into the scattering chamber and thus monitor the incident beam current. It is also capable of retracting the Faraday cup so that scattering can be observed.

The actuator is made of 347 stainless steel. The two bellows were constructed by Metal Bellows Corp. The actuating bellows is fixed spatially at the end away from the angle plate by the mounting arm attached to the gear wheel. By putting compressed air ($\approx$ 10 lbs/in^2) inside the outer bellows through a stainless steel line from the outside of the spectrometer it is possible to overcome the spring force of the return bellows and push the Faraday cup towards the scattering center. By pumping out the actuating bellows the spring constant of the inner spring bellows is sufficient to retract the Faraday cup. Insulation of the Faraday cup rod is achieved by surrounding it with a BN insulator where it passes through the entrance tube. At the other end it is coupled to a rod which is mounted in a ceramic insulated vacuum feedthrough (Photocon Research Products). The lead to the Faraday cup then attaches to the rod on the high vacuum side of this feedthrough. Metallic O-rings (United Aircraft Products) are

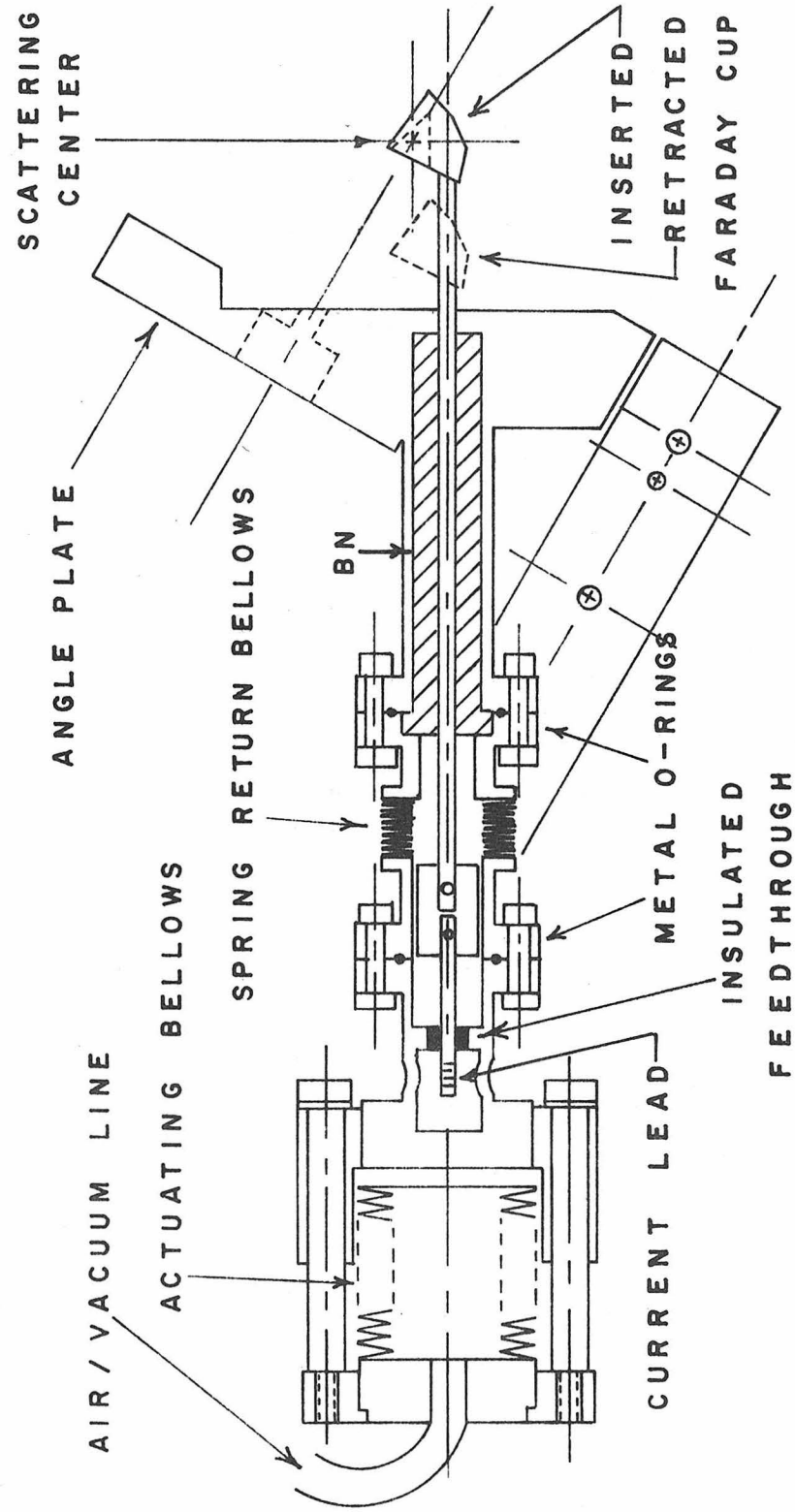

FIGURE II FARADAY CUP INSERTION MECHANISM

again employed to prevent the target gas from leaking out through the actuator mechanism.

The Faraday cup and rod is made of OFHC copper. The coupling between the feedthrough rod and the Faraday cup rod is a copper cylinder which has holes in its ends to hold each rod. Two pins go through the cylinder and pass through holes drilled in each rod to couple the rods rigidly together.

4.11. Gun Lens Mounting Plate

Figure 12 displays both a top and side view of the gun lens mounting plate which is made of aluminum. The two pins on the bottom of the plate fit tightly into reamed holes in the gear wheel. The three remaining holes are for screws which go into threaded holes in the gear wheel and secure the mounting plate to the gear wheel. The lenses are mounted on 0.250" diameter alumina or ceramic rods which pass through holes in the plate at both ends. Set screws are used to keep the rods from sliding back and forth in these holes. The lenses are held by screws coming up from the slots in the bottom of the mounting plate. Insulation is accomplished using a shouldered BN washer around each screw shaft.

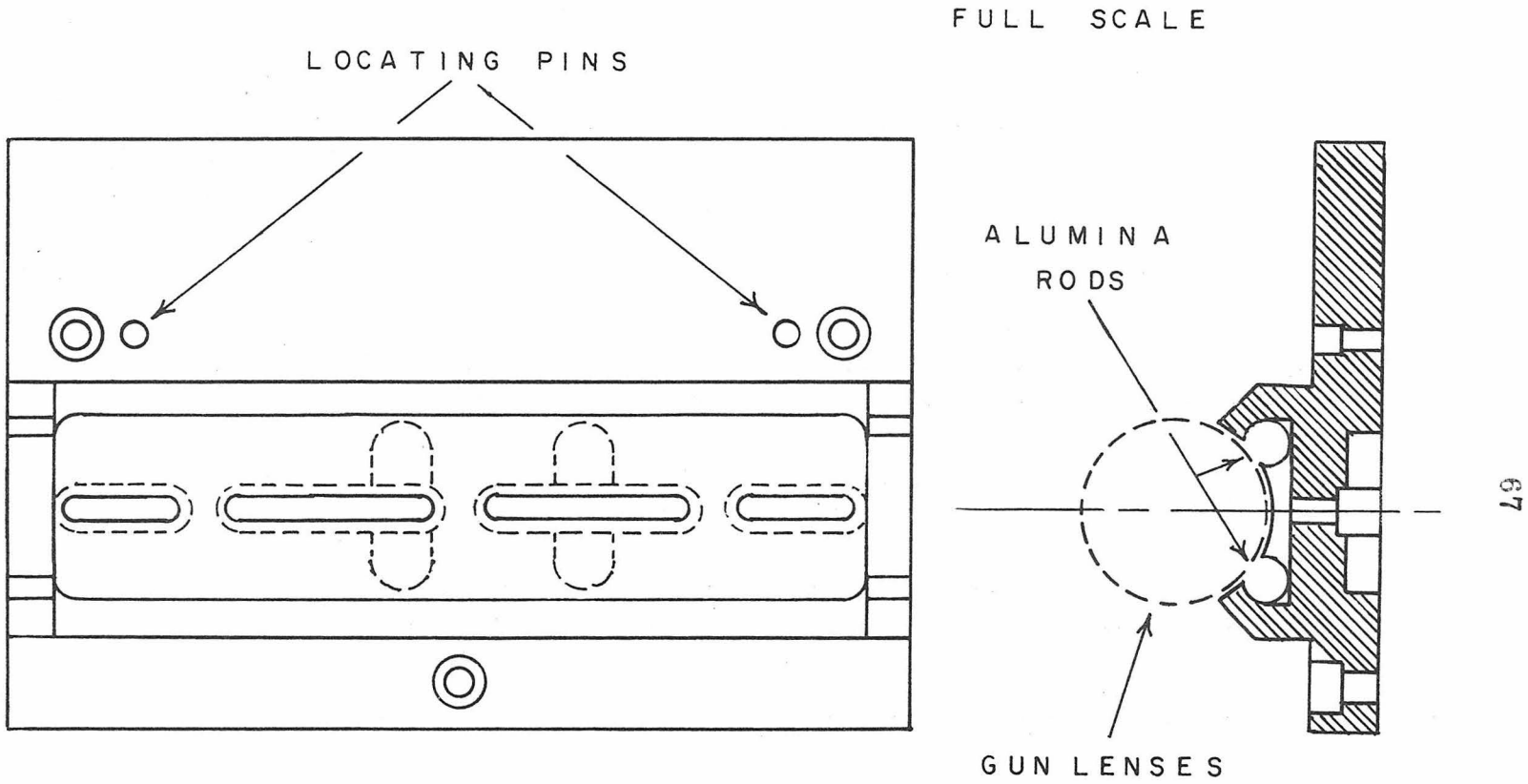

FIGURE 12 GUN MOUNTING PLATE

4.12. Detector Lens Mounting Plate

Figure 13 shows a side view of the detector lens mounting plate. The plate is made of aluminum. The method of securing the lenses is the same as discussed for the gun lens mounting plate. The detector lens mounting plate is attached to the upper horizontal frame piece. The locating surface fits tightly over the frame piece and they are then secured physically by two screws.

4.13. Bakeout Heaters

Internal bakeout heaters were used in the present instrument. 0.04" diameter chromel heater wire was wound through 0.25" diameter two-hole ceramic rods. The rods were then mounted on plates on the rear of both hemispheres and on the top of the angle plate. In addition, the lens mounting rods on the gun stage were single hole rods and heater wire was run through both rods.

It was found that the instrument could be operated successfully without utilizing the bakeout heaters. Adequate vacuum and lens surface conditions could be obtained 24 to 36 hr after pump down without baking. Baking was performed several times on the gun lenses but none of the other bakeout heaters were operated during the present study.

FULL SCALE

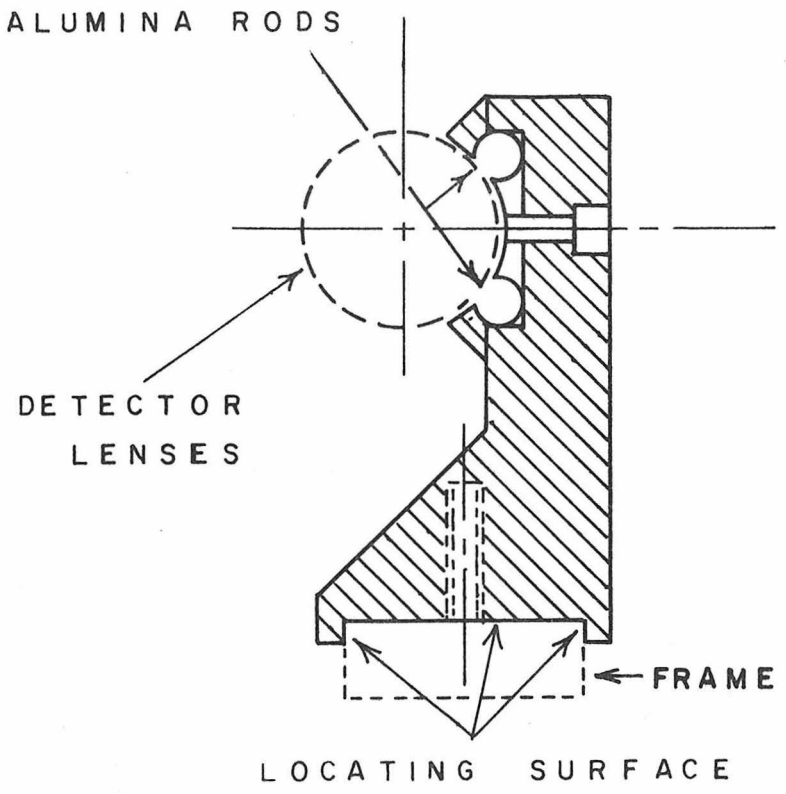

SIDE VIEW

FIG 13 DETECTOR MOUNTING PLATE

Thermocouples were installed on the angle plate, the outer sphere of the selector, and Herzog 1 to monitor temperatures during the bakeout.

4.14. Vacuum Feedthroughs

All feedthroughs were mounted on a 14" flange as shown in Figure 14. Feedthroughs 1 to 6 were constructed in the Caltech instrument shop using RCA 11 pin electrical feedthroughs and are sealed with 0.04" diameter gold wire. Feedthroughs 7 through 14 are standard Varian type 2 3/4 Conflat (Model 954-5072) feedthroughs which use copper sealing gaskets. The exact type of feedthrough and its function is described in Table 4.14-1. The connecting leads inside the spectrometer are woven glass insulated 22 gauge copper wires by Santa Fe Textiles Co. The liquid nitrogen cold shield lines, Faraday cup pressure line, and sample gas inlet lines utilize 1/4" diameter stainless steel tubing (either rigid or flexible wall type) with Cajon type fittings on each end to make vacuum tight seals.

The heating gas lines were never used during the present studies as mentioned earlier. In addition, the liquid nitrogen cooled plate, which mounts on the side of the frame inside the vacuum chamber was never used because adequate pumping speed was obtained with the diffusion pump alone. The liquid nitrogen plate might be

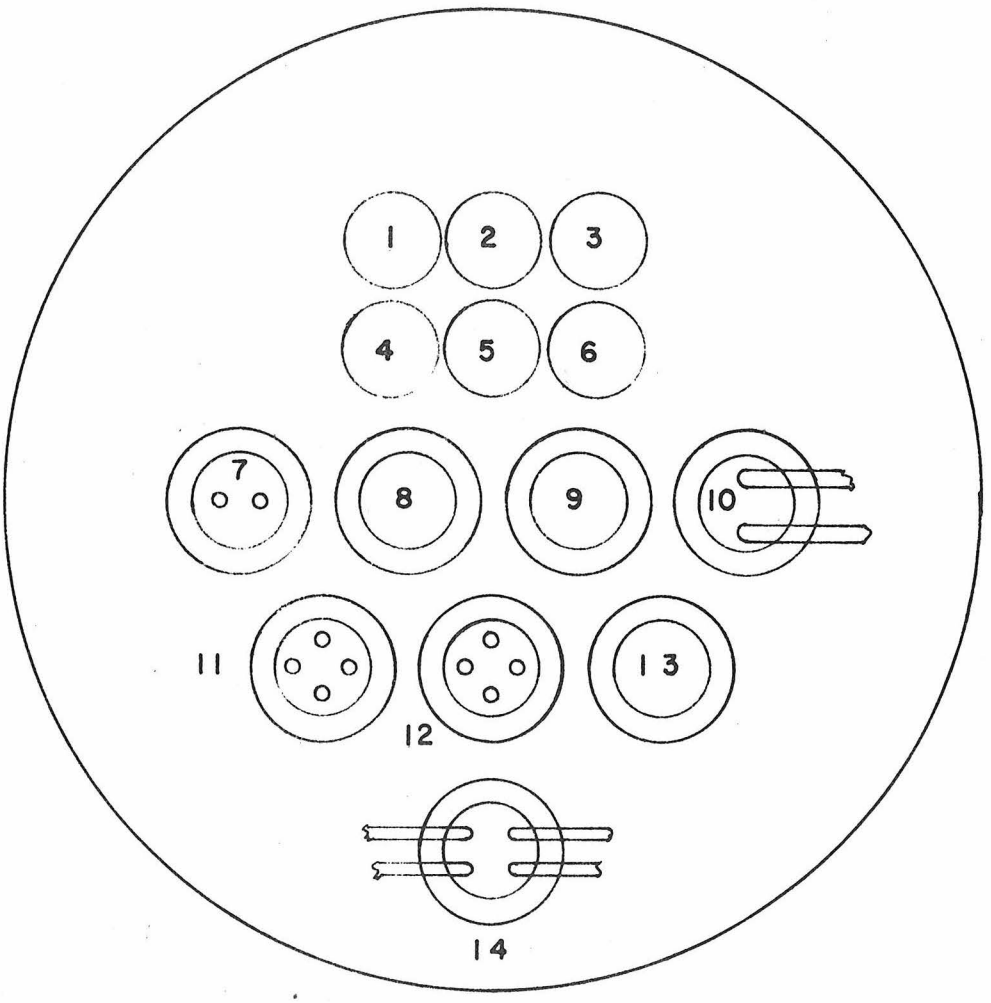

FIGURE 14 FLANGE FRONT VIEW

Table 4.14-1: Flange Feedthrough Listing

Feedthrough number	Use	Manufacturer
1, 2, 4, 5	Not used	Homemade RCA 11 pin electrical conductor
6	Ion gauge GE Model 22GT103	Homemade with gold O-ring seal
3	4 thermocouple leads 7 leads to Schulz-Phelps pressure gauge	Homemade 11 pin electrical conductor
7	High voltage to anode and rear of multiplier	Ceramaseal
8, 9	Lens voltages and 2 thermocouple leads	Varian Model 954-5013 20 pin electrical conductor
10	Liquid nitrogen feedthrough	Homemade. Two 1/4" stainless steel tubes welded into a Conflat blank
11	4 bakeout heater leads (20 amps per lead)	Ceramaseal
12	2 bakeout heater leads Faraday cup lead Outer sphere selector lead	Varian
13	Rotating motion feed-through	Cooke Vacuum Products Model D-909
14	2 heating gas tubes Sample gas tube Faraday cup actuator line	Four 1/4" stainless steel tubes welded into a Conflat blank

useful in protecting the whole system from a very reactive gas which is condensible at 77°K.

4.15. Spectrometer Shielding

The spectrometer is protected from RF interference by being located in a shielded room designed by Topatron Incorporated (Model 7322). This provides an attention of 10^5 of signal frequencies from 10^4 Hz to 10^{11} Hz. The room was normally operated with the door open during these studies and closing it produced no apparent changes. The room itself is probably not required for operation of the instrument at resolution values (defined as the full width at half maximum of the elastic peak) greater than 0.05 volts. Shielding may in fact be necessary to obtain higher resolution beams.

The earth's magnetic field is reduced to $\approx$ 1-3 milligauss in the area of the electron beam path by a μ-metal shield which fits inside the vacuum chamber. The shield was built by Williams Manufacturing Co.

4.16. Vacuum System

The vacuum system, the chamber specifications, the chamber pumping systems, the inlet system and its pumps have not been modified during the present research. These components have been previously described in detail by Rice.[4a]

4.17. Electrical Components

4.17.1 Impact Side Electronics

The impact side electrical system is shown in Figures 15 and 16. In Figure 15 the overall power supply configuration is shown. The impact energy power supply (Kepco Model HB2AM) is set to V_{imp} the voltage equal to the nominal desired impact energy. This voltage is applied to the filament through the 220Ω symmetrical biasing resistors. These resistors are employed to force the filament tip to be at the voltage set by the impact energy supply. If the impact energy supply negative side were simply attached to the negative side of the filament current supply, the voltage on the filament tip would be about 2 volts higher because $\approx$ 4 volts is put out by the filament current supply under the normal operating conditions.

The electrons which have just left the surface of the filament have a potential energy of qV_{imp} or $|V_{imp}|$ eV and a kinetic energy distribution which peaks around 0.5 eV.[4b] The most probable total energy, E_{tot}, is $[|V_{imp}| + 0.5]$ eV. When the electrons are in the scattering chamber V = 0 and thus T, their kinetic energy, is E_{tot}. One minor correction which must be included is any contact potential difference between the filament and the scattering chamber, which is designated V_{cp}. This term can be either positive or negative. The

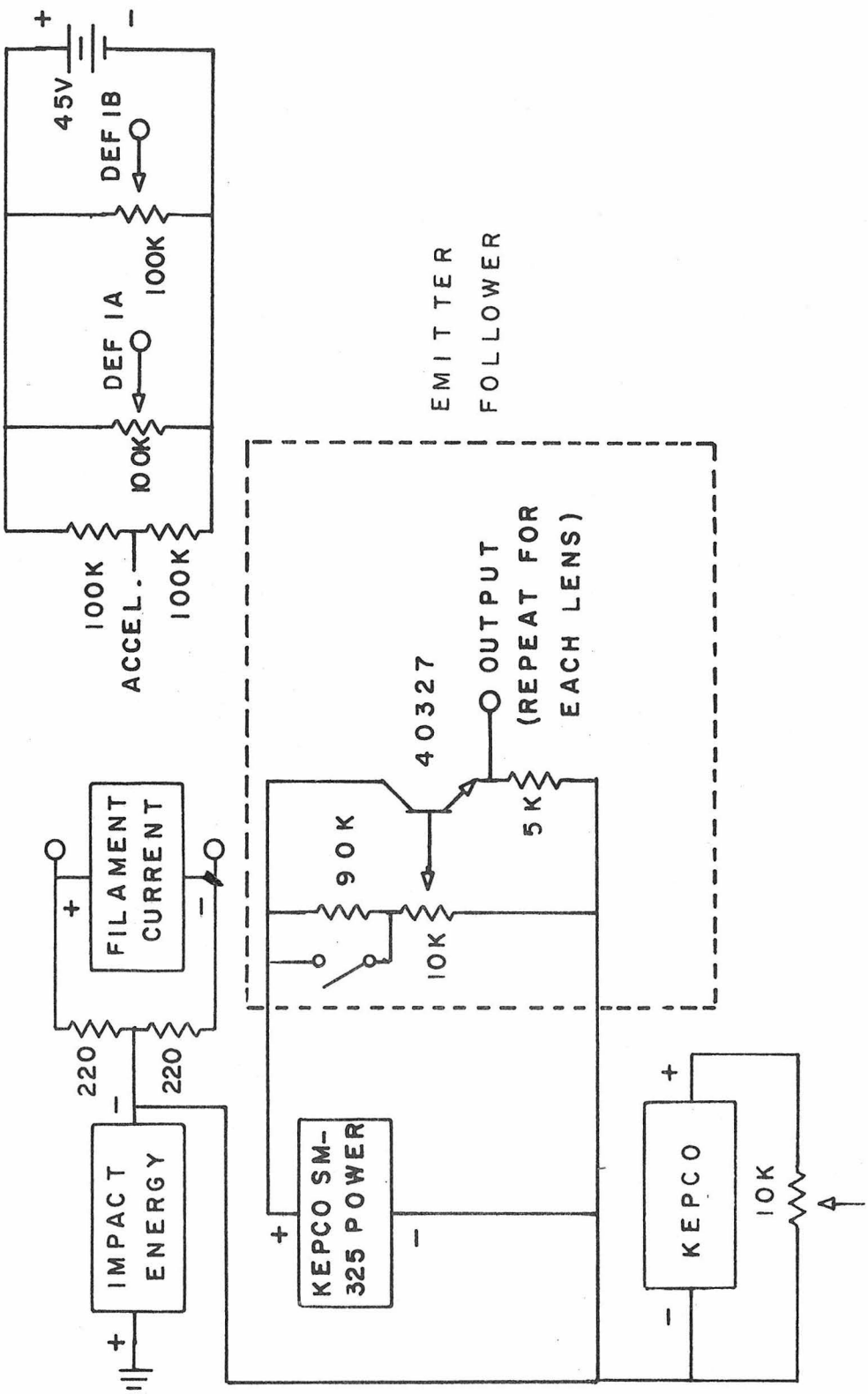

FIGURE 15 IMPACT SIDE ELECTRONICS I

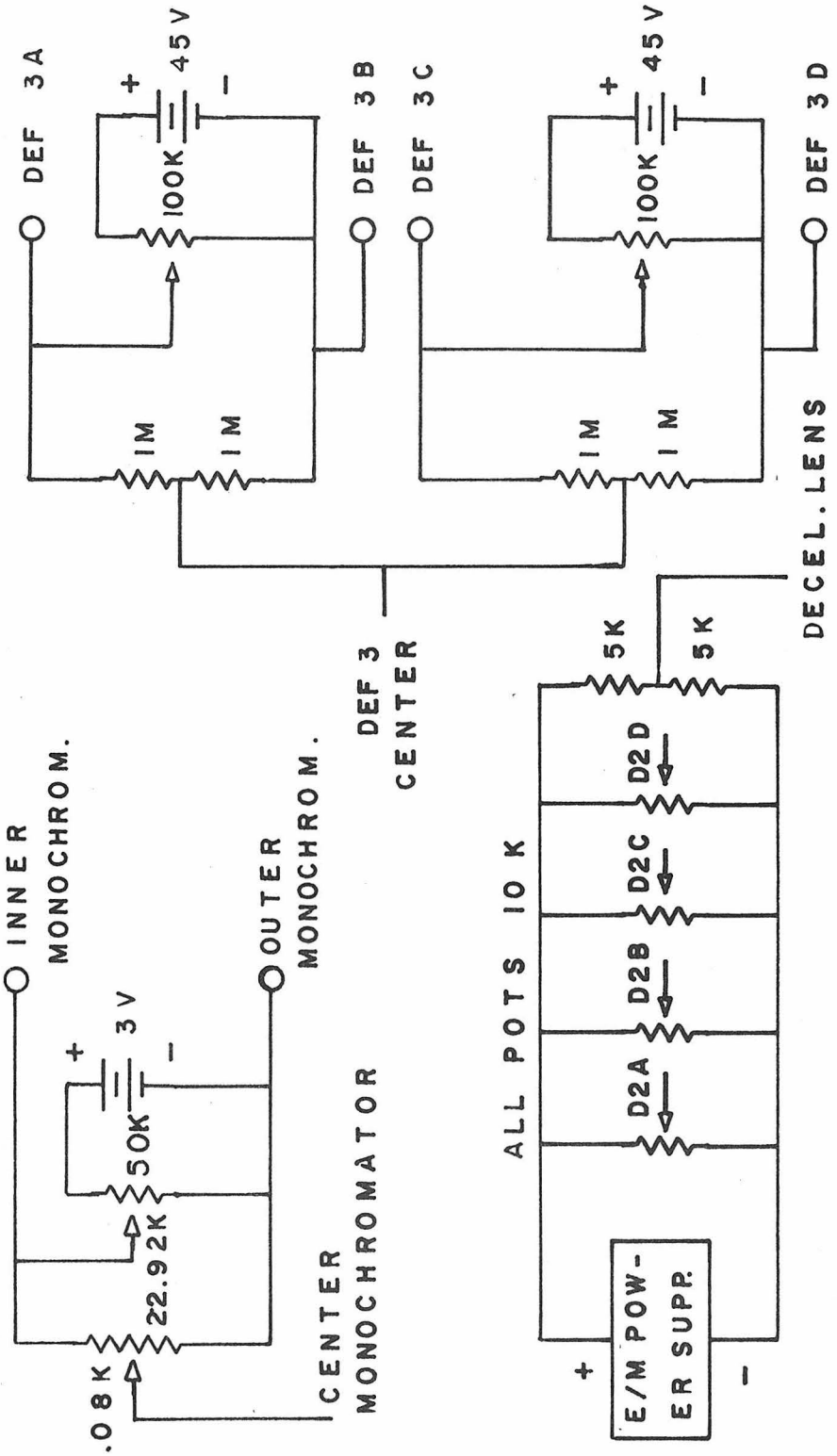

FIGURE 16 IMPACT SIDE ELECTRONICS II

actual impact energy in the scattering chamber is then $T_{sc} = [|V_{imp}| + 0.5 + V_{cp}]$ eV. Previous measurements [5] on both the 19.3 eV and 57 eV resonances in helium have shown that the real impact energy is usually within 1 eV of $|V_{imp}|$ and is often closer than 0.3 eV. Thus the value of $|V_{imp}|$ eV sets the actual impact energy to within 1 eV.

When the electrons are in any lens whose potential relative to the filament is V_ℓ volts then their potential energy is $qV = q[-V_{imp} + V_\ell]$ and thus $T_{lens} = [V_{lens} + V'_{cp} + 0.5]$ eV. The nominal kinetic energy is given by (V_{lens}) eV when V_{lens} is measured with respect to the filament and when V_{lens} is much larger than the contact potential or kinetic energy distribution terms.

The filament current supply (Kepco Model KS36-5) supplies the power to the filament. Typical current levels used to achieve the desired emission were 1.6 to 2.2 amps. The important parameter, however, is the power (voltage × amps) delivered to the filament. Because of the 22 gauge wire used in connecting the filament inside the machine to the power supply there is a significant voltage drop between the power supply and the filament itself. An experiment was performed to measure the true filament voltage by attaching separate non-current carrying leads directly to the filament housing. The filament was set up in a glass bell jar. Table 4.17.1-1 summarizes

Table 4.17.1-1

Emission Characteristics of 0.005" W Filament

I_{fil}	V_{fil}	Power (watts)	Filament temp	I_{grid} (10 volts accel)
1.4	2.22	3.108	875°C	$< 10^{-6}$
1.6	2.69	4.304	1240	
1.8	3.11	5.598	1555	
1.9	3.34	6.346	1660	
2.0	3.45	6.90	1780	
2.1	3.68	7.728	1960	1.05×10^{-3} amps
2.2	3.86	8.492	2050	5.2×10^{-3}
2.2	4.2	9.24	2180	15.2×10^{-3}

the relationship between actual filament power, filament temperature (as measured by an optical pyrometer) and the emission to a grid lens in front of the filament.

The lens voltages are taken from the amplifier shown in the box in Figure 15. This circuit is repeated for each lens voltage on the impact side. The power is supplied by the Kepco Model SM325 power supply. The total voltage is usually set to 100 volts. As mentioned above, this permits lenses to be set from 0 to 100 volts relative to V_{fil} and thus to select nominal electron kinetic energies in the range from 0 eV to 100 eV.

The emitter follower amplifier works in the following way. With the switch in parallel to the 90K resistor closed, 100 volts appears across the 10K 10-turn potentiometer. The voltage on the pot wiper is applied to the base of the 40327 transistor. The voltage at the emitter then is $V_{base} - V_{be}$ where V_{be} is the base-emitter drop in the transistor. This is typically about 0.7 volts so $V_{output} = V_{base} - 0.7$ volts. The purpose of the transistor is to reduce the high frequency impedance of the output back to ground and thus minimize A.C. pickup on the lens leads. The circuit gave D.C. voltages stable to ±0.01 volts over time scales of several hours with about 0.01 volt peak to peak 60 Hz ripple. Higher frequency noise was smaller than the 60 Hz component. Each output was fused (with a 1/32 or 1/100

amp fuse) to protect the amplifiers in case of short circuits between the lens and ground. When the shorting switch on the 90K resistor is open the range of voltages on the potentiometer is 0 to 10 volts. This permits more precise adjustment of voltages on lenses which are usually operated at <10 volts relative to V_{fil}.

Figure 15 also shows the circuit used to supply voltages to Deflectors 1A and 1B. These deflectors are located in the Accelerator lens. The 100K symmetrical bias resistors make the deflector voltages swing symmetrically above and below the accelerator lens voltage. The power for the 100K 10-turn potentiometers is supplied by two 22.5 volt batteries in series. With 45 volts available, the deflectors can both be set anywhere in the range $V_{accel} \pm 22.5$ volts using the potentiometers. A separate Kepco power supply (Model HB2M) is also included to provide the 250 volts necessary for the High Voltage lens.

Figure 16 shows the remaining impact side circuitry. The 2A to 2D deflectors, located in the Decelerator lens, are biased symmetrically about the Decelerator voltage. The E/M power supply (Model TR212A) was set to about 30 volts. Thus the 10 turn 10K pots could be used to adjust the deflector voltages in the range $V_{decel} \pm 15$ volts. The 3A to 3D deflectors have their center voltage adjusted by the DEF 3 center voltage and the voltage applied to each plate itself is

then adjusted by use of the 100K, 10 turn potentiometers. The center voltage for the monochromator is obtained from the center monochromator emitter follower amplifier. The biasing ratio between the inner and outer monochromator hemispheres is obtained by adjusting a 50K 10 turn pot. The desired ratio as shown in Figure 16 is 13/11. This is the value from the theoretical analysis [4c] of the spheres and is in fact the outer sphere radius divided by the inner sphere radius. The voltage across the sphere is taken from the wiper of a 50K 10 turn pot which is powered by a 3 volt battery.

4.17.2 Second Half Electronics

Figure 17 shows the second half circuit configuration. It is similar to the first half configuration. The Princeton Applied Research (Model TC-100 2R) power supply is set to a value near V_{imp}. The Kepco HB 2AM power supply is then set to 100 volts. Emitter follower amplifiers are again used to adjust the lens voltages in the range from 0 to 100 volts relative to V_{fil} (= - V_{imp}). The PAR is normally connected to ground but can also be connected to the sweep voltage source (see Section 4.17.3) to scan the energy-loss spectrum.

The circuit for the inner and outer selector voltages is identical to that used on the monochromator. The center voltage comes from the center selector amplifier output.

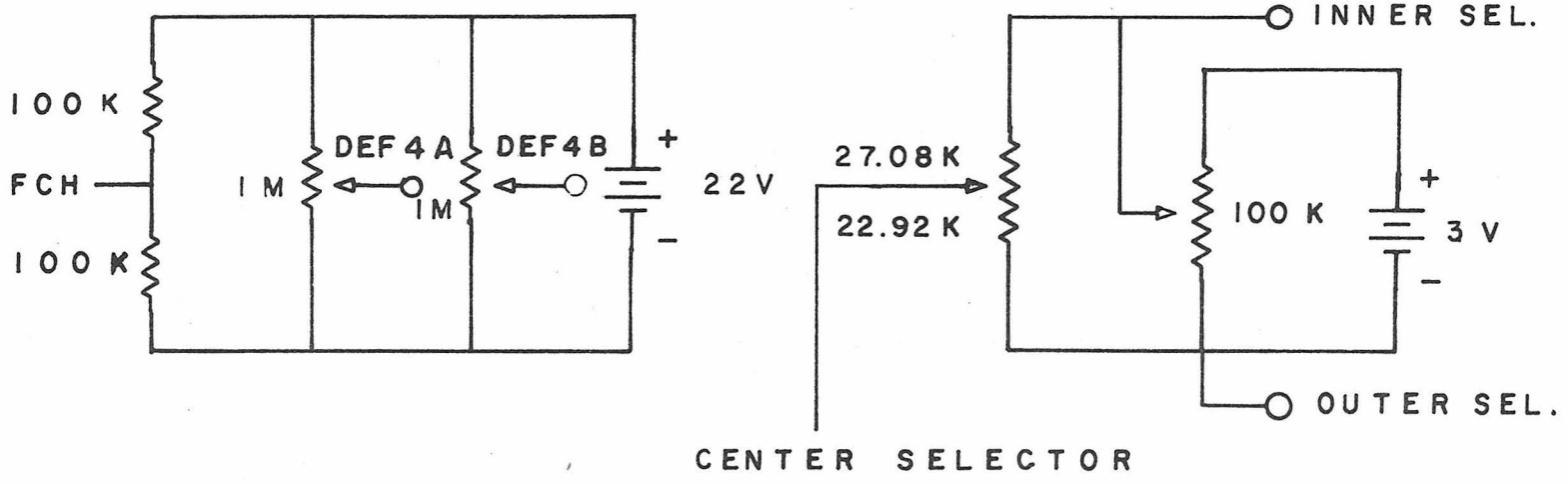

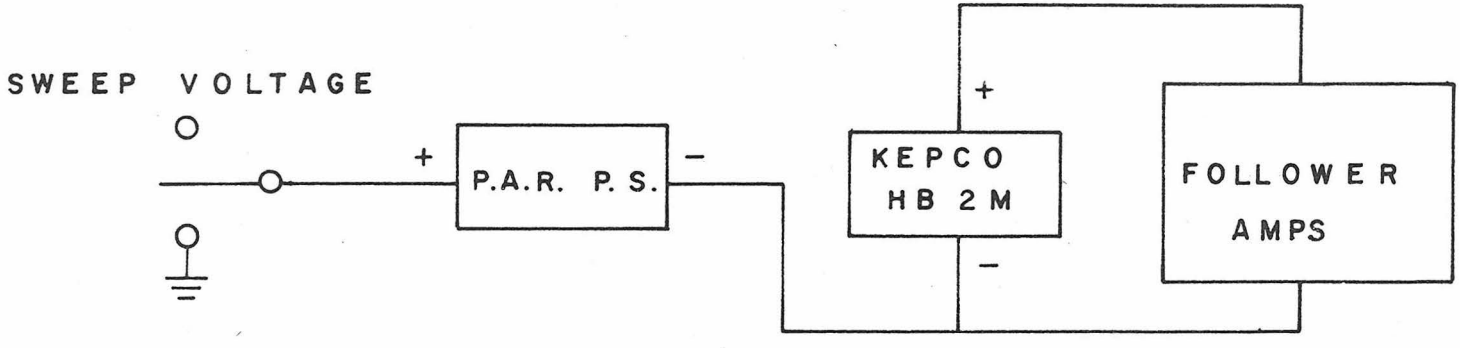

FIGURE 17 POST SCATTERING ELECTRONICS

Deflectors 4A and 4B, located in the Faraday Cup Housing lens, are biased symmetrically about the FCH voltage by the 100K resistors. Two 10 turn 1 Megohm potentiometers are used to adjust the deflector plate voltages in the range $V_{FCH} \pm 11$ volts.

4.17.3 Sweep Voltage Circuit

The circuits which provide the sweep voltage to the second half are shown in Figure 18. An energy loss spectrum is taken using a Nuclear Data Model 181-F multichannel scaler. The binary coded memory register in the M unit (bits C0 ... C9) is decoded by a Raytheon Model DAC20-10 digital to analog converter. The output voltage ranges from 0 to 10 volts and is proportional to the memory register contents.

In many molecules, there are no electronic excited states below 2 to 4 volts energy loss. It is very inefficient to scan a 10 volt energy-loss range and include a 2 to 4 volt region where no scattered electrons are expected. This problem has been overcome by including the jump voltage circuit. The desired jump voltage V_{jump} is set on the jump voltage power supply (Kepco Model HB2AM). When no current flows through the Potter and Brumfield Type ML17D relay coil the switches are connected to the upper contacts and the sweep voltage is equal to the Raytheon output. When the coil is energized

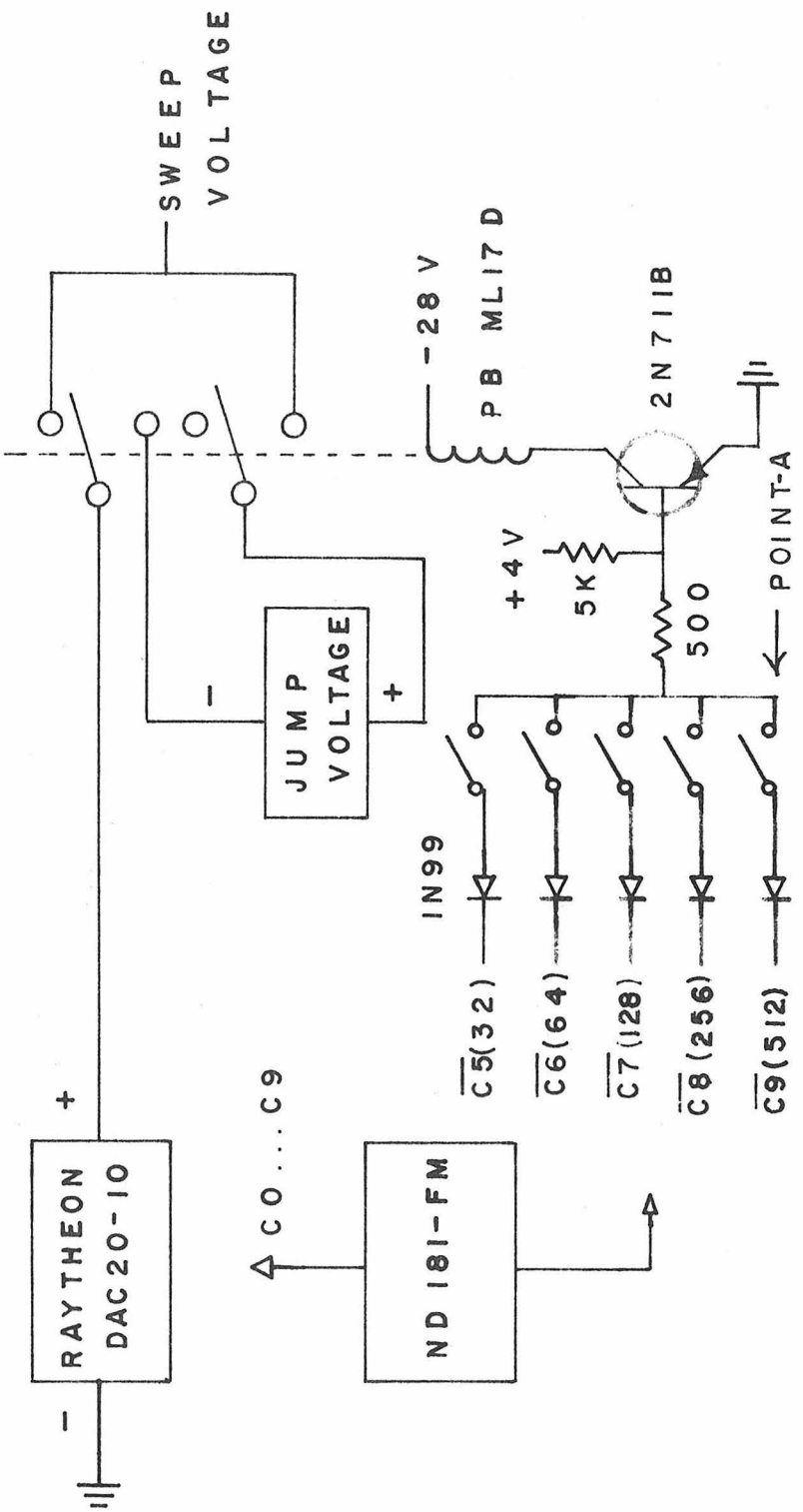

FIGURE 18 SWEEP / JUMP GENERATOR

the switches move to the lower contacts. The relay is wired so that the sweep voltage is now the Raytheon output plus V_{jump}. This permits the skipping of energy loss regions without any transitions.

The memory channel at which the jump is desired is set by the five switches shown in Figure 18. These are connected to the $\overline{C5}$ (channel 32) through $\overline{C9}$ (channel 512) output voltages from the M unit. When the memory register contents are below channel 32, $\overline{C5}$ is +4 volts. When channel 32 is reached $\overline{C5}$ is -4 volts. When any higher memory channel is reached $\overline{C5}$ will be -4 volts whenever the binary form of the number requires the 2^5 bit to be on. Similar voltages come from the other bits.

If the first 31 channels are used to store the number of elastically scattered electrons and a voltage jump is desired at channel 32, the $\overline{C5}$ switch as well as all remaining switches are closed. For the first 31 channels $\overline{C5}$ to $\overline{C9}$ are +4 volts. All the 1N99 diodes are nonconducting and the base of the 2N711B transistor is at +4 volts. This turns the transistor off (no current flows) and the relay is not energized. When channel 32 is reached $\overline{C5}$ goes to -4 volts. The diode conducts and the voltage at point A becomes -3.3 volts. The base voltage of the transistor is set by the voltage divider to be about -2.6 volts and the transistor begins to carry current. This energizes the relay and the

jump voltage is placed in series with the DAC output as discussed above. The subsequent switches are closed to keep the jump voltage in the circuit for the remainder of the memory channels (to 1023). If only $\overline{C5}$ were connected the circuit would turn on and off every 32 channels. If a jump is desired after 3 channels, switches $\overline{C6}$ to $\overline{C9}$ are closed but $\overline{C5}$ remains open.

4.18. Pulse Amplifier

The pulse amplifier which was used to convert the ≈ 0.01 volt output pulses of the multiplier into uniform width and height signals required by the multichannel scaler input circuits is shown in Figure 19. This circuit was developed in close collaboration with Doug Mason as mentioned in the acknowledgments.

The circuit is divided into three parts using a preamplifier with a gain of about 30 db, a differential comparator, and finally a monostable multivibrator to generate uniform width output pulses.

The preamplifier is a Motorola MC1550 video amplifier. The input is coupled to one side of the differential inputs by a 0.22 microfarad capacitor. The 5 millihenry coil across the amplifier inputs acts as a short for D.C. and low frequency (specifically 60 Hz pickup) signals while presenting a significant impedance to the pulses themselves which are in the 1 to 10 megahertz frequency range. The 1K

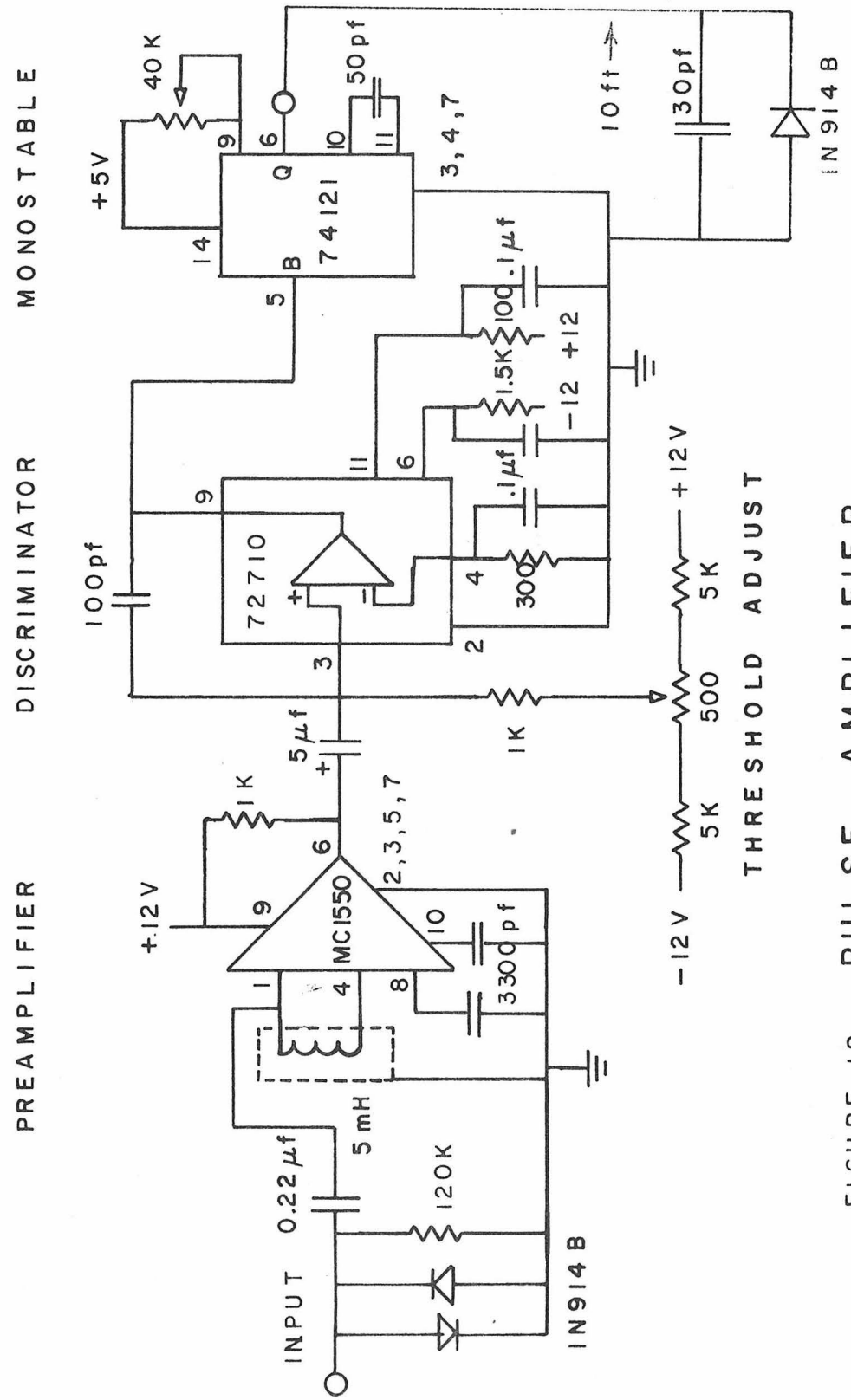

FIGURE 19 PULSE AMPLIFIER

resistor provides the feedback loop of the amplifier. The dotted lines around the 5 millihenry coil are simply a coil of 24 gauge insulated hookup wire wrapped around it. The ends of the shield wire are soldered to the board ground. This shield coil helps keep the MC1550 from picking up the output signals of the monostable and causing the circuit to oscillate. The 120K resistor establishes a D.C. ground voltage on the input. The 1N914B diodes are very high speed diodes (turning on in <10 nanoseconds) which should short excessively high voltage spikes to ground (from an arc in the machine) and thus protect the subsequent integrated circuits.

The discriminator is a Texas Instruments 72710 differential comparator. This device gives an output voltage of about 3 volts whenever the positive input is about 0.015 volts higher than the negative input. Otherwise the output is ≈ -0.3 volts. In the present configuration the negative input is tied to ground through a 300 ohm resistor. The output of the 1550 is coupled to the positive input by the 5 μf capacitor. A D.C. voltage is kept on the positive input by the threshold adjustment potentiometer. The pulses out of the MC1550 are positive going so the threshold pot is normally adjusted so that the D.C. voltage is about -0.05 volts. Any pulse out of the 1550 which is bigger than about 0.065 volts will cause the differential comparator output to go to +3 volts. A pulse out of the 1550 of 0.065 v corresponds

to a negative going input pulse from the Spiraltron of about 0.002 volts. The 100 picofarad capacitor helps speed up the transition time of the 72710 and prevent high frequency oscillations in the output during the turn on period.

The output stage is a Texas Instruments 74121 monostable multivibrator. The 40K pot is used to adjust the 3V output pulse to a desired width in the range from 100 nanoseconds to 500 nanoseconds. The monostable is triggered by the rising edge of the output from the differential comparator. The monostable can easily drive 10 ft of dual conductor cable as long as the cable is not shielded. To prevent ringing, the signal and ground wires are terminated into 30 pf of capacitance and a high speed diode to short out negative going ringing of the signal at the point where the cable is connected to the multichannel scaler or a counter.

The power supplies necessary for the pulse amplifier circuits were also integrated circuit types as shown in Figure 20. The Silicon General SG3501 takes the ±20 V.D.C. putput of a slightly filtered (0.5 volts RMS ripple at 60 Hz) power supply and converts it to ±12.00 V.D.C. with less than 0.01 volts ripple. A National Semiconductor LM309 was used to convert the +12 VDC to +5 VDC for the 74121.

A single-sided printed circuit board was designed to hold both the pulse amplifier and its power supplies. The overall dimensions of

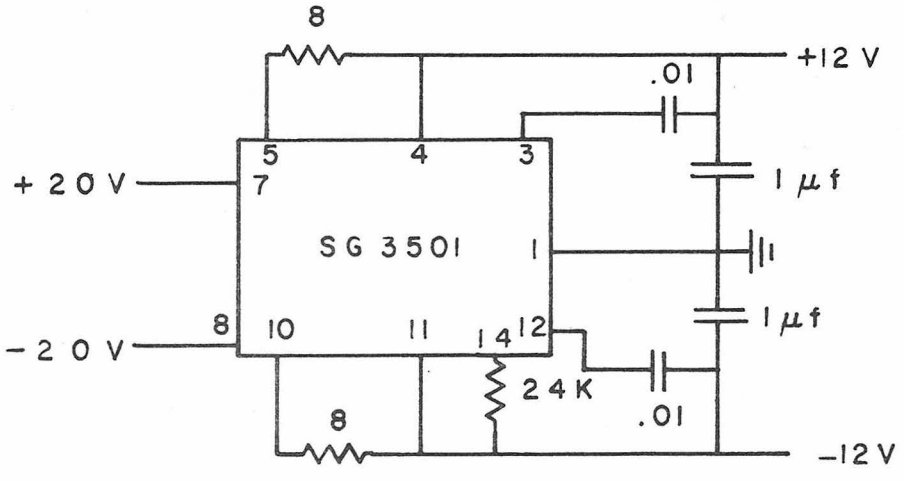

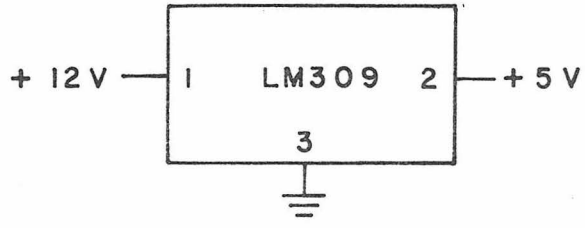

FIGURE 20 PULSE AMPLIFIER POWER SUPPLIES

the board were 4.5" × 8.375" and it was mounted in a chassis box. The board layout is shown in Figure 21.

4.19. Data Handling Devices

Figure 22 shows the data flow system used in these studies. The Nuclear Data MCS controls the voltages on the lenses and thus the energy loss of the electrons. The electrons striking the multiplier produce the small pulses which are transmitted to the pulse amplifier. The pulse amplifier converts these to standard 3 volt pulses which the ND accepts. The ND counts and then stores the number of pulses in each channel. After an adequate signal-to-noise ratio is achieved (3 to 8 hours of scanning at angles above 20°) the data is plotted on an X-Y plotter (Hewlett Packard Model 7005B) and then punched out on paper tape using a high speed punch (Teletype Model BRPE). The high speed punch interface controls the MCS during the punching operation. The interface also accepts and punches input from a teletype keyboard (Teletype Model ASR33) to permit each punched spectrum to be identified.

The oscilloscope is used for quick viewing of the spectrum to decide if it has achieved the desired signal to noise ratio. The counter (Hewlett Packard Model 5216A) is used to tune up the machine before actual scanning begins.

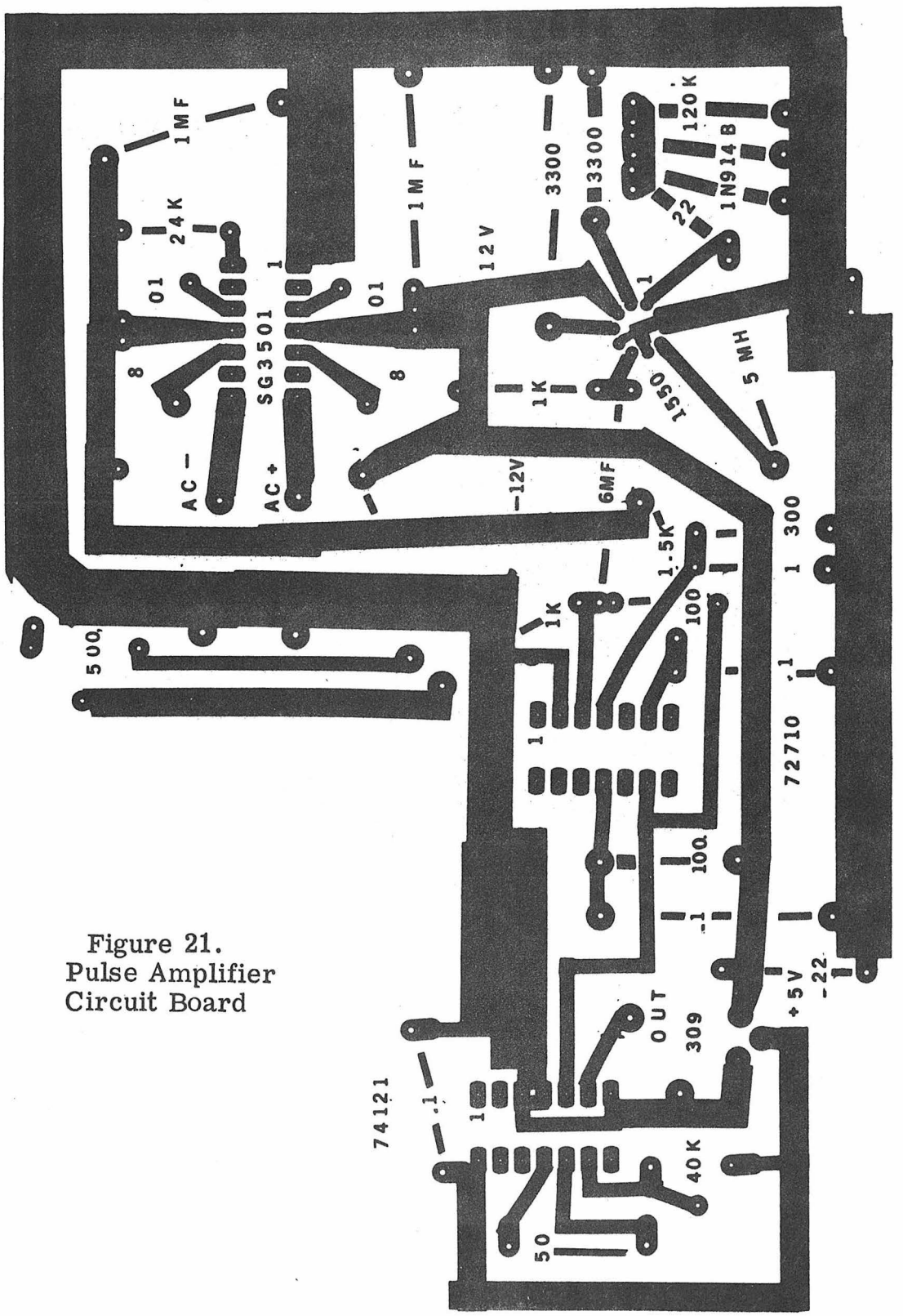

Figure 21.
Pulse Amplifier
Circuit Board

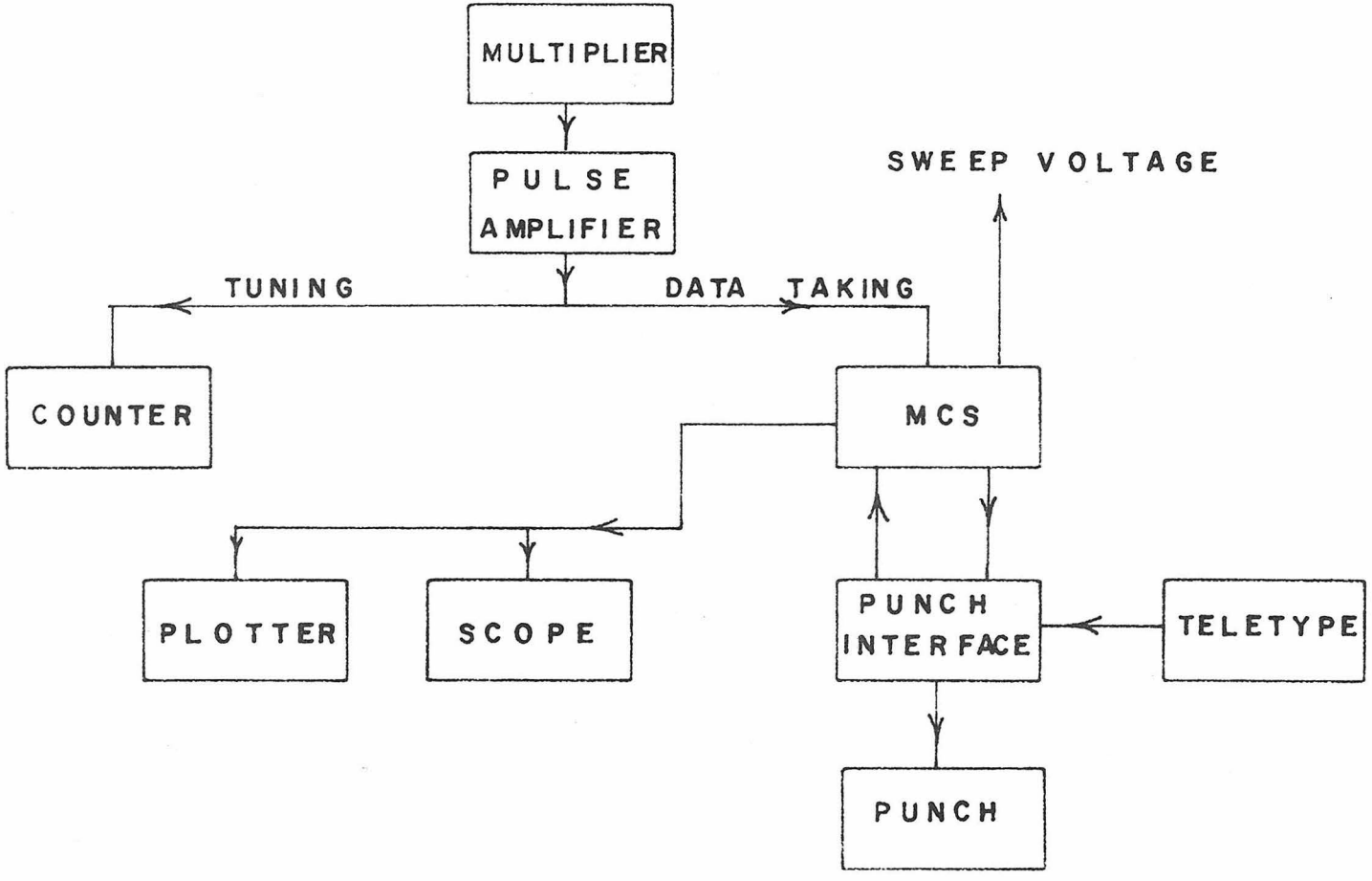

FIGURE 22 DATA HANDLING DEVICES

The paper tape which contains complete identifying information on the spectrum as well as the raw spectrum itself is then read into the SCC 4700computer system, the coding format is changed, non-numerics are removed from the data field, and the entire spectrum and heading is then written on magnetic tape. It is now ready for analysis on the IBM 370-158 computer at the Caltech Computing Center.

4.20. System Protection Interlock

An interlock was installed to protect the main diffusion pump, the filament, the electron multiplier, and the bakeout heaters whenever one of the following hazardous conditions occurs.

1. The system pressure rises above 1×10^{-4} torr.
2. The foreline pressure rises above 0.5 torr.
3. Water stops flowing through the diffusion pump cooling coils.
4. The mechanical pump is turned off.

If any of the above occurs the diffusion pump, filament power supply, high voltage power supply, and the bakeout heaters are turned off. The gate valve is also shut.

The sensors for each failure are described below.

1. The system pressure is continuously monitored by a G. E. Model 22GT103 ion gauge mounted on the pumping system above the diffusion pump. The ion gauge controller is a G. E. Model 22GC100

which has a switched A.C. outlet. The outlet is hot when the ion gauge is running but is turned off whenever an overpressure occurs and the ion gauge is shut off.

2. The foreline has a pressure sensor (Edwards Model VSK. 1.B.) which is a closed switch whenever the pressure is <0.5 torr but opens when the pressure is higher.

3. Water flow through the diffusion pump coils is monitored by a McDonnel No. FS1 flow switch. This is a single-pole double-throw switch which changes from one contact to the other when water flow ceases.

4. An additional pair of contacts on the mechanical pump power switch provides a normally closed switch which opens whenever the mechanical pump is turned off.

The A.C. putput of the ion gauge controller and the other sensors are hooked to a relay which supplies power to the spectrometer components in such a way that this relay is turned off in the event of any failure mentioned above.

References

1. J. A. Simpson and C. E. Kuyatt, Rev. Sci. Inst., 34, 265 (1963).

2. C. E. Kuyatt and J. A. Simpson, Rev. Sci. Inst., 38, 103 (1967).

3. K. Spangenberg and L. M. Field, Elec. Comm., 21, 194 (1943).

4. J. K. Rice, Ph.D. Thesis, California Institute of Technology, 1969; (a) pp. 120-127; (b) p. 208; (c) p. 82.

5. Sandor Trajmar, private communication.

5. Operating Procedures

5.1. System Pumpdown

The assembly and pumpdown of the spectrometer is performed in the following way. The lenses are mounted on the framework and all leads are connected. The lenses are then checked for shorts to each other or to the instrument framework. A check is also made to see that the electron multiplier leads, the thermocouples, the bakeout heaters and the Faraday Cup lead are all properly attached. The spectrometer is now ready to be closed. Just before closing a Freon Aerosol Duster was used (Miller-Stephenson Chemical Co. Type MS220) to "clean" all lens elements. This spray was developed for use in aerospace clean room applications and seems to permit a more rapid pumpdown of the instrument.

The frame and the flange on which it is mounted are pushed into the main vacuum chamber and secured with four bolts. The vacuum seal is made with a rubber (Buna-N) O-ring.

5.1.1. Pumpdown When System is Completely Shut Off

Start the main mechanical pump (MP) and pump down the diffusion pump (DP),the foreline,and the instrument itself through the DP bypass line. After 2 minutes turn on the compressor for the Freon baffle above the MP. After 10 to 15 minutes the foreline pressure should be less than 0.03 torr. Turn on the DP cooling water

and then start the DP. Also, start the compressor for the Freon baffle above the DP at this time. After 20 to 30 minutes DP warm-up time the liquid nitrogen (LN_2) cold trap above the DP can be filled with liquid nitrogen. Three to five minutes after the LN_2 is added the pressure above the DP should be less than 1×10^{-6} torr as read by a G.E. ion gauge. If the spectrometer main chamber pressure is below 0.03 torr, the bypass line to the mechanical pump is valved off, the ion gauge is turned off, and the gate valve leading to the diffusion pump is opened. The system is now being pumped by the diffusion pump. Within an hour the main chamber pressure should be 1 to 3×10^{-6} torr. If it is allowed to pump with no sample gas admission the ultimate pressure attained will be less than 1×10^{-7} torr.

5.1.2. Pumpdown When System Pumps are Running

If the mechanical pump and diffusion pump are already running, pumpdown is much simpler. The isolation valve on the outlet side of the DP is closed and then the system is roughed out through the DP bypass line. When the system pressure is less than 0.04 torr, the bypass valve is closed, the isolation valve is opened, the ion gauge is temporarily turned off, and the gate valve is opened. After one to two minutes, the ion gauge is restarted.

5.1.3. Spiraltron Startup and Lens Short Check

After the chamber pressure is below 5×10^{-6} torr the high voltage should be applied to the Spiraltron. This gives it several hours for its surfaces and its mounting plate to equilibrate and adjust to vacuum conditions.

The cables are also attached which carry the lens voltages, and a second check is made to see if any lens shorts have occurred. This check is made using a digital voltmeter to look at the voltage applied to each lens. Any shorts to the instrument frame will cause the lens voltage to be 0.0 volts with respect to ground. If only a momentary short occurred on insertion of the instrument, the lens voltage will now appear to be "floating" if the short duration was long enough to burn out the fuse. Shorts to other lenses are shown by the fact that the voltage adjustment potentiometer for a given lens does not affect the voltage applied to that lens. Finding the potentiometer which does cause a voltage change will show which lenses are shorted together.

The scattering angle, which was set near 0° to permit insertion of the instrument into the vacuum chamber, should now be changed to 30°. This will protect the Spiraltron from the unscattered primary beam when the filament is started.

5.2. Filament Startup

When the system pressure is below 1×10^{-6} torr the filament is started by slowly raising the heating current applied to it. The following scheme is used to control the rate at which its current is increased. An electrometer (Keithley 600A) is connected to the accelerator lens which is located directly in front of the cathode (see Section 4.2). The emission current from the filament can then be observed on the electrometer. The heating current is increased until an emission current of 1×10^{-9} amps is obtained. The heating current is kept constant for the next 15 to 20 minutes. During this period the emission current may increase by a factor of 2 to 3. After 20 minutes the heating current is increased until the emission current of 1×10^{-8} amp is obtained. The procedure is repeated every 20 minutes until the emission current reaches 1×10^{-5} amps. About 20 minutes later an additional increase in the heating current is made to bring the emission to 4×10^{-5} amps. The method seems to be a sensitive way to monitor the actual performance of the filament. Other methods, such as periodic equal increases in the heating current, can lead to too rapid a rise in filament temperature and cause it to burn out.

5.3. Sample Handling Procedures

All samples used in the present studies were purchased from

commercial sources with the exception of azomethane. Additional details on sources and purities are given in Section 6.

5.3.1. Room Temperature Liquid Samples

Since most of these samples were supplied in glass ampules they had to be transferred to sample bulbs or tubes. The samples were kept in glass tubes of 2.0 cm O.D. and about 10 cm length as shown in Figure 23. One tube end was closed and a 4 mm vacuum stopcock was attached to the other end. A Ŧ 14/35 male tapered joint was put on the other side of the stopcock to connect the sample tube a glass vacuum line. The following series of steps described the preparation of a liquid sample.

1. The mechanical pump is started to rough out the glass sample preparation line.

2. After 5 minutes the diffusion pump cooling water is turned on and the diffusion pump (DP) is started. The liquid nitrogen trap is filled to prevent back streaming of mercury from the DP.

3. After 1 to 3 hours the line pressure is about 1×10^{-5} torr. The sample tube is attached to the line, its vacuum stopcock cup is pumped down first and then the tube itself is pumped down.

4. A sample transfer tube, which is a test tube with a Ŧ 14/35 male tapered joint on one end is held using a test tube clamp on a

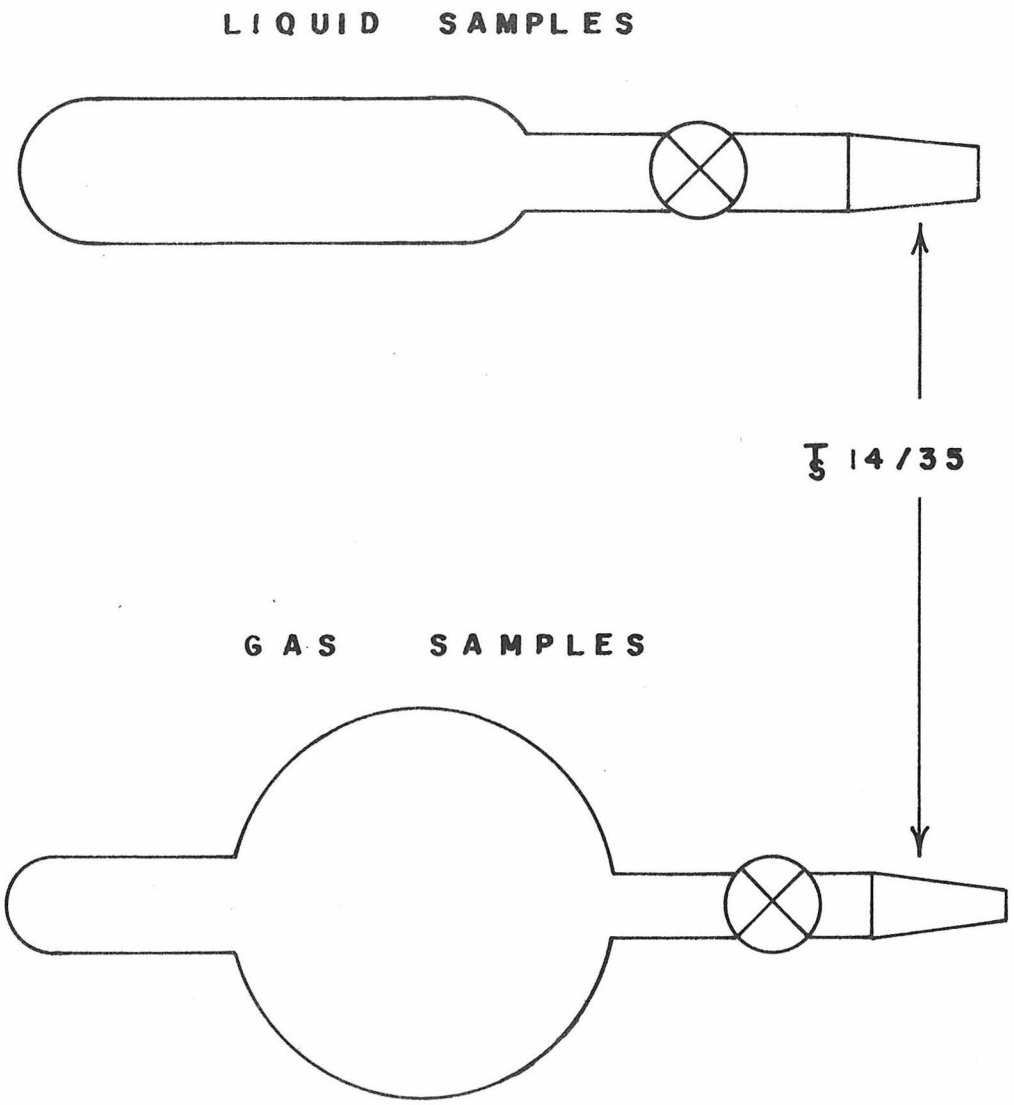

FIGURE 23 SAMPLE HOLDERS

ringstand in the fume hood.

5. The glass ampule is scratched with a glass file and broken open. It is important to have a rag or paper towel around the ampule as it sometimes shatters while it is being opened.

6. Three to 5 ml of the sample are pipetted into the transfer tube. The air above the sample in the tube is then purged of O_2 and H_2O with a stream of N_2 gas. A rubber plug is then used to cap the transfer tube. The remaining sample is put into a 100 ml brown storage bottle. The air above the sample in the storage bottle is flushed with N_2, the bottle is capped and then placed in a refrigerator. The combination of low temperature ($\approx 5\,^{\circ}C$) and the absence of light helps to prevent chemical decomposition of the sample.

7. If the vapor of the compound is very toxic (such as is the case for thiophosgene) the sample is frozen in the transfer tube using liquid nitrogen before moving the transfer tube into the lab and attaching it to the glass vacuum line. Less toxic compounds are carried unfrozen to the vacuum line.

8. After attaching the transfer tube to the glass line the sample is frozen using liquid nitrogen. The N_2 (with some air) which was in the transfer tube above the sample is pumped away.

9. When the pressure in the glass line is less than 1 or 2×10^{-3} torr, the DP is valved off and the liquid nitrogen dewar is

moved from the transfer tube to the sample tube. The sample warms up in the transfer tube and distills over into the sample tube.

10. After transfer is complete, the sample tube stopcock is closed and the sample is allowed to warm up. The glass line is opened to the DP and pumped on again. The sample is then frozen, the sample tube stopcock is opened, and remaining non condensible gases are pumped away. The liquid N_2 freeze-pump-thaw cycle is valuable for removing entrapped air from the sample. It is repeated until the remaining gas in the vacuum line condensed rapidly and completely (as indicated by a Wallace and Tiernan pressure gauge) when liquid nitrogen is placed around the sample tube.

11. The sample tube stopcock is now closed and the sample tube is removed from the line and stored in the refrigerator. The sample is now ready to be attached to the spectrometer inlet system and admitted to the scattering chamber. One problem with the present sample handling system is the fact that many of the organic molecules studied were good solvents for the stopcock grease. The samples could not safely be prepared more than a few days in advance because air started leaking into the sample through the areas in the stopcock where the grease was dissolved. All compounds containing a carbon-carbon double bond seemed to be good solvents for most of the stopcock greases. Apiezon L, M, N, and T were tried along with

Dow silicon HyVac and all dissolved to some extent. The spectra were checked for the presence of nitrogen impurity peaks during the experiments. The remaining portion of each sample was also checked for non-condensible gases using the sample preparation line following its use in the instrument.

5.3.2. Room Temperature Gaseous Samples

Samples which had a vapor pressure exceeding 760 torr at room temperatures were kept in 300 ml sample bulbs with a 4 mm vacuum stopcock and a ℱ 14/35 male tapered joint on the bulb. A sample bulb is shown in Figure 23. These sample gases were supplied in lecture bottles. These bottles were attached to the gas vacuum line using a stainless steel transfer line. The transfer tubing is pumped out and then the diffusion pump is valved off. The sample gas is admitted to the glass line through a manual metering valve. The pressure is observed on the Wallace and Tiernan gauge to prevent over pressurization. Enough sample gas is admitted so that the final bulb pressure is between 250 torr and 400 torr. The metering valve is then closed and the sample gas is frozen into the sample bulb freezeout arm using liquid nitrogen. Any non condensible gas is pumped away and the freeze-pump-thaw cycle is repeated until the sample gas in the line condenses rapidly and completely. Many samples which had a stated

purity of >95% had significant (up to 50%) amounts of air in them. This may result from incomplete evacuation of lecture bottles prior to their filling. The stopcock is now closed and the sample bulb is removed from the gas line. Gases which had absorption bands in the visible or near ultraviolet wavelength regions were protected by being wrapped in aluminum foil and then kept in a closed storage drawer.

5.3.3. Admission of Sample Gas to Spectrometer

The sample bulb or tube is attached to the spectrometer inlet system using the tapered glass joint. The inlet lines are pumped out using a mechanical pump and a diffusion pump. When the inlet line pressure is about 1×10^{-3} torr, the pumps are valved off. The pressure in the scattering chamber (SC) is measured by a Schulz-Phelps ionization gauge. This type of gauge is used because of its unique electrode configuration which permits accurate relative pressure measurements in the range from 10^{-4} torr to 10^{-1} torr pressure. The SC pressure should be less than 2×10^{-5} torr before admission of the sample gas. The gas is then admitted to the SC through a Granville Phillips (Model 203001-02-011) variable leak until the indicated pressure is about 5×10^{-3} torr. The spectrometer is now ready for tuning as described in Section 5.4.

5.4. Tuning The Spectrometer

Because there are about 30 independently adjustable lens voltages, there is no unique set of voltages or unique tuning method which always produces a beam of the desired intensity, resolution and angular divergence. The following series of steps will usually permit the successful tuning of the machine.

The voltages on the lenses are adjusted to somewhere in the range of values listed in Table 5.4-1. These values are typical for operation at 40 eV incident energy and energy resolution (defined as the full width at half maximum of the elastic peak) of 0.12 eV. The instrument should be set to observe 30° scattering if this was not done earlier.

The emission from the filament to the accelerator lens should be checked again. The filament heating current should be adjusted if necessary to achieve an emission of about 5×10^{-5} amps.

The electrometer can be connected to the decelerator lens to monitor the beam current hitting aperture 2. The deflectors 1A and 1B, the accelerator, and the high voltage lens voltages should be adjusted to maximize this current. It should be in the range from 1 to 3×10^{-6} amps.

The electrometer is moved to the outer sphere of the monochromator (OSM) and the deflector plate voltages and gun lens voltages

Table 5.4-1. Typical Lens Voltage Ranges
(Voltages w.r.t. Filament)

Cathode	0.0 (-40.0 w.r.t. ground)
Accelerator	50 → 70 V
Deflector 1A or 1B	Accel ± 10 V
High Voltage lens	200 to 250 V
Decelerator	50 → 70 V
Deflector 2A → 2D	Decelerator ± 10 V
Herzog 1	5 to 7 V
Center Monochromator	4.0 V
ΔM	1.9 V
Herzog 2	4 to 6 V
L2A	10 to 15 V
L2B	20 to 30 V
Deflector 3 center	60 to 80 V
Deflector 3A to 3D	Deflector 3 center
L3A	80 to 100 eV
L3B	10 to 20 eV
Herzog 3	4 to 6 V
Center selector	4.0
ΔS	1.9
Herzog 4	5 to 9 V
L4	10 to 20 V
FCH	60 to 90 V
Faraday Cup	FCH voltage
Deflector 4A, 4B	FCH ± 10V

are adjusted to maximize I_{osm}. Typical values for I_{osm} after tuning are 3×10^{-7} to 1×10^{-6} amps.

The electrometer can now be connected to the Faraday cup in the scattering chamber. It is important to bias the electrometer at least +90 volts with respect to ground in order to collect all the electrons entering the scattering chamber. The current with the 90 volt bias (giving a total electron collection energy of 130 volts) was more than three times the current collected with the electrometer grounded (40 volt collection energy). The voltage across the monochromator should be adjusted until a beam current is seen with the electrometer. The entrance lenses, the gun lenses, and deflector voltages can be adjusted to maximize this current. This process of monochromator and lens voltage adjustment should be continued until I_{FC} is in the range from 5×10^{-8} to 1×10^{-7} A at this impact energy. An effort was made to keep the voltages across deflectors 3A-D near zero volts in order to avoid deflecting the beam away from the mechanical zero angle of the machine. The gun deflectors could almost always be used to get the beam into the proper position to enter the scattering chamber with no voltage across the entrance deflector plates.

The beam is now tuned through the first half of the machine and into the scattering chamber. The Faraday cup is retracted and the lead to the Faraday cup is grounded to insure that no charge builds up on it. Because of the extreme sensitivity of the Spiraltron (it can detect

single electrons and 1 electron/sec = 1.6×10^{-19} amps) it was almost always possible to get the elastically scattered electrons through the second half to the multiplier by adjusting the voltage across the selector until the elastic peak was observed as a count rate from the Spiraltron as observed with the HP counter. The second half voltages were then adjusted from their nominal values to maximize the elastic scattering count rate. When no further increase is observed, the first half can be readjusted to further maximize the elastic count rate. This process is usually quite important because the first half had previously been tuned for maximum current to the Faraday cup. This was often achieved by increasing the angular divergence of the beam. The scattered current is only produced by electrons reaching the scattering volume (see Section 5.8) and this is aided by a narrow beam. After several more iterations of the tuning process (in both the first and the second half) the elastically scattered current at 30°, 40 eV incident energy, and an indicated target gas pressure of 5×10^{-3} should be in the range from 2×10^{3} to 2×10^{4} counts/sec. The stability of this scattered current is usually checked at this point by adjusting the PAR (second half reference supply) up one volt, (to limit the total number of counts reaching the Spiraltron) waiting 3 to 5 minutes, readjusting the PAR and checking to see if the count rate was the same within ±10%. If a larger variation had occurred, the voltages were readjusted and the test was repeated.

The resolution is checked by observing the elastic peak count rate on the counter while the PAR is adjusted in 0.01 volt steps. The total change in the PAR voltage from a counting rate of 1/2 the peak value on one side of the peak to the other side is defined as the full width at half maximum (FWHM) of the elastic peak. The resolution is typically 0.11 to 0.15 volts with the center voltages on each sphere set at 4.0 volts. If higher resolution is desired the sphere center voltages can be lowered with a corresponding adjustment of the voltages across each sphere. This lowering process is performed in small steps (say, 0.5 volts) on one sphere at a time and the instrument lens voltages are readjusted to maximize the scattered current. The Herzogs are very important lenses at the lower analyzing voltages and should be lowered along with the sphere center voltages. When the center monochromator is down to about 1.0 volts with respect to the filament and the center selector voltage is about 2.0 volts the resolution should be somewhere in the range from 0.05 to 0.08 volts. At these resolutions, however, the count rates are too low to observe singlet → triplet transitions except at very small scattering angles so most of the present experiments were made with a resolution of about 0.12 volts. The higher resolution spectra were very useful for observing vibrational fine structure, weak singlet → singlet transitions, and narrow Rydberg transitions.

The beam zero angle should also be checked before data taking begins. The direct beam zero angle may not be the same as the mechanical zero angle of the machine because of electron optical effects. This can be checked by first adjusting the PAR voltage so that electrons from a strong inelastic feature are transmitted by the second half. The gear wheel can be adjusted to observe a scattering angle of 0° (indicated angle) and the position of the true beam zero angle (given by the turns counter on the rotary motion feedthrough) is the indicated angle which gives the highest count rate. A second test is also to turn $\pm 3^\circ$ from this true zero angle and see if the count rate is the same on each side.

During the study of the molecules reported here the beam zero angle did not appear to be more than $\pm 1^\circ$ from the mechanical zero angle. This is in contrast to the results of Rice [1] on the previous version of this machine who found this variation to be as much as 7°. The explanation may involve the use of different electron lenses and the effort to keep the voltage across the scattering chamber entrance deflector plates close to zero volts (i.e., no deflection applied).

5.5. Obtaining An Energy Loss Spectrum

The instrument is now presumed to be tuned for the desired impact energy, resolution, and count rate stability. An energy-loss

spectrum is obtained in the following manner. The instrument is set to the desired scattering angle. The second half has been tuned to pass elastically scattered electrons with $V_{sweep} = 0$ volts. If a sweep voltage is applied to the second half reference supply and set to a value of V_s volts then electrons which have lost eV_s electron volts of energy in scattering would be reaccelerated to the same kinetic energy which the elastically scattered electrons have and would then be transmitted to the electron multiplier and detected. It should be noted that the elastically scattered electrons will have too much kinetic energy to get through the energy loss analyzer when $V_s \neq 0$. Electrons which have lost kinetic energy of eV_s electron volts will always be transmitted with highest efficiency when the sweep voltage has a value V_s. In this way by varying V_s the energy-loss spectrum can be obtained from the elastic peak out to any desired energy loss less than the incident energy value.

The actual spectrum is taken by the following series of steps.

1. The PAR is set about 0.3 volts lower so that when V_s is applied the energy-loss spectrum will start below the elastic peak. This permits measurement of the elastic intensity by integration of the area under the elastic peak, tests the peak shape symmetry and permits measurement of the instrumental resolution.

2. The Raytheon DAC is set to the desired total sweep range. It can be set to give a full scale voltage of from 1 to 10 volts using all 1024 MCS channels. A correspondingly smaller total sweep voltage is available by using only 256 or 512 channel of the MCS.

3. If a jump in the energy-loss spectrum is desired (to omit the region between the elastic peak and the onset of the first inelastic feature) the jump channel is selected and the necessary jump voltage is set on the jump power supply. The jump channel is selected so that at the chosen voltage step size the memory channels below the jump channel include the entire elastic peak.

4. The Nuclear Data MCS memory is erased, the scan counter (Beckman Preset Accumulator Model 6004) is cleared to zero and the pulse amplifier output is connected to the MCS input on the Nuclear Data.

Scanning is now started and continues until the desired signal-to-noise ratio is obtained. At scattering angles of 20° or less, when only the spin allowed transitions were studied, an adequate spectrum could be taken in 15 to 45 minutes. Whenever spin-forbidden transitions were also being studied the necessary scanning time ranged from 3 to 8 hours depending on the angle. By repeating the scan every 102 seconds any drifts in beam current, scattering chamber pressure, and lens voltages tend to affect both the elastic peak and the inelastic

features equally. This is more reliable than a single pass spectrum with a count ratemeter where instrumental conditions at the end of a 3-hour spectrum may be significantly different from those at the beginning.

5.6. Data Handling

The actual data handling devices have been described in Section 4.19. When the desired signal-to-noise ratio has been obtained the following series of steps is performed.

1. The following information is recorded in a log book: the date, spectrum number, molecule name, impact energy, scattering angle, the starting voltage (channel 0), the end voltage including the jump voltage, if any, the voltage at the jump channel without the jump voltage on, the jump channel voltage with the jump voltage included, the number of scans, the dwell time per channel, the time of day at the completion of the spectrum, the scattering chamber pressure, the pressure above the diffusion pump, the elastic peak count rate, the analyzing voltages in the monochromator and selector, the incident beam current to the Faraday cup and the approximate number of millivolts/channel. The first four voltages were measured on the center selector but could have been measured on any given second half lens.

2. The spectrum is plotted and labeled with spectrum number, molecule name, impact energy, scattering angle, number of scans, starting voltage, jump voltage, and step size.

3. The teletype is used to make an identifying heading on the paper tape and the spectrum is then punched out. The identifying heading is the spectrum number, molecule name, impact energy, scattering angle, date, the first four voltages recorded in step 1, the dwell time per channel, the number of scans, the total number of channels used and the channel at which the voltage jump occurred.

The spectrum is now complete and the instrument can be adjusted to another angle and the data taking process is repeated. A study at a given impact energy was usually made at 10° increments from 10° to 80° at a constant resolution value. In addition, a 0° spectrum was usually taken of the inelastic features at a higher resolution to provide a comparison with the optical spectra. If a given spectrum did not include the elastic peak because the count rate was too high the spectrometer was adjusted to 20° and the center selector voltage corresponding to the elastic peak was determined by adjustment of the PAR in 0.01 volt steps. This is necessary to determine the actual energy-loss values of the inelastic features in the spectrum at the scattering angle for which the elastic peak could not be included.

The paper tape containing the spectrum is read into the 4700 computer, the heading is verified and then the heading and the spectrum are written onto magnetic tape in a format compatible with the IBM 370-158 computer.

5.7. Computer Analysis

The data on the magnetic tape are subjected to a two-step analysis in programs written by W. M. Flicker (see acknowledgments). The programs called ANDATA1 and ANDATA2 are capable of many different types of manipulations on the data sets. These programs will be described in detail in the thesis of W. M. Flicker, so this report only summarizes the parts of these programs which were used to obtain the results reported in this thesis.

5.7.1. ANDATA1

ANDATA1 performs the following processes.

1. Because of arcs in the machine or arithmetic errors in the MCS some channels pick up many extra counts. These appear as noise spikes in the spectrum. They are detected and replaced by an average value of the contents of nearby channels.

2. A background function is subtracted from each channel's contents. The instrument has an angle dependent background count rate produced by elastically scattered electrons bouncing through the

selector instead of getting trapped on the inner or outer sphere surface when the sphere is tuned for inelastically scattered electrons. An additional source of noise is electrons which escape out of the monochromator or gun stage and drift across the instrument and get attracted into the detector lenses. In the present studies an energy-loss dependent background count rate was used which was sufficient to reduce the background just prior to the onset of the first inelastic feature to about O counts/second.

3. The ND MCS is dead (i.e., not capable of receiving data) for about 1 μsec following the leading edge of each pulse. During time time the signal is being added to the memory register value. Thus if the count rate in a channel corresponds to C counts/sec then the true count rate is actually

$$C_{true} = \frac{C}{1 - \tau C}$$

where $\tau = 1 \times 10^{-6}$ seconds. The program calculates count rates and then corrects for this dead time.

4. The smoothness of the data is limited by the accuracy of the counting process. The distribution of actual numbers of counts obtained in a given memory channel during repeated experiments where all other variables were held constant is given by the Poisson

distribution law.[2] It is defined as $P(n) = \bar{n}^n e^{-\bar{n}}/n!$ where $\bar{n}$ is the average number of counts/channel which would be obtained in a large number of repeated experiments. The standard deviation of this distribution is $\sqrt{n}$. The 95% confidence level intervals for a given number n (greater than 50) counts/channel obtained in one experiment are[2] $n + 1.92 \pm 1.96\sqrt{n+1.0}$. The 95% statistical significance level for the number of counts obtained in any channel when n ranges from 50 to 100 counts (typical for triplet states) is between ± 28% and ± 22%. Because of the limited statistical significance of the number of counts in any channel, the data is smoothed by averaging over anywhere from 3 to 9 adjacent channels.

5. The spectrum is plotted using several different scale factors. An energy loss scale and a count rate scale is put on each plot.

6. Peaks in the spectra are located and their voltages are calculated relative to the highest peak in the spectrum.

7. Slope breaks are located.

8. The areas under each peak are calculated.

9. The raw spectrum, the smoothed spectrum, the heading information, and the peak location information are all printed out.

The plotted output and the spectrum listing are analyzed to

determine the exact onset and end channels as well as the channels which contain peaks. This is the input information to ANDATA2.

5.7.2. ANDATA2

This program was used to perform the following operations.

1. Steps 1, 2, 3, 4 of the ANDATA1 description are repeated.

2. Band areas and area ratios from the specified onset and end channel numbers are calculated. The ratios are printed and also punched on cards.

3. The program calculates the voltages of all peaks, band onsets and band ends relative to a specified reference channel.

4. If a high angle spectrum contains a shoulder produced by a spin-forbidden excitation on an optically allowed transition, the program will deconvolute the shoulder to obtain its real band shape. This is done by subtracting an appropriately scaled low angle spectrum from the higher angle spectrum. In the low angle spectrum the band shape is primarily the band shape of the optically allowed transition. Thus by scaling and subtracting the low angle spectrum from the high angle spectrum, the band shape and area of the weak shoulder can be obtained. This method was utilized only for 1,3-butadiene. The results of the deconvolution are plotted along with the high angle spectrum itself to permit visual examination of the results.

The DCS ratios from ANDATA2 are used in conjunction with the measured elastic or inelastic DCS values (see Section 5.9) to obtain DCS values for all inelastic excitations.

5.8. Relationship of the Detected Current to the Differential Cross Section

The relationship of the DCS to the detected current has been treated in detail by Rice[3] for this instrument. Those results are discussed here in a slightly modified form.

The geometrical configuration is shown in Figure 24 for a scattering angle of 50°. If I_0 is the total incident current into the scattering chamber containing target molecules at a density ρ, then a current I_{SV}, given below, will reach the scattering volume. The other electrons will have been scattered out of the incident beam. The effective scattering volume is determined by the intersection of the incident beam cone and the detector view cone. Electron scattering events occurring outside of the scattering volume will not be detected.

$$I_{SV} = I_0 \exp(-\langle Q(E_0)\rangle \ell_1 \rho) \qquad (5.8\text{-}1)$$

$\langle Q(E_0)\rangle$ is the total scattering cross section for electrons of mean incident energy E_0 averaged over the beam energy distribution $f(E - E_0)$. This incident beam energy distribution is peaked sharply at

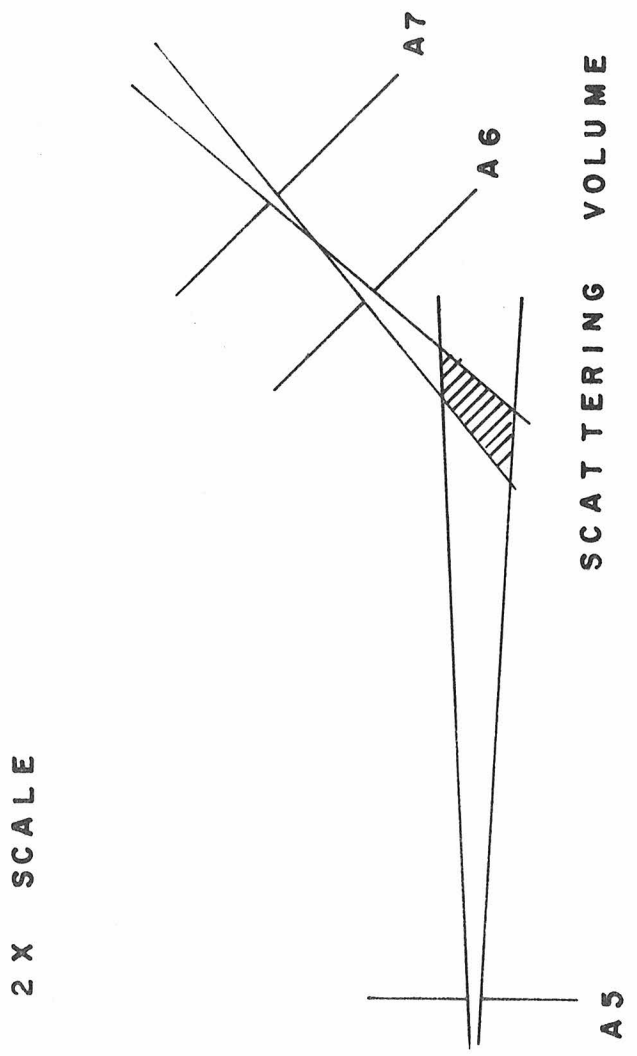

FIGURE 24 SCATTERING VOLUME GEOMETRY

E_0 and usually has a FWHM of less than 0.1 volts as described previously. $\langle Q(E_0) \rangle$ can be written as

$$\langle Q(E_0) \rangle = \int_{E=0}^{\infty} f(E - E_0)\, Q_{tot}(E)\, dE \qquad (5.8\text{-}2)$$

with $Q_{tot}(E)$ equal to the total scattering cross section at energy E.

The scattered current of electrons into solid angle χ which have lost an energy W for electrons in the incident energy range E to E + dE can be written as

$$di_{sc} = \frac{I_{SV}\, \sigma(E, W, \chi) \rho\, V(\theta)\, f(E - E_0)\, dE}{A} \qquad (5.8\text{-}3)$$

σ is the differential cross section for the energy-loss process which leads to an energy loss W. A is the cross sectional area of the beam at the scattering center. The current which leaves the scattering chamber is given by the integral of di_{sc} over the range of acceptance angles Ω determined by apertures 6 and 7. In addition, this current is also attenuated by scattering out of the exiting beam before it reaches aperture 6. Thus

$$I_{out}\, dE = \exp(-\langle Q(E_0 - W) \rangle\, \ell_2 \rho)\, dE \int_{\Omega} i_{sc}\, d\Omega \qquad (5.8\text{-}4)$$

$$\text{and} \qquad \langle Q(E_0 - W) \rangle = \int_{E=0}^{\infty} f(E - E_0 - W)\, Q_{tot}(E - W)\, dE \qquad (5.8\text{-}5)$$

Once the electrons are out of aperture 6 the following factors determine if they lead to an output pulse from the pulse amplifier.

1. The selector transmits electrons with an efficiency which depends on the energy loss of the electrons. The transmission efficiency can be defined as the percentage of the electrons incident on the entrance plane of the selector which are transmitted through aperture 8 (the detector stage aperture). The transmission function is gaussian shaped.[3] If $\epsilon_s^{opt}(W)$ is the transmission efficiency for scattered electrons which have lost an amount of energy W with the second half optimally tuned to pass them, then the transmission efficiency at any given energy loss or gain W is

$$\epsilon_s(W) = \epsilon_s^{opt}(W) \exp-[(V_{sweep} - W)^2/\alpha\Delta^2] \qquad (5.8\text{-}6)$$

Δ is the full width at half maximum (typically .07 to 0.1 volts) of the elastic peak in the selector itself and $\alpha = -1/(4 \ln 1/2)$. For elastically scattered electrons (W = 0) as V_{sweep} changes from negative values to positive values the gaussian elastic line shape is reproduced. In addition, for $W \neq 0$ as V_{sweep} changes from below W to above W a similar gaussian line shape will result. The optimized efficiency

will be the same if $\epsilon_s^{opt}(W = 0) = \epsilon_s^{opt}(W)$.

2. Other detection determining factors include the fact that the second half optics do not transmit electrons with 100% efficiency. This efficiency may also depend on energy loss. In addition, the multiplier and pulse amplifier may not detect electrons with unit efficiency. A second quantity $\epsilon_1(W)$ is defined as the product of the lens transmission and the detection system efficiencies. The result is that the detected current I_D will be I_{out} integrated over all E and W and multiplied by the above efficiencies

$$I_D = \int_E \int_W I_{out}(E, W)\, \epsilon_s(W)\, \epsilon_1(W)\, dE\, dW . \qquad (5.8\text{-}7)$$

Inserting all previous expressions leads to

$$I_D(V_{sweep}, \chi) = \frac{I_0\, V(\theta)\, \rho}{A} \exp(-\langle Q(E_0)\rangle\, \ell_1 \rho) \times$$

$$\int_E \int_W \int_\Omega \epsilon_s(W)\, \epsilon_1(W)\, f(E - E_0)\, \sigma(E, W, \chi) \exp(-\langle Q(E_0 - W)\, \ell_2 \rho)\, d\Omega\, dw\, dE \qquad (5.8\text{-}8)$$

The triple integral in (5.8-8) can be simplified by noting that $f(E - E_0)$ measures the incident beam energy distribution and is sharply peaked at $E = E_0$. This leads to the simplifications below.

1. If no resonance process is occurring then $\sigma(E, W, \chi)$ is only a slowly varying function of E in the ± 0.2 eV range about E_0 where the E integral is nonzero. Thus $\sigma(E, W, \chi)$ can be replaced by $\sigma(E_0, W, \chi)$ and removed from the integral over E.

2. Both $\epsilon_S(W)$ and $\epsilon_1(W)$ may also depend on the incident energy E but over the small effective range of the E integral the selector transmission efficiencies and the lens transmission efficiencies are constants.

3. $\langle Q(E_0 - W) \rangle$ is the averaged total scattering cross section for electrons of energy near E_0-W. This quantity changes with E for a constant W but since it is primarily the elastic total cross section, it does not undergo rapid changes with E anywhere in the 20 to 100 eV region over a small ± 0.2 eV range.[4] This may not be true if there is a resonance scattering process occurring but even in those cases the elastic cross section often shows only small oscillations around its non resonance value. In He at $\theta = 72^\circ$ the resonance at 19.3 eV leads to a temporary drop of only 14% in the scattered signal while for Neon the 16.0 eV resonance gives a drop of only 3%.[5] There are now no terms contained in the energy integral which depend on E other than $f(E - E_0)$. If f is defined such that

$$\int_{E=0}^{\infty} f(E - E_0)\, dE = \delta(E - E_0) \qquad (5.8\text{-}9)$$

then 5.8-8 becomes

$$I_D(V_{sweep}, \chi) = \frac{I_0 V(\theta) \rho}{A} \exp(-\langle Q(E_0) \rangle \ell_1 \rho) \times$$

$$\int_W \int_\Omega \epsilon_s(W) \epsilon_1(W) \sigma(E_0, W, \chi) \exp(-\langle Q(E_0 - W) \rangle \ell_2 \rho) \, dW \, d\Omega \tag{5.8-10}$$

The view cone determining apertures have been kept small enough so that there are only small variations in θ and ϕ over the solid angle range accepted. (Except at very small scattering angles.) For values of θ above a few degrees $\sigma(E_0, W, \chi)$ is approximately constant over the range of sampled solid angles. $\sigma(E_0, W, \chi)$ can then be replaced by $\sigma(E_0, W, \theta_{mean}, \phi_{mean})$ where θ_{mean} and ϕ_{mean} are the values determined by the angles between the axes of the beam and view cones. As mentioned in Section 1 only one value of ϕ is studied here because for randomly oriented target molecules the observed scattering will not depend on ϕ. Thus $\sigma(E_0, W, \theta_{mean}, \phi_{mean})$ can be written as $\sigma(E_0, W, \theta)$ where θ now means θ_{mean}. The Ω integration can now be performed and $\Delta\Omega$ is defined as

$$\Delta\Omega = \int_\Omega d\Omega \tag{5.8-11}$$

$\Delta\Omega$ is simply the acceptance solid angle subtended by the exit lens

system at the scattering center. Equation (5.8-10) now reduces to

$$I_D(V_{sweep}, \theta) = \frac{I_0 V(\theta) \rho}{A} \Delta\Omega \exp(-\langle Q(E_0) \rangle \ell_1 \rho \times$$

$$\int_W \epsilon_S(W)\, \epsilon_1(W)\, \sigma(E_0, W, \theta) \exp(-\langle Q(E_0 - W) \rangle \ell_2 \rho)\, dW \qquad (5.8\text{-}12)$$

$\epsilon_S(W)$ is a gaussian peaked sharply at $W = V_{sweep}$. Thus the value of W in $\epsilon_1(W)$ and $\langle Q(E_0 - W) \rangle$ can be set equal to V_{sweep}. In addition, the selector optimum efficiency term $\epsilon_s^{opt}(W)$ can also be set equal to $\epsilon_s^{opt}(V_{sweep})$ and all 3 terms can be removed from the integral. The result is

$$I_D(V_{sweep}, \theta) = \frac{I_0 V(\theta) \rho\ \Delta\Omega}{A} \epsilon_s^{opt}(V_{sweep}) \epsilon_1(V_{sweep}) \times$$

$$\exp\left(-[\langle Q(E_0) \rangle \ell_1 + \langle Q(E_0 - V_{sweep}) \rangle \ell_2]\, \rho\right) \times$$

$$\int_W \sigma(E_0, W, \theta) \exp -([V_{sweep} - W]^2 / \alpha \Delta^2)\, dW . \qquad (5.8\text{-}13)$$

The following definitions are useful to simplify this expression. The ideal gas law is also used to convert ρ to pressures P ($\rho = P/kT$).

$$P_0(V_{sweep}) \equiv [\langle Q(E_0) \rangle \ell_1 + \langle Q(E_0 - V_{sweep}) \rangle \ell_2]^{-1} kT \qquad (5.8\text{-}14)$$

$$\epsilon(V_{sweep}) \equiv \epsilon_s^{opt}(V_{sweep})\, \epsilon_1(V_{sweep}) \qquad (5.8\text{-}15)$$

$$Z(E_0, V_{sweep}, \theta) \equiv$$

$$\int_W \sigma(E_0, W, \theta) \exp -([V_{sweep} - W]^2/\alpha\Delta^2)\, dW \qquad (5.8\text{-}16)$$

$$I_D(V_{sweep}, \theta) = \frac{I_0[V(\theta)\Delta\Omega]}{AkT} \epsilon(V_{sweep}) P \exp(-P/P_0) Z \qquad (5.8\text{-}17)$$

5.8.1. Measurement of Cross Section Ratios

In these experiments differential cross sections for inelastic features were obtained at most angles (see further discussion in 5.9) by using the measured ratio to the elastic peak and subsequently measuring the elastic DCS. By insertion in (5.8-17) for V_{sweep} of 0 and then for a value V_{sweep} it is seen that this ratio is

$$\frac{I_D(V_{sweep}, \theta)}{I_D(V_{sweep}=0, \theta)} = \frac{\epsilon(V_{sweep})}{\epsilon(0)} \frac{\exp(-P/P_0(V_{sweep})}{\exp(-P/P_0(0))} \frac{Z(E_0, V_{sweep})}{Z(E_0, 0, \theta)} \qquad (5.8\text{-}18)$$

The other terms all cancel. It is important to notice that the term $[V(\theta)\Delta\Omega]$ cancels so that the ratios are correct even if the scattering volume correction cannot be accurately evaluated. Rice has shown previously[6] that $\epsilon(V_{sweep}) = \epsilon(0) \pm 0.05\, \epsilon(0)$ when $E_0 \geq 10$ eV, $E_0 - w \geq 10$ eV, and the lens following aperture 7 was at a voltage $\geq E_0$. These conditions were used in the present studies. At impact energies of 20 eV, features beyond 10 eV loss to be significantly lower in

intensity when compared with the spectra at 25 eV incident energy and the same scattering angle. This suggests that for $E_0 - W < 10$ eV the transmission efficiency may decrease. P_0 depends on V_{sweep} through $\langle Q(E_0 - V_{sweep})\rangle$. This total scattering cross section is essentially the total elastic cross section at the energy E_0 or at $E_0 - V_{sweep}$. Over the energy loss ranges used here (no ratio was taken for features whose peaks were more than 9 eV apart) the elastic cross section is assumed to vary slowly enough so that $P_0(V_{sweep})$ is approximately equal to $P_0(0)$. In N_2, for example, the observed variation from 10 eV to 35 eV is less than 10%.[4] Thus the exponential and the ϵ terms cancel in 5.8-18 and the detected signal ratio reduces to the ratio of the cross sections integrated over W.

$$\frac{I_D(V_{sweep}, \theta)}{I_D(V_{sweep} = 0, \theta)} = \frac{\int_W \sigma(E_0, W, \theta) \exp -([V_{sweep} - W]^2/\alpha\Delta^2)\, dW}{\int_W \sigma(E_0, W, \theta) \exp -(W^2/\Delta^2)\, dW} \tag{5.8-19}$$

Both integrals are strongly peaked at $V_{sweep} = W$ in each case so $\sigma(E_0, W, \theta)$ can be replaced by $\sigma(E_0, V_{sweep}, \theta)$ and removed from the integrals. The integrals are then over gaussians of the same shape (Δ^2 is the same in all parts of a given energy loss spectrum) and will cancel leading to

$$\frac{I_D(V_{sweep},\ \theta)}{I_D(V_{sweep}=0,\ \theta)} = \frac{\sigma(E_0,\ V_{sweep},\ \theta)}{\sigma(E_0,\ V_{sweep}=0,\ \theta)} \qquad (5.8\text{-}20)$$

The ratios of areas under peaks are thus seen to lead directly to cross section ratios in the absence of energy loss dependence of the optics and rapid variations in the total elastic cross sections.

5.8.2 Direct Measurement of a Cross Section

The elastic scattering cross section was obtained directly from rapid measurements of $I_D(V_{sweep}=0,\ \theta)$ over the range from $\theta = 20°$ to $\theta = 80°$. The details are discussed in Section 5.9. Examination of expression 5.8-17 for I_D shows that if the results for $I(0,\ \theta)$ are divided by $[V(\theta)\Delta\Omega]$ an expression is gotten as follows:

$$\frac{I_D(0,\ \theta)}{[V(\theta)\Delta\Omega]} = \frac{I_0}{A\,kT}\,\epsilon(0)P\,\exp(-P/P_0)\,Z(E_0,\ 0,\ \theta) \qquad (5.8\text{-}21)$$

All terms on the right except Z do not depend on θ. $\epsilon(0)$ and A are constant as long as the electron optics are not retuned. If in addition, P, I_0, and T are kept constant during an elastic DCS measurement then the terms may be replaced by a constant C. Thus

$$\frac{I_D(0,\ \theta)}{C[V(\theta)\Delta\Omega]} = \int_W \sigma(E_0,\ W,\ \theta)\,\exp -(-W^2/\alpha\Delta^2)\,dW \qquad (5.8\text{-}22)$$

The integral is sharply peaked near W = 0. Thus $\sigma(E_0, W, \theta)$ can be replaced by $\sigma(E_0, 0, \theta)$ and removed from the integral. The remaining integral is a constant which does not depend on θ. Defining a new proportionality constant C′ 5.8-23 is written as

$$\frac{I_D(0, \theta)}{[V(\theta)\Delta\Omega]} = C' \sigma(E_0, 0, \theta) . \qquad (5.8\text{-}23)$$

C′ does not depend on θ. If the values for $I_D(0, \theta)$ are divided by the product of scattering volume and the acceptance angle, an accurate relative cross section for the process in question is obtained. This means that the cross section values for any angle are accurate with respect to those of other angles but the value at one angle is chosen arbitrarily. A measurement of absolute cross section values is beyond the capability of the present instrument because of an inability to measure A, $\epsilon(0)$, P (absolutely), and to determine the proper value for P_0 and the effect of the energy loss integral on $\sigma(E_0, V_{sweep}, \theta)$.

5.8.3. Pressure Dependence of the Detected Signal

Equation (5.8-17) also shows the expected pressure dependence of the detected signal for single scattering events. For a specified value of V_{sweep} this formula can be written as

$$\ell n\left(\frac{I_D}{I_0 P}\right) = C - P/P_0 \qquad (5.8\text{-}24)$$

where

$$C = \ell n\left[\frac{V(\theta)\Delta\Omega}{A\,kT}\,\epsilon(V_{sweep})\,Z(E_0, V_{sweep}, \theta)\right] \qquad (5.8\text{-}25)$$

Rice [7] has shown that this expression is accurate to at least .012 torr for He. Doering [8] has also shown that it holds to .05 torr for 90° scattering in Helium in the E_0 range from 10 to 30 eV. Double scattering events would artificially increase the measured cross section at a given angle for an inelastic process by having elastic scattering at the scattering angle θ proceeded or followed by zero angle inelastic scattering. The pressure dependence of double scattering events is different from that of single scattering and thus departures from single scattering conditions would be indicated by failure of equation 5.8-24.

In the present study no specific effort was made to verify that the pressure dependence in equation 5.8-24 was being obeyed. Our approach was to keep the pressure low enough so that double scattering was unlikely. The typical indicated pressures were .003 to .006 torr. In addition, for some molecules, spectra were repeated at the same θ and E_0 but with increased pressures of up to .01 torr without any noticeable change in the observed cross section ratios. This method

does in fact sacrifice some potential scattered signal but it does circumvent the relatively tedious process of determining that only single scattering is occurring for each new molecule.

5.9. DCS Measurement Techniques

5.9.1. Scattering Volume Corrections

In Section 5.8.2 it was shown how the detected current at each scattering angle can be related to the relative DCS for a process. This required that the incident current, temperature and target gas pressure be kept constant during the period of the angular measurement. In addition, the raw count rates must be divided by $V(\theta)\Delta\Omega$ which is the product of the scattering volume times the effective solid angle. A crude approximation to $V(\theta)\Delta\Omega$ is to simply set it equal to sine θ where θ is the scattering angle. This approximation is justified only when the beam and view cone angles are very small compared to the scattering angle. A more accurate numerical integration has been perfomed by Trajmar et al.[9] for a scattering geometry identical to that of the present study. This method involved the assumption of an incident electron beam with a half angle of 1°, 3° or 5° and a gaussian type current density distribution relative to the center of the cone. The DCS for the process was assumed to be either isotropic or $\propto 10^{-.0122\theta}$ or $\propto 10^{-.0322\theta}$. This affects the calculation because the

finite size of the view cone leads to a number of slightly different values of θ contributing. The effective value of scattering volume times solid angle of acceptance was calculated for each point in the intersection of the view cone and the beam cone and then summed over all the contributing points to obtain $V(\theta)\Delta\Omega$.

The results are tabulated in Table 5.9-1 for the various beam half angles. One problem in using these values is the fact that the beam half angle is not well defined. The first half of the machine can be rotated about the scattering center and this is also equivalent to rotating the second half about the scattering center. By measuring the current to the first dynode of an electron multiplier as a function of rotation angle Rice measured [10] the angular resolution of the system. He obtained a half angle of 2.0° at 30 eV incident energy. This number provides only a lower bound to the beam half angle because rotation is about the scattering center rather than about aperture 5 which is the source of the electron beam cone. In the DCS curves reported here it has been assumed that in the range of incident energies below 25 eV the appropriate beam angle is 5° while from 25 eV to 70 eV a 3° beam angle was assumed. The effect of this assumption in terms of relative errors in DCS values is discussed in 5.10.

Table 5.9-1. Effective Value of $V(\theta)\Delta\Omega$ for $\sigma \propto 10^{-.0122\theta}$

θ (Deg)	sin θ	Beam angle		
		5°	3°	1°
10	0.174	.2619	.218	.225
20	0.342	.423	.358	.361
30	0.50	.544	.496	.434
40	0.643	.675	.639	.637
50	0.766	.787	.764	.726
60	0.866	.879	.865	.864
70	0.949	.946	.939	.939
80	0.985	.987	.984	.984
90	1.0	1.0	1.0	1.0

5.9.2. Elastic DCS Measurement

After the instrument was tuned at 30° and the count rate was stable on the elastic peak as indicated by the counter an elastic DCS could be taken. The count rate was measured at 30° by a 10 second integration on the counter. The scattering angle was quickly moved to 40° and the count rate was obtained there. The process continued until $\theta = 80°$ was reached. At least two 10 second integrations were taken at 80°. Then the instrument was moved back to 20° in 10° steps and the count rates from 10 second integrations were recorded every 10°. Finally, the count rate was checked a third time at 30° to determine that no major drifts had occurred. If the value at 30° had shifted by more than ±10% the measurement was usually repeated.

The raw count rates were averaged over the numbers obtained for each angle. They were then corrected for pulse amplifier dead time following each pulse (0.5 μseconds) by the formula

$$C_{true} = \frac{C_{measured}}{1 - (5 \times 10^{-7})\, C_{measured}} \qquad (5.8\text{-}26)$$

The dead time corrected count rates were then multiplied by the values of $V(\theta)\Delta\Omega$ appropriate for each angle obtained from Table 5.9-1. The resulting relative DCS values were arbitrarily normalized so that the elastic DCS value at 40° was 1.0. The elastic DCS was not

measured below 15° or 20° for most molecules. Below 20° the elastic scattering signal includes unscattered electrons from the edges of the primary beam. This effect can produce artificially inflated low angle elastic DCS values. This was a greater problem at lower impact energies where the beam angle is in fact larger.

5.9.3. Inelastic DCS Measurements

Because of the inability to measure the elastic DCS reliably below 20° the DCS for the strongest inelastic feature was measured directly at 10°, 20°, and 30°. The second half was tuned on the desired inelastic feature at 20°. The count rate for 1 or 2 10 second integration times was recorded. Similar measurements were made at 30°, then 20° again, 10° and finally 20° again. Because of the low absolute value of the observed count rates (typically 100 to 500 counts/second at 20°) at least 3 10 second integration periods were used and in some cases as many as 10 periods were employed (100 seconds total observation time). The resulting values were averaged and then multiplied by the appropriate value of $V(\theta)\Delta\Omega$ to give the DCS values in one set of arbitrary units.

The ratios of the same inelastic feature to the elastic peak could be used along with the elastic DCS to get the inelastic DCS values at 20° and 30°. This represents a second arbtrary unit set of

inelastic DCS values. The inelastic DCS values from the direct measurement are normalized so that they equal the value from the ratio method at 20°. The results from the two methods at 30° provide an indication of the consistency of the two methods. This consistency is discussed in percentage terms in the error analysis in Section 5.10.

5.10 Estimated Uncertainties in DCS Values and Cross Section Ratios

The previous sections have discussed the data collection methods used in this study. In this section an estimate will be made of the errors involved in these measurements.

A study was made of the short-term repeatability of the cross section ratios by studying the spectrum of cis-2-trans-4-hexadiene at $E_0 = 45$ eV and $\theta = 40^\circ$ on 3 separate occasions during one week of data taking on this molecule. The sample standard deviation is defined as follows

$$s = \sqrt{\frac{\sum_{i=1}^{n} (x_i - \bar{x})^2}{n - 1}} \qquad (5.10\text{-}1)$$

where n is the number of separate experiments to measure x and $\bar{x}$ is the mean value obtained in the n experiments. The percentage sample standard deviation is defined by $100\ s/\bar{x}$. For one triplet/singlet ratio this was 18.7% and for the other triplet/singlet ratio it was 19.1% while the singlet/elastic peak ratio percentage deviation was 7.5%. Thus the net uncertainty in the ratios of spin forbidden to spin allowed transition are on the order of ±20% while the ratio of the singlets to the elastic peak is uncertain to ±10%. These numbers are also consistent with the only long term (more than 1 year) repetition of a spectrum.

The 35 eV and $\theta = 45^\circ$ spectrum of butadiene repeated to ±4% on the singlet/elastic ratio and ±13% on the triplet/singlet ratios. A second source of error is from the elastic DCS measurements. The elastic cross section measurements were repeated for both 1, 3-pentadiene and for 1, 4-cyclohexadiene. The average value of the two measurements was calculated and then the percentage sample standard deviation was obtained. The values are listed in the Table 5.10-1. The average percentage sample standard deviation was 21.8% and this is presumably a measure of the uncertainty in elastic DCS measurements. To be conservative a value of ±25% for the elastic DCS measurement error will be used and this will also be assumed to apply to the directly measured inelastic DCS at $\theta = 10^\circ$ and $\theta = 20^\circ$.

An additional error due to the volume correction is important at $\theta = 10^\circ$ and $\theta = 20^\circ$. The present study used the volume correction for an intermediate forward peaked DCS and a beam half angle of 3°. The beam half angle may have been 5° and it is conceivable that the correct angle dependence of the DCS was closer to a sharply forward peaked DCS such as the $10^{-.032\theta}$ type used by Trajmar in the same volume correction calculations. The volume correction would have been increased from 0.218 to 0.290. If it is assumed that the "real" value is in the middle of this range then the volume correction error is ±14% at 10°. A similar calculation at $\theta = 20^\circ$ gave ±11.5%.

Table 5.10-1. Percentage Sample Standard Deviations for Some Elastic DCS Measurements

	1,4-Cyclohexadiene		1,3-Pentadiene	
θ	E_0 = 30 eV	E_0 = 50 eV	E_0 = 30 eV	E_0 = 55 eV
20	70 %	59 %	46	22
30	34	5.7	24	11
40[a]	0	0	0	0
50	9.5	2.6	19	1.6
60	10	8.8	23	3.9
70	11	10	27	5.0
80	20	11	48	40.7

[a] The value at 40° is always zero because elastic DCS values are normalized to 1.0 at this angle.

Above $\theta = 30^\circ$ the error is less than 5%. Table 5.10-2 summarizes the discussion in this section and gives the total error from all three sources.

One additional uncertainty arises when spectra are run at two different times under different tuning conditions. As will be seen in Section 6 of this thesis most of the singlet→triplet DCS curves are smooth even if they are not flat. Some notable exceptions are 1,3-butadiene ($E_0 = 35$ eV, $\theta = 10^\circ$), 1,3-hexadiene ($E_0 = 45$ eV, $\theta = 10^\circ$), 1,3-cyclohexadiene ($E_0 = 40$ eV, $\theta = 10^\circ$), and 1,5-hexadiene ($E_0 = 25$ eV, $\theta = 10^\circ$). In all cases the DCS point in question is much higher than would be expected from a smooth curve fitted to the higher angle points. Although the increase may be real it was also noted that in all cases the cross section ratio was obtained from a spectrum taken weeks or months after the initial set of ratios at the higher angles. Thus these results are somewhat uncertain and should be used with caution. A possible explanation of this effect may be changes in the beam zero angle relative to the mechanical zero angle of the machine. Because the triplet/singlet ratios are rising very rapidly with increasing θ around 10°, a shift of 2° or 3° in the beam zero angle to give the true 12° or 13° ratio at an indicated angle of 10° could produce the "increase" in the calculated DCS point.

Table 5.10-2. Summary of Estimated Errors

	Ratios		DCS Values		
θ	Triplet/Singlet	Singlet/Elastic	Elastic	Singlet	Triplet
10	± 20	± 10	± 39%	± 49%	± 59%
20	± 20	± 10	± 37%	± 47%	± 57%
30-80	± 20	± 10	± 25	± 35	± 45

References

1. J. K. Rice, Ph.D. Thesis, California Institute of Technology, 1969, pp. 209-211.

2. E. B. Wilson, Jr., An Introduction to Scientific Research (McGraw-Hill Book Co., Inc., New York, 1952), pp. 191-5.

3. J. K. Rice, op. cit., pp. 224-229.

4. Some typical elastic cross section plots as a function of incident energy are given in H. S. Massey, E. H. S. Burhop, and H. B. Gilbody, Electronic and Ionic Impact Phenomena, Vol. II (Oxford Press, London, 1969) p. 709.

5. G. J. Schulz, Phys. Rev., A136, 650 (1964).

6. J. K. Rice, op. cit., pp. 234-238.

7. J. K. Rice, op. cit., pp. 229-234.

8. J. P. Doering and A. J. Williams IV, J. Chem. Phys., 47, 4180 (1967).

9. S. Trajmar, D. C. Cartwright, J. K. Rice, R. T. Brinkmann, and A. Kuppermann, J. Chem. Phys., 49, 5464 (1968).

10. J. K. Rice, op. cit., pp. 209-211.

6.1. 1,3-Conjugated Polyenes

Introduction

The conjugated dienes and trienes chosen for study here are members of a class of molecules called the conjugated polyenes. The role of triplet excited states of the large polyene, 11-cis retinal, in the vision process has been recently discussed.[1] The primary photochemical event in the vision process involves cis → trans isomerization of 11-cis retinal.[2] The aldehyde is initially bound to the protein opsin through a Schiff base.[3] The role of the low-lying triplet state in the visual isomerization process is still not definitely established but it is known[1] that cis → trans isomerization does occur following triplet energy transfer to 11-cis retinal in solution. Two recent studies[4,5] of the optical spectra of substituted polyenes have also indicated that there is a singlet state (the $2\ ^1A_g$) at an energy just below that of the $1\ ^1B_u$. The $1\ ^1B_u$ state is the upper state for the intense N → V type[6] absorption in these molecules. The energy locations of low-lying singlet and triplet states in the smaller polyenes could aid in understanding which of the excited states of 11-cis retinal are part of the vision mechanism.

The small polyenes have been the subject of many photochemical studies.[7] Much of the interest arose from the discovery of

the photochemical conversion of ergosterol to pre-vitamin D_2 (pre calciferol). Both of these molecules are larger polyene systems and their photochemical transformations have been discussed by Havinga and Schlatmann.[8] Excited state energy locations developed from the study of smaller polyenes should be useful in developing a reaction scheme for the ergosterol-vitamin D_2 system.

In the simplest polyene, 1,3-butadiene, several ab initio π electron approximation calculations[9-11] are available for comparison with experimental results. Further if the σ and π electron separation approximation is correct for a specific excited electronic state in butadiene, then that state should be relatively unaffected by alkyl substituion for the H atoms in butadiene. Several of the polyenes studied here are alkyl substituted derivatives of 1,3-butadiene and the results obtained will be interpreted in terms of the applicability of the π electron approximation to each of the several excited states which are observed.

6.1.1. s-trans-1,3-Butadiene

1,3-Butadiene, the simplest polyene, has been studied previously at impact energies E_0 of 20 eV, 35 eV, and 55 eV and the results have been published.[12,13] In addition to the work reported in

these papers, the DCS values for the various transitions have now been obtained. Spectra taken at higher resolution values have also permitted observation of a number of singlet → singlet transitions which were not seen in the previously published spectra. To facilitate comparison of the results for the other polyenes with those of butadiene the present section will review the earlier butadiene studies and provide further discussion based on the more recent studies.

Figure 24 shows a low-resolution (0.16 eV FWHM) spectrum of butadiene for E_0 = 20 eV and $\theta = 85°$ while Figure 25 is a higher resolution spectrum at E_0 = 90 eV and $\theta = 0°$. The DCS values for the transitions to be discussed below are shown for incident electron energies of 20 eV, 35 eV, and 55 eV in Figures 26-28. The DCS numerical values are given in Tables 6.1.1-1 to 6.1.1-3.

6.1.1.1 The $1\ ^3B_u$ State

The first inelastic feature produces an onset at about 2.4 eV and a peak at 3.22 ± 0.04 eV. The DCS curves shown in Figure 26-28 indicate that the excitation probability for this transition is independent of the electron scattering angle. This behavior is typical[14] for exchange excitation and confirms the earlier assignments[12, 13, 15] of this feature to the lowest singlet → triplet transition. The onset of optical absorption in the high pressure oxygen perturbation study of Evans[15]

is at 2.51 eV. The electron impact onset is about 0.1 eV below the optically-determined 0-0 energy because of the spread in energy (FWHM $\approx$ 0.12 to 0.15 eV) of the electron beam.

The theoretical calculations[9-11] predict that the lowest singlet $\rightarrow$ triplet transition is the $\tilde{X}^1A_g \rightarrow 1\,^3B_u$. The vertical excitation energy is predicted at 3.24 eV[9] or 3.45 eV[10,11] in excellent agreement with the present experimental value of 3.22 eV. The agreement between theory and experiments permits the assignment of the 3.22 eV peak to the $\tilde{X}^1A_g \rightarrow 1\,^3B_u$ transition.

The $1\,^3B_u$ state has been previously identified as the initial excited state in sensitized cycloaddition reactions of butadiene in the liquid state.[16] The products are varying amounts of cis and trans 1,2-divinylcyclobutane and 4-vinylcyclohexene.

6.1.1.2 The $1\,^3A_g$ State

The second inelastic feature peaks at 4.91 $\pm$ 0.03 eV as shown in Figure 24. The DCS curves shown in Figures 26-28 are similar in both shape and magnitude to those of the $\tilde{X}^1A_g \rightarrow 1\,^3B_u$ transition and permit assignment to the second singlet $\rightarrow$ triplet transition. The theoretical calculations predict that the second singlet $\rightarrow$ triplet transition is the $\tilde{X}^1A_g \rightarrow 1\,^3A_g$ and put the vertical excitation energy at 4.95 eV[9] or 5.04 eV[10,11] in good agreement with our experimental

value.

Two hydrogen migration reactions are observed following mercury ($^3P_1$) sensitized photolysis of butadiene in the vapor phase. One reaction leads to H_2 and a product which is presumed to be vinylacetylene.[7] A second process leads to vibrationally "hot" 1,2-butadiene. This molecule can either be stabilized by collision[17] or undergo dissociation to methyl and propargyl ($CH{\equiv}C{-}\dot{C}H_2$) radicals[18] from which subsequent reactions occur. The initially excited state in these reactions is a triplet state because the total spin of the atom plus molecule system is conserved. The rate of triplet → triplet energy transfer in the condensed phase is proportional to the spectral overlap of the normalized donor phosphorescence spectrum and the absorption spectrum.[19, 20] Recent studies have also suggested that a similar criterion applies in the gas phase.[21, 22] An examination of the overlap of the 4.89 eV mercury line with each of the triplet states indicates that the $1\,^3A_g$ is initially excited by energy transfer from the $^3P_1$ state of mercury if this criterion is applicable.

6.1.1.3 The $1\,^1B_u$ state

The strongest feature in the electron impact spectrum is the transition which peaks at 5.92 ± 0.02 eV. The DCS curves for this transition are sharply forward peaked. The forward peaking and the

strong relative intensity confirm the earlier assignment [23] to the optically allowed $\tilde{X}^1A_g \rightarrow 1\,^1B_u$ transition. The spectrum in Figure 25 at a higher resolution shows vibrational fine structure on the 5.92 eV peak with shoulders at 5.76 ± 0.03 eV and 6.05 ± 0.03 eV. These values agree within experimental error with the optical values of 5.75 eV, [24] 5.92 eV [24] and 6.09 eV. [24, 25] The vibrational spacing of about 0.17 eV has been identified [25] as a progression in the symmetric carbon-carbon double bond stretching vibration.

Two additional narrow features appear at 6.64 ± 0.02 eV and 6.80 ± 0.02 eV. These states are also seen in the optical spectra [26] at about 6.65 eV and 6.81 eV and were attributed to a Rydberg series.

6.1.1.4 The 6.9 eV to 7.8 eV Region

The excitation region between 6.9 eV and 7.9 eV in butadiene has been the subject of controversy for many years. The region has been attributed to a $\tilde{X}^1A_g \rightarrow 2\,^1A_g$ transition, [27] a $\tilde{X}^1A_g \rightarrow 2\,^1B_u$ transition, or to a Rydberg type transition [25] in the s-trans form of butadiene (trans with respect to the C2-C3 single bond). In the previously published papers [12, 13] these bands with peaks at 7.08 eV, 7.28 eV, and 7.48 eV have also been discussed. In the low resolution and low impact energy spectra (see Figure 24), this region appears to be one electronic transition. At higher impact energies and at higher

resolution the appearance of this feature changes (see Figure 25) and it also grows weaker with respect to the $\tilde{X}^1A_g \rightarrow 1\,^1B_u$ transition at 5.92 eV. The optical absorption studies of butadiene [28, 29] indicate that the region contains a number of Rydberg like features superimposed on an absorption continuum. The appearance of the optical spectrum does not indicate that the peaks at 7.08 eV, 7.28 eV, and 7.48 eV are necessarily part of the same electronic transition as was assumed earlier. They appear to be one electronic transition in the electron impact spectra because of the much lower resolution.

An estimate of the oscillator strength, ϵ, in the region from 6.9 eV to 7.8 eV from the data of Pottier et al. [28] was made with a classical dispersion theory formula. [30] The resulting value of .057 is somewhat low for a fully allowed transition but still not small enough to rule out such an assignment. The DCS curves for the 6.9 eV to 7.8 eV region shown in Figure 26-28 are not as sharply forward peaked as those of the $\tilde{X}^1A_g \rightarrow 1\,^1B_u$ but do not permit a definite assignment of these bands to any one of the three previously suggested assignments.

6.1.1.5 Higher States

Rydberg state excitations are seen at 8.00 eV, 8.18 eV, 8.39 eV, 8.54 eV, and 8.69 eV in good agreement with the results from optical studies. [25, 28, 29] Transitions to states above the first

Figure Captions

Figure 24. The electron energy-loss spectrum of 1,3-butadiene from 2 eV to 9 eV for 20 eV incident beam energy at a scattering angle (θ) of 85° and 0.16 eV resolution (FWHM).

Figure 25. Electron energy-loss spectrum of 1,3-butadiene from 5.0 eV to 11.5 eV at $\theta = 0°$; 90 eV incident electron energy; an uncalibrated sample pressure reading (P_{ind}) of 3.9×10^{-3} torr; 0.07 eV resolution (FWHM).

Figure 26. Differential cross sections as a function of θ at an incident electron energy of 20 eV for elastic scattering (+) and for transitions to the following excited states: $1\,^3B_u$ (Δ), $1\,^3A_g$ ($\bigcirc$), $1\,^1B_u$ ($\square$), and the 7.28 eV singlet ($\times$).

Figure 27. Same as Figure 26 for an incident electron energy of 35 eV.

Figure 28. Same as Figure 26 for an incident electron energy of 55 eV.

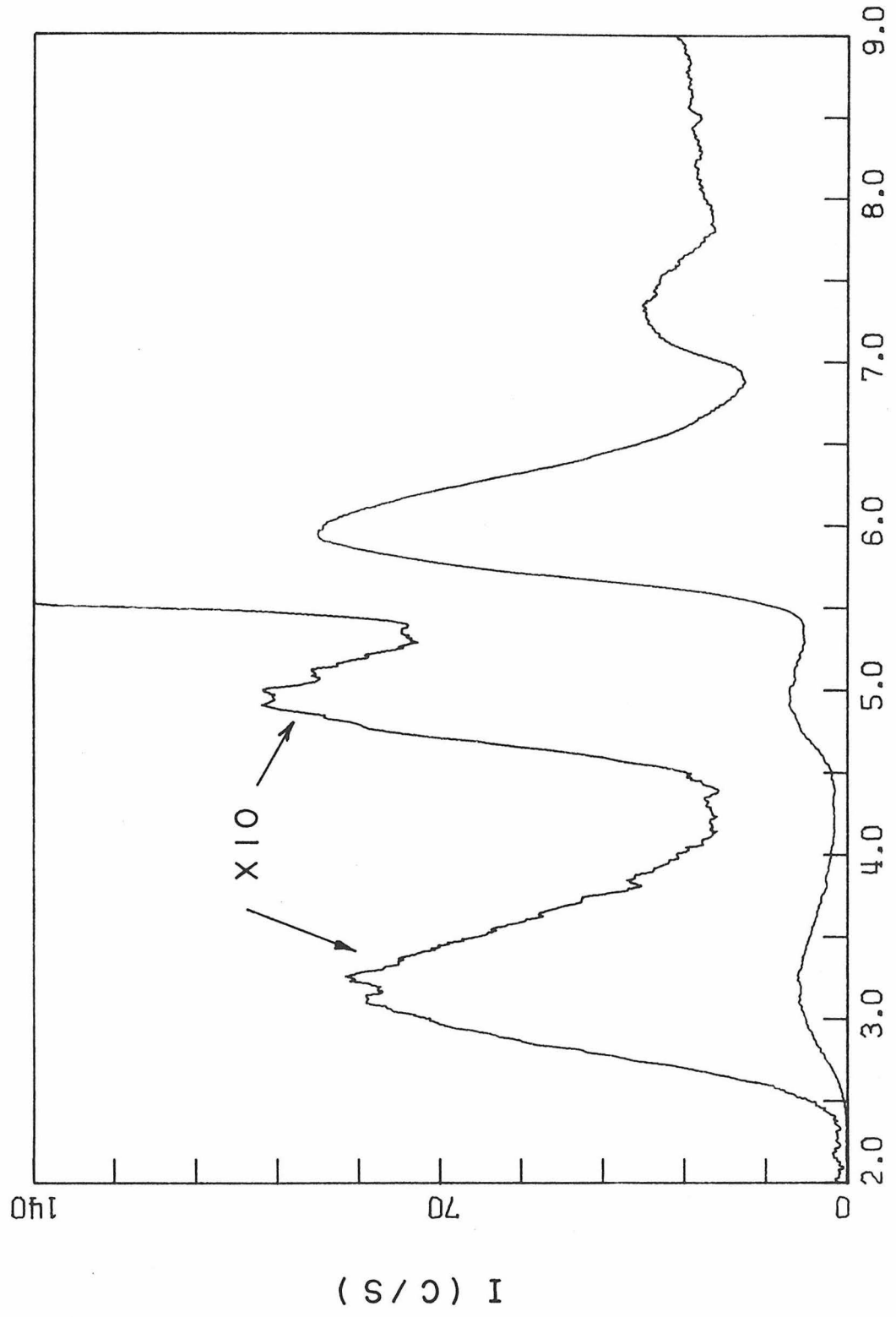

FIG. 24

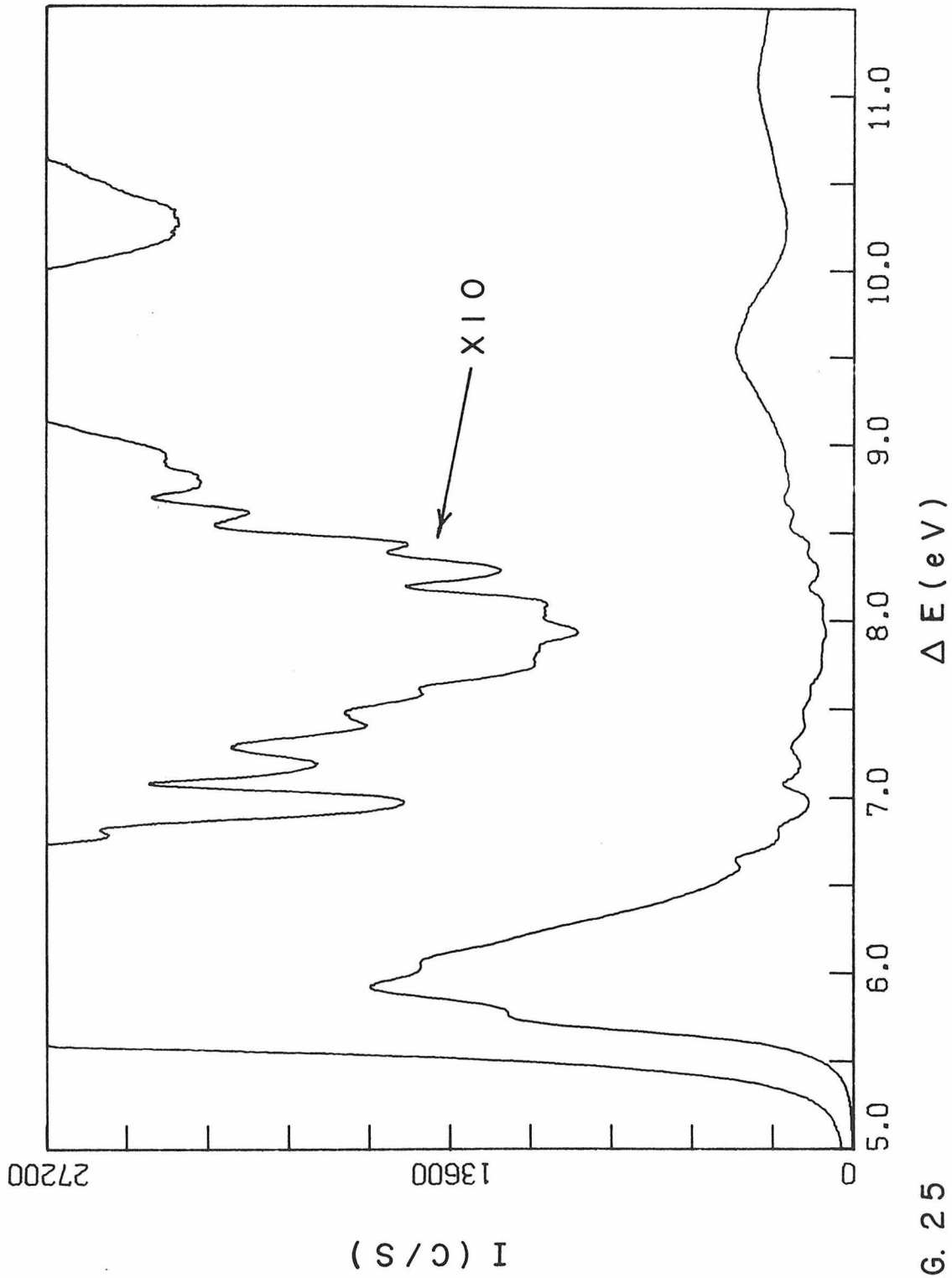

FIG. 25

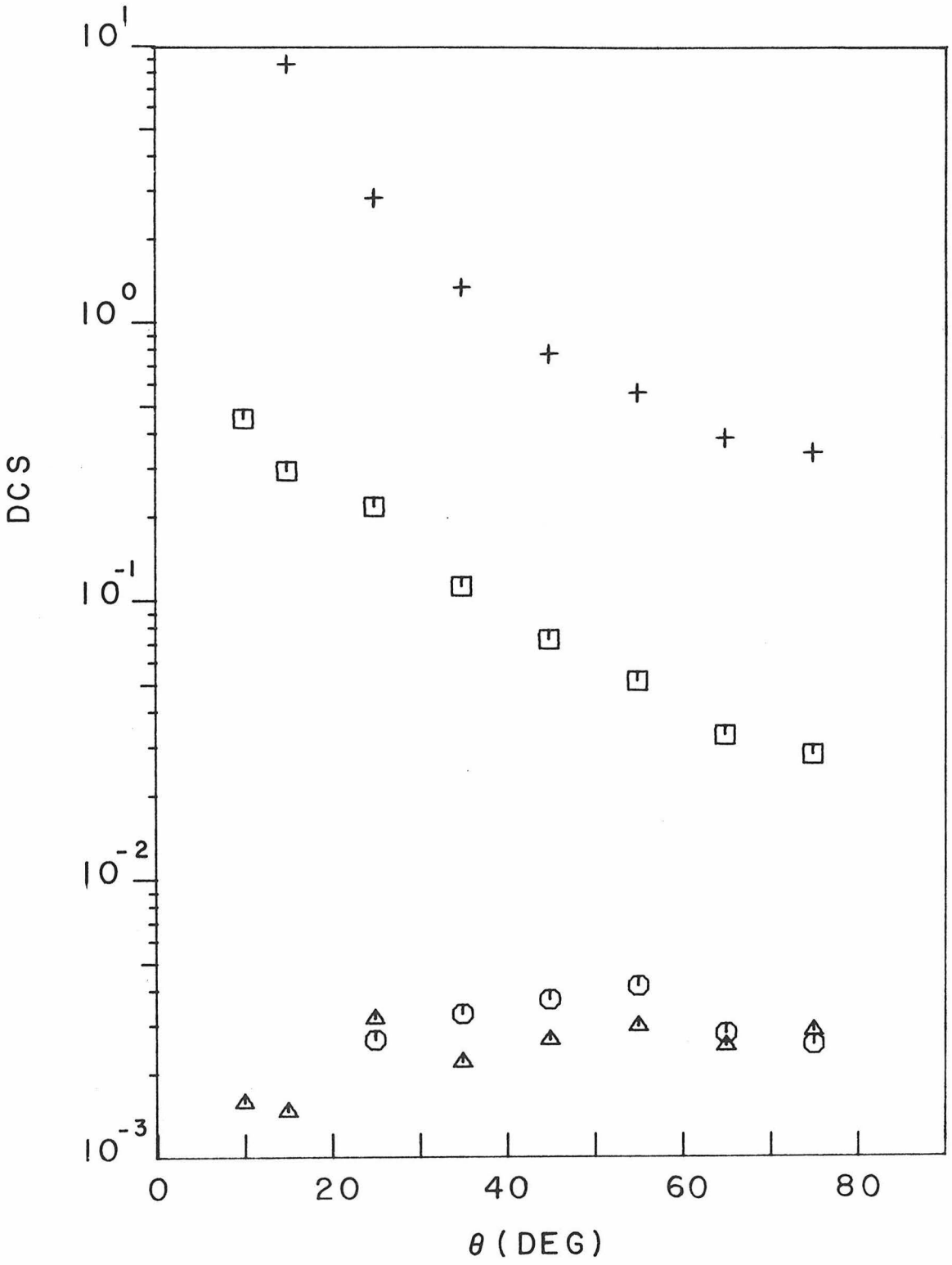

FIGURE 26

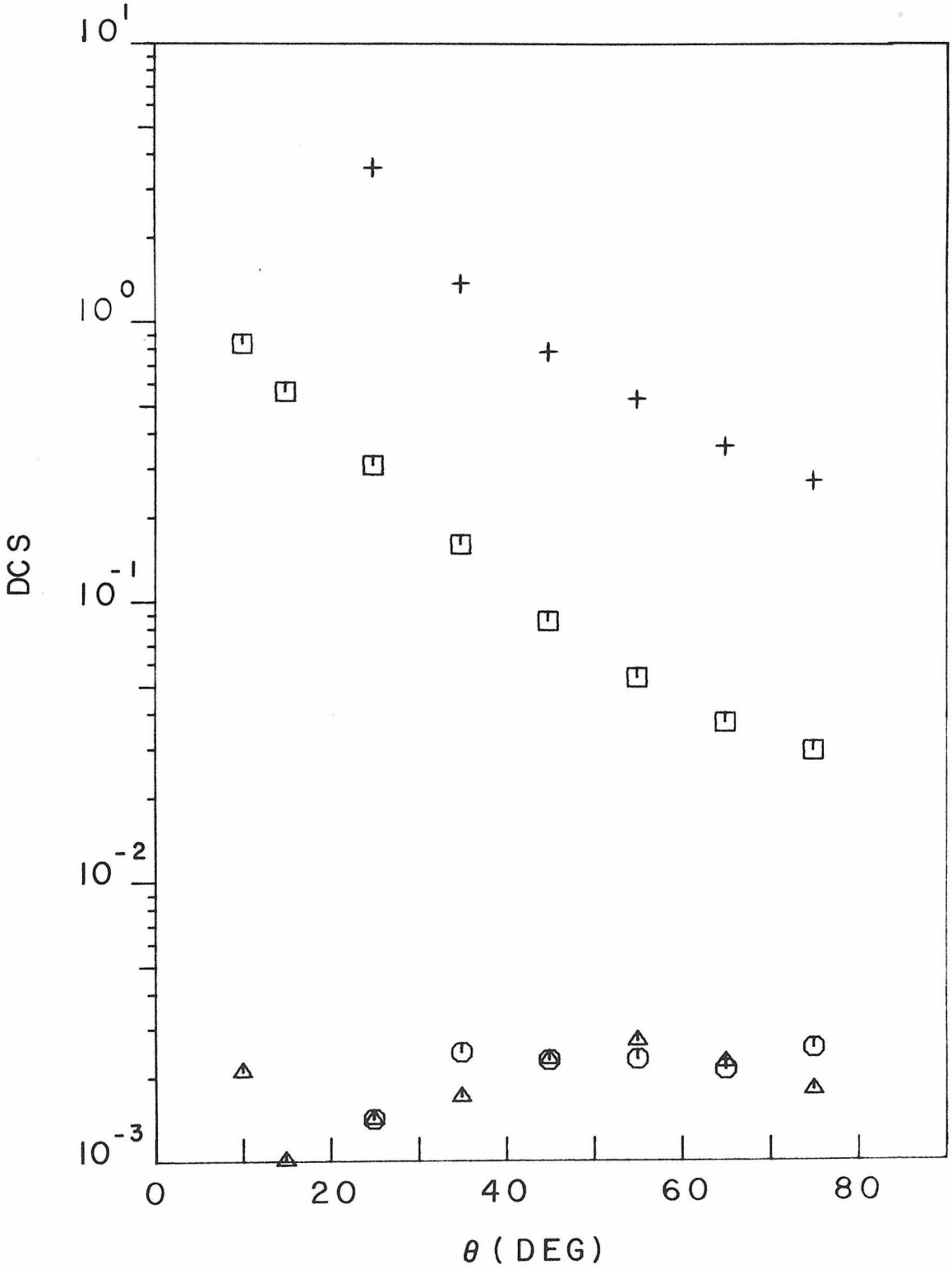

FIGURE 27

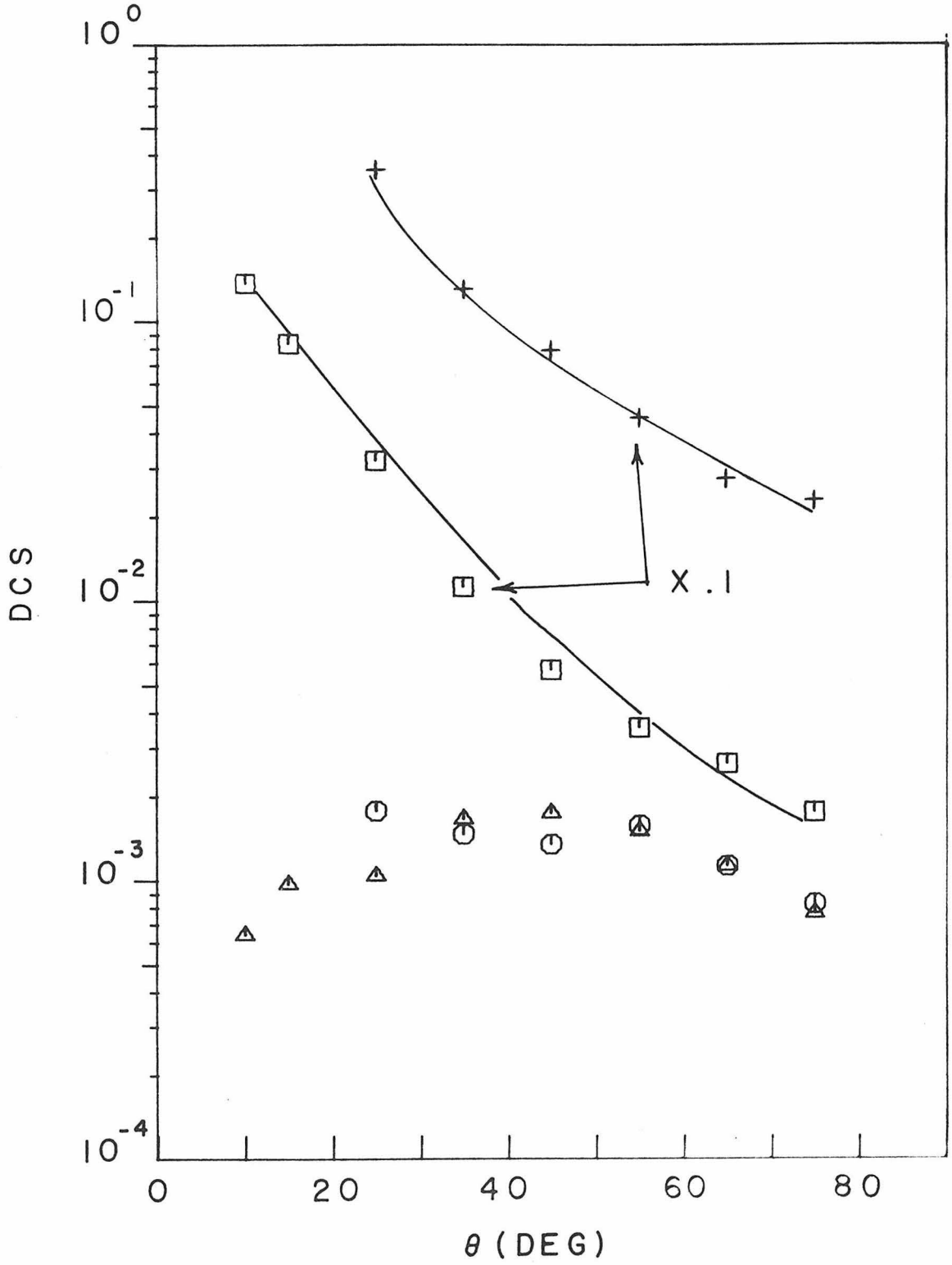

FIGURE 28

Table 6.1.1-1. DCS Values for 1,3-Butadiene at 20 eV Incident Energy[a]

		Scattering Process			
θ	Elastic	$\tilde{X}^1A_g \rightarrow 1^3B_u$	$\tilde{X}^1A_g \rightarrow 1^3A_g$	$\tilde{X}^1A_g \rightarrow 1^1B_u$	$\tilde{X}^1A_g \rightarrow V_2$
10	–	0.00157	–	0.449	0.0606
15	8.56	0.00146	–	0.291	0.0544
25	2.80	0.00315	0.00264	0.216	0.0458
35	1.33	0.00220	0.00328	0.112	0.0246
45	0.767	0.00264	0.00369	0.0723	0.0207
55	0.554	0.00296	0.00412	0.0514	0.0153
65	0.381	0.00251	0.00279	0.0328	0.0111
75	0.339	0.00284	0.00253	0.0280	0.0101

[a] Elastic peak at 40° is arbitrarily set equal to 1.0.

The two values for the $\tilde{X}^1A_g \rightarrow 1^1B_u$ DCS from both the direct and ratio methods are set equal for $\theta = 25°$.

Table 6.1.1-2. DCS Values for 1,3-Butadiene at 35 eV Incident Energy[a]

θ	Elastic	Scattering Process $\tilde{X}^1A_g \rightarrow 1\,^3B_u$	$\tilde{X}^1A_g \rightarrow 1\,^3A_g$	$\tilde{X}^1A_g \rightarrow 1\,^1B_u$	$\tilde{X}^1A_g \rightarrow V_2$
10	–	0.00209[b]	–	0.835	0.185
15	13.97	0.00101	–	0.562	0.134
25	3.57	0.00141	0.00141	0.307	0.0694
35	1.37	0.00170	0.00246	0.160	0.0462
45	0.775	0.00231	0.00230	0.0853	0.0276
55	0.528	0.00269	0.00231	0.0533	0.0179
65	0.357	0.00225	0.00213	0.0368	0.0142
75	0.269	0.00179	0.00254	0.0293	0.0120

[a] Elastic peak at 40° is set equal to 1.0. The values for the $X^1A_g \rightarrow 1\,^1B_u$ DCS from the alternate methods are set equal at $\theta = 35°$.

[b] Reliability is not certain. See discussion in 5.10.

Table 6.1.1-3. DCS Values for 1,3-Butadiene at 55 eV Incident Energy

	Scattering Process				
θ	Elastic	$\tilde{X}^1A_g \rightarrow 1\,^3B_u$	$\tilde{X}^1A_g \rightarrow 1\,^3A_g$	$\tilde{X}^1A_g \rightarrow 1\,^1B_u$	$\tilde{X}^1A_g \rightarrow V_2$
10	–	0.000640	–	1.377	0.348
15	19.0	0.000979	–	0.837	0.208
25	3.54	0.00105	0.00179	0.319	0.0858
35	1.31	0.00168	0.00148	0.113	0.0337
45	0.791	0.00175	0.00136	0.0571	0.0182
55	0.452	0.00151	0.00158	0.0353	0.0121
65	0.275	0.00113	0.00113	0.0262	0.00941
75	0.230	0.000762	0.000824	0.0176	0.00637

Table 6.1.1-4. Excited Electronic States of s-trans 1,3-Butadiene[i]

State	Nature of state	Present results[f] Peak	Present results[f] Franck-Condon region	Optical results	Theory Shih et al.[a]	Theory Hosteny et al.[b]
1^3B_u	Valence[a, b]	3.22 ± 0.04	2.4 → 4.4	3.22[c]	3.24	3.45
1^3A_g	Valence[a, b]	4.91 ± 0.03	4.0 → 5.5		4.95	5.04
1^1B_u	Diffuse[a, b]	5.76 ± 0.03 5.92 ± 0.02 6.05 ± 0.03	5.0 → 6.9	5.75[d] 5.92[d] 6.09[d]	6.60	7.05
	Rydberg[e]	6.64 ± 0.02		6.65[e]		
	Rydberg[e]	6.80 ± 0.02		6.81[e]		
See discussion in text. These may be composite in nature.		7.08 ± 0.02 7.28 ± 0.02 7.48 ± 0.02		7.07[d] 7.27[d]		
		7.60				
	Rydberg	8.00 ± 0.03		8.00[g]		
	Rydberg	8.18 ± 0.03		8.17[g]		
	Rydberg	8.39 ± 0.03		8.38[g]		
	Rydberg	8.54 ± 0.03		8.50[g]		
	Rydberg	8.69 ± 0.03		8.73[g]		
	Superexcited	9.53 ± 0.03		9.56[h]		
	Superexcited	11.04 ± 0.04				

[a] Reference 9. [b] Reference 10, 11. [c] Reference 15. [d] Reference 24. [e] Reference 26.
[f] See references 12 and 13. [g] Reference 25. [h] Reference 28. [i] All values in eV.

ionization potential produce broad maxima at 9.53 ± 0.03 eV and 11.04 ± 0.04 eV.

6.1.2. 1-trans-3-Pentadiene

Electron impact spectra of 1,trans-3-pentadiene (trans piperylene) were taken at impact energies of 30 eV, 55 eV, and 75 eV and scattering angles from 0° to 80°. Some typical spectra are shown in Figures 29-31. The cross section ratios and the cross section curves are shown in Figures 32-35. Table 5.1.2-1 summarizes the state designations discussed below and gives the measured peak locations while Table 6.1.2-2 is a tabulation of the DCS values.

In the following discussion the π electronic states are labeled by the symmetry they would have in the C_{2h} point group. 1-trans-3-Pentadiene does not actually belong to this symmetry group but the similarity of the spectrum (for the low lying $\pi \rightarrow \pi^*$ transitions) to that of butadiene supports this use of a local symmetry designation for these states. A similar method of describing these electronic states will also be used for the other conjugated polyenes reported in this study.

The 1-trans-3-pentadiene sample was obtained from Aldrich Chemical Company. It has a stated purity of 99% and was subjected to several liquid nitrogen freeze-pump-thaw cycles prior to being used in

the spectrometer.

6.1.2.1 The $1\,^3B_u$ State

The lowest energy loss peak in the spectrum occurs at 3.14 ± 0.05 eV as shown in Figures 29 and 30. The cross section ratio in Figure 32 of this transition to the strong $\tilde{\chi}^1A_g \rightarrow 1\,^1B_u$ transition at 5.80 eV (see discussion in 6.1.2.3) shows the sharp increase[12-14] with increasing scattering angle expected for a singlet → triplet transition. The DCS curves for excitation of this state are also roughly isotropic as expected for such a transition as shown in Figures 33 and 34. The results are similar to the results for the $\tilde{\chi}^1A_g \rightarrow 1\,^3B_u$ transition in butadiene. The effect of alkyl substitution on this state in butadiene is only a slight lowering (about 0.08 eV) of the vertical transition energy. The energy is still close to the value predicted for the $\tilde{\chi}^1A_g \rightarrow 1\,^3B_u$ transition in butadiene by the ab initio calculations.[9-11] Semiempirical Pariser-Parr type calculations of Allinger et al.[31] on 1-trans-3-pentadiene place the ^3B_u state at 3.11 eV in excellent agreement with the present experimental value. The cross section behavior permits unequivocal identification of this transition as singlet → triplet in nature. Comparison with the results in butadiene and the theoretical calculations indicate that this is the $\tilde{\chi}^1A_g \rightarrow 1\,^3B_u$ transition.

The 0-0 band for this transition has been measured using the high pressure oxygen perturbation technique.[32] The lowest vibrational peak comes at 2.57 eV. The absorption onset in the electron impact spectra is at about 2.5 eV in good agreement with the optical value.

Trans → cis isomerization of pentadiene has been studied[33,34] in solution following energy transfer from a sensitizer molecule in its lowest triplet electronic state. Hammond et al.[33] have made a careful study of the steady state [trans]/[cis] concentration ratio as a function of sensitizer triplet energy for sensitizers whose triplet energies range from 2.3 eV to 3.2 eV. Turro has suggested[34] that isomerization is occurring via the lowest diene triplet state in these studies, which is the $1\,^3B_u$. This conclusion is also consistent with the results of recent calculations[35] on the energy of the lowest triplet states of butadiene as a function of twist angle around the double bond. The ground state has a high barrier to isomerization but both the lowest singlet and triplet excited states are predicted[35] to be most stable in the twisted form. Thus if a sensitizer triplet state excites the $1\,^3B_u$ state in 1-trans-3-pentadiene, the molecule will twist to a roughly antiplanar form about the C3-C4 double bond. When the molecule returns to the ground state it can twist in one direction to give the cis form and in the other direction to give the trans form.

6.1.2.2 The $1\,^3A_g$ State

A feature which appears as only a shoulder on the low energy side of the $\tilde{X}^1A_g \rightarrow 1\,^1B_u$ transition at low scattering angles (see Figure 29) but is easily visible as a separate peak at higher scattering angles (see Figure 30) can be identified as the second singlet → triplet transition on the basis of its DCS and cross section ratio behavior. The maximum intensity transition energy is at 4.87 ± 0.06 eV with a Franck-Condon region from 4.4 eV to beyond 5.5 eV. Allinger et al.[31] calculate the second singlet → triplet to be at 4.70 eV. The similarity of the results to those in butadiene (see 6.1.1.2) permits assignment of this transition as the $\tilde{X}^1A_g \rightarrow 1\,^3A_g$.

The photochemical reactions of 1,3-pentadiene have been studied in the condensed phase using 4.89 eV light[36] and in the gas phase following energy transfer from mercury in the $^3P_1$ (4.89 eV) state.[37] In the condensed phase the light directly excites only the singlet excited state and the important reactions are trans → cis isomerization (Φ = 0.083), and 3-methylcyclobutene formation (Φ = 0.030). The cyclobutene formation is postulated[37] to be the only true primary photochemical reaction of the excited singlet state. In the gas phase Hg sensitized studies ring closure is also observed but the product is 1,3-dimethylcyclopropene (20% yield).[38] Cis-trans isomerization is also important in these gas phase studies. The state

which is initially excited in the Hg sensitized studies is presumably the $1\,^3A_g$ because of spin conservation rules and the very favorable spectral overlap. The reaction to give the dimethylcyclopropene is probably[37,38] a multistep process involving 1,3 diradical formation and then a 1,3 hydrogen migration.

6.1.2.3 The 1^1B_u State

The largest peak in the electron impact spectrum occurs at 5.80 ± 0.03 eV with a Franck-Condon region from below 5.0 eV to about 6.8 eV. The DCS behavior shown in Figures 33 and 34 is strongly forward peaked and confirms an assignment to the lowest fully allowed $\pi \rightarrow \pi^*$ singlet $\rightarrow$ singlet transition, the $\tilde{X}^1A_g \rightarrow 1\,^1B_u$. The peak location is in good agreement with optical spectroscopic studies which gave peak values of 5.80 eV,[39] 5.81 eV,[40] or 5.77 eV.[24] The peak location agrees closely with the 5.79 eV theoretical value of Allinger et al.[31]

6.1.2.4 Higher Energy Singlet $\rightarrow$ Singlet Transitions

In the spectrum show in Figure 31 a number of higher energy singlet $\rightarrow$ singlet transitions are apparent with peaks at 6.87 ± 0.04 eV, 7.06 ± 0.04 eV, 7.69 ± 0.04 eV, 7.92 ± 0.04 eV, 9.33 ± 0.1 eV, and 11.60 ± 0.1 eV. The first four peaks are very similar in appearance to Rydberg features in 1,3-butadiene between 7.6 and 8.7 eV. The

Table 6.1.2-1. Excited Electronic States of 1-trans-3-Pentadiene [a]

State	Peak	Franck-Condon region	Optical results	Theoretical Calculations [c]
$1\,^3B_u$	3.14 ± 0.05	2.5 → 4.0	2.57 (0-0 band) [b]	3.11
$1\,^3A_g$	4.87 ± 0.06	4.4 to beyond 5.2	–	4.70
$1\,^1B_u$	5.80 ± 0.03	below 5.0 to 6.8	5.80, [d] 5.81 [e]	5.79
Rydberg like in appearance	6.87 ± 0.04 7.06 ± 0.04 7.69 ± 0.04 7.92 ± 0.04		6.88 [f] 7.07, [g] 7.04 [h]	
Superexcited	9.33 ± 0.1			
Superexcited	11.60 ± 0.1			

[a] All values in eV. [b] Reference 32. [c] Reference 31. [d] Reference 39. [e] Reference 40. [f] Reference 24. [g] Reference 42. [h] Reference 39.

Table 6.1.2-2. DCS Values for 1-trans-3-Pentadiene [a]

θ (DEG)	Scattering Process [b] Elastic	$\tilde{X}^1A_g \rightarrow 1^3B_u$	$\tilde{X}^1A_g \rightarrow 1^3A_g$	$\tilde{X}^1A_g \rightarrow 1^1B_u$
		30 eV		
10	–	0.00115	–	0.298
20	2.98	0.000824	–	0.165
30	1.43	0.000842	0.00190	0.0912
40	1.00	0.00123	0.00189	0.0707
50	0.829	0.00151	0.00127	0.0315
60	0.602	0.00234	0.00212	0.0511
70	0.481	0.00252	0.00154	0.0301
80	0.507	0.00231	0.00175	0.0250
		55 eV		
10	–	0.000321	–	0.938
20	2.75	0.000596	–	0.359
30	1.35	0.000934	0.00149	0.164
40	1.00	0.00138	0.00132	0.109
50	0.634	0.00111	0.00111	0.0682
60	0.388	0.000744	0.000886	0.0440
70	0.365	0.000816	0.000959	0.0409
80	0.188	0.000465	0.000557	0.0219

[a] The fitting of the $\tilde{X}^1A_g \rightarrow 1^1B_u$ DCS from the direct and indirect methods was performed at 30°. [b] The symmetry designations are for an idealized C_{2h} symmetry polyene.

Figure Captions

Figure 29. The electron energy-loss spectrum of 1-trans-3-pentadiene from 2 eV to 10 eV energy loss for 30 eV incident energy, 10° scattering angle, 7.0×10^{-8} amperes (A) incident electron current (I), $P_{ind} = 6.6 \times 10^{-3}$ torr, and 0.17 eV resolution (FWHM).

Figure 30. The 2 eV to 10 eV energy loss spectrum of pentadiene for $E_0 = 30$ eV, $\theta = 60°$, $I = 1.05 \times 10^{-7}$ A, $P_{ind} = 6.0 \times 10^{-3}$ torr, and a resolution of 0.15 eV (FWHM).

Figure 31. The pentadiene energy-loss spectrum from 5 eV to 14 eV for $E_0 = 75$ eV, $\theta = 10°$, $P_{ind} = 1.2 \times 10^{-2}$ torr, and a resolution of 0.17 eV (FWHM).

Figure 32. Ratios of intensities I of the $\tilde{X}^1A_g \rightarrow 1^3B_u$ and $\tilde{X}^1A_g \rightarrow 1^3A_g$ transitions to that of the $\tilde{X}^1A_g \rightarrow 1^1B_u$. The excited states for the curves shown are 1^3B_u (+) at 30 eV, 1^3B_u (○) at 55 eV, 1^3A_g (Δ) at 30 eV, and 1^3A_g (□).

Figure 33. DCS curves as a function of θ at an incident electron energy of 30 eV for elastic scattering (+) and for transitions to the following excited states: 1^3B_u (Δ), 1^3A_g (○), and the 1^1B_u (□).

Figure 34. Same as Figure 33 for an incident electron energy of 55 eV.

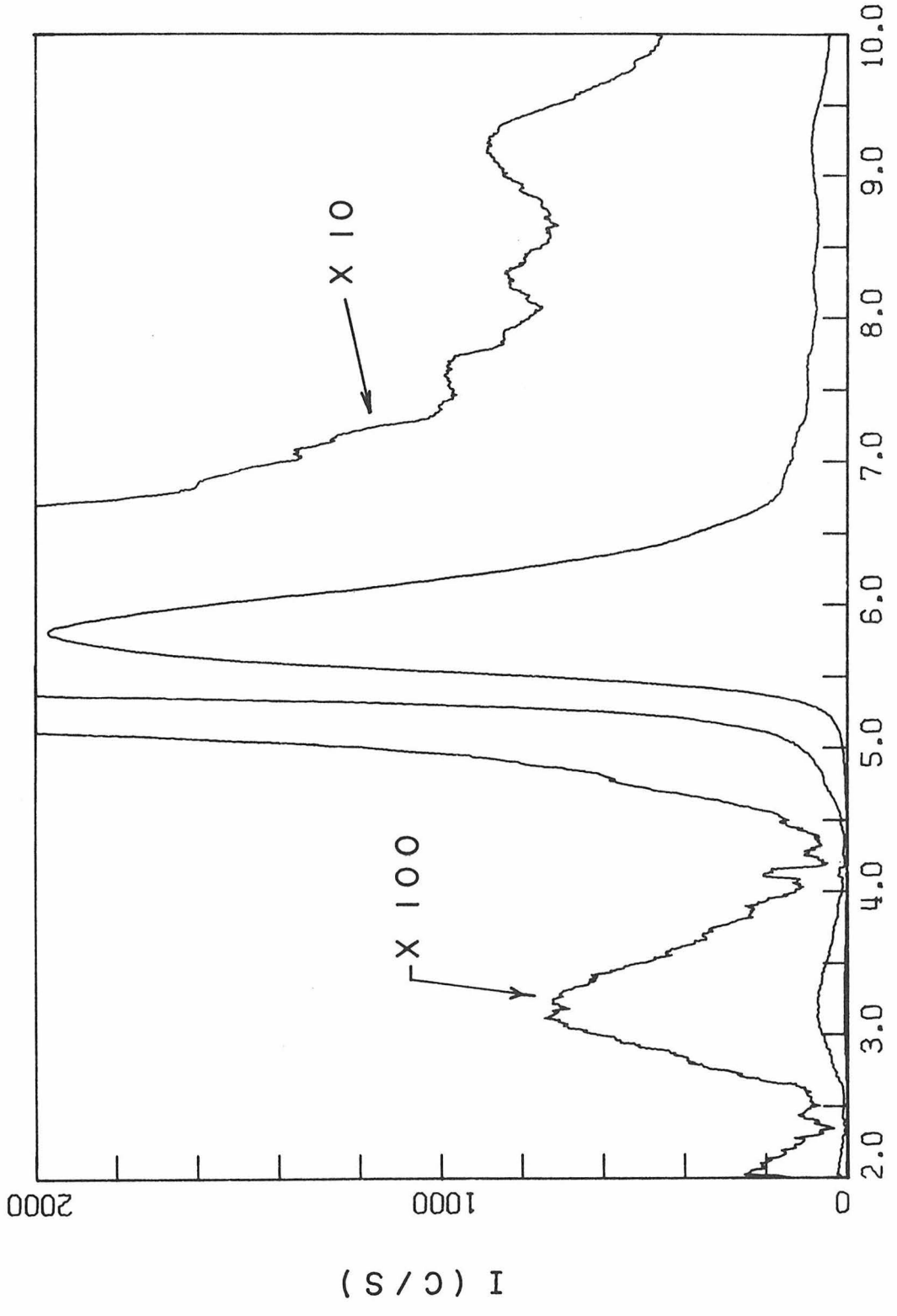

FIG. 29

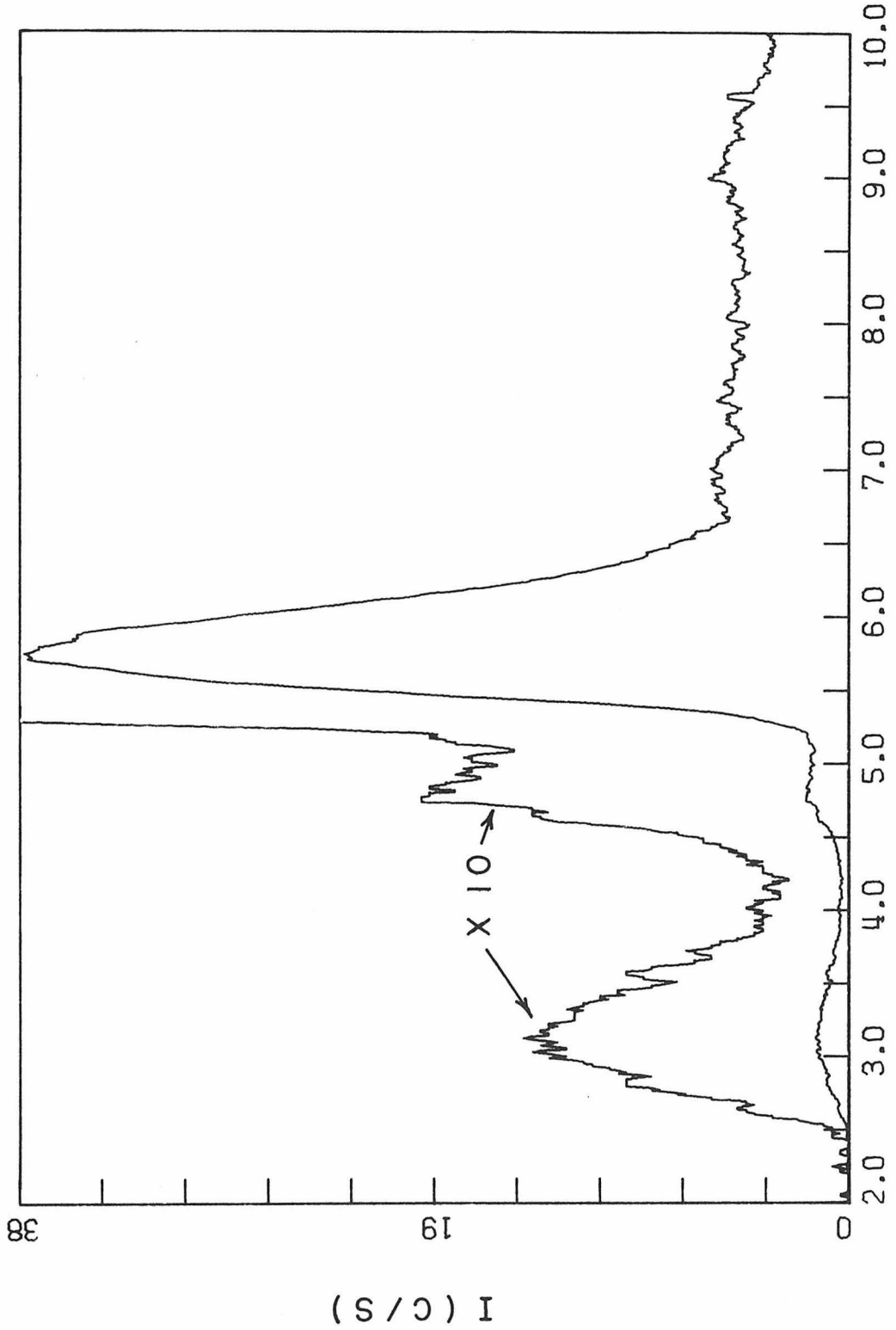

FIG. 30

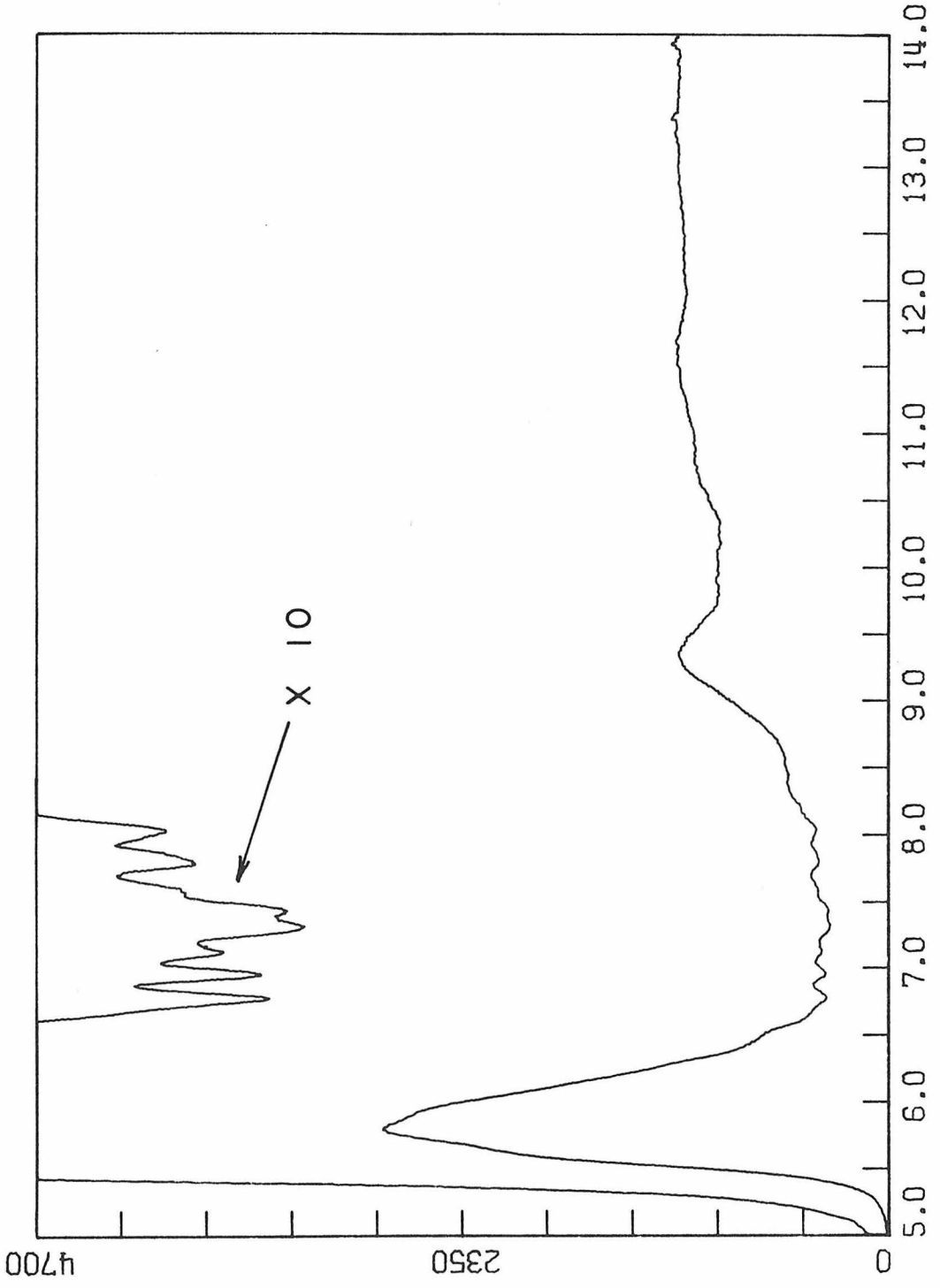

FIG. 31

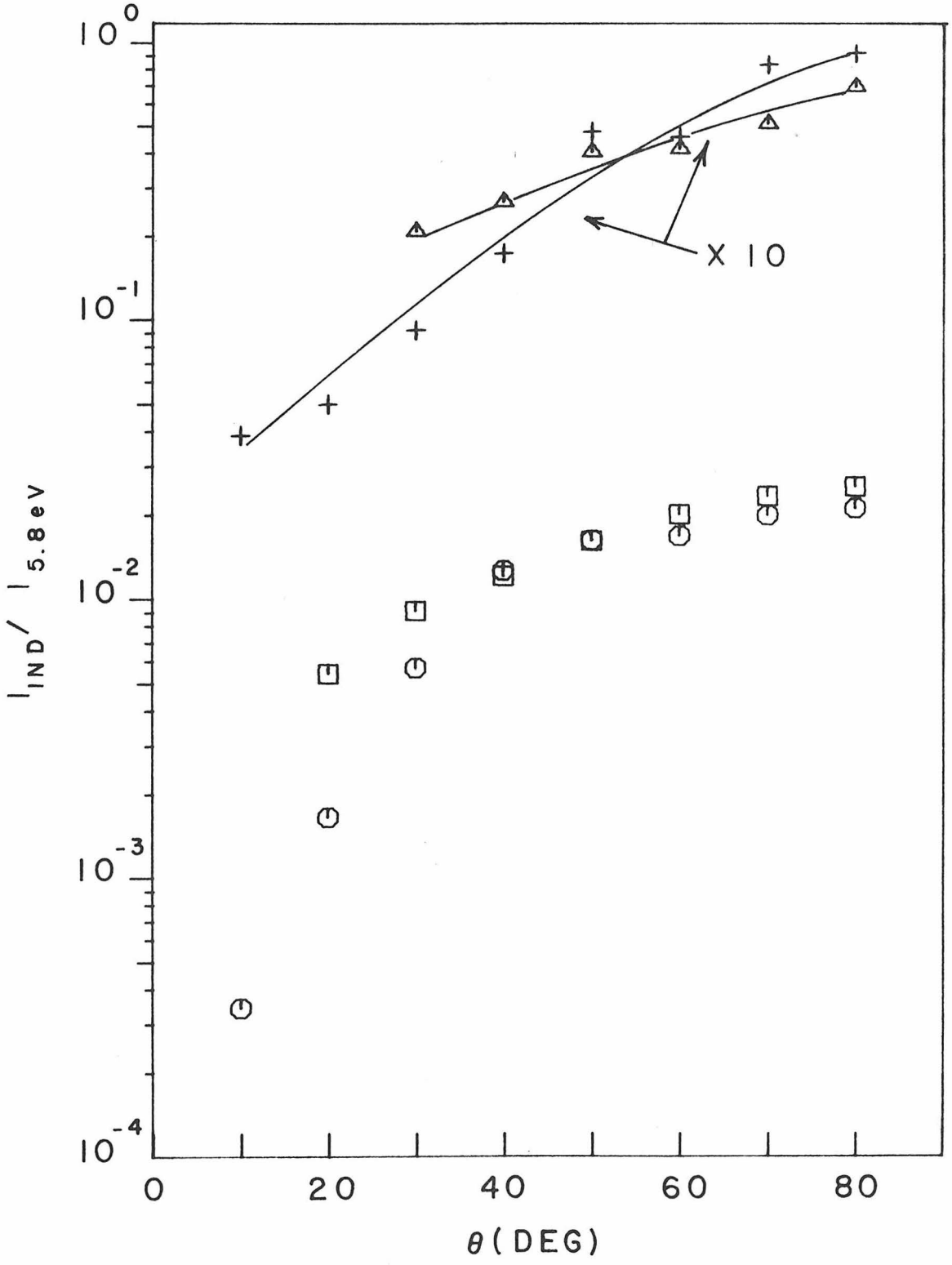

FIGURE 32

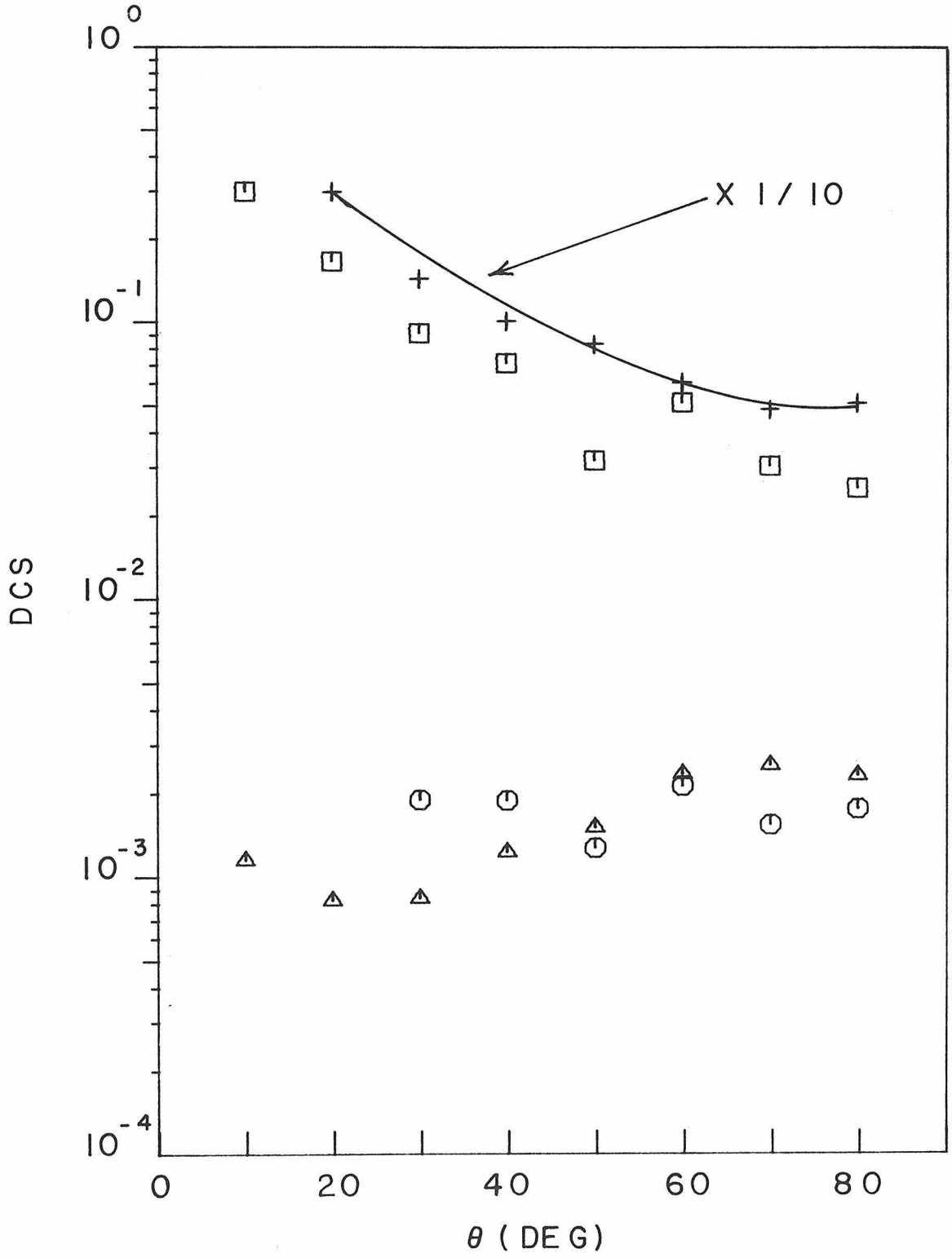

FIGURE 33

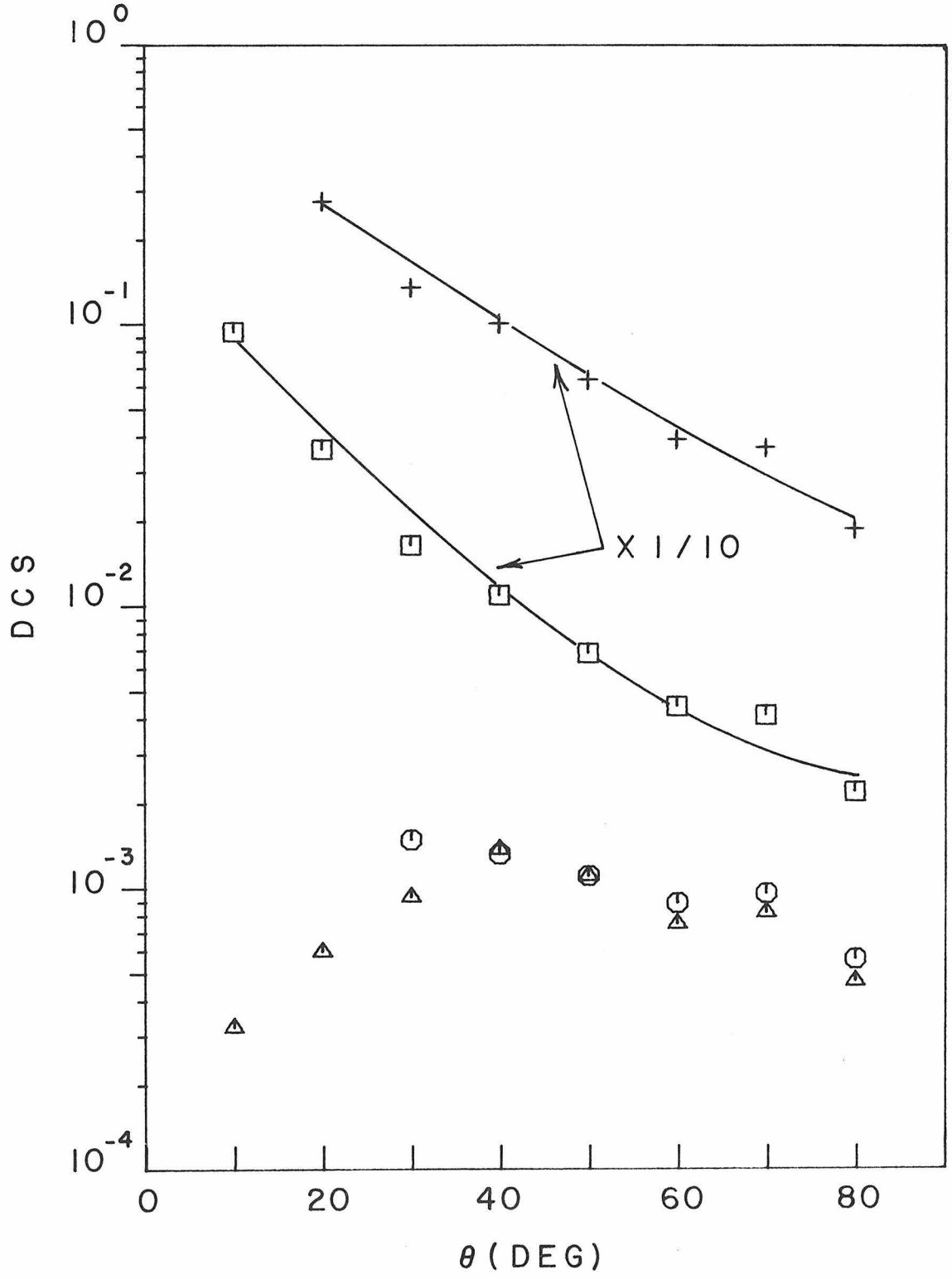

FIGURE 34

two broad absorption features at 9.33 and 11.60 may correlate with the peaks at 9.53 eV and 11.04 eV in 1,3-butadiene. Both peaks are beyond the first ionization energy of pentadiene (8.68 eV)[41] and are thus superexcited states.

6.1.3. Cis and Trans 1,3-Hexadiene

Electron impact spectra of an isomeric mixture of cis and trans 1,3-hexadiene were obtained at impact energies of 25 eV and 45 eV. The spectra, as shown in Figures 35 to 37, are similar to those of butadiene and pentadiene. The peak locations reported here are apparently the first published values for these states. A survey of the literature did not reveal any previous studies of the electronic excited states in this molecule. The cross section ratios are plotted in Figure 38 in the same way as they were for pentadiene. Figures 39 and 40 display the DCS curves. Table 6.1.3-1 summarizes the following discussion and the peak locations while Table 6.1.3-2 lists the DCS values.

The 1,3-hexadiene sample was obtained from the Aldrich Chemical Co. The stated purity was 99% with respect to other chemical compounds but it was a combination of the cis and trans forms of 1,3-hexadiene. The sample was subjected to the usual freeze-pump-thaw cycles prior to its use.

6.1.3.1 The $1\,^3B_u$ State

The lowest peak occurs at 3.20 ± 0.05 eV with a Franck-Condon region from about 2.5 eV to 4.1 eV. The DCS curves in Figures 39 and 40 confirm the singlet→triplet nature of this transition. The similarity of the results to those in butadiene permit assignment of this band to the $\tilde{X}^1A_g \rightarrow 1\,^3B_u$ transition.

6.1.3.2 The $1\,^3A_g$ State

The second peak in the spectrum, as shown in Figure 36, occurs at 4.93 ± 0.05 eV. The DCS curves show that this is a singlet→triplet transition and comparison with butadiene indicates that this is the $\tilde{X}^1A_g \rightarrow 1\,^3A_g$ transition.

The vapor phase Hg ($^3P_1$) sensitized photochemistry of 1,3-hexadiene has been studied.[38] The principal reaction is isomerization to the 2,4-hexadienes (cis-cis, cis-trans, and trans-trans). A minor process is the ring closure analogous to that seen in butadiene and pentadiene.[37,38] The products in the 1,3-hexadiene experiment are 1-methyl-3-ethylcyclopropene and 1-ethyl-3-methylcyclopropene. The initial excited state is presumably the $1\,^3A_g$ but the reactions may actually occur from the lower triplet or even the ground state singlet.

Figure Captions

Figure 35. The electron energy-loss spectrum of 1,3-hexadiene from 2.3 eV to 8.0 eV for E_0 = 45 eV, $\theta = 20°$, $P_{ind} = 4.6 \times 10^{-3}$ torr, and a resolution of 0.14 eV (FWHM).

Figure 36. The electron energy loss spectrum of 1,3-hexadiene from 2.3 eV to 7.5 eV for E = 45 eV, $\theta = 80°$, $P_{ind} = 4.6 \times 10^{-3}$ torr and a resolution of 0.16 eV.

Figure 37. The 5 eV to 13 eV energy-loss region of 1,3-hexadiene for E_0 = 45 eV, $\theta = 4°$, and $P_{ind} = 4.6 \times 10^{-3}$ torr.

Figure 38. Ratios of the indicated intensity I to that of the $\tilde{X}^1A_g \rightarrow 1^1B_u$ transition as a function of scattering angle θ. The excited states and impact energies for the curves shown are 1^3B_u (+) at 25 eV, 1^3B_u (○) at 45 eV, 1^3A_g (△) at 25 eV, and 1^3A_g (□) at 45 eV.

Figure 39. DCS curves as a function of θ at an incident electron energy of 25 eV for elastic scattering (+) and for transitions to the following excited states: 1^3B_u (△), 1^3A_g (○), and the 1^1B_u (□).

Figure 40. Same as Figure 39 for an incident electron energy of 45 eV.

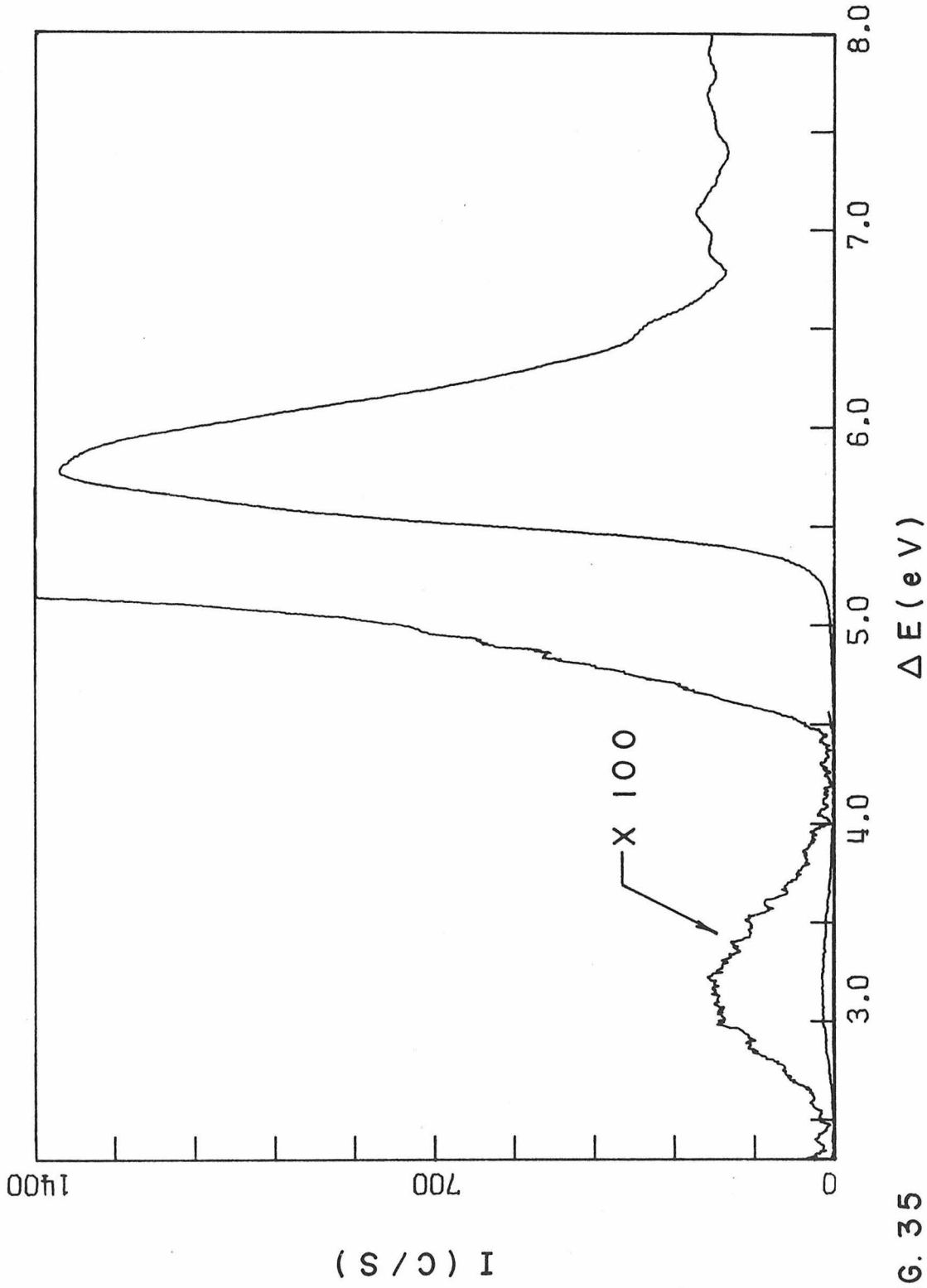

FIG. 35

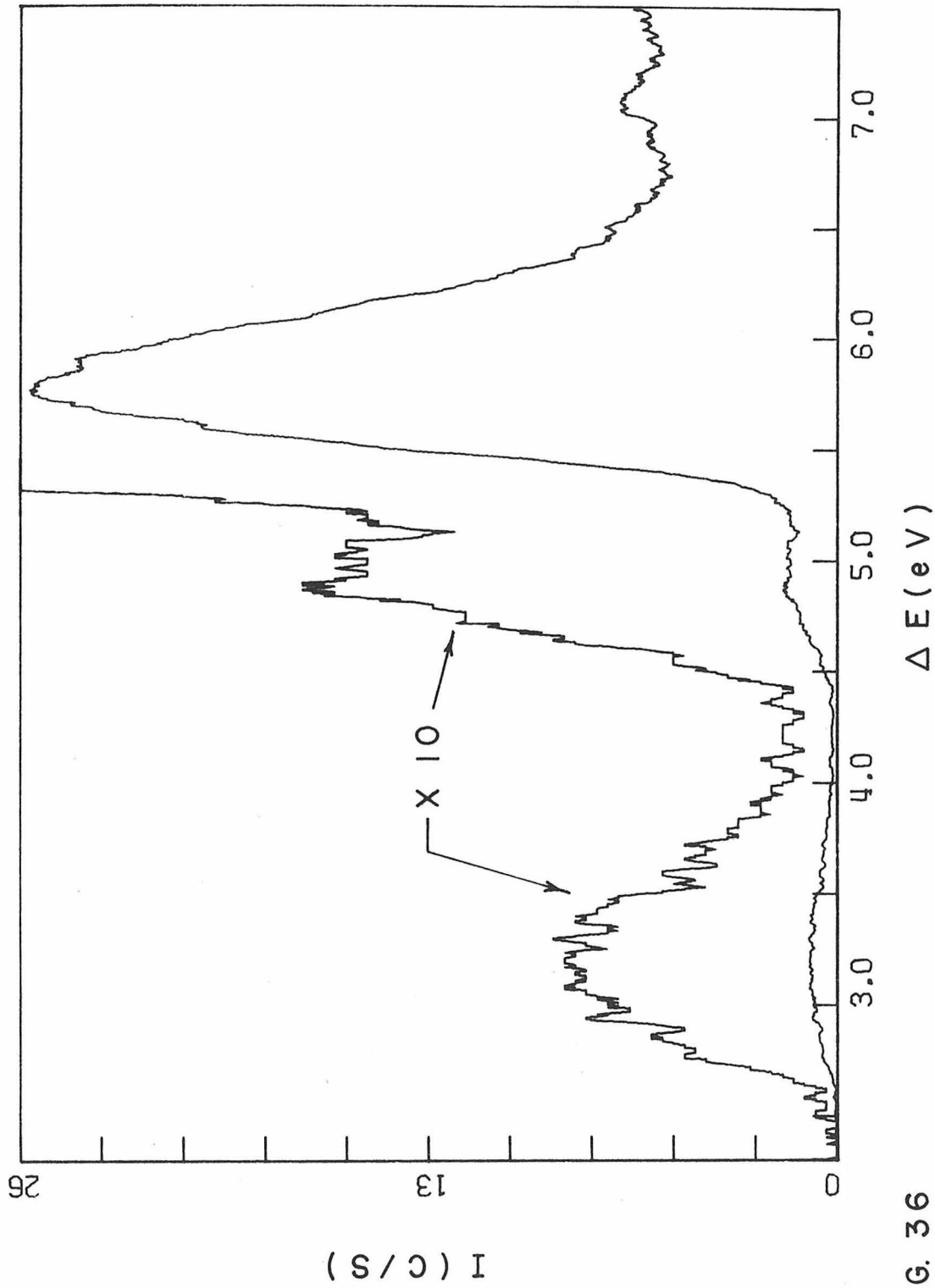

FIG. 36

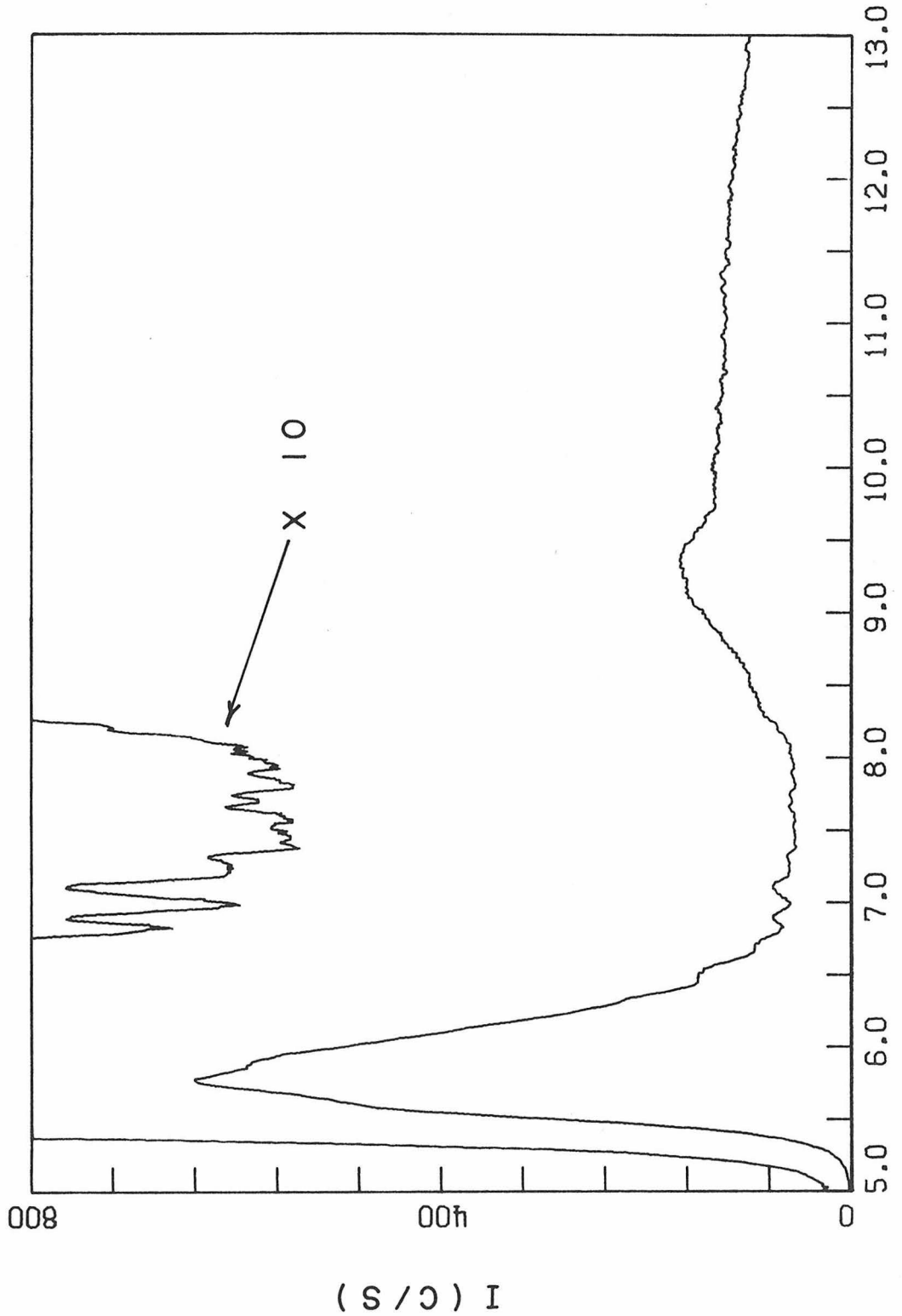

FIG. 37

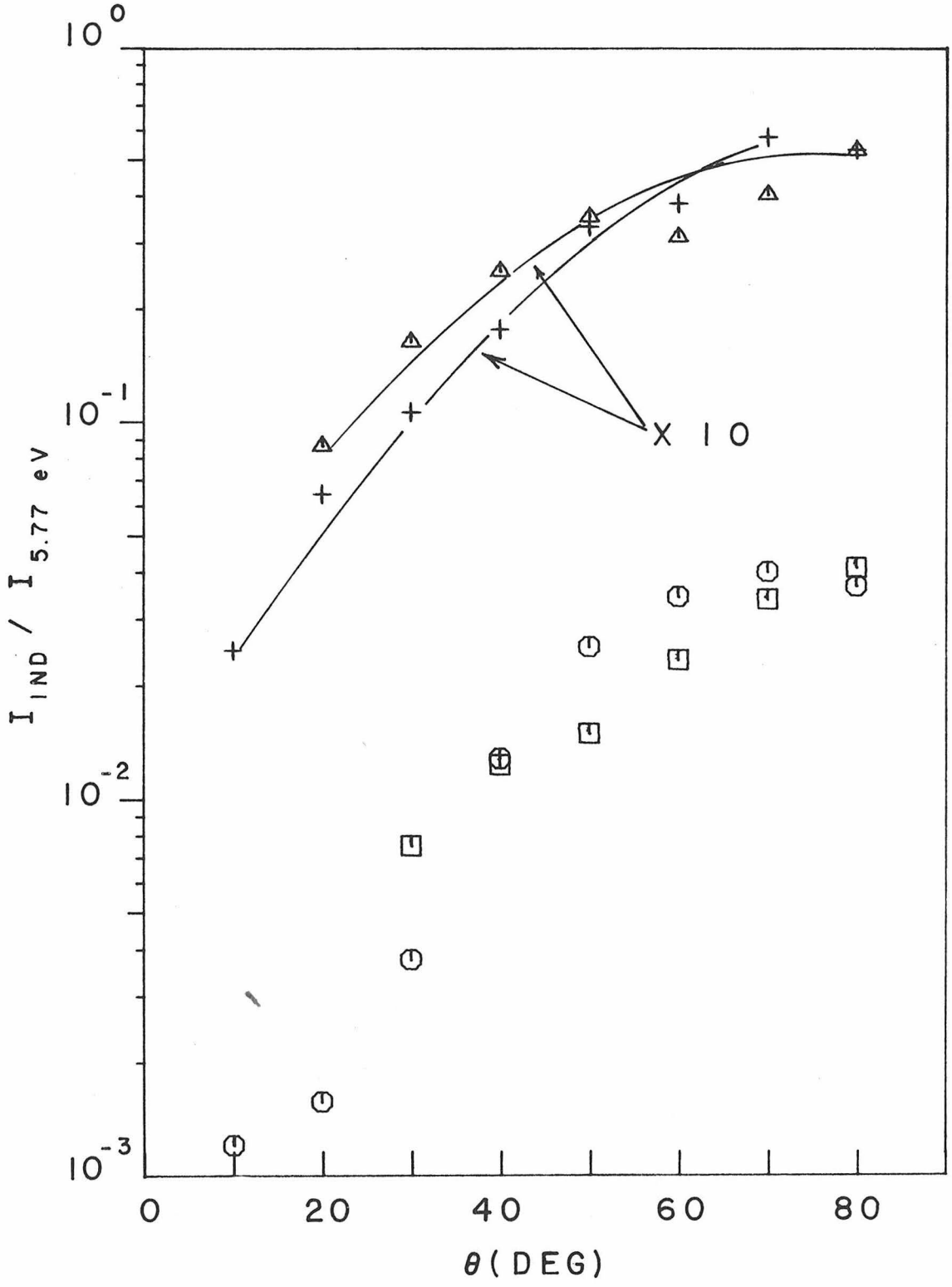

FIGURE 3 8

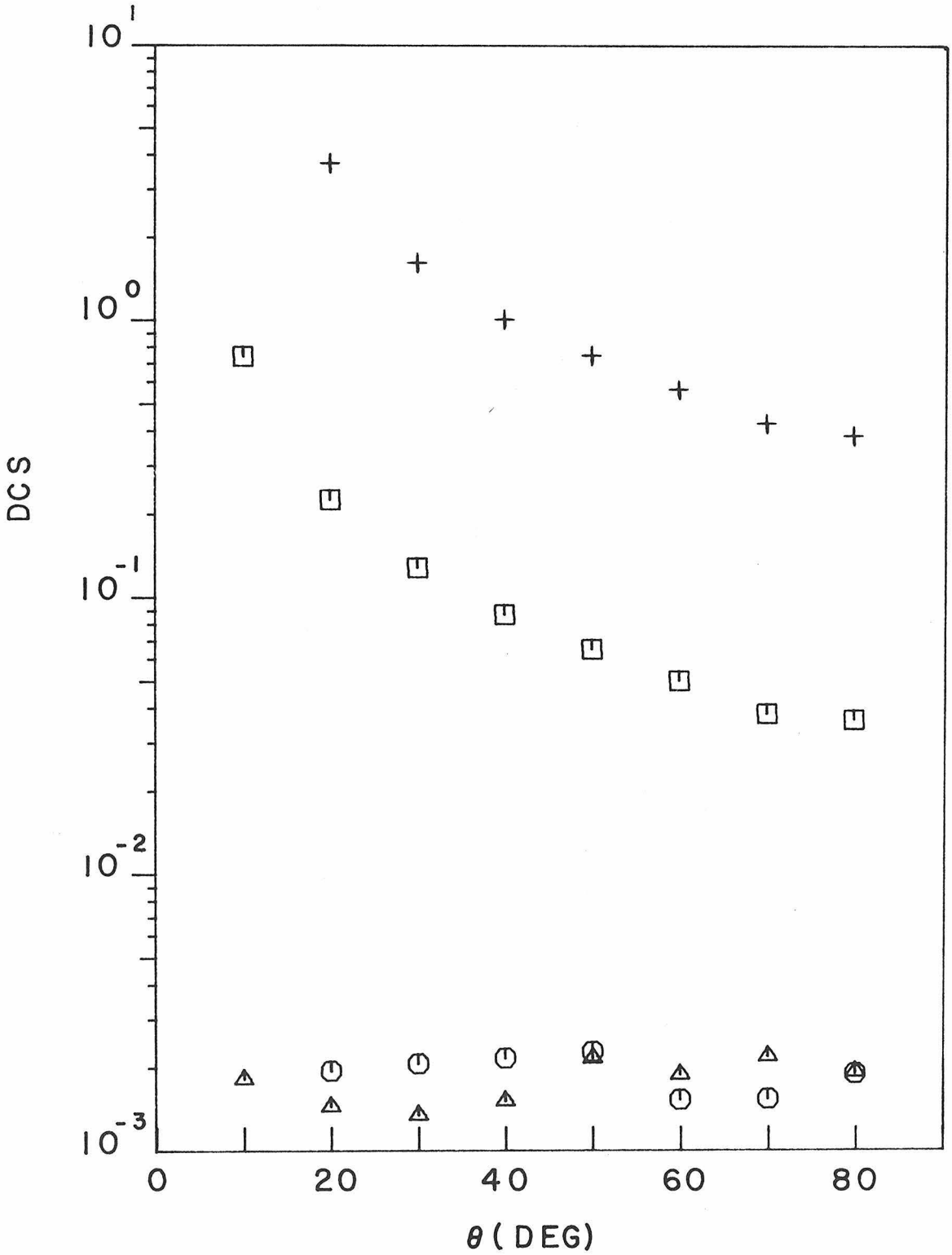

FIGURE 39

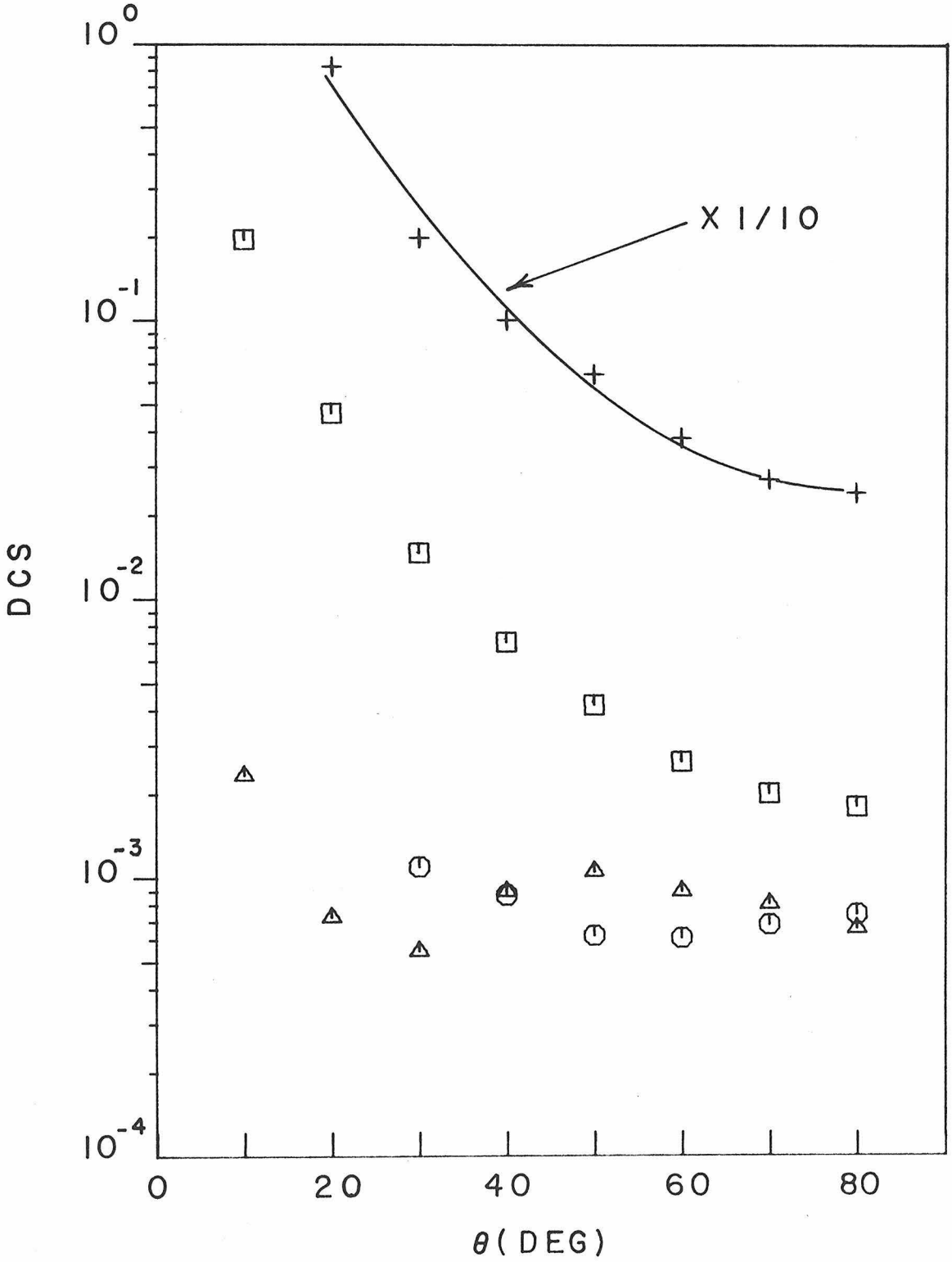

FIGURE 40

Table 6.1.3-1. Excited Electronic States of a Mixture of cis and trans 1,3-Hexadiene [a]

State [b]	Peak location	Franck-Condon region
$1\,^3B_u$	3.20 ± 0.05	2.5 eV to 4.1 eV
$1\,^3A_g$	4.93 ± 0.05	4.4 eV to beyond 5.2 eV
$1\,^1B_u$	5.77 ± 0.05	Below 5.0 eV to 6.9 eV
Rydberg like	6.90 ± 0.03	
in appearance	7.09 ± 0.03	
	7.29 ± 0.03	
	7.69 ± 0.05	
Super excited	9.3 ± 0.1	

[a] All values in eV.

[b] The symmetry designations are for an idealized C_{2h} symmetry polyene.

Table 6.1.3-2. DCS Values for 1,3-Hexadiene (isomeric mixture)

	Scattering Process [a]			
θ	$\tilde{X}^1A_g \rightarrow 1^3B_u$	$\tilde{X}^1A_g \rightarrow 1^3A_g$	$\tilde{X}^1A_g \rightarrow 1^1B_u$	Elastic
		25 eV		
10	0.00183	–	0.743	–
20	0.00145	0.00195	0.226	3.72
30	0.00135	0.00207	0.128	1.61
40	0.00152	0.00217	0.0866	1.00
50	0.00216	0.00229	0.0652	0.737
60	0.00189	0.00153	0.0496	0.558
70	0.00220	0.00154	0.0384	0.420
80	0.00193	0.00190	0.0363	0.383
		55 eV		
10	0.00235 [b]	–	1.958	–
20	0.000729	–	0.465	8.27
30	0.000549	0.00110	0.147	1.99
40	0.000900	0.000869	0.0705	1.00
50	0.00106	0.000624	0.0419	0.640
60	0.000899	0.000610	0.0262	0.378
70	0.000808	0.000681	0.0202	0.274
80	0.000659	0.000738	0.0180	0.244

[a] The symmetry designations are for an idealized C_{2h} symmetry polyene.

[b] Reliability is not certain. See discussion in 5.10.

6.1.3.3 The $1\,^1B_u$ State

The most intense feature in the spectrum is the peak at 5.77 ± 0.05 eV. The intensity and the sharply forward peaked DCS for this transition indicate that it is a fully allowed singlet→singlet transition. The similarity with the butadiene and pentadiene spectra show that this the the $\tilde{X}^1A_g \rightarrow 1\,^1B_u$ transition.

6.1.3.4 Higher Energy Singlet→Singlet Transitions

A number of narrow weak peaks are seen in Figure 37 in the energy-loss region between 6.8 eV and 8.0 eV. Peaks are seen at 6.90 ± 0.03 eV, 7.09 ± 0.03 eV, 7.29 ± 0.03, and 7.69 ± 0.05 eV. The features are similar in appearance to the Rydberg peaks in butadiene.

A broad absorption peak at 9.3 ± 0.1 eV is again quite similar to the peaks in butadiene and pentadiene at 9.53 eV and 9.33 eV, respectively. It presumably is a transition to a superexcited state.

6.1.4. Cis-2, trans-4-Hexadiene

Figures 41 to 43 show some representative spectra of cis-2, trans-4-hexadiene. (This will be called 2, 4-hexadiene in the following discussion.) Other spectra were obtained at both 25 eV and 45 eV over the range of scattering angles from 10° to 80°. Figure 44 displays the cross section ratios while Figures 45 and 46 show the

DCS curves. The discussion below is summarized in Table 6.1.4-1 and the numerical listing of the DCS values is in Table 6.1.4-2.

The sample of cis-2, trans-4-hexadiene was obtained from the Aldrich Chemical Co. with a stated purity of 99%. The usual liquid nitrogen freeze-pump-thaw preparation procedure was followed.

6.1.4.1 The $1\,^3B_u$ State

The lowest electronic transition in 2, 4-hexadiene produces the peak at 3.11 ± 0.04 eV as shown in Figures 41 to 43. The cross section ratio behavior and the DCS curves show that this is a singlet → triplet transition. The similarity to the butadiene spectrum indicates that this is the $\tilde{X}^1A_g \rightarrow 1\,^3B_u$ transition. The peak location is in good agreement with the theoretical value (3.08 eV) of Allinger et al.[31] for this transition in trans-2, trans-4-hexadiene. The Franck-Condon region for this transition is between 2.45 eV and 4.0 eV. The excitation onset energy is in fair agreement with the position of the 0-0 band peak (2.55 eV) in the oxygen induced optical absorption studies.[32] The isomeric composition of the "2, 4-hexadiene" sample used in the optical absorption study was not specified.

6.1.4.2 The $1\,^3A_g$ State

A shoulder is seen in Figure 42 at about 4.85 ± 0.1 eV. Because the $\tilde{X}^1A_g \rightarrow 1\,^1B_u$ transition is at a lower energy than it was in

butadiene (the peak is at 5.69 eV instead of 5.92 eV), the singlet → singlet transition overlaps strongly with the 4.85 eV feature even at low impact energies and large scattering angles. Thus it is not possible to give an accurate peak location. The DCS curves for this shoulder, however, show that it is the second singlet → triplet transition and a comparison with the other polyenes indicates that this is the $\tilde{X}^1A_g \rightarrow 1^3A_g$ transition. The Franck-Condon region is from 4.35 eV to beyond 5.1 eV.

6.1.4.3 The 1^1B_u and Higher Singlet States

The strongest transition in 2, 4-hexadiene produces the peak at 5.69 ± 0.03 eV. The strongly forward peaked DCS curves confirm the earlier assignment by Mulliken[23] of this transition as the $\tilde{X}^1A_g \rightarrow 1^1B_u$. The peak location is also in good agreement with the 5.70 eV value from the most recent optical absorption study.[40]

A weak singlet → singlet transition is observable in Figures 41 and 43 at 6.78 ± 0.04 eV. This peak is also seen optically at about 6.75 eV.[26] Transitions to super excited states are seen at 9.13 ± 0.05 eV, 9.78 ± 0.05 eV, and 10.85 ± 0.05 eV.

Figure Captions

Figure 41. The electron impact spectrum of cis-2, trans-4-hexadiene from 2.5 eV to 6.5 eV energy loss for E_0 = 45 eV, θ = 10°, P_{ind} = 4.8×10 torr, $I = 6.4 \times 10^{-8}$ A, and a resolution of 0.17 eV (FWHM).

Figure 42. Same as Figure 41 except for θ = 60°, $P_{ind} = 5.6 \times 10^{-3}$ torr, $I = 6.0 \times 10^{-8}$ A, and a resolution of 0.14 eV.

Figure 43. The 4 eV to 12 eV energy-loss spectrum of cis-2, trans-4-hexadiene for E_0 = 45 eV, θ = 20°, $P_{ind} = 3.9 \times 10^{-3}$ torr, $I = 6.8 \times 10^{-8}$ A, and a resolution of 0.16 eV.

Figure 44. Ratios of the indicated intensity I to that of the $\tilde{X}^1A_g \rightarrow 1^1B_u$ transition as a function of scattering angle θ. The excited states for the curves shown are 1^3B_u (+) at 25 eV, 1^3B_u (○) at 45 eV, 1^3A_g (△) at 25 eV, and 1^3A_g (□) at 45 eV.

Figure 45. DCS curves for cis-2, trans-4-hexadiene as a function of θ at an incident electron energy of 25 eV for elastic scattering (+) and for transitions to the following excited states. 1^3B_u (△), 1^3A_g (○), and the 1^1B_u (□).

Figure 46. Same as Figure 45 for an incident energy of 45 eV.

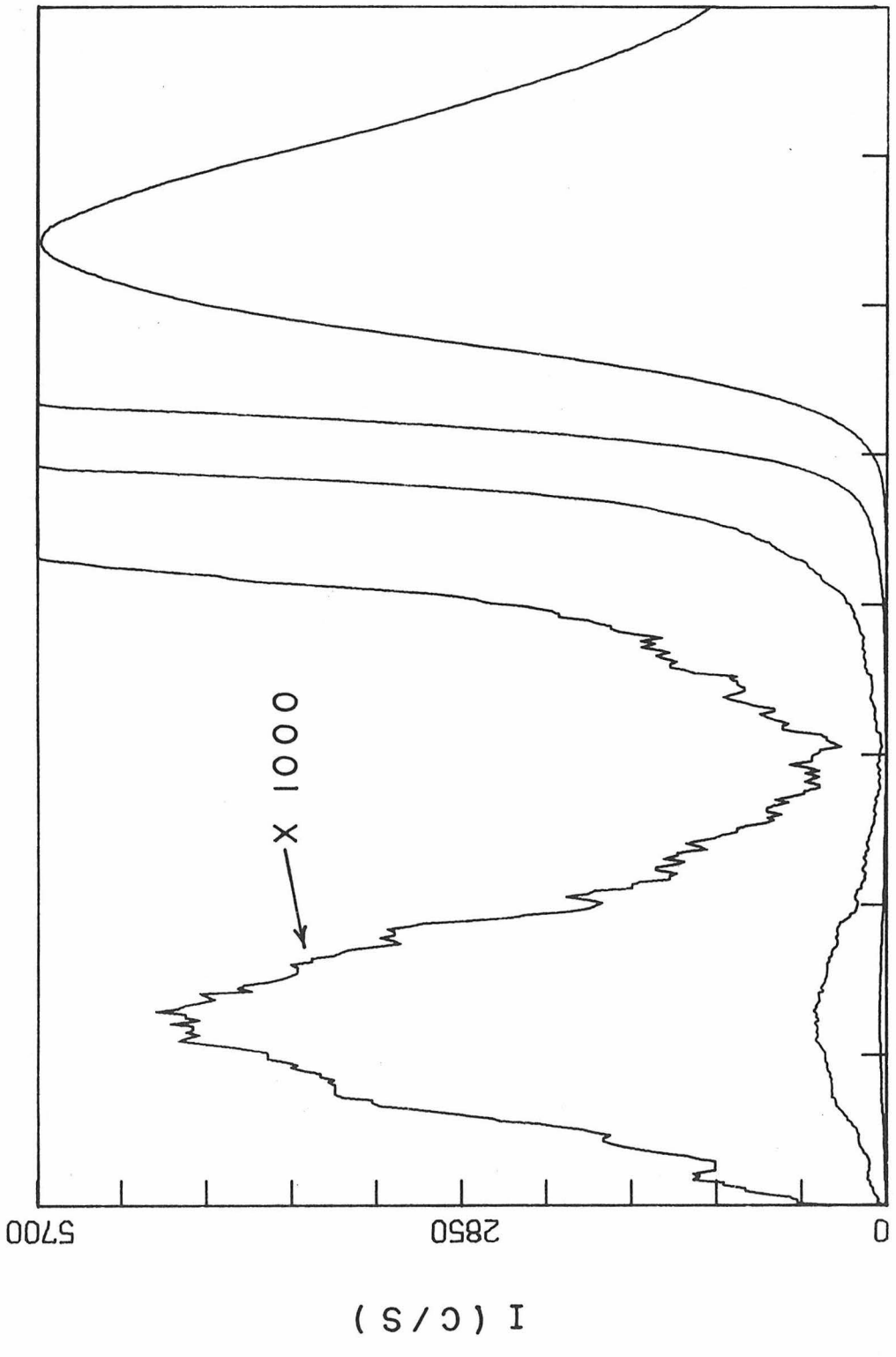

FIG.41

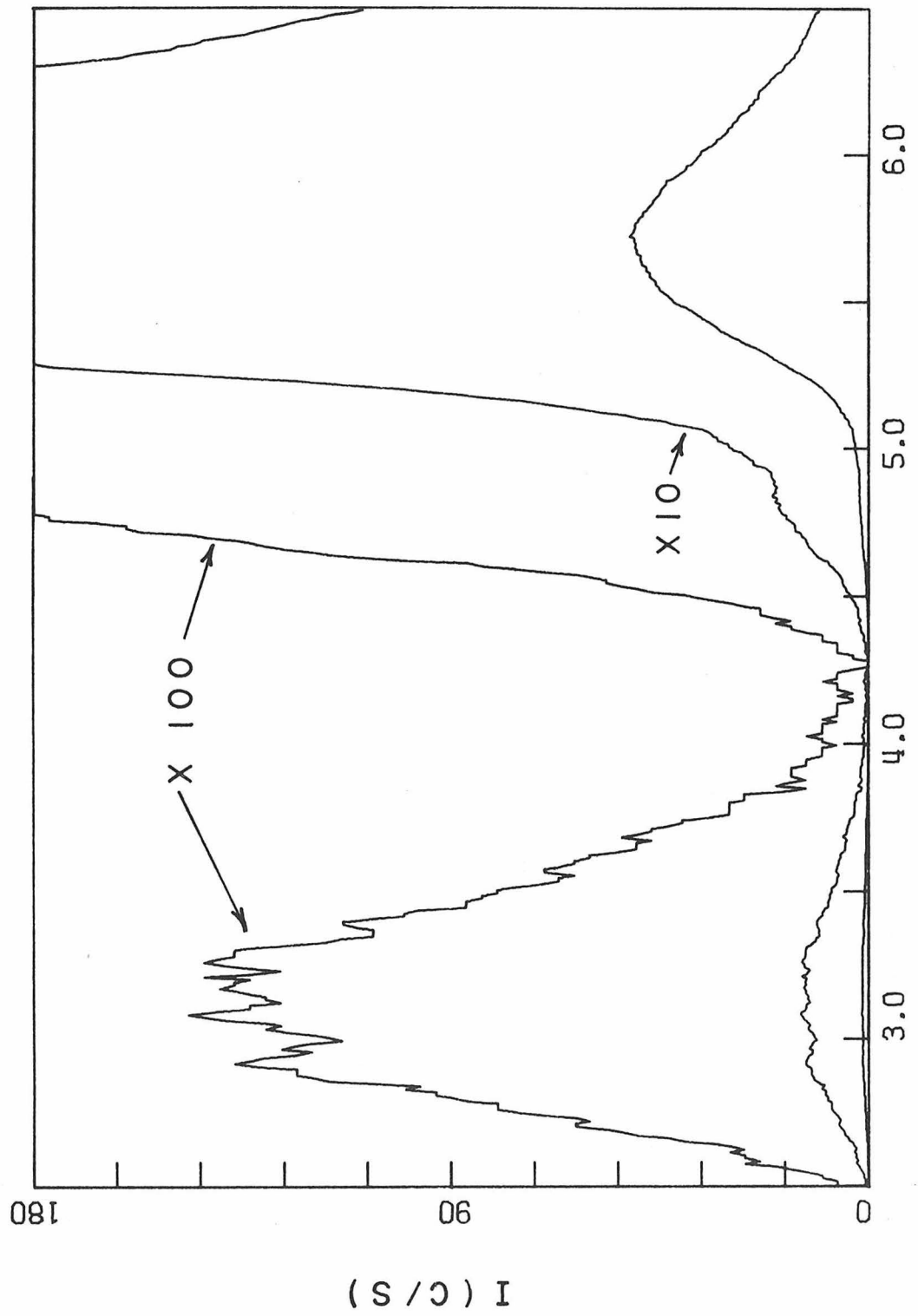

FIG.42

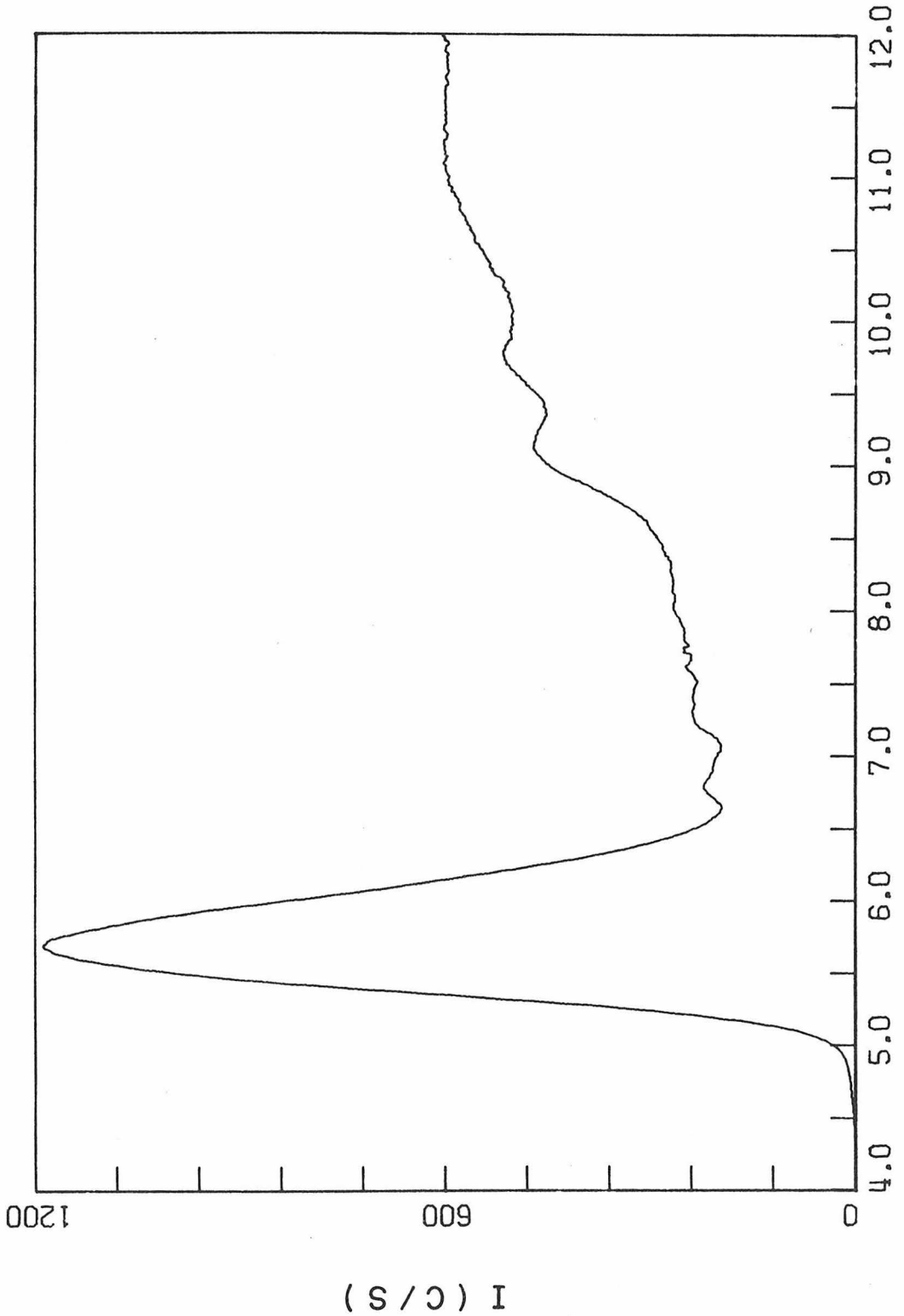

FIG. 43

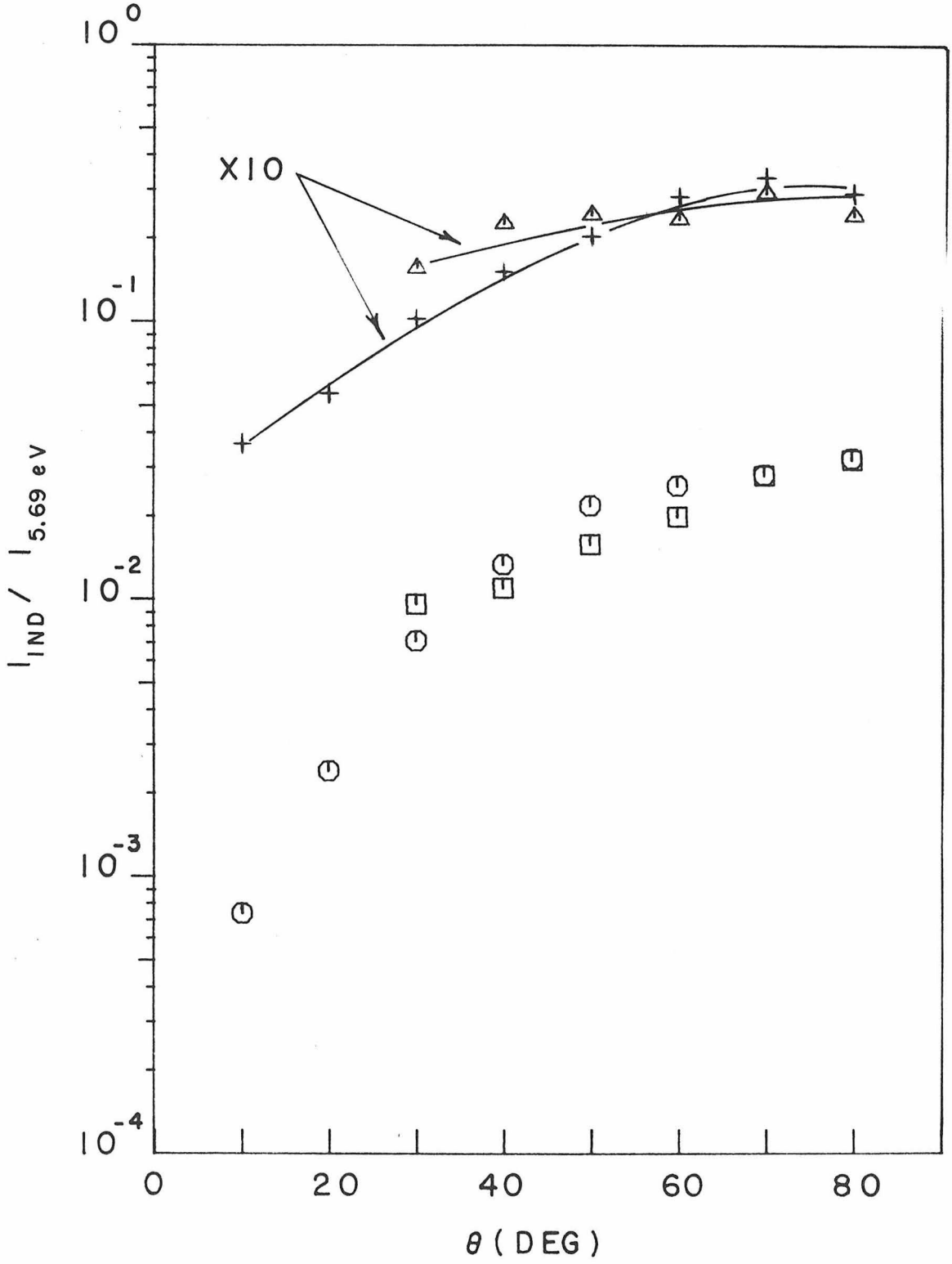

FIGURE 44

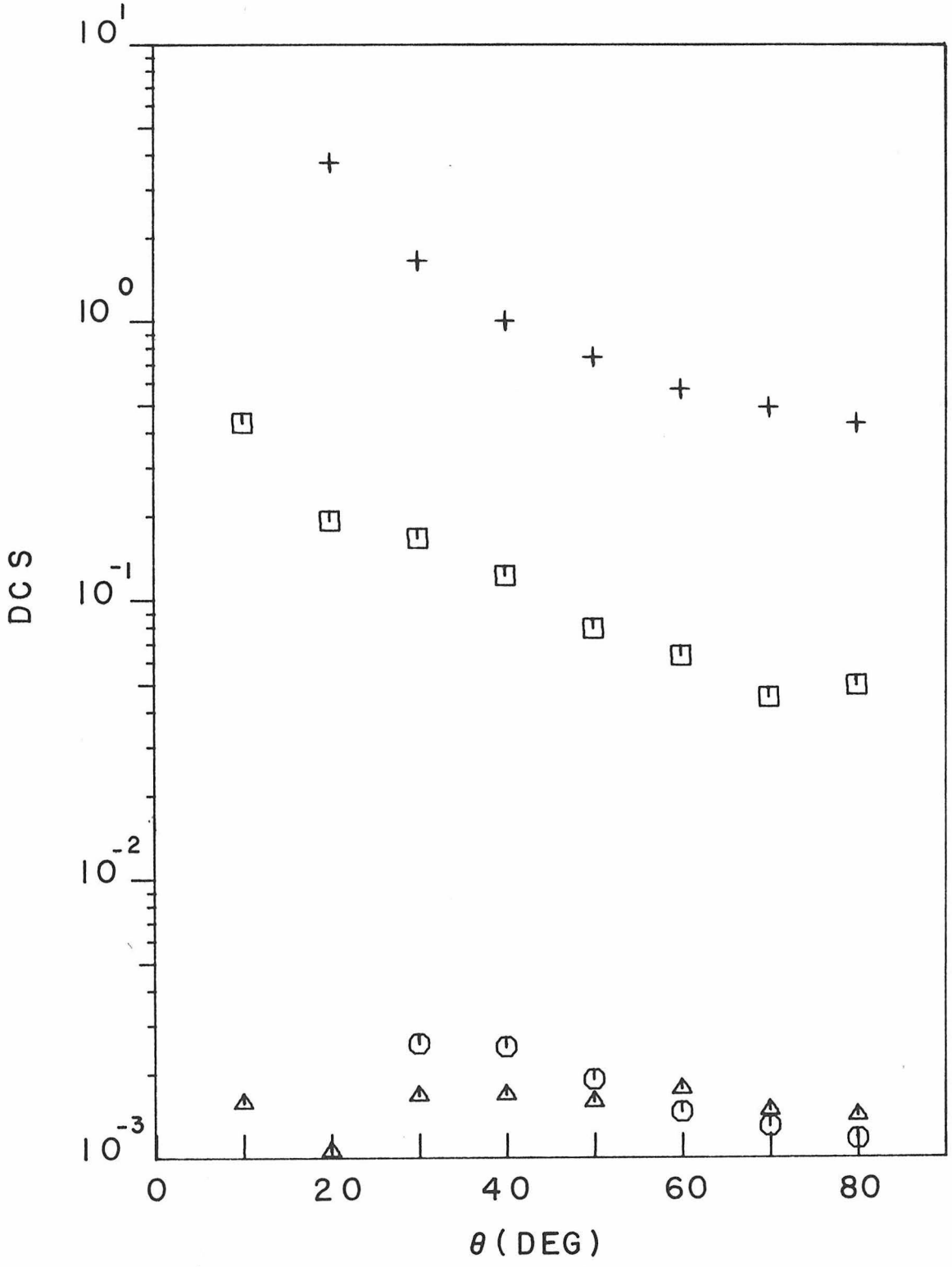

FIGURE 45

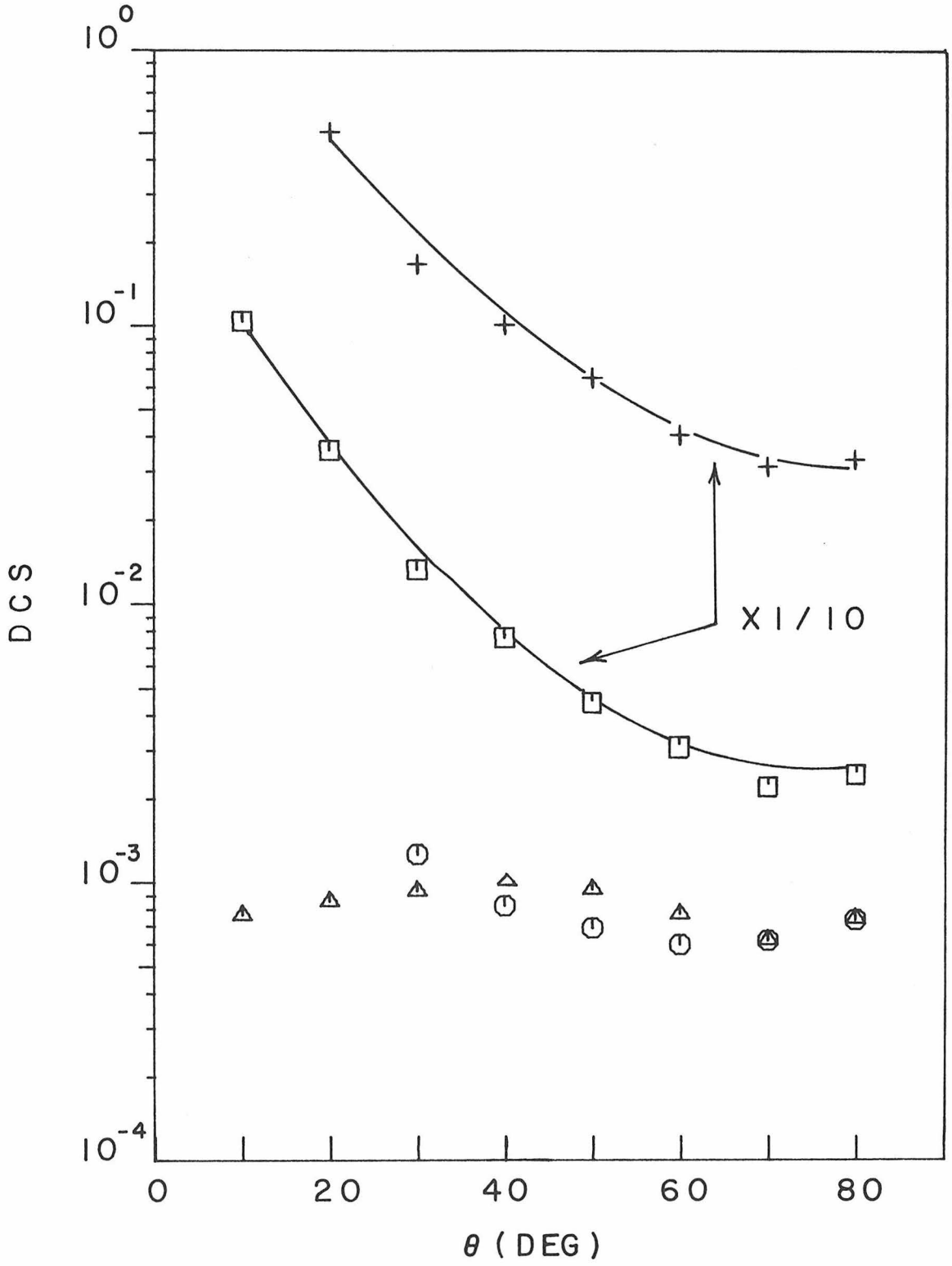

FIGURE 46

Table 6.1.4-1. Excited Electronic States of cis-2-trans-4-Hexadiene [a]

State [b]	Peak location	Franck-Condon region	Theoretical values	Optical values
$1\,^3B_u$	3.11 ± 0.04	2.45 → 4.0	3.08 [c]	2.55 (0-0 band) [d]
$1\,^3A_g$	4.85 ± 0.1 [g]	4.35 to beyond 5.1	4.62 [c]	–
$1\,^1B_u$	5.69 ± 0.03	Below 4.8 to 6.7	5.71 [c]	5.70 [e]
Singlet	6.78 ± 0.04			6.75 [f]
Super excited	9.13 ± 0.05 9.78 ± 0.05 10.85 ± 0.05			

[a] All values in eV. [b] Symmetry designations are for a C_{2h} symmetry polyene. [c] Reference 31 for trans-2, trans-4-hexadiene. [d] Reference 32 for a 2, 4-hexadiene of unspecified isomeric composition. [e] Reference 40. [f] Reference 26. [g] Seen as a shoulder only in all spectra.

Table 6.1.4-2. DCS Values for cis-2-trans-4-Hexadiene

	Scattering Process [a]			
θ	$X^1A_g \rightarrow 1^3B_u$	$X^1A_g \rightarrow 1^3A_g$	$X^1A_g \rightarrow 1^1B_u$	Elastic
		25 eV		
10	0.00157	–	0.432	–
20	0.00106	–	0.193	3.729
30	0.00168	0.00257	0.166	1.649
40	0.00169	0.00251	0.112	1.00
50	0.00159	0.00191	0.0794	0.74
60	0.00177	0.00146	0.0631	0.573
70	0.00148	0.00130	0.0451	0.488
80	0.00141	0.00117	0.0496	0.434
		45 eV		
10	0.000764	–	1.04	–
20	0.000856	–	0.355	5.045
30	0.000936	0.00126	0.132	1.668
40	0.00100	0.000824	0.0754	1.00
50	0.000943	0.000687	0.0437	0.645
60	0.000772	0.000597	0.0304	0.403
70	0.000621	0.000616	0.0225	0.310
80	0.000742	0.000734	0.0235	0.328

[a] The symmetry designations are for an idealized C_{2h} symmetry polyene.

6.1.5 1,3-Cyclohexadiene

1,3-Cyclohexadiene has been the subject of many photochemical studies because its reactions are typical of those seen in the Vitamin D system. Photolysis of 1,3-cyclohexadiene with uv light in the gas phase[43,44] leads to 1,3,5-hexatriene, benzene, H_2, and other products. Photolysis of 1,3,5-hexatriene also gives these products.[44] Similar interconversions among 1,3-cyclohexadiene, 1,3,5-hexatriene, and benzene are also observed following photolysis in solution.[45-47] The exact relationship of these interconversions to those seen in the Vitamin D_2-steroid system has been discussed by several authors.[7,8,44]

1,3-Cyclohexadiene is also of interest because it is a polyene which is forced to be in the s-cis conformation. Ab initio calculations[9] have been very accurate in predicting triplet state energies in the acyclic polyenes using the results for s-trans-1,3-butadiene. The calculations were also performed for s-cis-1,3-butadiene and can be compared with the present experiment. Spectra were taken at 20 eV and 40 eV incident electron energy. Some typical spectra are given in Figures 47 to 49, the cross section ratios are plotted in Figure 50, and the DCS curves are displayed in Figures 51 and 52. The usual summary and DCS value listings are given in Tables 6.1.5-1 and 6.1.5-2.

The sample was obtained from Aldrich Chemical Co. with a stated purity of 99%. The sample was used as soon after its arrival as possible because 1,3-cyclohexadiene is known to undergo decomposition to benzene and cyclohexene.[45] Small amounts of hexatriene could also be formed following electron impact excitation of the sample. The discussion below considers the effect that these impurities might have on the observed spectra. In the following discussion the state designations will be those of an s-cis-polyene of C_{2v} symmetry.

6.1.5.1 The $1\,^3B_2$ State

The lowest energy electronic transition in 1,3-cyclohexadiene produces the peak at 2.94 ± 0.05 eV with a Franck-Condon region from 2.1 eV to 3.8 eV. The cross section ratio to the $1\,^1B_2$ state at 4.9 eV (see next section) shows a sharp increase with increasing scattering angle which is typical of a singlet→triplet transition. The DCS behavior shown in Figures 51 and 52 also confirms this conclusion. The calculations on s-cis-butadiene[9] place the $\tilde{X}\,^1A_g \rightarrow 1\,^3B_2$ transition at 2.95 eV in excellent agreement with the present results. The semi-empirical calculations of Allinger et al.[31] put the lowest triplet at 3.01 eV. The good agreement between experiment and the calculations of Shih et al.[9] indicate that the correct assignment of the 2.94 eV peak is to the $\tilde{X}\,^1A_g \rightarrow 1\,^3B_2$ transition. This transition is also seen in optical

absorption studies. The peak occurs at 2.9 eV in an oxygen and chloroform solution[15] or at 2.79 eV in methyl iodide solution.[48] The 0-0 band is placed at 2.27 eV in the oxygen and chloroform solution.[32]

The photosensitized dimerization of 1,3-cyclohexadiene has been studied in solution.[49] The suggestion was made that the dimerization reaction involved the diene triplet excited states for linear dienes and therefore the $1\,^3B_2$ state is the precursor state for these dimerization processes of 1,3-cyclohexadiene.

No other triplet state is seen below the onset of the $\tilde{X}\,^1A_1 \rightarrow {}^1B_2$ transition at 4.2 eV in contrast with the results for the other polyenes. The calculations on s-cis-butadiene, however, put the $1\,^3A_1$ state at 4.90 eV while the semiempirical calculations place it at 4.61 eV. The $\tilde{X}\,^1A_1 \rightarrow 1\,^3A_1$ is probably hidden underneath the strong $\tilde{X}\,^1A_1 \rightarrow 1\,^1B_2$ transition.

6.1.5.2 The $1\,^1B_2$ State

The intense transition peaking at 4.94 ± 0.03 eV was assigned to the $N \rightarrow V$ or $\tilde{X}\,^1A_1 \rightarrow 1\,^1B_2$ transition by Mulliken.[23] The DCS curves for this transition are sharply forward peaked as would be expected for a fully allowed singlet $\rightarrow$ singlet transition. The earlier optical spectra showed some vibrational structure on this peak[49] but the more

recent studies have shown only a smooth feature with a peak centered at 4.95 eV.[48, 50, 51] The vibrational fine structure was shown to be that of 1, 3, 5-hexatriene produced by photochemical conversion of the 1, 3-cyclohexadiene sample. In the spectrum shown in Figure 49, there is a slight indication of vibrational structure on the 4.94 eV peak, indicating a very small amount of 1, 3, 5-hexatriene is present in the sample. The absence of any discernible peaks however indicates that the contamination level is small.

6.1.5.3 Higher Singlet States

Three peaks are seen in Figure 49 at 6.05 ± 0.03 eV, 6.20 ± 0.03 eV, and 6.39 ± 0.05 eV. These peaks are seen in the optical spectra[48, 52] and have been attributed to a vibrational progression of a Rydberg type singlet → singlet transition.[53]

The next peak occurs at about 6.93 ± 0.03 eV. A peak is seen at about 7.00 eV in one optical study[48] but an earlier optical study[52] showed only smooth continuous absorption in this region. Benzene however is known to have an extremely intense (f = 1.2) transition peaking at 6.93 eV.[54] If the intensity ratio in the electron impact spectra between two singlet → singlet transitions is the same as their optical f number ratio, then the area ratio in Figure 52 (about 5 to 1) could be obtained with as little as 2% benzene contamination because

Figure Captions

Figure 47. The electron impact spectrum of 1, 3-cyclohexadiene from 2 eV to 6 eV energy loss for $E_0 = 40$ eV, $\theta = 10°$, $P_{ind} = 5.5 \times 10^{-3}$ torr and an incident current $I = 5.4 \times 10^{-8}$ A.

Figure 48. Same as Figure 47 for $\theta = 60°$, $P_{ind} = 4.6 \times 10^{-3}$ torr and a resolution of 0.15 eV (FWHM).

Figure 49. The 4 eV to 9 eV energy-loss spectrum of 1, 3-cyclohexadiene for $E_0 = 40$ eV, $\theta = 0°$, and $P_{ind} = 4.5 \times 10^{-3}$ torr.

Figure 50. Ratios of the intensity of the $\tilde{X}\,^1A_1 \rightarrow 1\,^3B_2$ transition to that of the $\tilde{X}\,^1A_1 \rightarrow 1\,^1B_2$ as a function of scattering angle θ for E = 20 eV (+) and E = 40 eV (Δ).

Figure 51. DCS curves for 1, 3-cyclohexadiene as a function of θ at an incident electron energy of 20 eV for elastic scattering (+) and for transitions to the $1\,^3B_2$ (Δ) and the $1\,^1B_2$ ($\bigcirc$) excited states.

Figure 52. Same as Figure 51 for an incident electron energy of 40 eV.

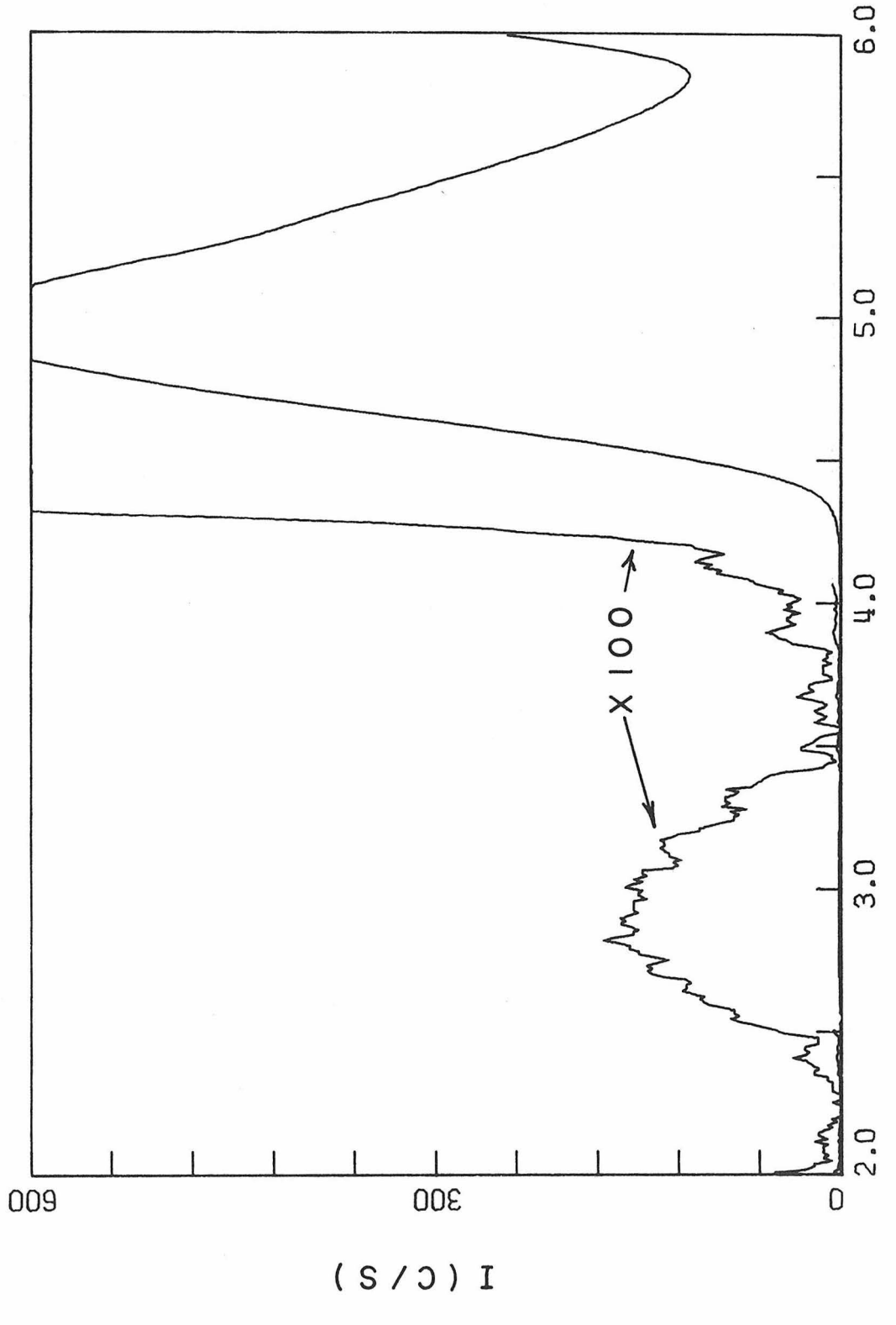

FIG. 47

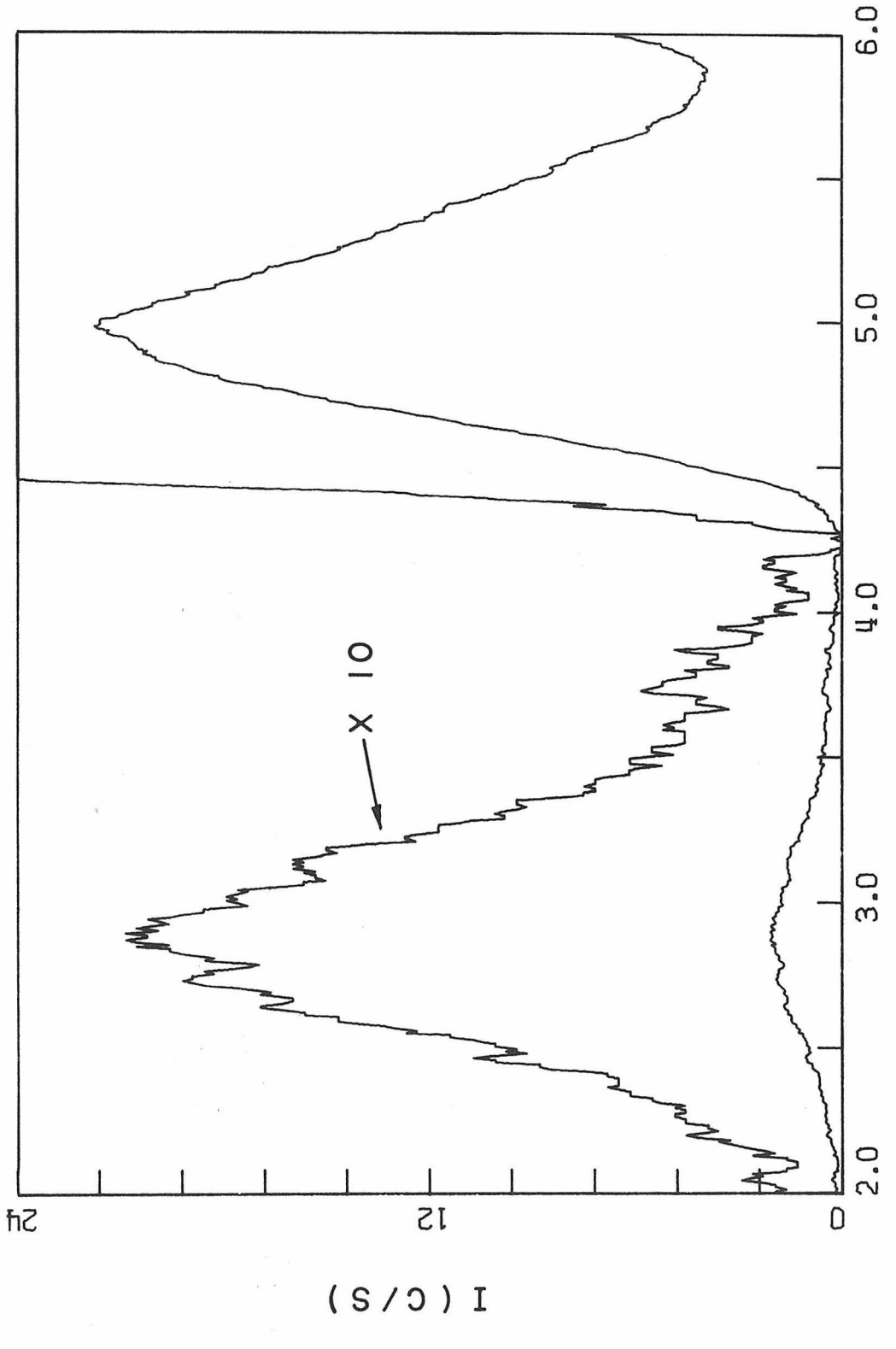

FIG.48

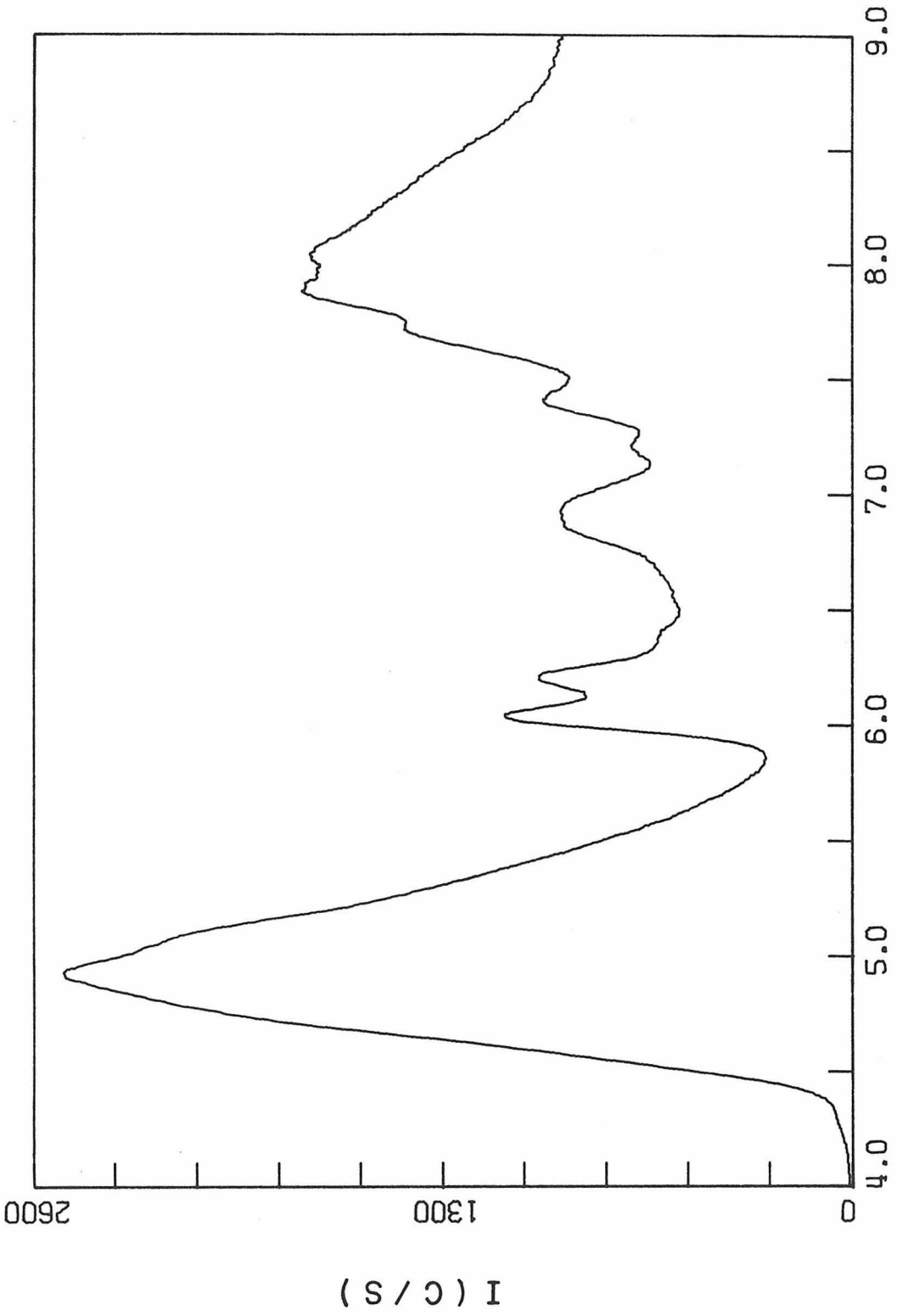

FIG. 49

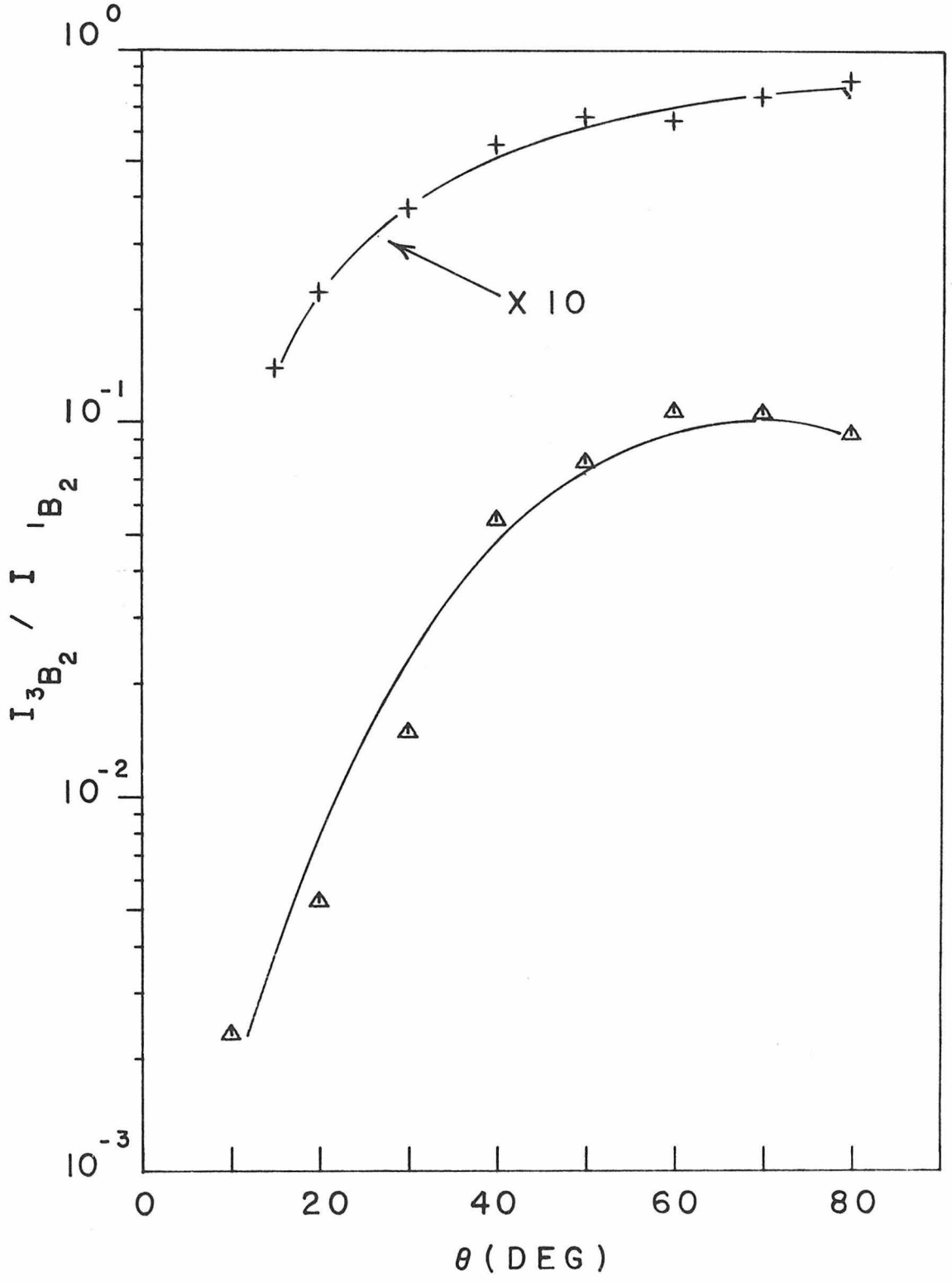

FIGURE 50

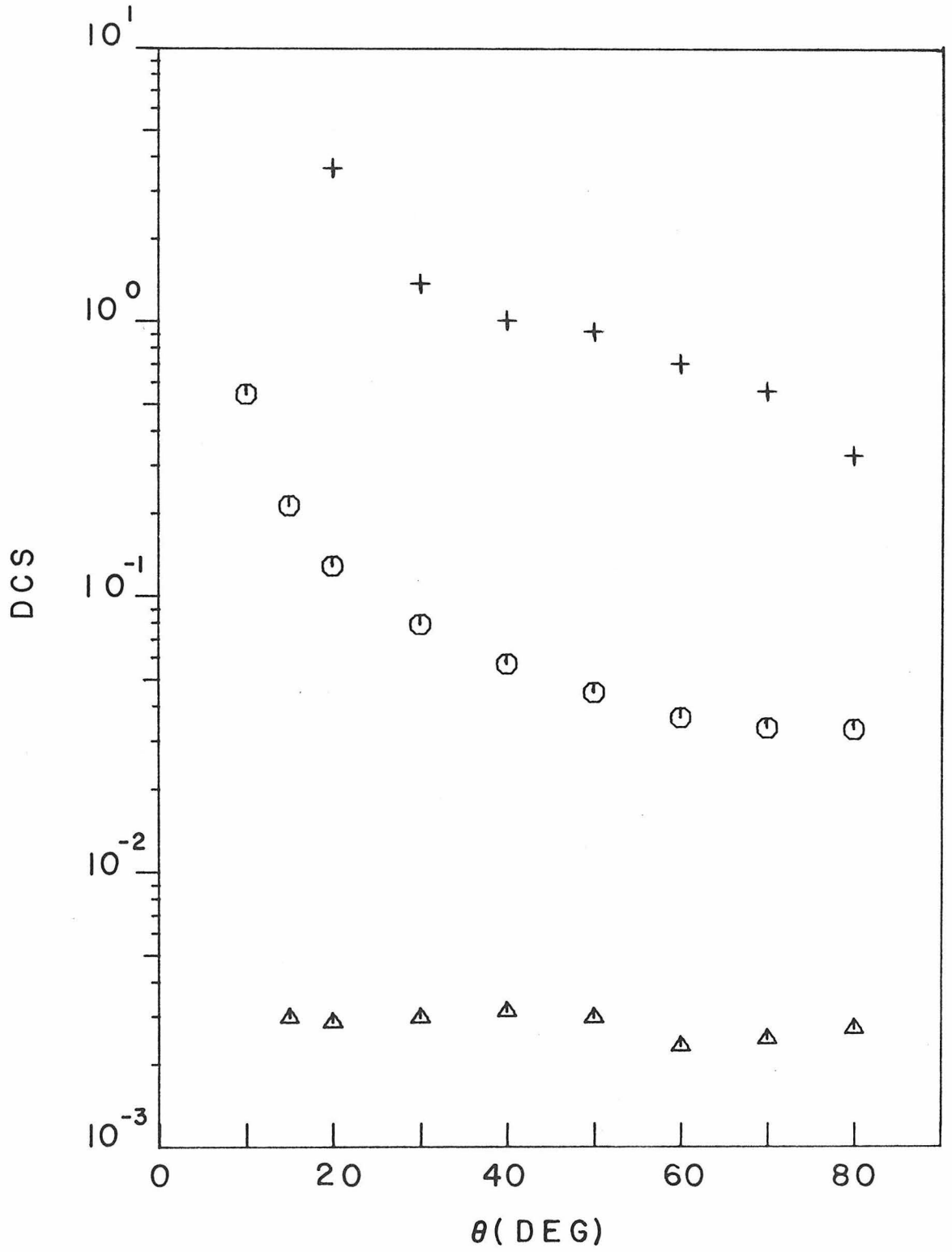

FIGURE 51

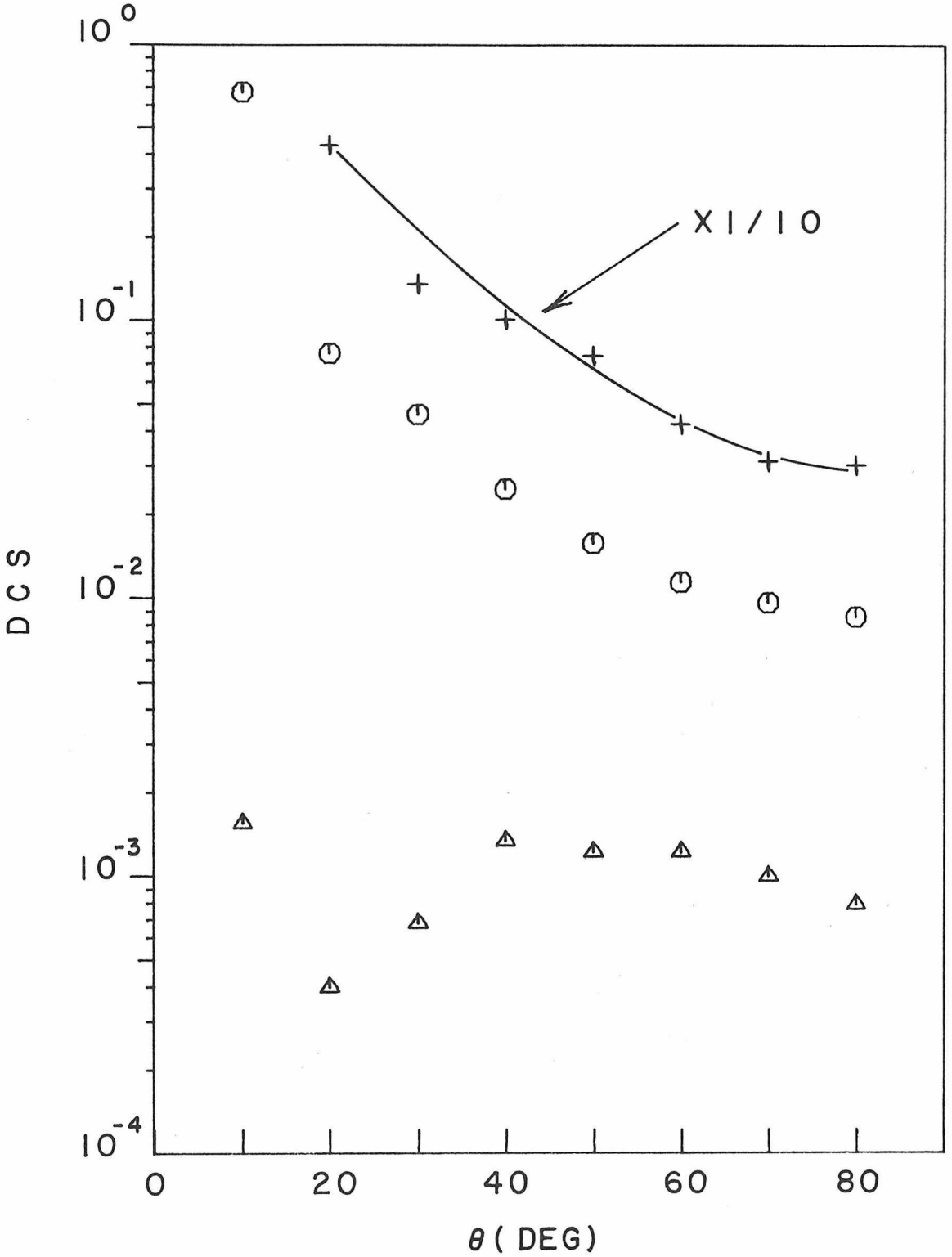

FIGURE 52

Table 6.1.5-1. Excited Electronic States of 1,3-Cyclohexadiene [a]

State [b]	Peak	Franck-Condon region	Theoretical values	Optical values	
$1\,^3B_2$	2.94 ± 0.05	2.1 to 3.8	2.95, [c] 3.01 [d]	2.79 (peak) [e] 2.9 (peak) [f] 2.27 (0-0) band [g]	
$1\,^1B_2$	4.94 ± 0.03	4.2 to 5.9	6.35, [c] 5.21 [d]	4.95 [h]	
Attributed to a Rydberg transition [i]	6.05 ± 0.03			6.05 [j]	6.02 [k]
	6.20 ± 0.03			6.24 [j]	6.20 [k]
	6.39 ± 0.05			6.41 [j]	6.39 [k]
Appears to be part of one transition	7.21 ± 0.05				
	7.42 ± 0.05				
	7.73 ± 0.05				
	7.88 ± 0.05				
	8.05 ± 0.05				

[a] All values in eV. [b] State symmetry designations are given for a C_{2V}, s-cis-polyene.
[c] Reference 9 for s-cis-butadiene. [d] Reference 31. [e] Reference 48. [f] Reference 15.
[g] Reference 32. [h] References 48, 50, 51. [i] Reference 53. [j] Reference 52. [k] Reference 48.

Table 6.1.5-2. DCS Values for 1,3-Cyclohexadiene

θ	Scattering Process [a] $\tilde{X}^1A_g \rightarrow 1\,^3B_2$	$\tilde{X}^1A_g \rightarrow 1\,^1B_2$	Elastic
		20 eV	
10	–	0.541	–
15	0.00295	0.212	–
20	0.00284	0.128	3.62
30	0.00295	0.0787	1.37
40	0.00312	0.0565	1.00
50	0.00295	0.0448	0.918
60	0.00233	0.0362	0.698
70	0.00247	0.0332	0.556
80	0.00270	0.0328	0.525
		40 eV	
10	0.00155 [b]	0.668	–
20	0.000398	0.0758	4.30
30	0.000675	0.0456	1.35
40	0.00134	0.0245	1.00
50	0.00122	0.0157	0.737
60	0.00122	0.0114	0.421
70	0.000999	0.00955	0.312
80	0.000784	0.00850	0.295

[a] The symmetry designations are for an s-cis polyene of C_{2V} symmetry. [b] Reliability is not certain. See 5.10.

the f number for the $\tilde{X}^1A_1 \rightarrow 1\,^1B_2$ transition in 1, 3-cyclohexadiene is only 0.13.[48] Thus the 6.93 eV peak may be produced by the benzene impurities.

Additional singlet → singlet transitions are seen at 7.21 ± 0.05 eV, 7.42 ± 0.05 eV, 7.73 ± 0.05 eV, 7.88 ± 0.05 eV, and 8.05 ± 0.05 eV. The benzene electron impact spectrum has only very weak features in this energy range[55] so these peaks can be reliably assigned to 1, 3-cyclohexadiene transitions. The last 3 peaks appear to be part of a vibrational progression on a very strong electronic transition between about 7.2 eV and 8.8 eV.

6.1.6. Cis, trans-1, 3, 5-Hexatriene

1, 3, 5-Hexatriene is the simplest example of a conjugated linear triene. The presence of the third double bond should make the electronic excited states more like those of the retinal polyenes when compared with the excited states in the dienes previously discussed (see 6.1.1 to 6.1.5).

Several recent experimental studies of substituted polyenes (1, 8-diphenyloctatetraene,[56, 57] 1, 4-diphenylbutadiene,[58] and 2, 10-dimethylundecapentaene[59]) have indicated that an optically forbidden transition, the $\tilde{X}^1A_g \rightarrow 2\,^1A_g$, lies at an energy below that of the strong $\tilde{X}^1A_g \rightarrow 2\,^1B_u$ transition. Most theoretical calculations on

butadiene [10, 11, 31, 60] and hexatriene [31, 60, 61] predict a similar energy ordering of these transitions. The optical [48, 50, 62, 63] and threshold electron impact [61] spectra of hexatriene, however, have not given evidence for a low-lying ^1A_g excited state. Electron impact spectroscopy in the intermediate energy range (10 eV to 100 eV) sometimes permits observation of transitions which are not seen in either the threshold electron impact or optical studies (see discussion in Section IIID of Appendix I). The present experiments were initiated with the hope of observing the $\tilde{X}^1A_g \rightarrow 2\,^1A_g$ transition in hexatriene. The excited states of hexatriene are also of interest because of their role in the Vitamin D_2-steroid photochemical system (see discussion in 6.1.5). The strong $\tilde{X}^1A_g \rightarrow 1\,^1B_u$ transition in hexatriene (see discussion in 6.1.6.3) is also a good model for a number of similar bands in alkyl-substituted hexatrienes. [64]

Electron impact spectra were taken at both 20 eV and 40 eV incident electron energy. Representative spectra are shown in Figures 53 to 55. The cross section ratios are plotted in Figure 56 and the DCS curves are in Figures 57 and 58. Table 6.1.6-1 summarizes the following discussion while Table 6.1.6-2 gives the numerical DCS values.

The sample of 1, 3, 5-hexatriene was obtained from Aldrich Chemical Co. The sample had a stated purity of 99% but is a mixture of the cis and trans isomers. Other investigators [63] have reported that samples of 1, 3, 5-hexatriene from Aldrich contain 60%± 4% trans and 40%± 4% cis isomeric forms.

6.1.6.1 The $1\,^3B_u$ State

The lowest energy transition in hexatriene peaks at 2.61 ± 0.05 eV with a Franck-Condon region from about 1.9 eV to 3.5 eV. The cross section ratios and the DCS curves at both impact energies permit an assignment of this band to the lowest singlet → triplet transition. Theoretical calculations place the $\tilde{X}^1A_g \rightarrow 1\,^3B_u$ transition at 2.66 eV [31] or 2.40 eV [61] for trans-1, 3, 5-hexatriene in good agreement with the experimental results. The $\tilde{X}^1A_g \rightarrow 1\,^3B_u$ transition has also been seen in the threshold electron impact spectrum [61] at 2.6 eV (trans isomer), in the optical spectrum in chloroform and oxygen [15] at 2.6 eV (trans), and in the optical spectrum in methylene iodide solution [48] at 2.57 eV (trans) or 2.63 eV (cis). All values are in good agreement with the present results for an isomerically mixed sample.

Cis ⇌ trans isomerization of 1, 3, 5-hexatriene is observed [47] in solution following excitation by triplet sensitizers such as biacetyl. Spectral overlap arguments can be applied to show that the biacetyl

triplet (T_{00} = 2.37 eV)[65] is only capable of efficiently exciting the $1\,^3B_u$ state and not the $1\,^3A_g$ state (see 6.1.6.2).

6.1.6.2 The $1\,^3A_g$ State

The second transition in hexatriene peaks at 4.11 ± 0.05 eV with a Franck-Condon region from about 3.6 eV to beyond 4.6 eV. The DCS curves are isotropic as shown in Figures 57 and 58 and permit assignment to the second singlet → triplet transition. The same feature was observed in the threshold spectrum[61] at ≈ 4.2 eV and assigned to the $\tilde{X}\,^1A_g \rightarrow 1\,^3A_g$ transition. Theoretical calculations put the transition at 3.87 eV[61] or 4.13 eV[31] in the trans isomer.

6.1.6.3 The $1\,^1B_u$ State

The strongest feature in the spectrum occurs between about 4.3 eV and 6.0 eV with peaks at 4.95 ± 0.03 eV, 5.13 ± 0.02 eV, and 5.30 ± 0.03 eV. The transition has been studied previously by both optical[48, 50, 62, 63] and threshold electron impact studies[61] and assigned[61, 62] to the $\tilde{X}\,^1A_g \rightarrow 1\,^1B_u$ transition. Peak locations in the optical studies are in good agreement with the results of the present studies. The optical spectra under high resolution[48, 50, 63] show vibrational fine structure in addition to the C=C double bond stretching progression which is observed in Figure 55. The vibronic structure in this transition has been studied theoretically by Warshel and

Karplus [66] and the results were similar to the vibronic pattern in the optical experiments. The DCS curves for the $\tilde{X}^1A_g \rightarrow 1\,^1B_u$ transition are sharply forward peaked as expected for an allowed transition. Theoretical calculations put the transition at 5.14 eV, [31] 5.26 eV, [61] 5.18 eV, [60] or 5.409 eV. [40]

Several additional spectra were taken under higher resolution conditions to search for a ^1A_g state on the low energy side of the $\tilde{X}^1A_g \rightarrow 1\,^1B_u$ transition. Examination of the spectra failed to reveal such a state as either a peak or as a slope break in the smoothly rising $\tilde{X}^1A_g \rightarrow 1\,^1B_u$ excitation curve. The results are in agreement with optical [63] and threshold electron impact studies. [61] The failure to observe such a state indicates that it may be nearly coincident in energy with the $1\,^1B_u$ state. If they are at the same energy (within, say, 0.1 to 0.2 eV) it would be very difficult to see the $\tilde{X}^1A_g \rightarrow 2\,^1A_g$ transition because of the strong intensity of the $\tilde{X}^1A_g \rightarrow 2\,^1B_u$ transition.

6.1.6.4 Higher Singlet States

Higher energy singlet → singlet transition produce peaks which are seen in Figure 55 at 6.25 eV, 6.42 eV, 6.57 eV, 6.75 eV, 6.93 eV, 7.08 eV, 7.48 eV, 7.77 eV and 8.06 eV. Some of the peaks below 7.0 eV have also been observed in the optical spectrum. [48, 62] The peaks at 6.75 eV, 6.93 eV, and 7.08 eV appear to be vibronic peaks in a single electronic transition.

Figure Captions

Figure 53. The electron impact spectrum of cis-trans-1, 3, 5-hexatriene from 2 eV to 6 eV for E_0 = 40 eV, $\theta = 10°$, and a resolution of 0.12 eV (FWHM).

Figure 54. The 2 eV to 6 eV energy-loss spectrum of cis-trans-1, 3, 5-hexatriene for E_0 = 40 eV, $\theta = 70°$, and a resolution of 0.17 eV (FWHM).

Figure 55. The energy-loss spectrum from 4.5 eV to 8.5 eV for E_0 = 40 eV, $\theta = 0°$, and $P_{ind} = 3.9 \times 10^{-3}$ torr.

Figure 56. Ratios of the indicated intensity I to that of the $\tilde{X}^1A_g \rightarrow 1^1B_u$ transition as a function of θ. The excited states and incident energies for the curves shown are 1^3B_u (+) at 20 eV, 1^3B_u (○) at 40 eV, 1^3A_g (△) at 20 eV, and 1^3A_g (□) at 40 eV.

Figure 57. DCS curves for cis, trans-hexatriene as a function of θ at an incident energy of 20 eV for elastic scattering (+) and for transitions to the following excited states: 1^3B_u (△), 1^3A_g (○), and the 1^1B_u (□).

Figure 58. Same as Figure 57 for an incident electron energy of 40 eV.

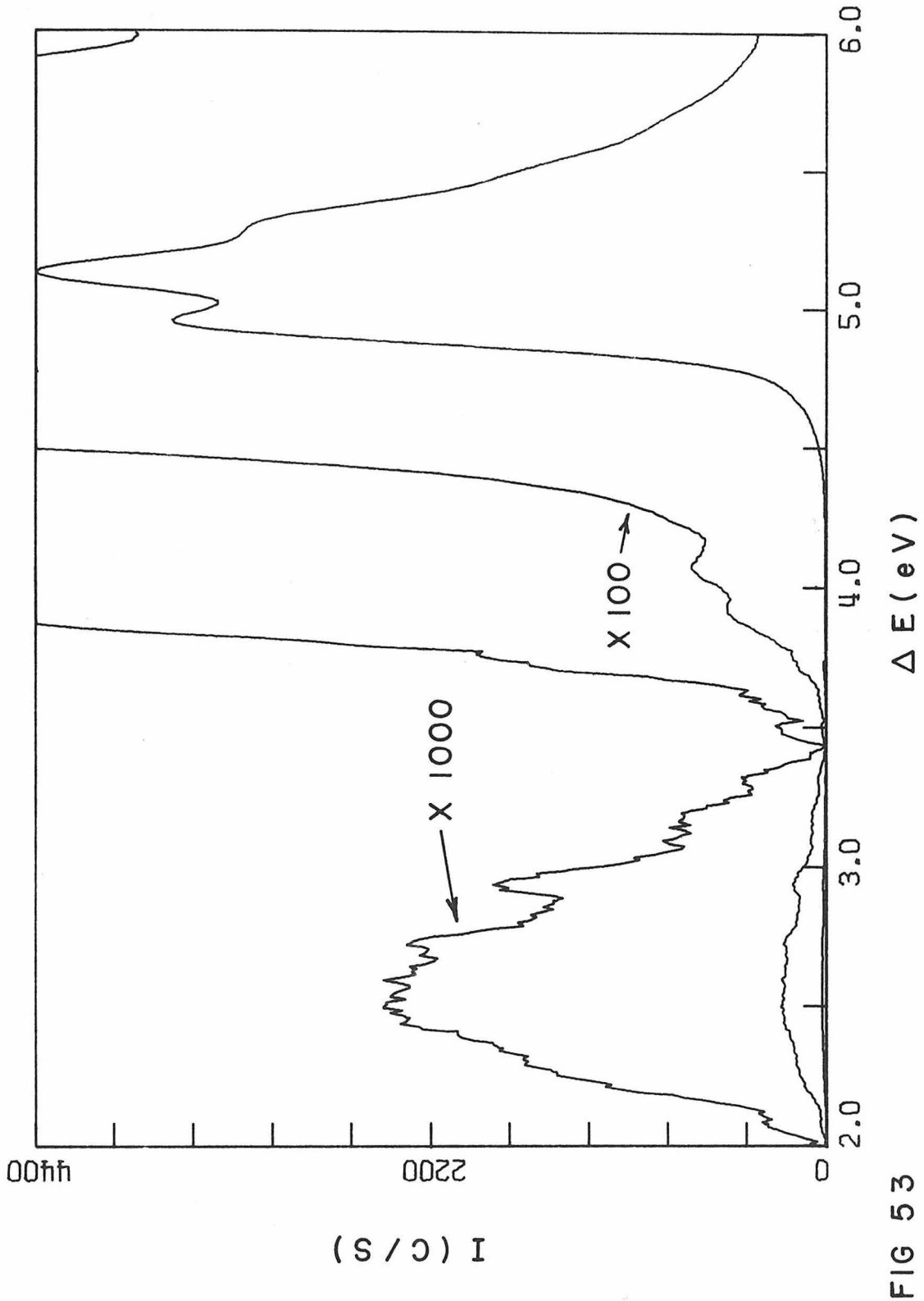

FIG 53

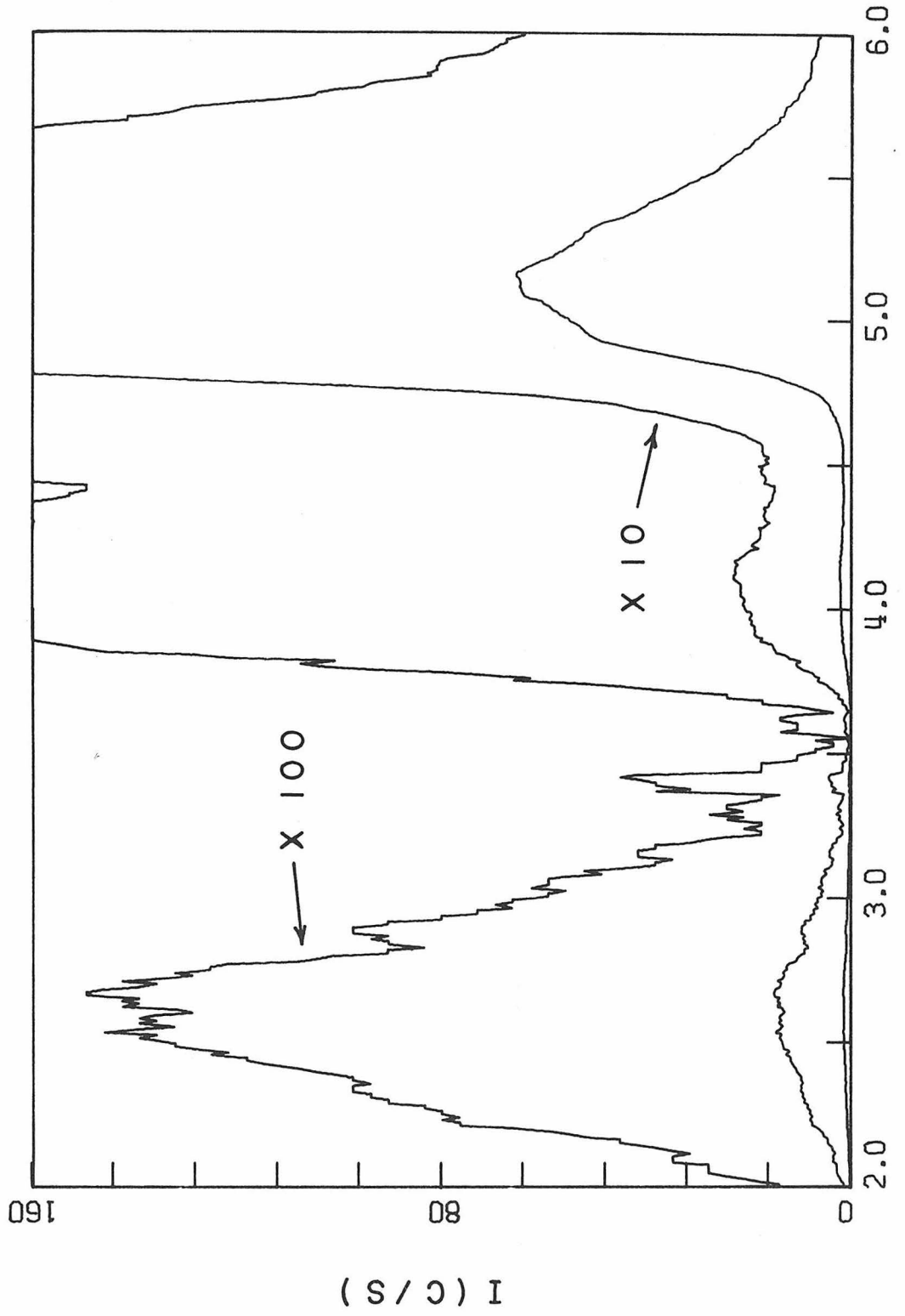

FIG. 54

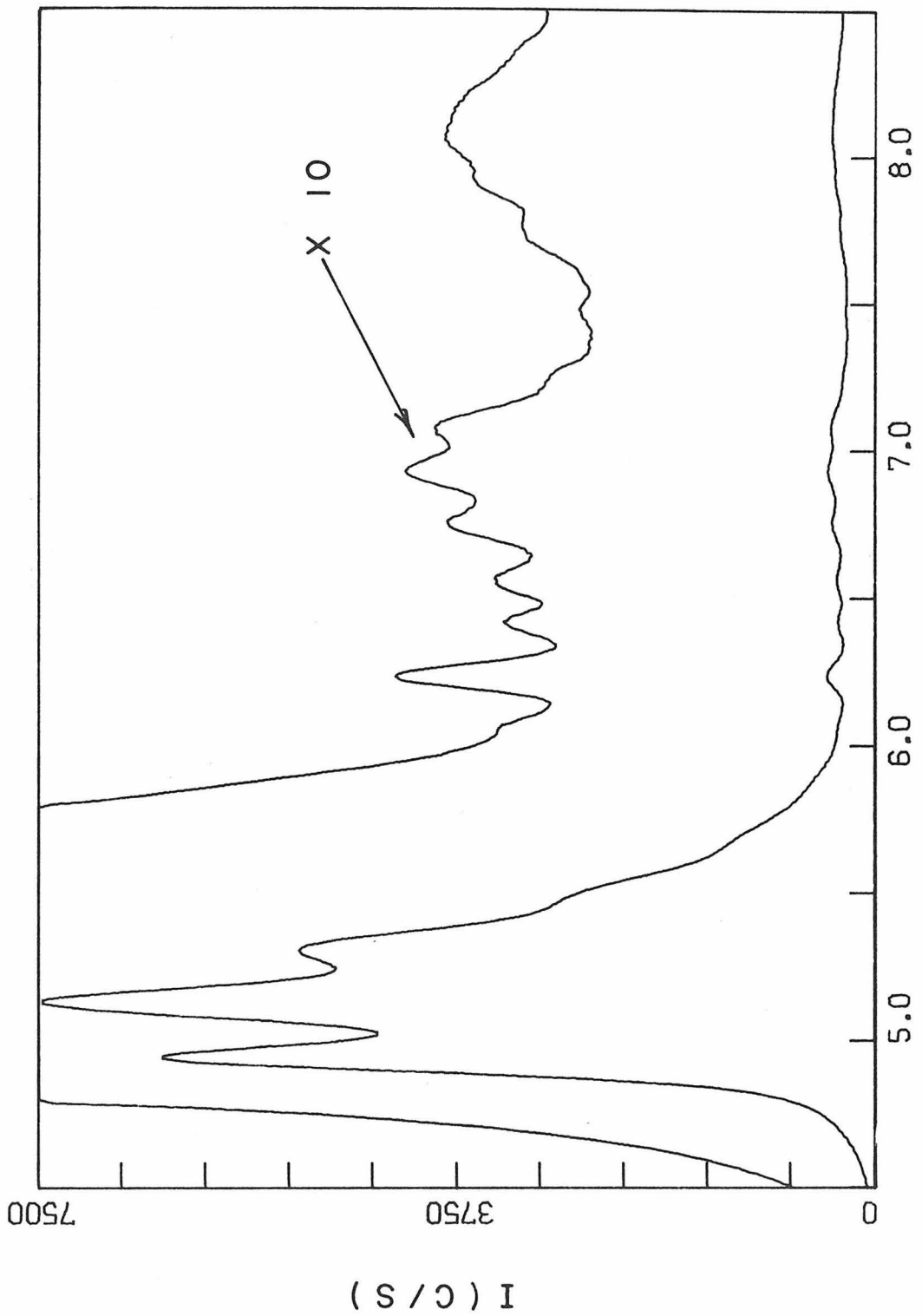

FIG. 55

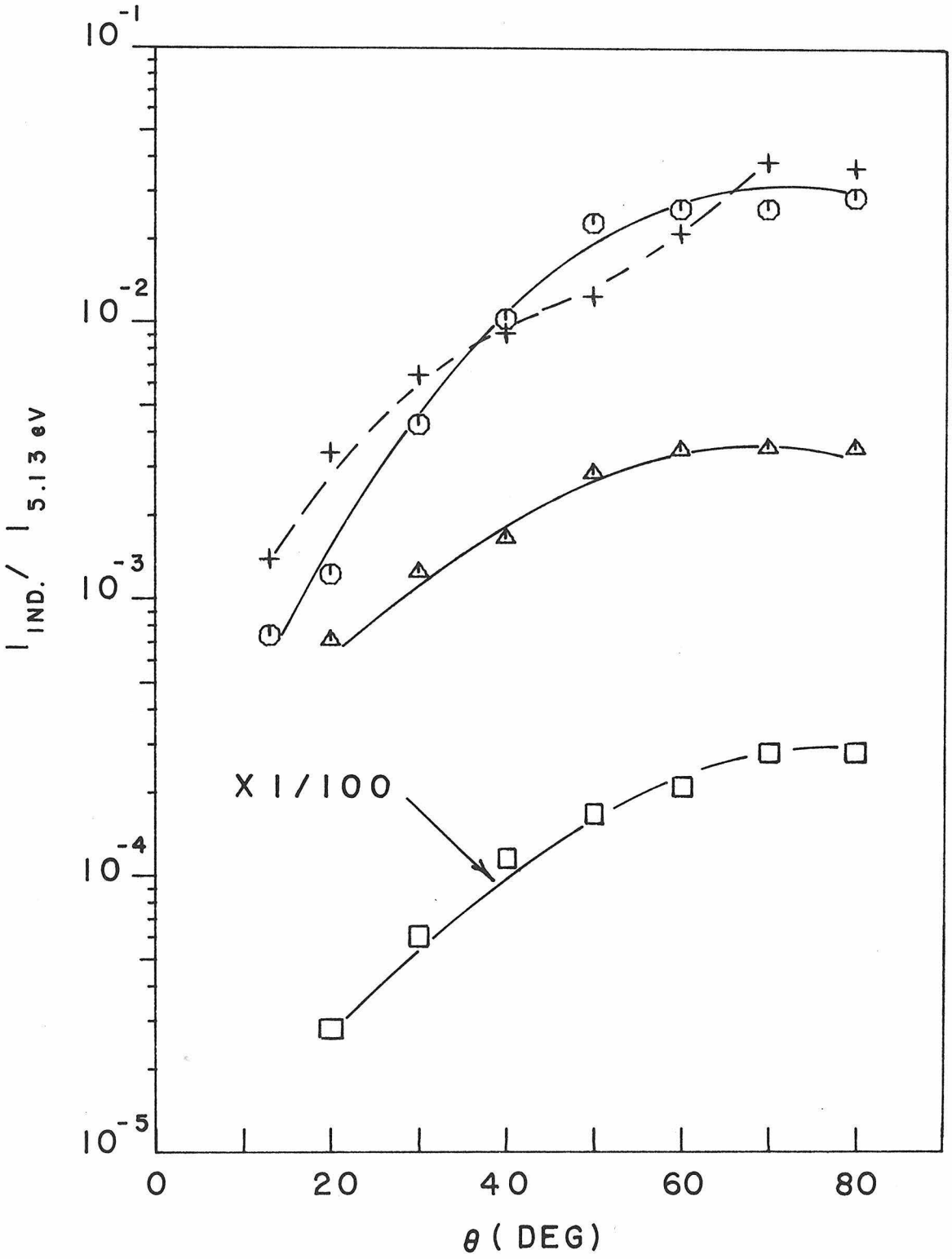

FIGURE 56

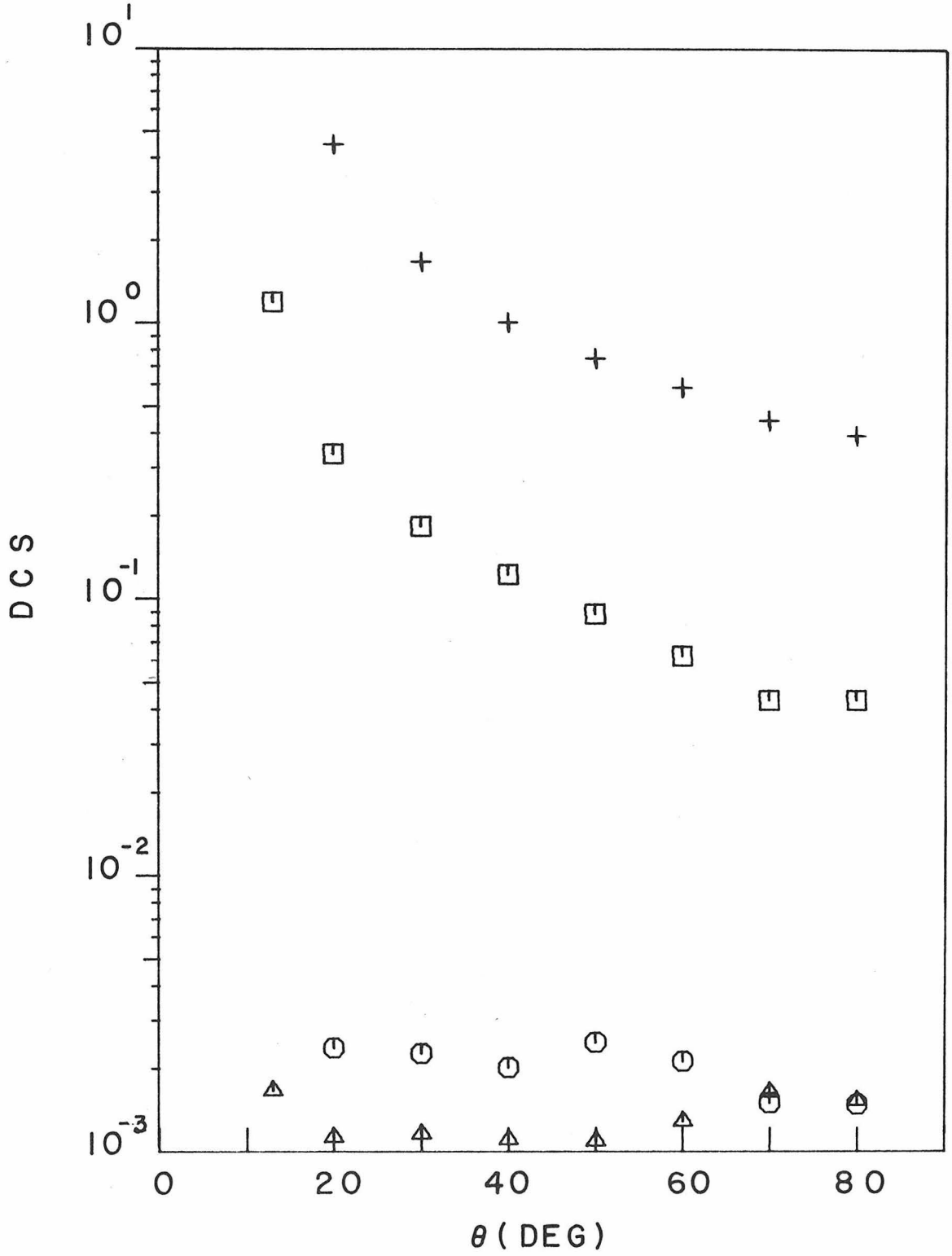

FIGURE 57

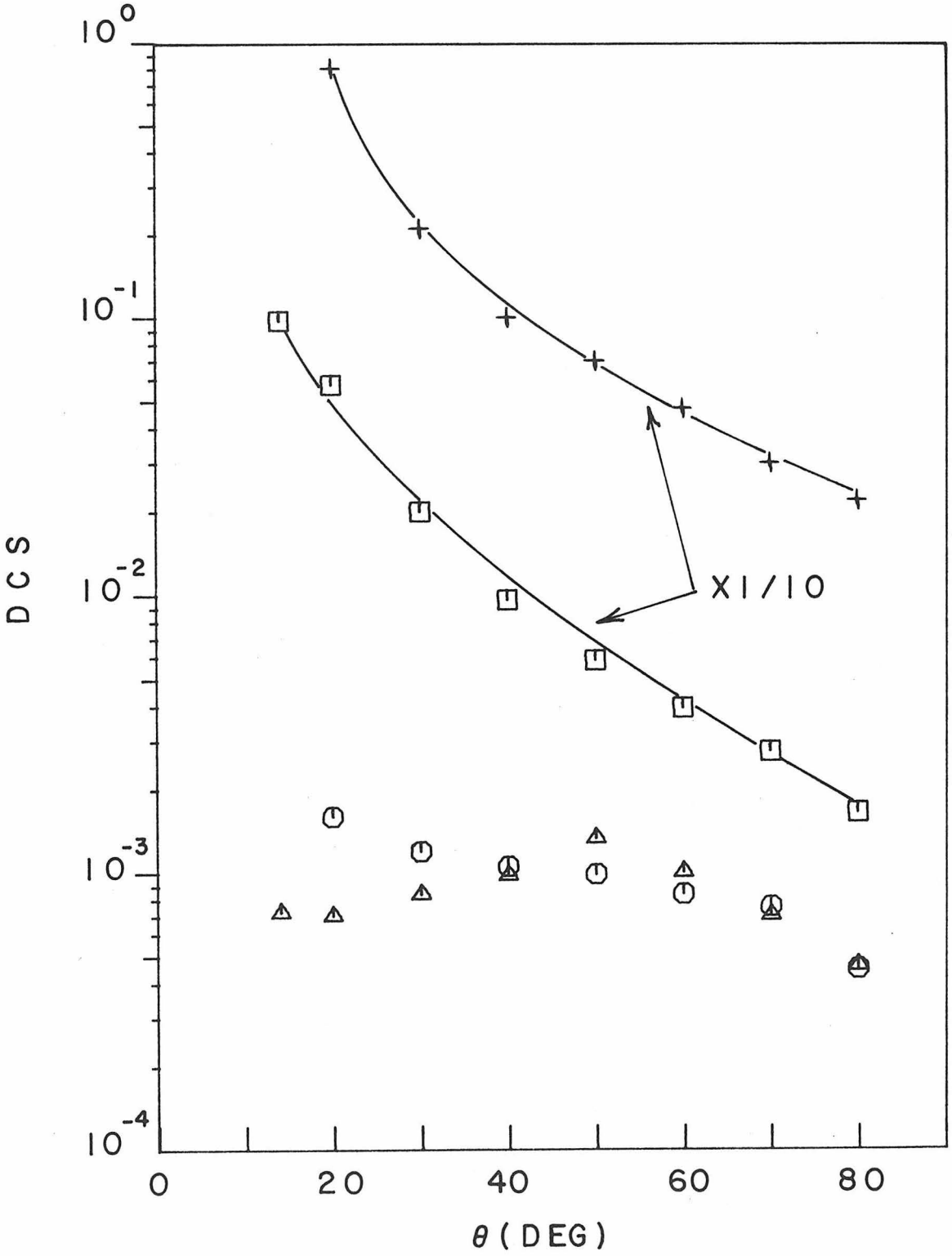

FIGURE 58

Table 6.1.6-1. Excited Electronic States of 1, 3, 5-Hexatriene [a]

State [b]	Peak [c]	Franck-Condon region [c]	Theoretical values	Other experimental values: Threshold electron impact [d]	Other experimental values: Optical (for trans)
$1\,^3B_u$	2.61 ± 0.05	1.9 to 3.5	2.66 (trans) [e]		2.6 [f]
			2.40 (trans) [d]	2.6 (trans)	2.57 [g]
$1\,^3A_g$	4.11 ± 0.05	3.6 to beyond 4.6	3.87 [d]	≈ 4.2	–
			4.13 [e]		
$1\,^1B_u$	4.95 ± 0.03		5.14 [e]		4.934 [j, k]
	5.13 ± 0.02	4.3 to 6.0	5.26 [d]	5.1	5.140 [j] 5.136 [k]
	5.30 ± 0.03		5.18 [h]		5.291 [j] 5.288 [k]
			5.41 [i]		
Singlets	6.25 ± 0.05				
	6.42 ± 0.05				
	6.57 ± 0.05				6.53 [g]
	6.75 ± 0.05	Appear to be			6.72 [g]
	6.93 ± 0.05	part of one			6.90 [g]
	7.08 ± 0.05	transition			
	7.48 ± 0.05				
	7.77 ± 0.05				
	8.06 ± 0.05				

[a] All values in eV. [b] For trans-1, 3, 5-hexatriene. [c] For an isomeric mixture. [d] Reference 61. [e] Reference 31. [f] Reference 15. [g] Reference 48. [h] Reference 60. [i] Reference 40. [j] Reference 50. [k] Reference 63.

Table 6.1.6-2. DCS Values for cis, trans-1, 3, 5-Hexatriene

	Scattering Process [a]			
θ	$\tilde{X}^1A_g \rightarrow 1^3B_u$	$\tilde{X}^1A_g \rightarrow 1^3A_g$	$\tilde{X}^1A_g \rightarrow 1^1B_u$	Elastic
		20 eV		
13	0.00166	–	1.186	–
20	0.00113	0.00237	0.335	4.476
30	0.00116	0.00227	0.182	1.668
40	0.00111	0.00201	0.122	1.00
50	0.00109	0.00248	0.0876	0.741
60	0.00129	0.00212	0.0616	0.577
70	0.00164	0.00150	0.0429	0.437
80	0.00153	0.00148	0.0425	0.392
		40 eV		
14	0.000722	–	0.979	–
20	0.000702	0.00160	0.575	8.099
30	0.000840	0.00119	0.200	2.107
40	0.000986	0.00106	0.0965	1.00
50	0.00134	0.000994	0.0586	0.701
60	0.00101	0.000843	0.0395	0.469
70	0.000704	0.000755	0.0274	0.301
80	0.000463	0.000452	0.0165	0.219

[a] The scattering process symmetry designations are for trans-1, 3, 5-hexatriene.

6.2. Non 1,3-Conjugated Polyenes

6.2.1. Cis-1,4-Hexadiene and trans-1,4-Hexadiene

Polyenes which are acyclic and have two C–C single bonds separating the ethylenic subunits should presumably have little interaction between the subunits when either one is excited electronically. The spectra of such molecules should be more like those of alkyl substituted ethylenes than of a 1,3-conjugated polyene such as butadiene. These studies of 1,4-hexadiene were undertaken to see whether such arguments are applicable to 1,4-hexadiene. There also do not appear to be any previous determinations of electronic transition peak locations for 1,4-hexadiene although one study of the optical spectrum in solution reported a featureless absorption onset.[67] Both cis- and trans-1,4-hexadiene are commercially available and each isomer was studied to determine what effects the different geometric forms had on the electronic transition energies.

Spectra were taken of both an isomerically mixed sample of 1,4-hexadiene and of the pure cis and trans isomers. No significant differences were observed among the three different samples in terms of electronic transition energies. Spectra of the isomerically mixed sample are shown in Figures 59 and 60, while the cross section ratios are shown in Figure 61 and the DCS curves are plotted in Figures 62

and 63. The peak locations and the observed electronic transitions indicate that the 1, 4-hexadienes are basically alkyl substituted ethylene systems rather than conjugated polyenes, as discussed below.

The isomerically mixed sample was obtained from Aldrich Chemical Co. and had a stated purity of 99%. The samples of cis-1, 4-hexadiene and trans-1, 4-hexadiene were purchased from Chemical Samples Co. and each had a specified purity of 98%. The usual liquid nitrogen freeze-pump-thaw cycles were employed during sample preparation.

6.2.1.1 The T State

The lowest energy-loss peak occurs at 4.25 ± 0.05 eV as shown in Figure 59 and 60. The cross section ratio to the N-V transition (see 6.2.1.2) shows a sharp increase with increasing scattering angle while the DCS curves are nearly isotropic. Both facts permit identification of this feature between 3.4 eV and 5.3 eV as the lowest singlet → triplet transition. The molecule ethylene [14, 68, 69] and its methyl [14, 68, 69] or ethyl [69] derivatives show a singlet → triplet transition which peaks between 4.1 eV and 4.4 eV. This transition is known as the N → T transition in ethylene [70] and the same designation will be used here for 1, 4-hexadiene.

Figure Captions

Figure 59. The electron impact spectrum of cis, trans-1, 4-hexadiene from 3.5 eV to 12.0 eV energy loss for E_0 = 40 eV, $\theta = 10^\circ$, $P_{ind} = 4.9 \times 10^{-3}$ torr, and a resolution of 0.12 eV (FWHM).

Figure 60. The 3.3 eV to 9 eV energy loss region of 1, 4-hexadiene for E_0 = 40 eV, $\theta = 50^\circ$, $P_{ind} = 3.1 \times 10^{-3}$ torr, and a resolution of 0.13 eV.

Figure 61. Ratio of the intensity of the N → T transition to that of the N → V transition as a function of scattering angle for E_0 = 25 eV (+) and E_0 = 40 eV (Δ).

Figure 62. DCS curves for cis, trans-1, 4-hexadiene as a function of θ at an incident electron energy of 25 eV for elastic scattering (+) and for the N → T (Δ) and N → V (○) transitions.

Figure 63. Same as Figure 62 for an incident energy of 40 eV.

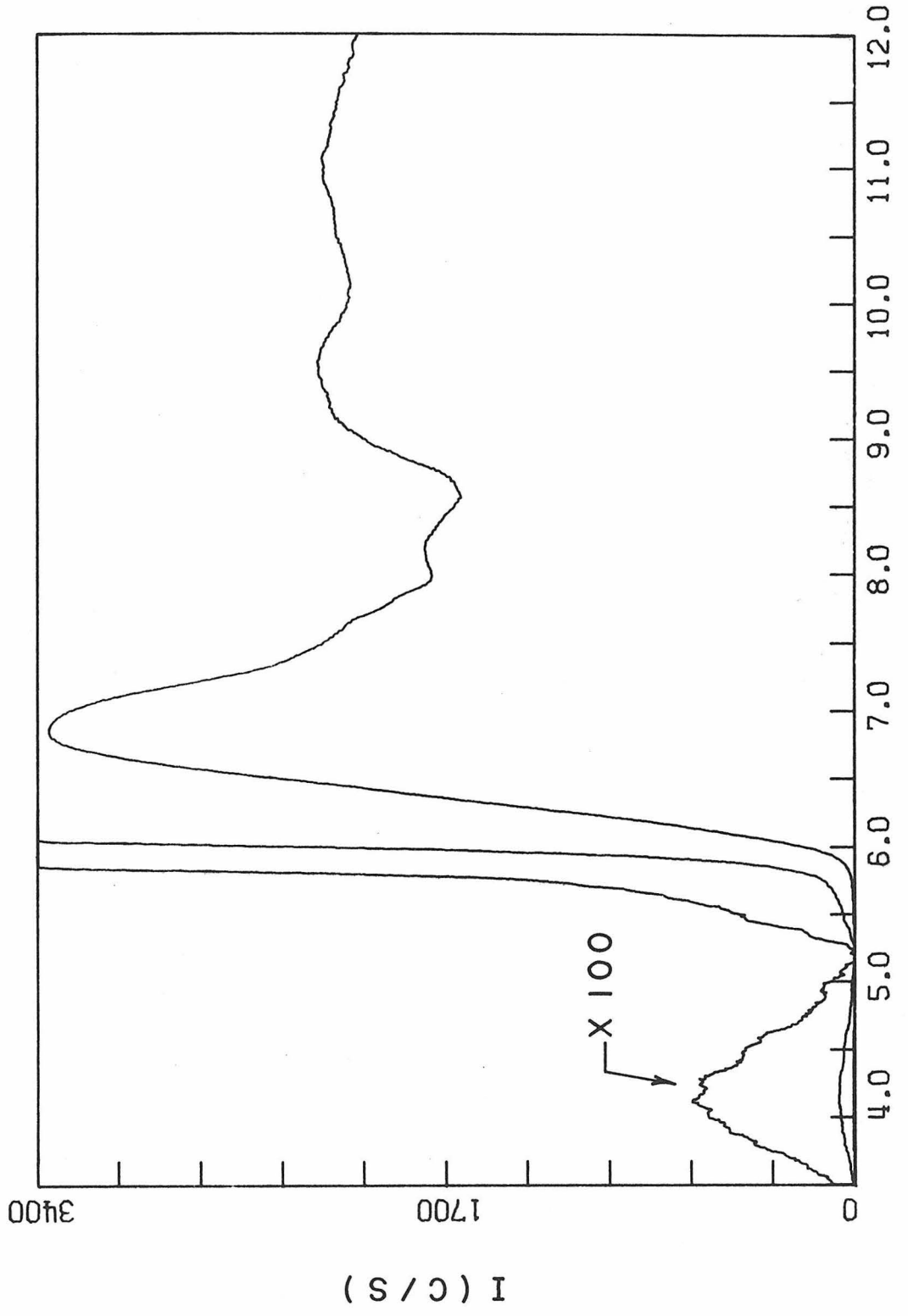

FIG. 59

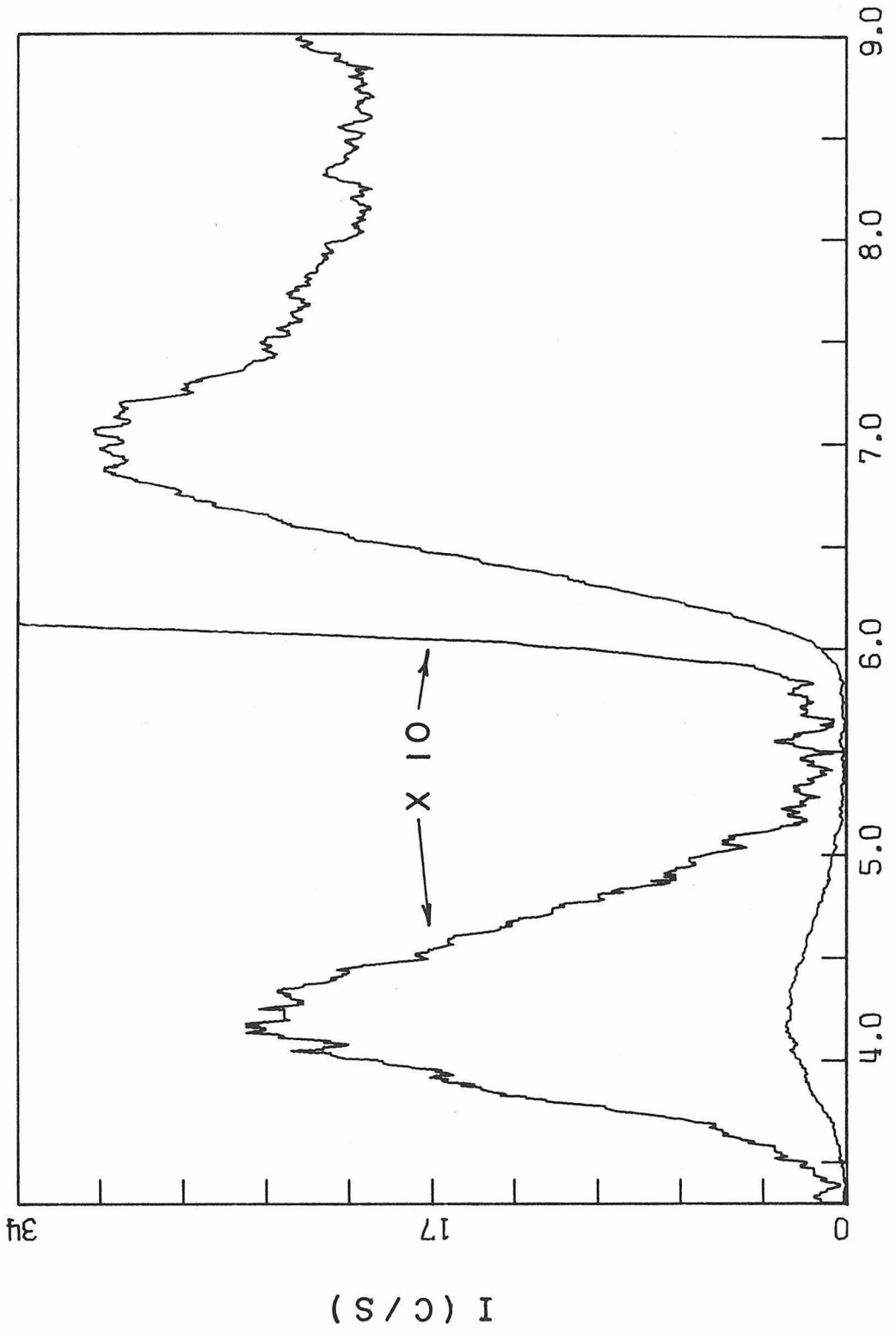

FIG.60

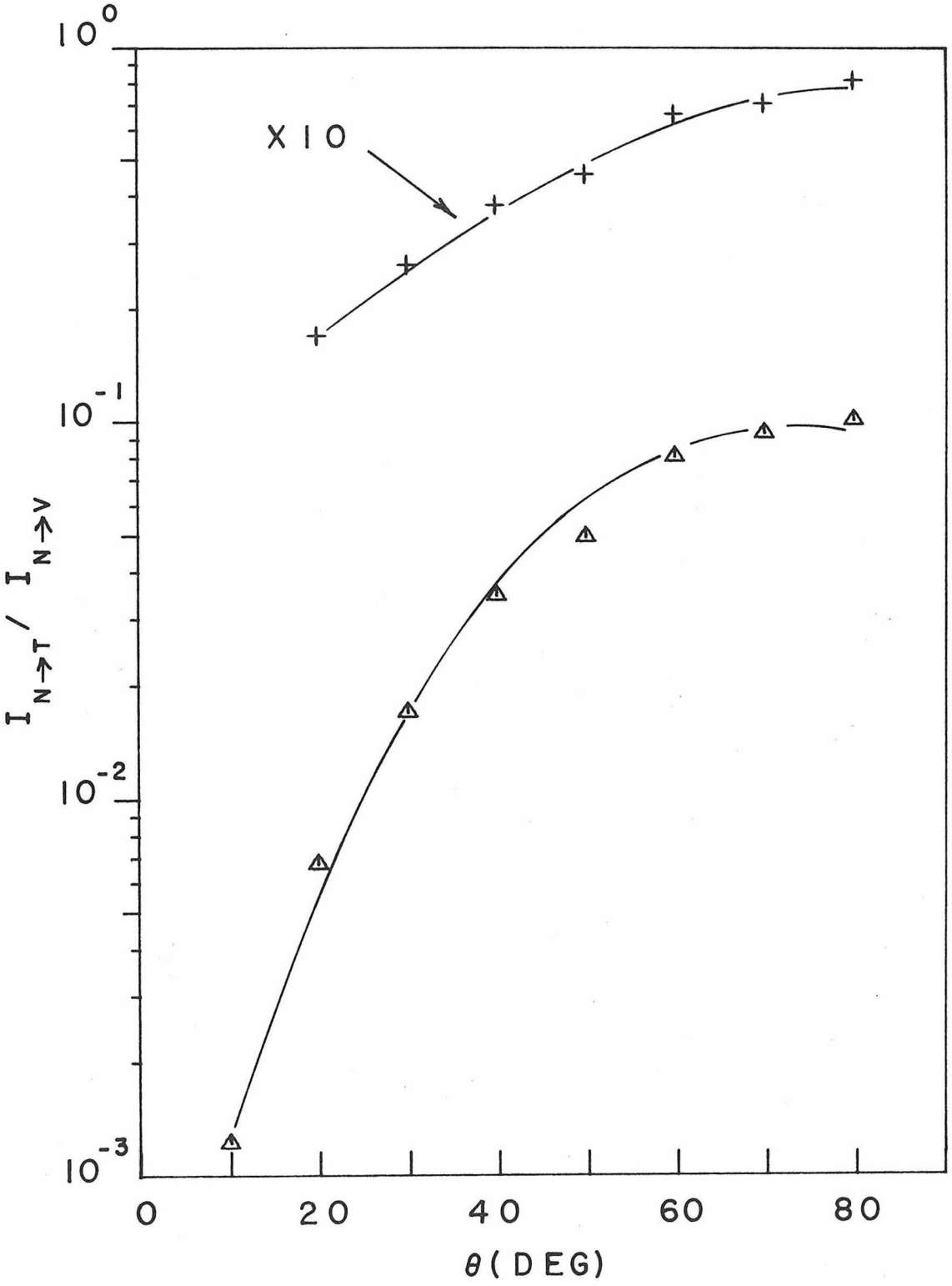

FIGURE 61

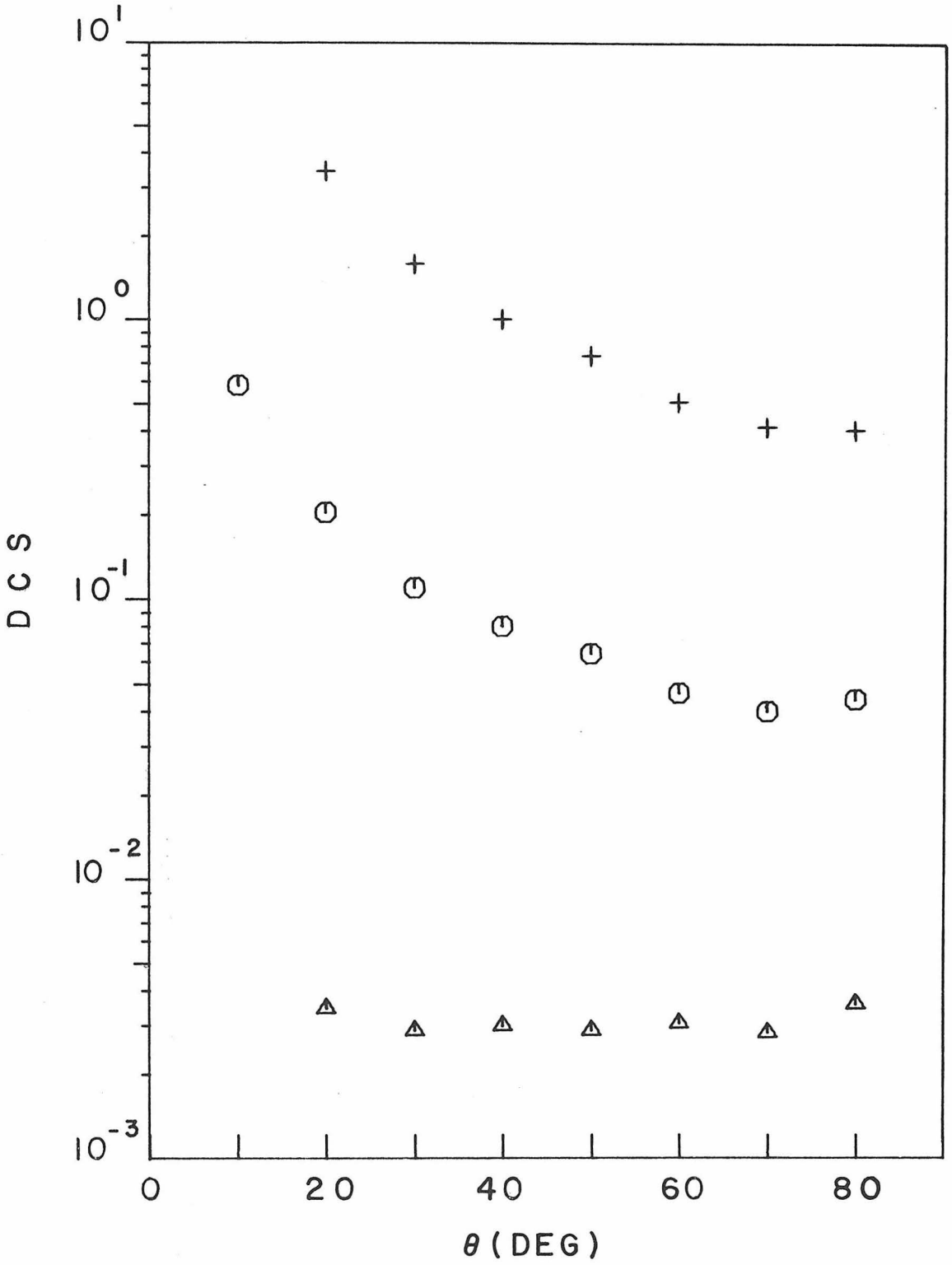

FIGURE 62

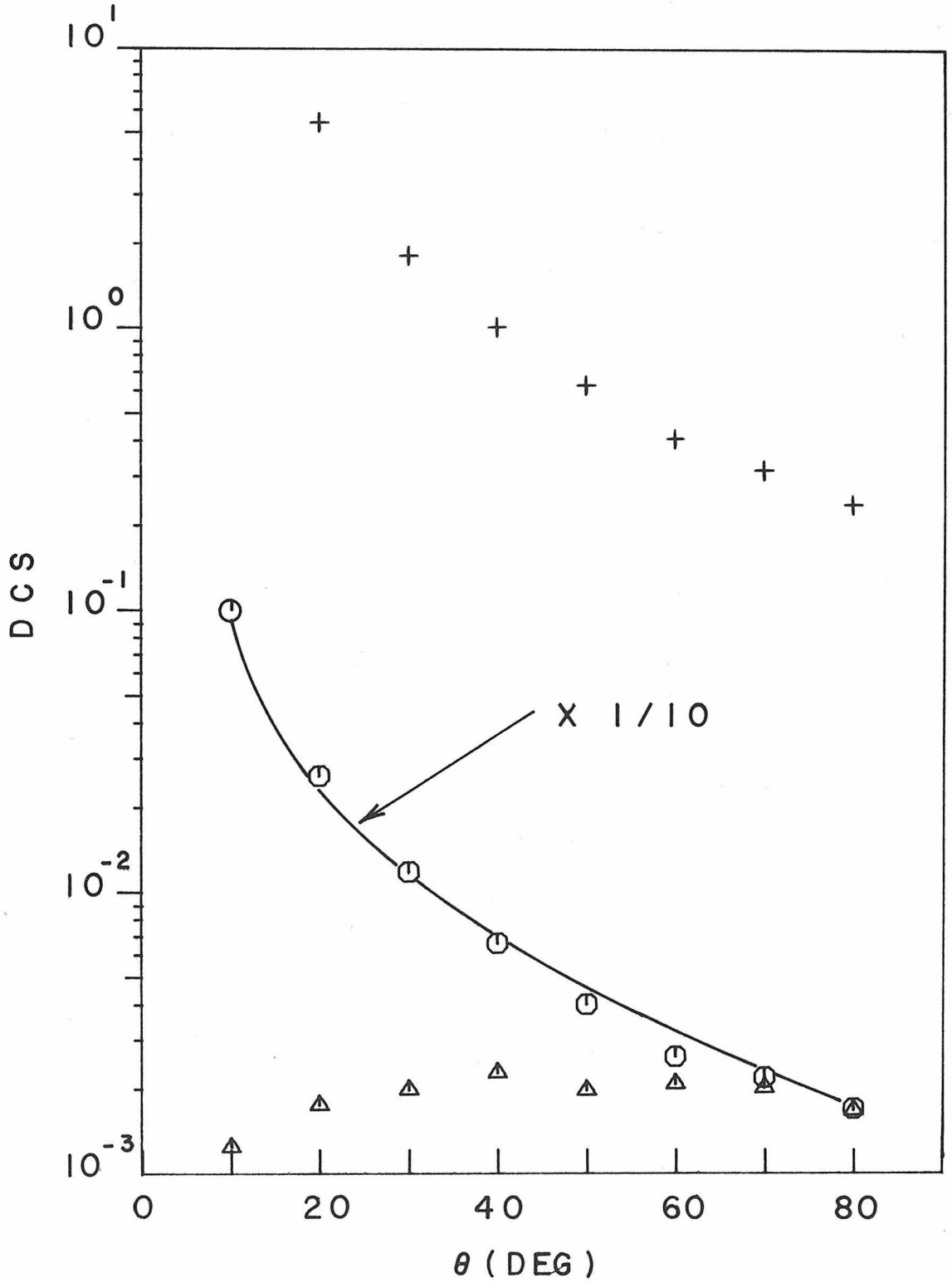

FIGURE 63

Table 6.2.1-1. DCS Values for cis, trans-1, 4-Hexadiene

	Scattering Process [a]		
θ	N → T	N → V	Elastic
	25 eV		
10	–	0.581	–
20	0.00345	0.204	3.43
30	0.00287	0.110	1.59
40	0.00300	0.0800	1.00
50	0.00288	0.0638	0.739
60	0.00304	0.0464	0.506
70	0.00281	0.0402	0.414
80	0.00357	0.0443	0.403
	40 eV		
10	0.00125	1.023	–
20	0.00175	0.259	5.42
30	0.00199	0.118	1.80
40	0.00228	0.0663	1.00
50	0.00198	0.0402	0.624
60	0.00208	0.0260	0.404
70	0.00201	0.0217	0.314
80	0.00168	0.0168	0.236

[a] The states are designated by the corresponding transition in ethylene.

6.2.1.2 The V State and Higher States

The strongest feature in the spectrum peaks at 6.84 ± 0.06 eV although the peak is very broad and gives a fairly flat excitation curve between 6.8 eV and 7.0 eV in many of the spectra. The DCS curves are strongly forward peaked and indicate that this is an optically allowed transition. The strong N → V transition in ethylene peaks at around 7.6 eV [14, 68] while in alkyl substituted ethylenes the corresponding peaks occur [24, 68, 70] between 6.6 and 7.2 eV. The strong absorption at 6.84 eV can be assigned to the N → V type transition in 1, 4-hexadiene based on its intensity, DCS behavior, and peak location. The optical spectrum [67] only included the area of absorption onset for the N → V transition.

A broad maximum occurs at 9.4 ± 0.2 eV in the isomerically mixed sample and in the trans isomer. This feature is not readily apparent, however, in the spectra of the cis isomer.

6.2.2. 1, 5-Hexadiene

The electron impact spectrum of 1, 5-hexadiene (diallyl) was studied at incident electron energies of 25 eV and 40 eV. The results which are discussed below indicate that the two lowest excited states are similar to those observed in alkyl substituted ethylenes and in 1, 4-hexadiene (see Section 6.2.1). Spectra of 1, 5-hexadiene at 40 eV

incident energy and scattering angles of 10°, 70°, and 0° are shown in Figures 64 to 66. The cross section ratios are plotted in Figure 67 and the DCS curves appear in Figures 68 and 69.

The 1, 5-hexadiene sample was obtained from Aldrich Chemical Co. and had a stated purity of 98%. The usual freeze-pump-thaw procedure was applied to the sample before using it in these studies.

6.2.2.1 The T State

The lowest energy transition in 1, 5-hexadiene produces the peak at 4.25 ± 0.05 eV with a Franck-Condon region from 3.5 eV to 5.3 eV. The cross section ratio to the N → V transition (see 6.2.2.2) and the DCS curves permit assignment to a singlet → triplet transition. Comparison with the results in 1, 4-hexadiene (6.2.1.1) and other alkyl substituted ethylenes [14, 68, 69] indicate that this transition corresponds to the N → T transition in ethylene. [70] The T state is the triplet state which was identified as the initial excited state in the mercury-photosensitized decomposition studies [71] of 1, 5-hexadiene. The principal products were hydrogen, ethylene, propene, and 1, 3-butadiene.

The peak at 5.9 eV is due to an unidentified impurity in the sample. The ratio in the electron impact spectra of the areas under this feature to that of the N → V transition is less than 1%. If the

Figure Captions

Figure 64. The electron impact spectrum of 1, 5-hexadiene from 3.5 eV to 8 eV energy loss for E_0 = 40 eV, $\theta = 10°$, $P_{ind} = 5.9 \times 10^{-3}$ torr, and a resolution of 0.14 eV.

Figure 65. Same as Figure 64 except $\theta = 70°$ and $P_{ind} = 5.7 \times 10^{-3}$ torr.

Figure 66. The 6 eV to 14 eV energy-loss region in 1, 5-hexadiene for E_0 = 40 eV, $\theta = 0°$, and $P_{ind} = 4.0 \times 10^{-3}$ torr.

Figure 67. The ratio of the intensity of the N → T transition to that of the N → V transition as a function of scattering angle for E_0 = 25 eV (+) and E_0 = 40 eV (Δ).

Figure 68. DCS curves for 1, 5-hexadiene as a function of θ at an incident electron energy of 25 eV for elastic scattering (+) and for the N → T (Δ) and N → V (○) transitions.

Figure 69. Same as Figure 68 for an incident energy of 40 eV.

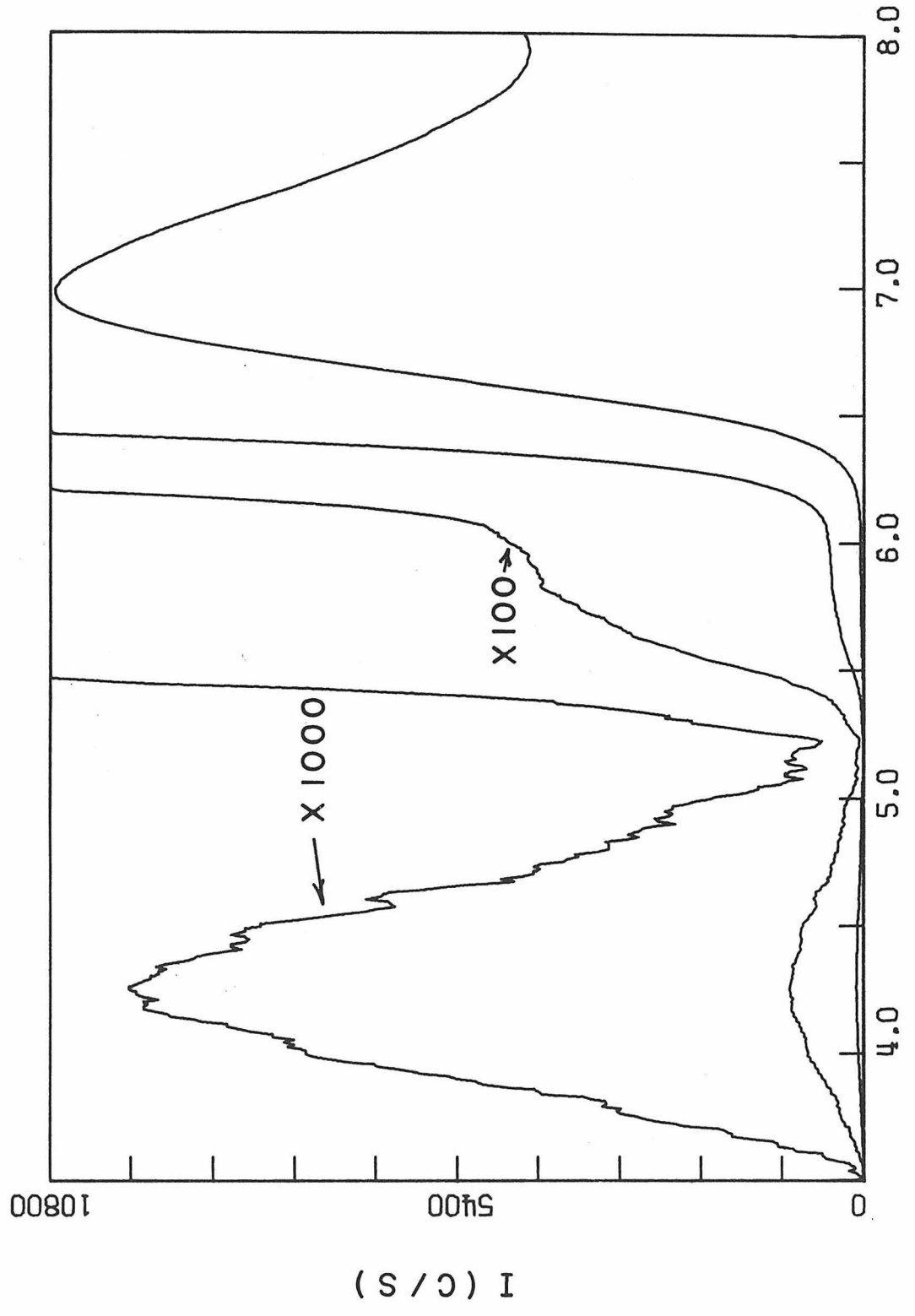

FIG. 64

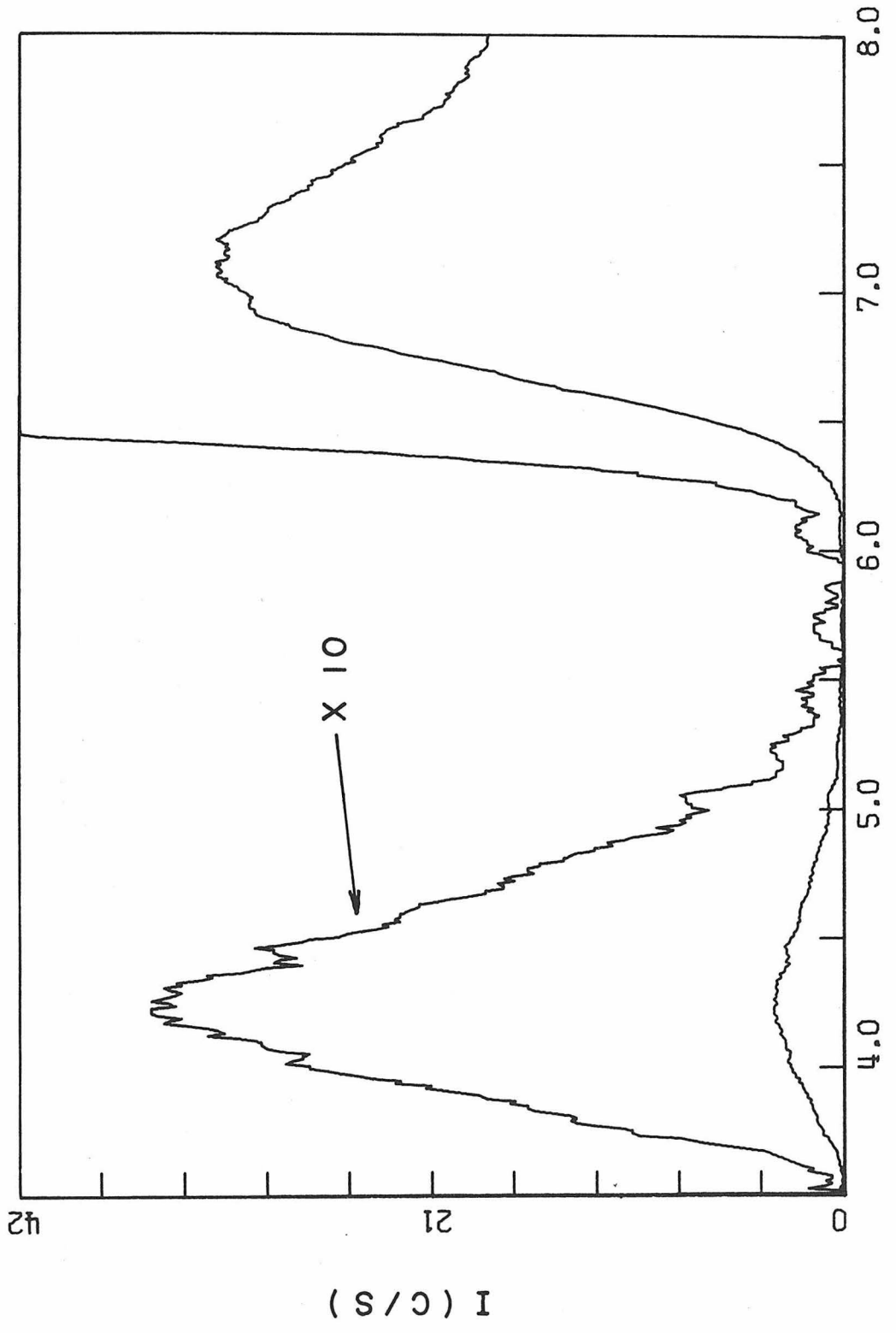

FIG. 65

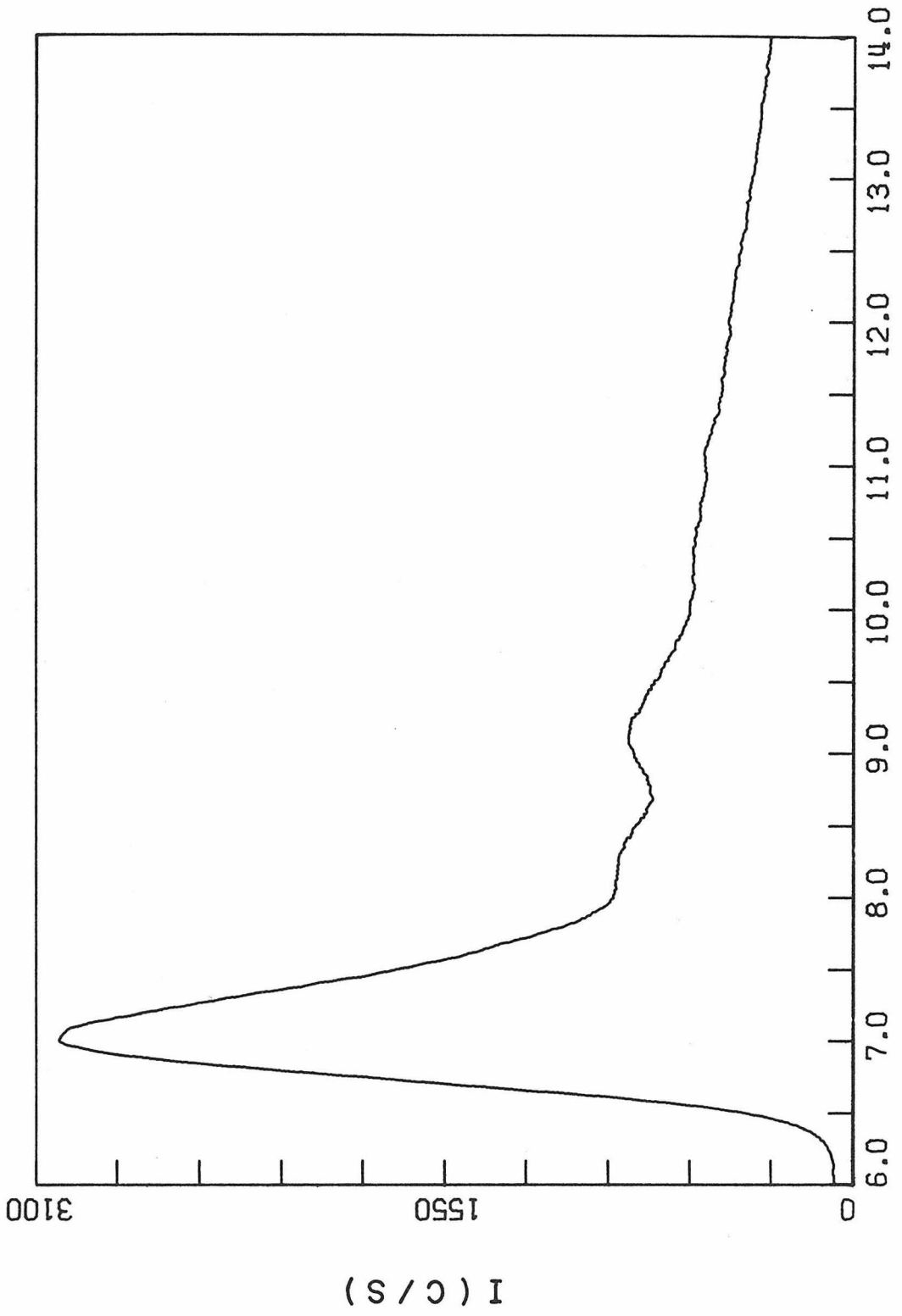

FIG 66

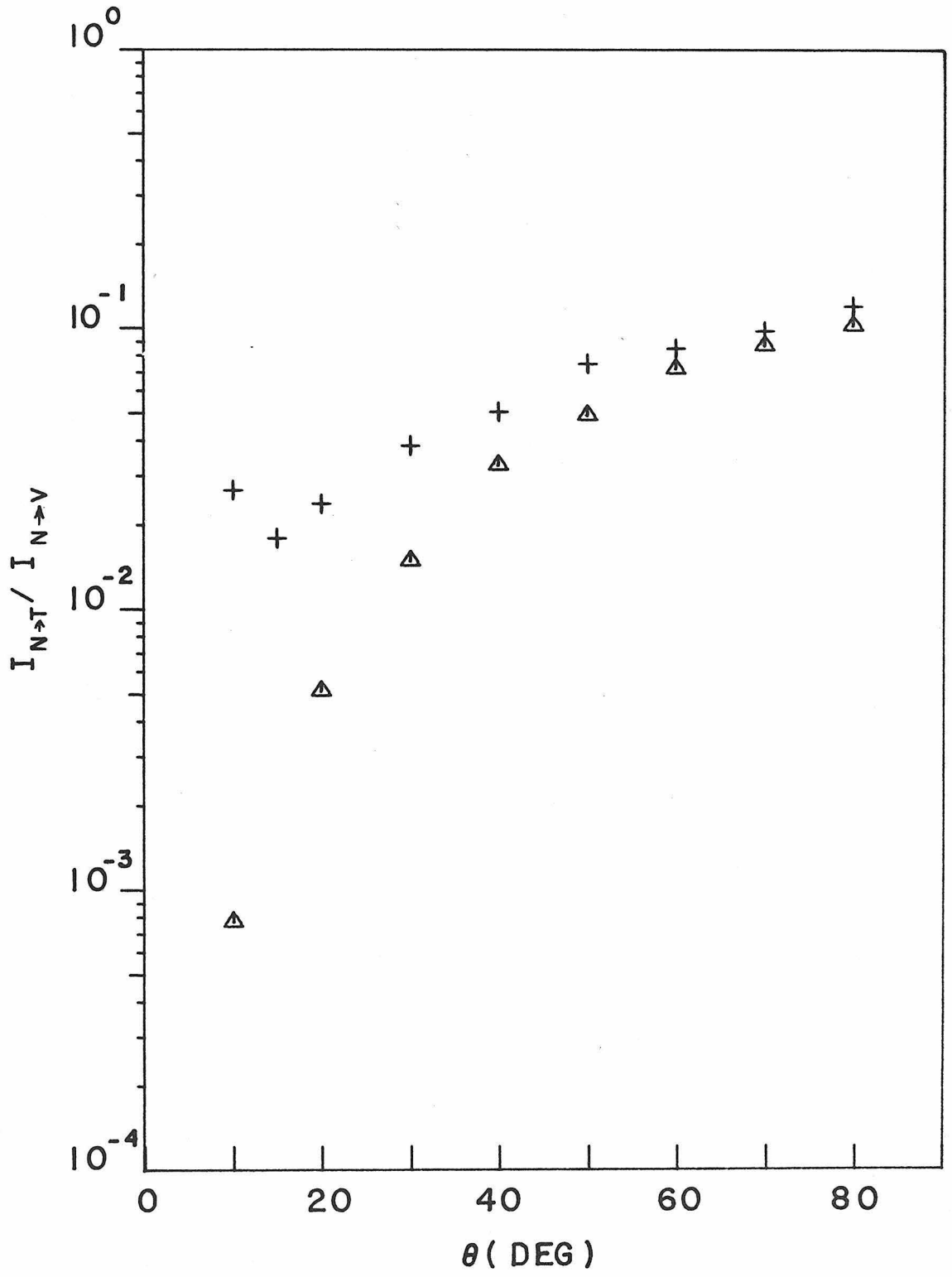

FIGURE 67

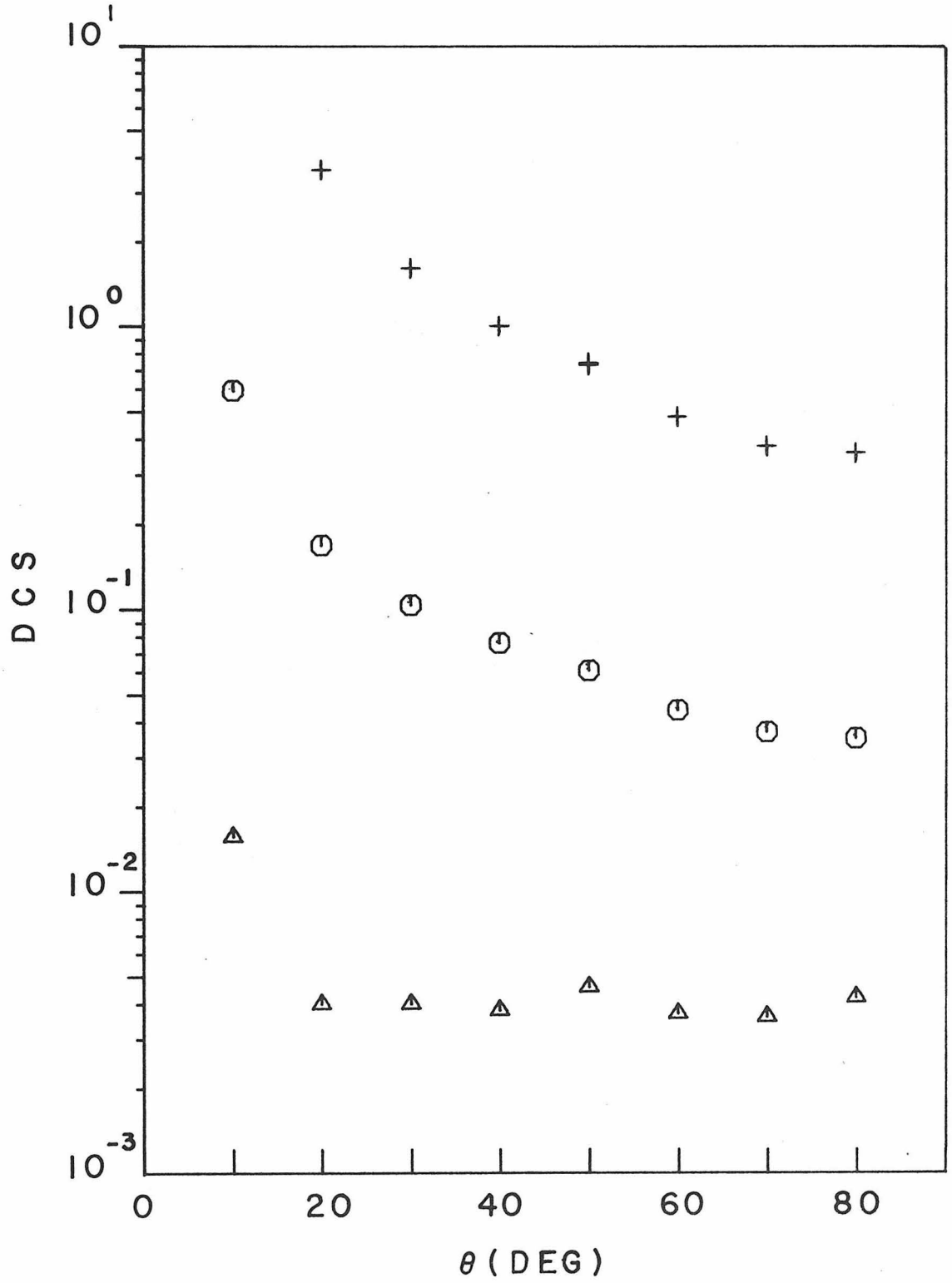

FIGURE 68

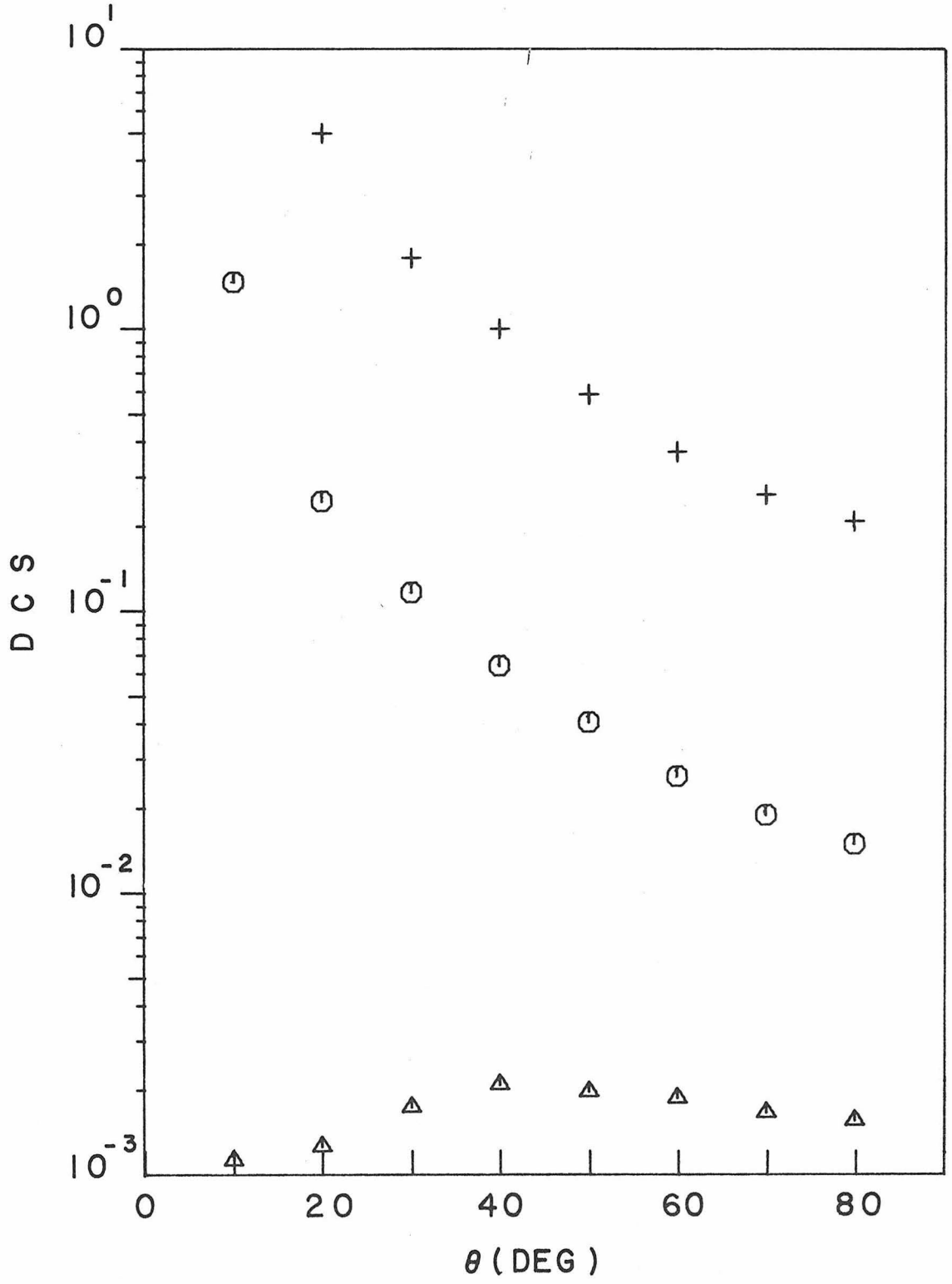

FIGURE 69

Table 6.2.2-1. DCS Values for 1,5-Hexadiene

θ	Scattering Process [a] N→T	N→V	Elastic
	25 eV		
10	0.0157 [b]	0.592	–
20	0.00402	0.169	3.62
30	0.00397	0.104	1.61
40	0.00383	0.0762	1.00
50	0.00458	0.0612	0.726
60	0.00374	0.0442	0.484
70	0.00361	0.0370	0.382
80	0.00415	0.0346	0.356
	45 eV		
10	0.00113	1.47	–
20	0.00126	0.246	5.01
30	0.00174	0.117	1.79
40	0.00209	0.0641	1.00
50	0.00198	0.0404	0.594
60	0.00188	0.0262	0.371
70	0.00167	0.0192	0.261
80	0.00156	0.0153	0.212

[a] The states are designated by the corresponding transition in ethylene. [b] Reliability is not certain. See 5.10.

intensity of the 5.9 eV impurity transition and that of the N → V transition are comparable, then this indicates that the impurity concentration is well below the specified maximum value of 2%.

6.2.2.2 The V State and Higher States

The peak at 7.00 ± 0.04 with a Franck-Condon region from below 6.1 eV to 7.9 eV corresponds to the N → V type transition in the alkyl substituted ethylenes.[24, 68, 70] The sharply forward peaked DCS curves and the intensity of the transition confirm this assignment. The transition has also been seen by optical absorption.[24, 42] The peak itself is quite broad but has a maximum at either 6.99 eV[24] or 7.13 eV.[42]

Broad maxima are seen in Figure 66 with peaks at 8.3 ± 0.1 eV and 9.1 ± 0.1 eV. These regions involve singlet → singlet excitations.

6.2.3. 1,4-Cyclohexadiene

The results discussed previously (6.2.1 and 6.2.2) for 1,4-hexadiene and 1,5-hexadiene indicated that there was very little interaction between the ethylenic groups in the 1,4 or 1,5 positions in these linear dienes. Cyclic 1,4-dienes, however, may have significant interactions because of the physical proximity of the double bonds or because other σ bonds in the molecule are oriented in such a way as to permit hyperconjugation.

Hoffmann has given a summary of the interactions of orbitals through space or through bonds.[72, 73] When the geometry of the molecule permits direct spatial overlap of the orbitals on each of two chromophores, the interaction is of the "through-space" type.[72, 74] The interaction splits the degenerate π and π^* orbitals and is manifested by the presence of two π-electron ionization potentials (IP_S), one of which will be lowered from the value for the geometrically similar olefin. An example of this behavior is seen in the IP_S of norbornene (π_{IP} = 8.97 eV) and norbornadiene (π_{IP_S} = 8.69 eV, 9.55 eV).[75] The effect of interaction on the energy of the intense $\pi \rightarrow \pi^*$ transition is more difficult to predict. The energy of the lowest $\pi \rightarrow \pi^*$ transition will be shifted from the value in the corresponding olefin, but this transition may then be symmetry forbidden.[72] Thus the strong $\pi \rightarrow \pi^*$ transition may come from the second or third $\pi \rightarrow \pi^*$ transition whose energy may be either above or below that of the N → V type transition in the corresponding olefin.

In 1,4-cyclohexadiene the "through-space" interaction is expected to be small[72] because the molecule is almost planar (dihedral angle = 159.3°)[76] and this geometry gives poor direct overlap between the p type π orbital lobes. The H atoms on C_3 and C_6 however are at an angle[76] of 96.1° with respect to the plane defined by C_1, C_2, C_4 and C_5 and the σ_{CH} bonds can couple the π

systems together. This "through-bond" interaction [72, 73, 77] by hyperconjugating σ orbitals leads to lowering of the first IP and to two separate π_{IP} values as discussed above. This is confirmed by studies [75] on cyclohexene (π_{IP} = 9.12 eV) and 1,4-cyclohexadiene (π_{IP_s} = 8.80 eV, 9.80 eV). The interaction diagram for 1,4 cyclohexadiene [72] shows that the lowest $\pi \rightarrow \pi^*$ transition ($\tilde{X}^1A_1 \rightarrow 1\,^1A_2$) is symmetry forbidden. The first allowed $\pi \rightarrow \pi^*$ transition should be the $\tilde{X}^1A_g \rightarrow 1\,^1B_2$ whose energy shift with respect to the N $\rightarrow$ V transition in cyclohexene is not predictable for the reasons discussed above.

Spectra of 1,4-cyclohexadiene are shown in Figures 70 and 71. Figure 72 displays the cross section ratios while Figures 73 and 74 contain the DCS plots. Table 6.2.3-1 lists the DCS values.

Samples of 1,4-cyclohexadiene were obtained from Aldrich Chemical Co. (97% stated purity) and from PCR Inc. (99% stated purity). The sample from Aldrich was used for only a few of the spectra because a benzene impurity gave a noticeable peak at 6.93 eV(see Figure 71). Most of the spectra were taken with the PCR sample where the benzene peak was not noticeable (see Figure 70). The two samples gave similar results for the other transitions reported here.

6.2.3.1 The T State

The lowest energy transition has a Franck-Condon region between 3.4 eV and 5.4 eV and produces the peak at 4.29 ± 0.05 eV. The shape and magnitude of the DCS curves for this transition, as shown in Figures 73 and 74, permit assignment to the lowest singlet $\rightarrow$ triplet transition. This transition was also observed in the threshold excitation spectrum at 4.3 eV and assigned to a triplet state.[78] The results of both experimental studies are in fair agreement with the theoretical calculations[31] which put the lowest triplet state at 4.07 eV.

The energy of the T state is about the same as in 1, 4 and 1, 5-hexadiene and in alkyl substituted ethylenes.[14, 68, 69] This result is somewhat surprising because the strong $\pi \rightarrow \pi^*$ transition (see 6.2.3.3 below) is shifted upwards by about 1 eV. One possible reason for this is the fact that the T state in ethylene is a compact valence type state while the V state is calculated to be more diffuse or Rydberg like.[79] The hyperconjugation with the σ_{CH} orbitals could be more effective for the V state because of the increased spatial overlap of the π and σ_{CH} orbitals producing the shift observed in the N $\rightarrow$ V transition energy. This explanation must be viewed with caution, however, because other ab initio calculations suggest that the V state

has a valence character rather than a diffuse character.[80, 81]

6.2.3.2 The 6.15 eV State

The next transition in 1, 4-cyclohexadiene produces the peak at 6.15 ± 0.07 eV. The Franck-Condon region extends from 5.5 eV to beyond 6.5 eV. The qualitative angular behavior of this feature indicates that it is a singlet → singlet transition. This feature is also seen in the optical spectrum[31] at 6.20 eV and in the threshold electron impact spectrum[78] at 6.3 eV. Both studies classified it as a $\pi \rightarrow \pi^*$ transition. Theoretical calculations[31] place a forbidden singlet→ singlet $\pi \rightarrow \pi^*$ transition at 6.42 eV and the intensity of the peak relative to that of the N → V type transition (see 6.2.3.3) is consistent with this assignment. An alternate assignment to a transition corresponding to the N → R (3s) transition[70, 82] in ethylene is also possible. The N → R transition arises from excitation of a π electron to the 3s type atomic orbital. In ethylene the N → R transition is superimposed on the N → V transition but in a substituted ethylene like cis-2-butene it occurs[70, 82] between 5.9 eV and 6.45 eV.

The peak at 6.93 eV in Figure 71 is produced by a benzene impurity in the sample as discussed previously.

Figure Captions

Figure 70. The electron impact spectrum of 1, 4-cyclohexadiene from 3.3 eV to 12.0 eV for E_0 = 50 eV and $\theta = 10°$.

Figure 71. The 3.3 eV to 8.8 eV energy-loss region for E_0 = 50 eV, $\theta = 80°$, and a resolution of 0.15 eV (FWHM).

Figure 72. Ratio of the intensity of the N → T transition to that of the N → V transition as a function of scattering angle for E = 30 eV (+) and E = 50 eV (Δ).

Figure 73. DCS curves for 1, 4-cyclohexadiene as a function of θ at an incident electron energy of 30 eV for elastic scattering (+) and for the N → T (Δ) and N → V (○) transitions.

Figure 74. Same as Figure 73 for an incident electron energy of 50 eV.

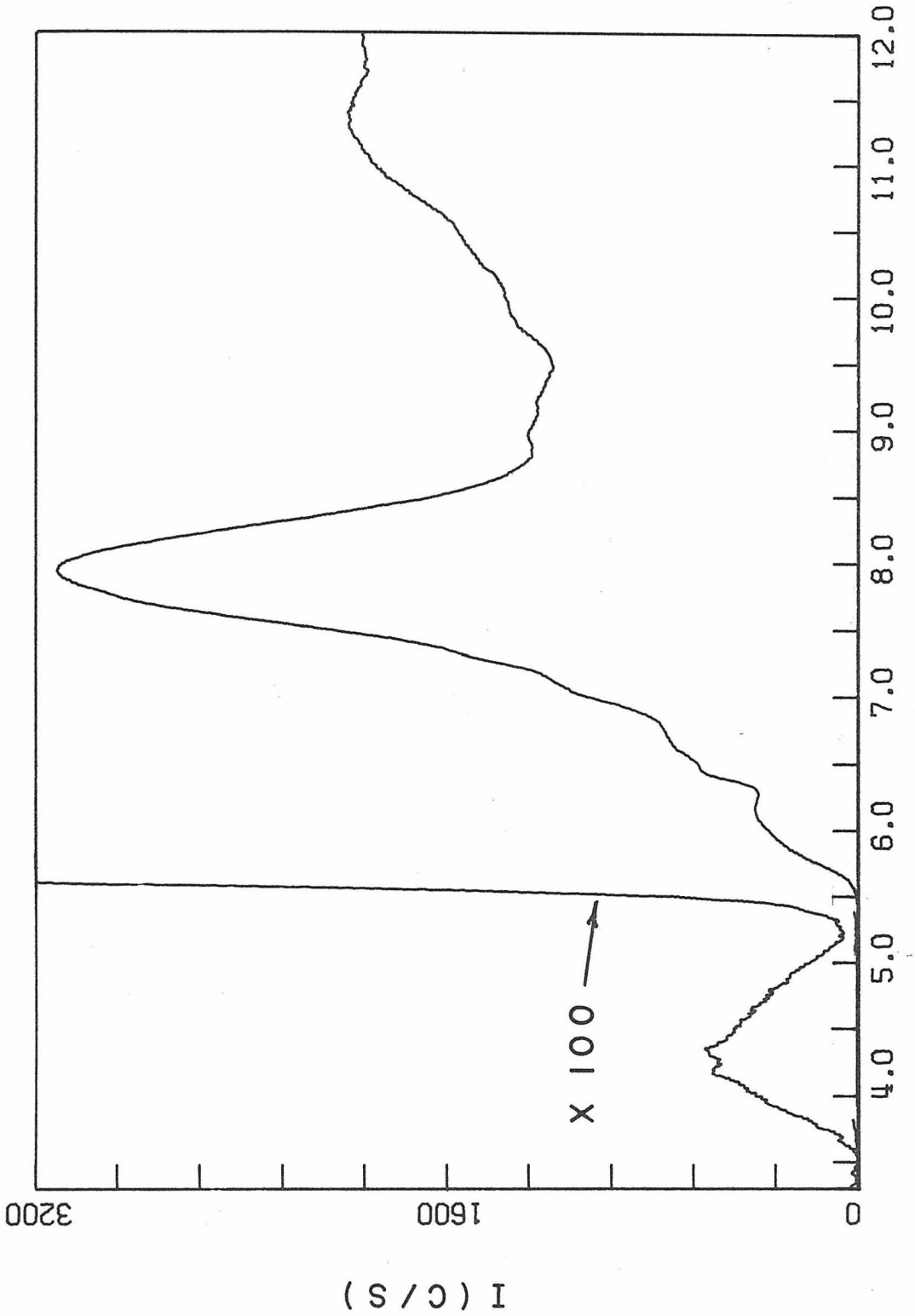

FIG. 70

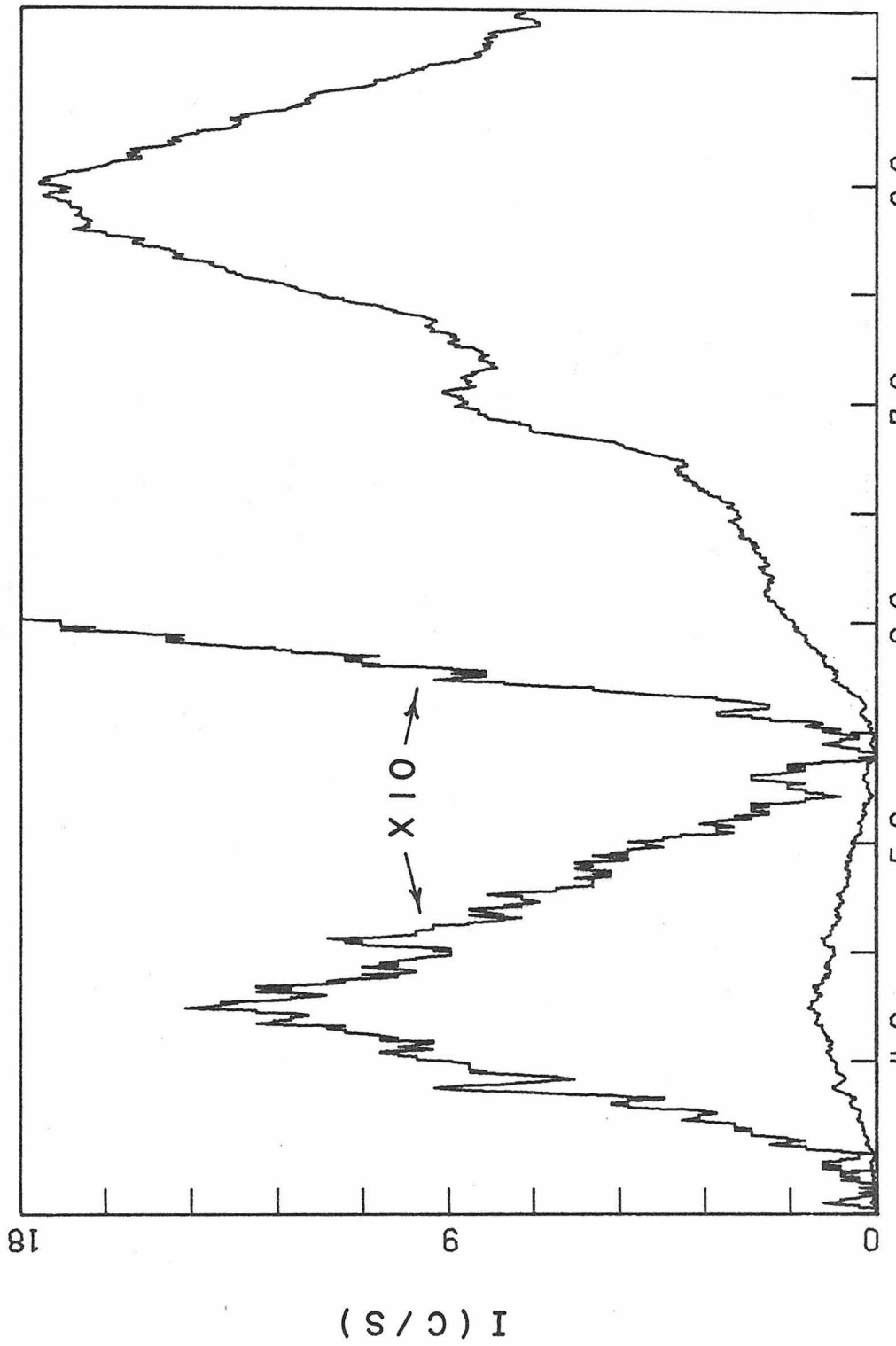

FIG. 71

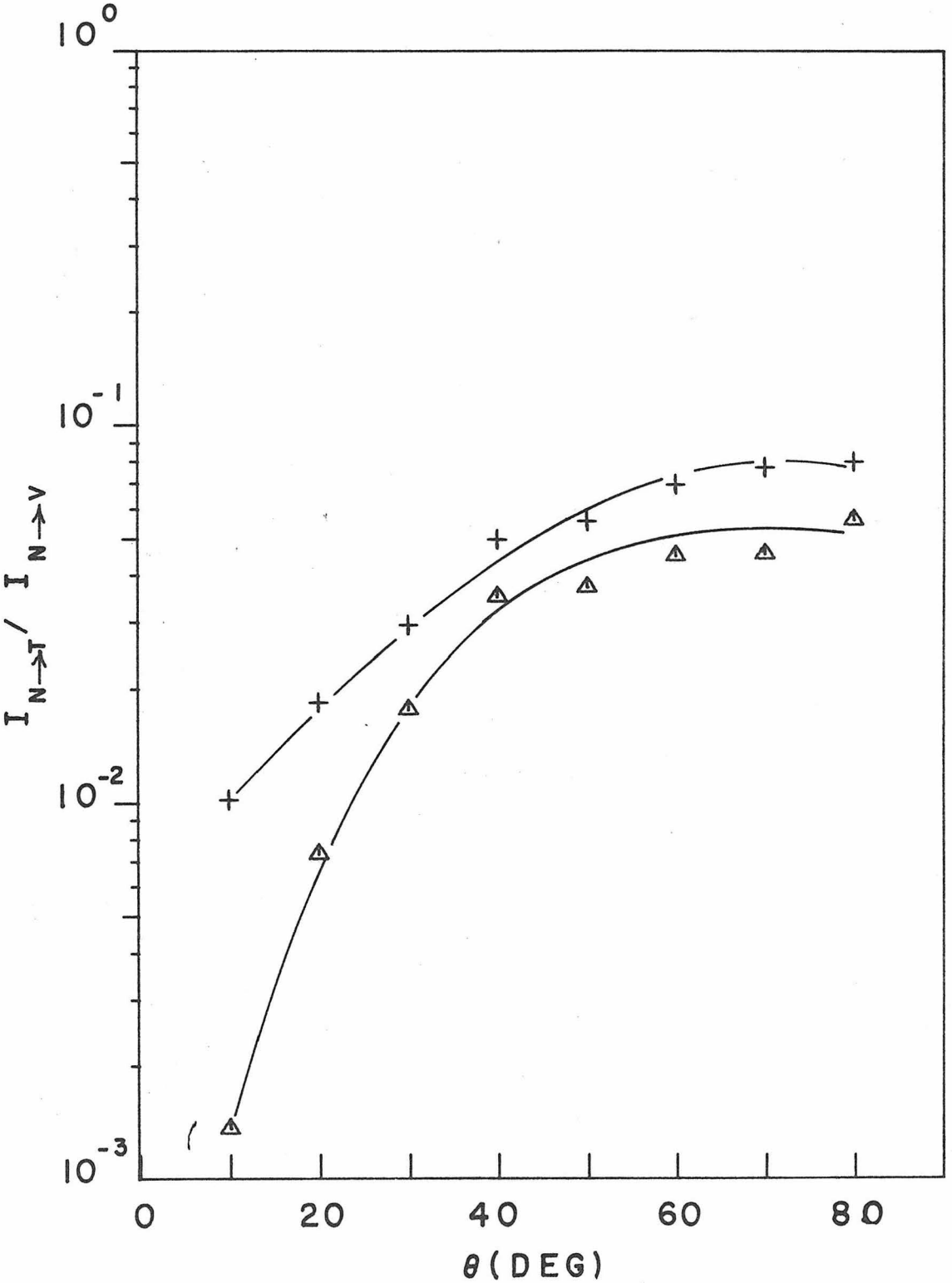

FIGURE 72

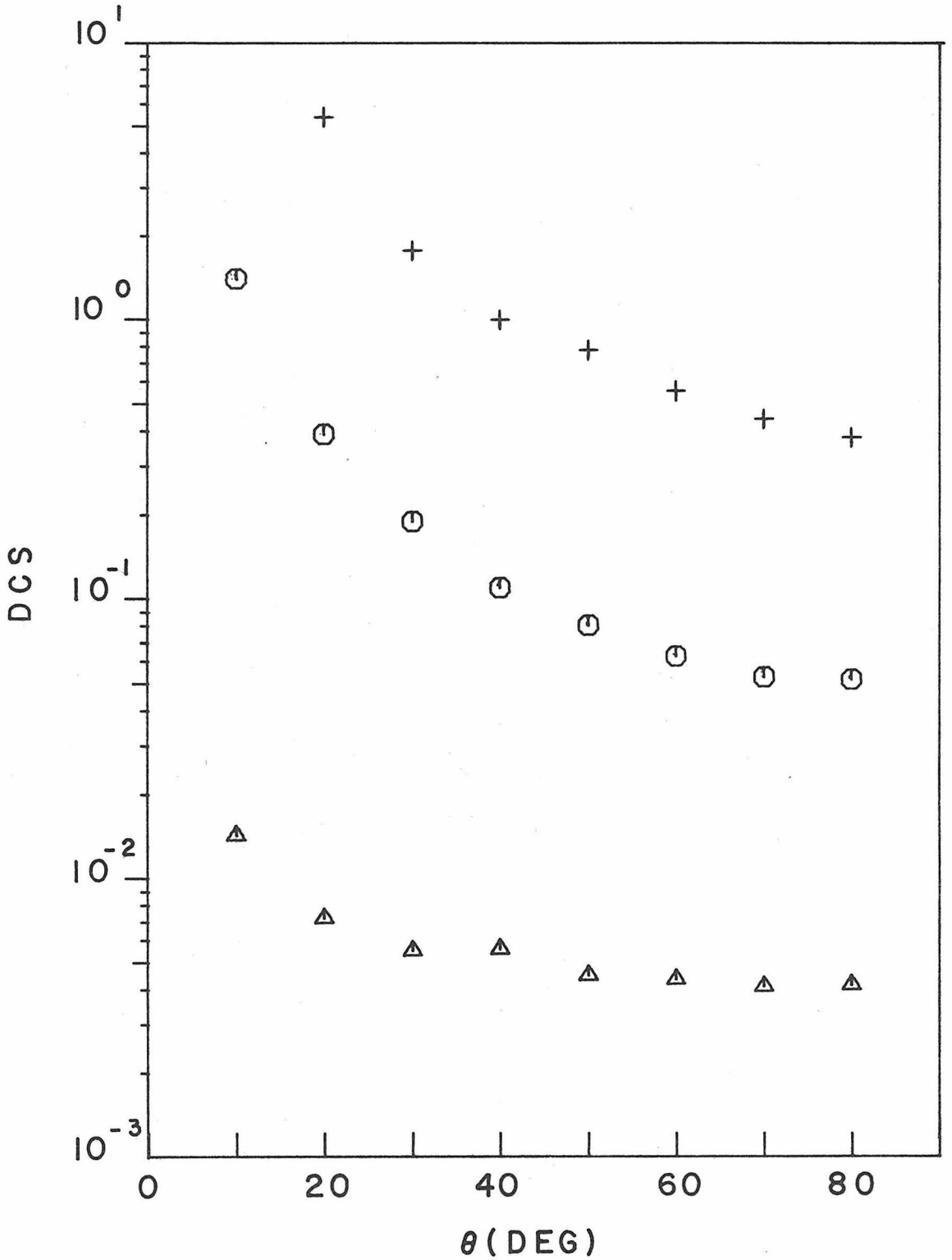

FIGURE 73

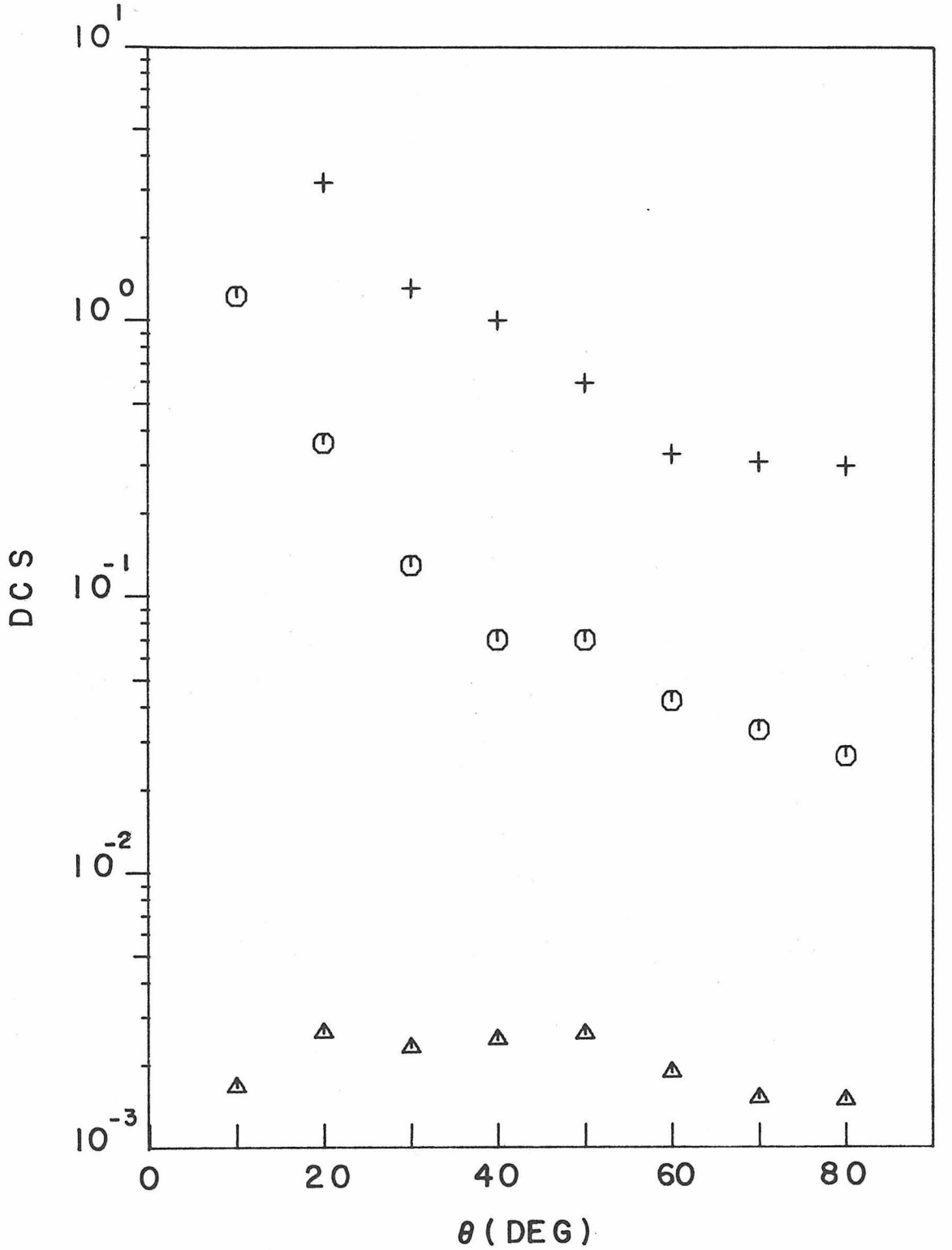

FIGURE 74

Table 6.2.3-1. DCS Values for 1,4-Cyclohexadiene

θ	Scattering Process [a] N→T	N→V	Elastic
		30 eV	
10	0.0143	1.399	–
20	0.00719	0.391	5.41
30	0.00553	0.188	1.78
40	0.00562	0.113	1.00
50	0.00451	0.0812	0.781
60	0.00435	0.0627	0.560
70	0.00408	0.0530	0.445
80	0.00415	0.0520	0.382
		50 eV	
10	0.00166	1.224	–
20	0.00263	0.360	3.19
30	0.00231	0.131	1.31
40	0.00247	0.0701	1.00
50	0.00258	0.0697	0.596
60	0.00187	0.0417	0.328
70	0.00151	0.0333	0.311
80	0.00148	0.0265	0.297

[a] The states are designated by the corresponding transition in ethylene.

6.2.3.3 The V State

The strongest feature in the spectrum peaks at 7.95 ± 0.07 eV. The DCS behavior indicates that this is a fully allowed singlet → singlet transition. As discussed in the introduction, this transition may not correspond to the first $\pi \rightarrow \pi^*$ transition but may be the second or third transition of this type. The transition appears at 8.1 eV in the trapped electron spectrum.[78] Theoretical calculations[31] predict that the lowest energy allowed $\pi \rightarrow \pi^*$ transition should be at 7.37 eV in poor agreement with the experimental results.

The higher energy loss features in Figure 70 were not studied at a sufficient number of impact energies and scattering angles to extract peak locations at the present time.

6.3 Azo Compounds

The azo compounds ($R_1-N=N-R_2$) have been the object of many photochemical studies. The results have been reviewed by several authors.[83-85] The effect of uv radiation on azo compounds is to produce N_2 elimination, cis-trans isomerization, and tautomerization to a hydrazone. The N_2 elimination reaction has been used in many experiments because it provides a clean source of alkyl radicals for synthetic procedures.

Although earlier studies[85, 86] had located the 0-0 band for the lowest singlet → triplet transition in diazabicycloheptene by energy transfer arguments, the results in the papers on azomethane in Appendices I and II and in section 6.3.2 for azo-t-butane represent the first direct spectroscopic observation of azo compound triplet states. The energy locations of these transitions should provide important information in discussions of which states are involved in the various photochemical reactions.

6.3.1. Trans-Azomethane

Azomethane ($H_3C-N=N-CH_3$) has been studied in conjunction with M. S. Foster and J. L. Beauchamp who studied the trapped electron spectrum. The results are described in the papers in Appendices I and II of this thesis. The paper in Appendix I has been accepted for publication by the Journal of Chemical Physics while the second paper has been submitted to Chemical Physics Letters.

Singlet → triplet transitions are seen with maxima at 2.75 ± 0.04 eV and $4.8_4 \pm 0.1$ eV. A comparison of calculations for diimide (H-N=N-H) suggests that these are the $n_+ \rightarrow \pi^*$ ($\tilde{X}^1A_g \rightarrow 1\,^3B_g$) and $\pi \rightarrow \pi^*$ ($\tilde{X}^1A_g \rightarrow 1\,^3B_u$) transitions, respectively. The $n_+ \rightarrow \pi^*$ ($\tilde{X}^1A_g \rightarrow 1\,^1B_g$) transition peaks at 3.50 ± 0.04 eV. It has been previously seen optically[84, 87] and assigned[87, 88] on the basis of its optical intensity

Table 6.3.1-1. DCS Values for trans-Azomethane

	Scattering Process [a]				
θ	$1\,^3B_g$	$1\,^1B_g$	4.84 eV	6.71 eV	Elastic
			20 eV		
15	0.000438	0.00935	0.00140	0.0725	6.05
20	0.000651	0.00560	0.00244	0.0431	3.68
30	0.000588	0.00298	0.00245	0.0287	1.69
40	0.000740	0.00243	0.00321	0.0223	1.00
50	0.000742	0.00196	0.00353	0.0187	0.648
60	0.000736	0.00159	0.00219	0.0153	0.428
70	0.000794	0.00146	0.00206	0.0113	0.326
80	0.000739	0.00130	0.00175	0.00980	0.285
10	0.000618	0.0358	0.00135	0.710	–
20	0.000645	0.0118	0.000685	0.134	8.00
30	0.000685	0.00432	0.00119	0.0527	2.50
40	0.000412	0.00161	0.00110	0.0234	1.00
50	0.000469	0.00146	0.00132	0.0154	0.70
60	0.000393	0.00112	0.00138	0.00970	0.473
70	0.000576	0.000971	0.00154	0.00859	0.337
80	0.000597	0.000849	0.00121	0.00615	0.242

[a] The scattering process is identified as either the energy of the peak for the transition or by the symmetry of the corresponding excited state in trans-diimide.

and by comparison with theoretical calculations. Higher energy loss singlet→singlet transitions are seen in the 5 eV to 10 eV transition energy range. Peaks are seen at 6.01 eV, 6.71 eV, 7.8 eV, and 9.5 eV. The nature of these transitions is not clear at present although the first is a symmetry-forbidden or Rydberg-like singlet→singlet transition and the higher peaks are produced by allowed singlet→singlet transitions.

More detailed discussions of the trans-azomethane results appear in the papers in the appendices. Table 6.3.1-1 gives a listing of the numerical DCS values which were used to make the plots in the papers.

6.3.2. Azo-t-Butane

The results for azomethane suggested that the low-lying states of the azo compounds are quite similar to those of diimide (H–N=N–H), as discussed in Appendix I. Azo-t-butane ($(H_3C)_3$–C–N=N–C–$(CH_3)_3$) can be derived formally from azomethane by exhaustive substitution of methyl radicals for each H atom. It was hoped that the spectra of azo-t-butane would be similar to that of azomethane for the low-lying transitions. This was found to be true as discussed below.

Spectra of azo-t-butane were taken at incident energies of 50 eV and 70 eV. Examples of the spectrum are shown in Figures 75

and 76 while the DCS curves are plotted in Figures 77 and 78. The results of these studies for both azo-t-butane and azomethane are summarized in Table 6.3.2-1 and the DCS values for azo-t-butane are listed in Table 6.3.2-2. The sample of azo-t-butane was obtained from Fairchild Chemical Co. and subjected to the usual liquid nitrogen freeze-pump-thaw purification cycle.

6.3.2.1 The $1\,^3B_g$ State

The first inelastic transition in azo-t-butane peaks at 2.67 ± 0.05 eV with a Franck-Condon region from 2.2 eV to beyond 3.1 eV. The DCS curves are isotropic within a factor of 2 from 10° to 80° at both impact energies. The shape and the magnitude of the DCS curves for this transition indicate that it is a singlet → triplet transition. The lowest singlet → triplet transition in azomethane is the $\tilde{X}^1A_g \rightarrow 1\,^3B_g$ which peaks at 2.75 eV. The similarity in energy of these features strongly suggests that the 2.67 eV peak in azo-t-butane is produced by its $\tilde{X}^1A_g \rightarrow 1\,^3B_g$ transition.

6.3.2.2 The $1\,^1B_g$ State

The second peak in the spectrum occurs at 3.37 ± 0.02 eV. The Franck-Condon region for the band ranges from 2.9 eV to 4.1 eV. The transition has been seen by optical absorption methods and assigned to the $\tilde{X}^1A_g \rightarrow 1\,^1B_g$ ($n_+ \rightarrow \pi^*$) transition.[87] The peak in the

optical spectrum occurs at 3.37 eV, in excellent agreement with the present results. The forward peaked behavior of the DCS for this transition confirms the assignment to a spin-allowed transition. This state corresponds to the 3.50 eV state in azomethane.

6.3.2.3 The 4.9 eV State

A very weak feature is seen in both Figures 75 and 76 at 4.9 ± 0.1 eV. The ratio of the peak height at 4.9 eV to that of the 2.67 eV ($1\,^3B_g$) peak was independent of θ within a factor of two. This suggests that the 4.9 eV state is produced by a singlet → triplet transition because the constant peak ratio indicates that the DCS for the 4.9 eV feature is also independent of θ. More quantitative measurement of the DCS for this region was not performed because it is a shoulder in the onset region for stronger singlet → singlet transitions. In azomethane the second singlet → triplet transition occurs at 4.8_4 eV in close agreement with the results in azo-t-butane. The similarity of the results for the three low lying transitions in azo-t-butane and azomethane lends further support to the assumption that these states arise from excitations of the azine group (–N=N–) electrons.

Theoretical calculations [87-90] for diimide predict that the second triplet state is the $1\,^3B_g$ ($\pi \rightarrow \pi^*$) and the applicability of diimide calculations to both azomethane and azo-t-butane is supported by the

Figure Captions

Figure 75. The electron impact spectrum of azo-t-butane from 2 eV to 9 eV energy loss for E_0 = 50 eV, $\theta = 10°$, and a resolution of 0.12 eV (FWHM).

Figure 76. The electron impact spectrum of azo-t-butane from 2 eV to 6 eV energy loss for an incident electron energy of 70 eV, $\theta = 70°$, and a resolution of 0.14 eV (FWHM).

Figure 77. DCS curves for azo-t-butane as a function of θ at an incident electron energy of 50 eV for elastic scattering (+) and for the $\chi^1A_g \rightarrow 1^3B_g$ (Δ) and the $\chi^1A_g \rightarrow 1^1B_g$ ($\bigcirc$) transitions.

Figure 78. Same as Figure 77 for an incident electron energy of 70 eV.

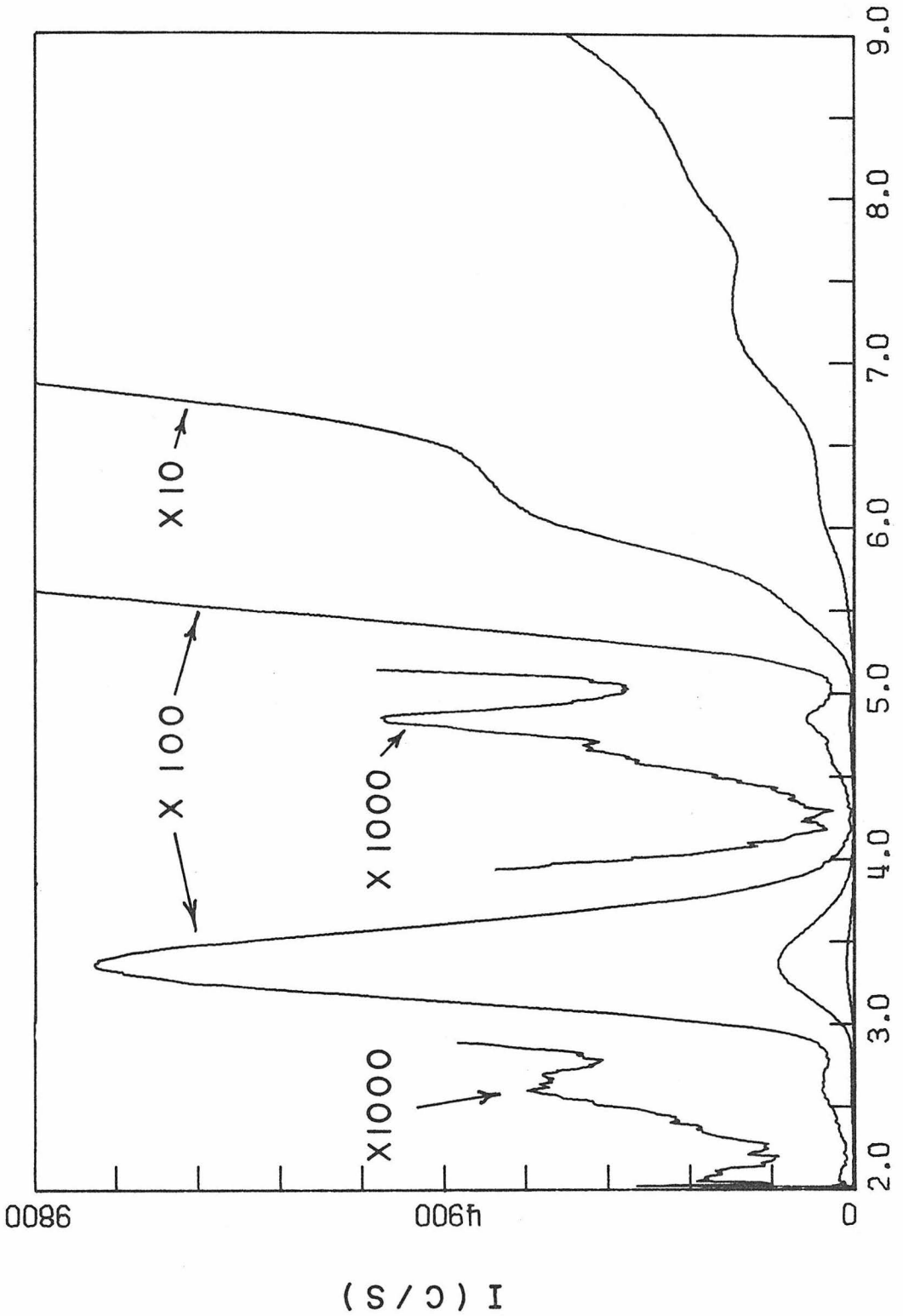
9800
4900
0
I (C/S)
X10000
X 100
X 1000
X 10
2.0
3.0
4.0
5.0
6.0
7.0
8.0
9.0
ΔE(eV)

FIG. 75

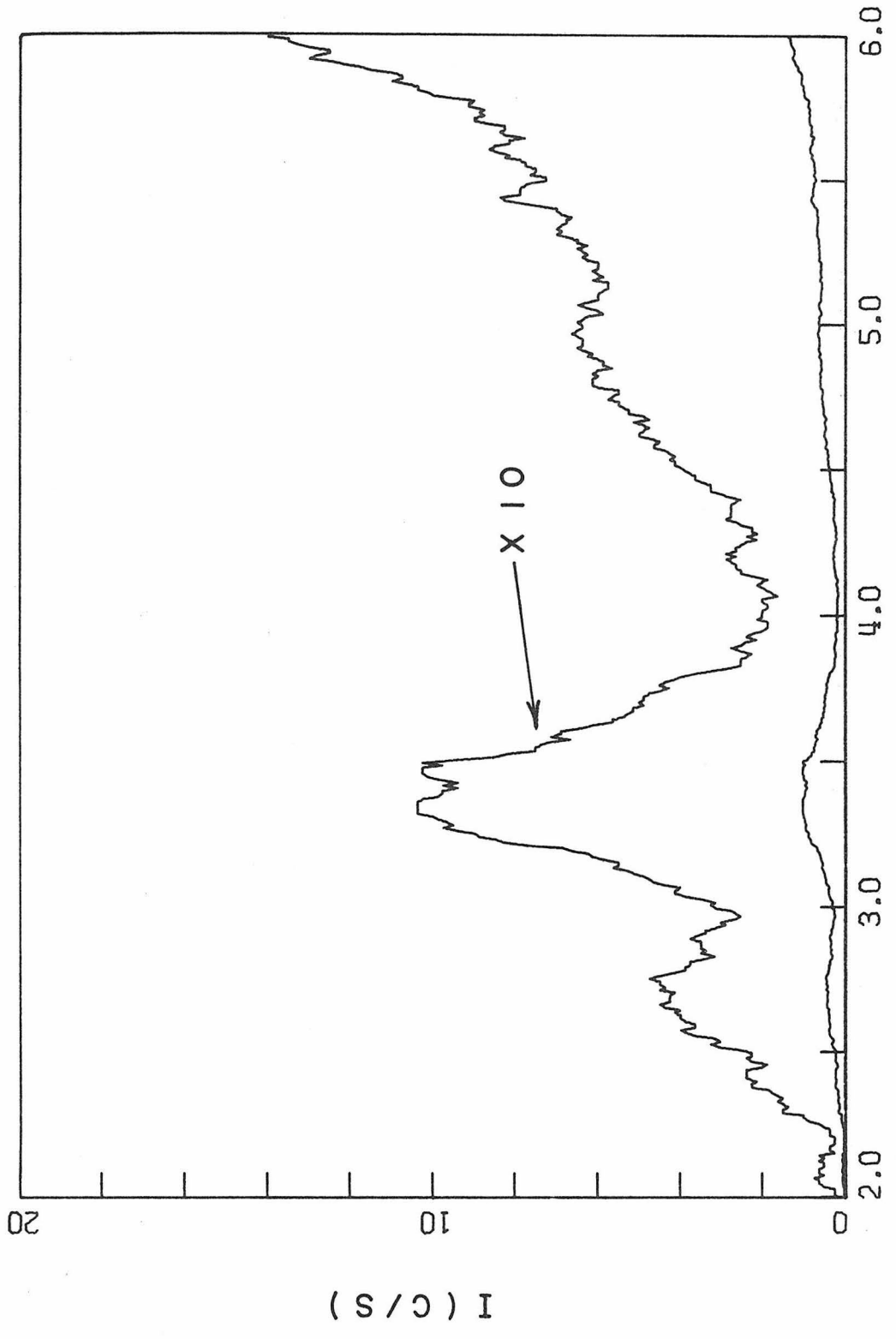

FIG. 76

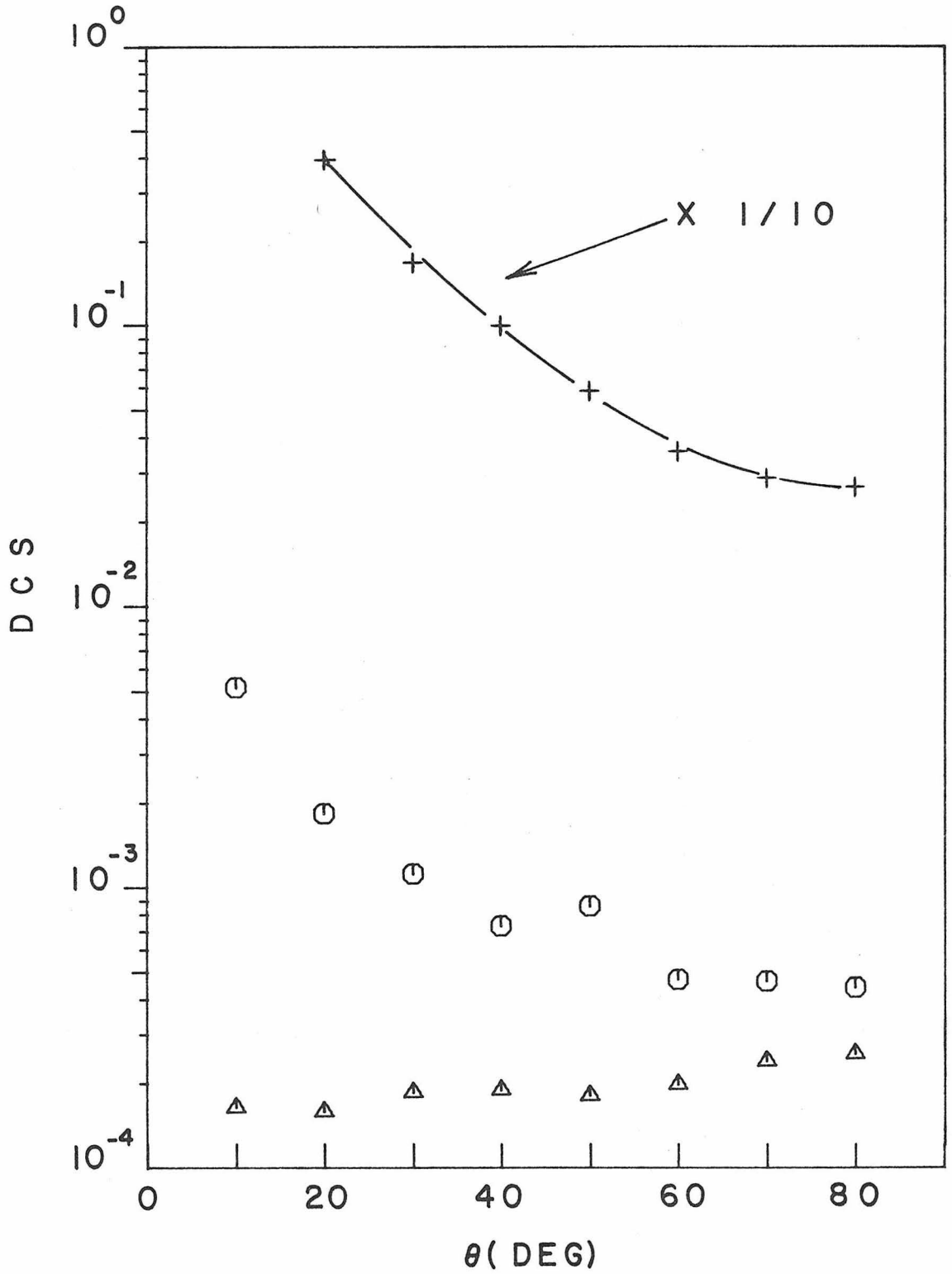

FIGURE 77

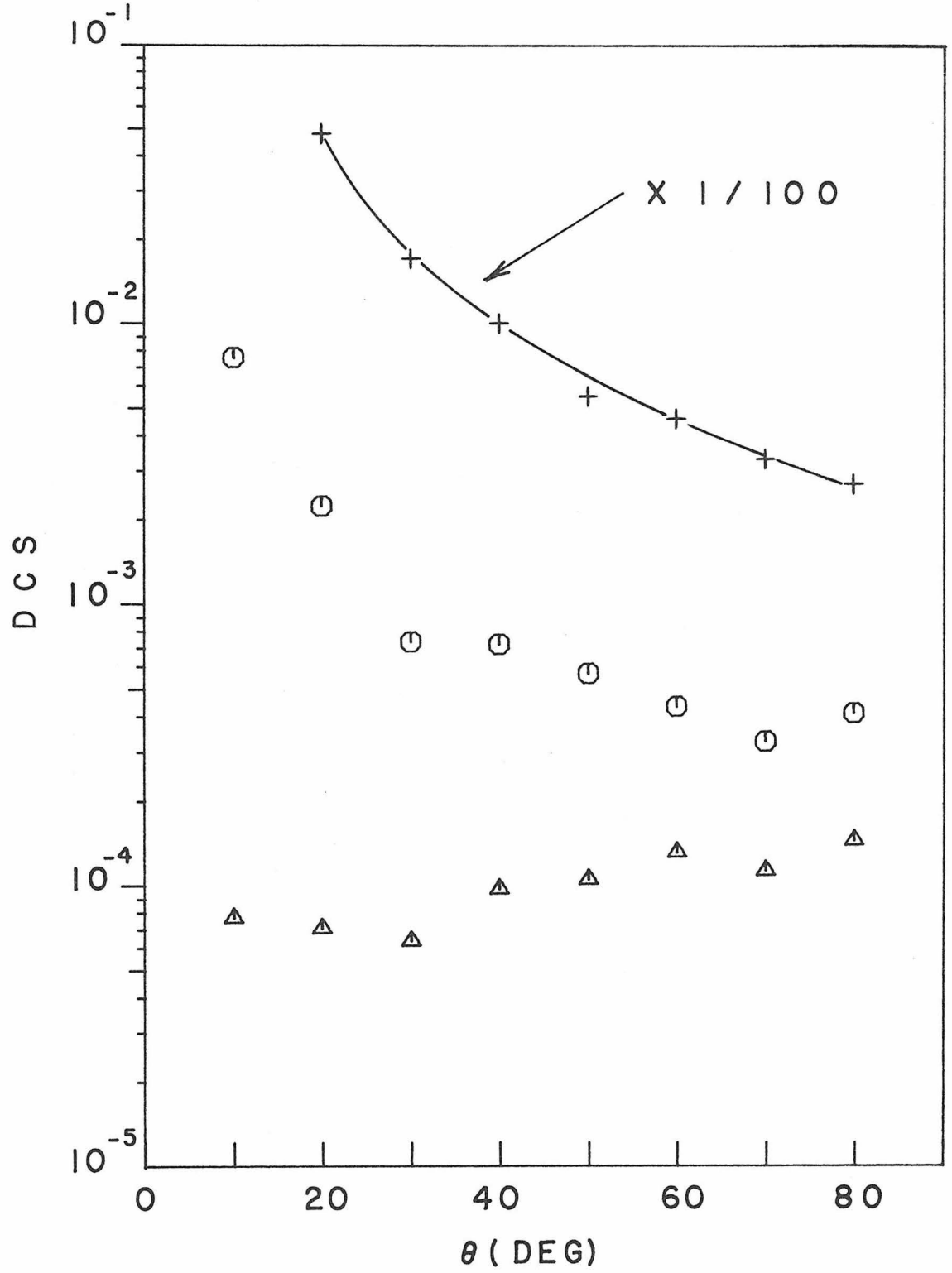

FIGURE 78

Table 6.3.2-1. Excited Electronic States of Some Azo Compounds

Excited state	Transition energy (eV) Azomethane	Azo-t-butane Present study	Azo-t-butane Optical [a]
$1\,^3B_g$	2.75 ± 0.04 (2.3 → 3.1) [b]	2.67 ± 0.05 (2.2 → 3.1)	–
$1\,^1B_g$	3.50 ± 0.04 (2.9 → 4.2)	3.37 ± 0.02 (2.9 → 4.1)	3.37
Triplet ($1\,^3B_u$?)	4.8_4 ± 0.1	4.9 ± 0.1	–
Singlets [c]	6.01 ± 0.1	6.1 ± 0.1	6.1
	6.71 ± 0.03	7.35 ± 0.1	7.35
	7.8 ± 0.1	8.1 ± 0.1	8.14
	9.5 ± 0.1		9.2

[a] Reference 87.

[b] The numbers in parenthesis give the estimated band onsets and ends.

[c] The listing of the singlets is in the order of increasing energy and does not imply that these higher states in the two molecules are correlated with each other.

Table 6.3.2-2. DCS Values for Azo-t-butane

θ	Scattering Process [a] $\tilde{X}^1A_g \rightarrow 1^3B_g$	$\tilde{X}^1A_g \rightarrow 1^1B_g$	Elastic
		50 eV	
10	0.000164	0.00516	–
20	0.000159	0.00184	3.93
30	0.000186	0.00112	1.69
40	0.000190	0.000734	1.00
50	0.000181	0.000864	0.588
60	0.000199	0.000472	0.363
70	0.000241	0.000466	0.288
80	0.000255	0.000441	0.272
		70 eV	
10	0.0000773	0.00758	–
20	0.0000709	0.00224	4.80
30	0.0000636	0.000735	1.71
40	0.0000978	0.000723	1.00
50	0.000106	0.000570	0.553
60	0.000132	0.000436	0.462
70	0.000114	0.000328	0.328
80	0.000146	0.000413	0.270

[a] The scattering process is identified as the corresponding transition in trans-diimide.

similarity of the spectra of both molecules.

6.3.2.4 Higher Singlet States

Broad maxima on a rising background are seen in Figure 75. Peaks or stepouts are apparent at 6.1 ± 0.1 eV, 7.35 ± 0.1 eV, and 8.1 ± 0.1 eV. The intensity and angular behavior of these features suggest that all are singlet → singlet transitions. The results are similar to those of the optical absorption spectrum[87] which has peaks at 6.1 eV, 7.35 eV, 8.14 eV, and 9.2 eV. The intensity of the three higher peaks indicates that these are fully allowed transitions while the intensity of the lowest peak ($f \approx .023$ using a classical dispersion theory formula[30]) suggests that it may be a symmetry forbidden or Rydberg-like singlet → singlet transition.

6.4. Propadiene

Propadiene (allene) has been studied and the results are discussed extensively in the manuscript in Appendix III. The manuscript has been accepted for publication in the Journal of Chemical Physics.

6.5 Thiophosgene

Thiophosgene (Cl_2CS) provides an interesting spectrum for comparison with that of formaldehyde and other carbonyls and

thiocarbonyls. Both thiophosgene and formaldehyde have low-lying $n \rightarrow \pi^*$ transitions and both are non-planar in this excited state. It was hoped that higher energy transitions such as the $\pi \rightarrow \pi^*$ transitions in each molecule might also show such similarities. This does not appear to be the case as discussed below.

Low resolution spectra in the 2.0 eV to 6.0 eV energy loss range are shown in Figures 79 to 81. Peaks were also seen at higher energy losses but are not reported here because some of these peaks may have been produced by impurity molecules in the sample.

The thiophosgene sample was obtained from the Aldrich Chemical Co. and did not have a specified purity level. Commercial samples of thiphosgene are known[91] to contain variable amounts of phosgene, CS_2, OCS, SO_2, and thiophosgene dimer as impurities. The sample used in the present study was subjected to the normal liquid nitrogen freeze-pump-thaw cycle but was not subjected to the gas-liquid chromatography process which is necessary to prepare a spectroscopically pure sample. The spectra of the first four impurity compounds have been studied in this laboratory and were used to look for impurity peaks in the spectrum of thiophosgene.

6.5.1. The $1\,^1A_2$ and $1\,^3A_2$ States

The first transition in the electron impact spectrum has an

onset at about 2.1 eV and produces a peak at 2.61 ± 0.05 eV. The optical spectrum in this region has been studied extensively[91-95] and it is known that two strongly overlapping transitions are present. The optical studies show that the first is the $n \rightarrow \pi^*$ $\tilde{X}^1A_1 \rightarrow 1^3A_2$ transition whose origin is at 2.16 eV[95] and extends from 2.08 eV[95] to 2.34 eV[94] while the second transition is the $n \rightarrow \pi^*$ $\tilde{X}^1A_1 \rightarrow 1^1A_2$ whose origin is at 2.32 eV[91] and extends from 2.16 eV to 3.18 eV.[94] Both excited states are non-planar,[91,95] like the corresponding $n \rightarrow \pi^*$ states in formaldehyde. The two states were never seen as separate peaks in the present study because of the low resolution used here and the fact that they are strongly overlapped with each other.

6.5.2. The 3.1 eV State

A second peak is observable on the high energy loss side of the 1^1A_2 peak in Figures 79 and 80. The peak occurs at 3.1 ± 0.1 eV and has an estimated Franck-Condon region from 2.5 eV to 3.6 eV. This feature has not been reported optically and none of the impurity molecules mentioned in the introduction have a strong transition at this energy. At 40 eV impact energy the peak height ratio of the 3.1 eV feature to that of the singlet → singlet transition at 4.88 eV (see 6.5.4) increases by at least a factor of 10 in going from $\theta = 10^\circ$ to $\theta = 80^\circ$. The increase is probably greater because the 1^1A_2 state is

still very intense at 3.1 eV energy loss for E = 40 eV and $\theta = 10°$ as shown in Figure 81. Thus, the 3.1 eV peak intensity is artificially increased by overlap of the $1\,^1A_2$ state. The peak height ratio increase and the energy dependence of the 3.1 eV feature indicate that it is the second singlet → triplet transition in the molecule. It may correspond to the singlet → singlet transition at 4.88 eV which has been attributed to the $\pi \rightarrow \pi^*$, $\tilde{X}\,^1A_1 \rightarrow {}^1A_1$ transition (see 6.5.4). A splitting of 1.8 eV between the singlet → triplet and singlet → singlet components of a $\pi \rightarrow \pi^*$ transition is comparable to the corresponding split of 2.5 eV to 3 eV in the $\pi \rightarrow \pi^*$ transition in substituted olefins.[14, 24, 68-70]

6.5.3. The 3.95 eV State

A peak is seen at 3.95 ± 0.05 eV in Figure 81. This feature has an angular behavior which is consistent with a singlet → singlet transition. A peak has also been seen at this energy in optical studies with an oscillator strength f of 2.42×10^{-5} and attributed to an n(Cl) → π^* transition on the basis of theoretical calculations.[96] Although the present results cannot eliminate the possibility that this is a correct assignment, the extremely weak intensity of the transition in the electron impact spectrum strongly suggests that this is an impurity peak. CS_2 is known to have a singlet → singlet transition at 3.9 eV in both optical[97] and electron impact studies[98] and must be

considered as a possible source of the 3.95 eV peak.

6.5.4. The 4.89 eV State

The most intense transition in the 2 eV to 6 eV energy loss region occurs at 4.89 ± 0.02 eV with a Franck-Condon region from 4.4 to 5.5 eV. This band has been studied optically [93, 94, 99] and attributed [96, 99] to a $\pi \rightarrow \pi^*$, $\tilde{X}^1A_1 \rightarrow 2^1A_1$ transition. The peak in the optical spectrum [99] occurs at 4.88 eV, in good agreement with the present study. The qualitative angular behavior and the intensity confirm an assignment to a singlet → singlet transition. The location of the corresponding $\pi \rightarrow \pi^*$ transition in formaldehyde is not known. Theoretical calculations [100, 101] place the $\pi \rightarrow \pi^*$ transition in formaldehyde at 10 eV or more about the ground where it can interact strongly with a number of Rydberg states. Thus if the 4.89 eV state is in fact the $\pi \rightarrow \pi^*$ transition in thiophosgene, then the thiophosgene spectrum is analogous to that of formaldehyde for only the low-lying $n \rightarrow \pi^*$ transitions.

Figure Captions

Figure 79. The electron impact spectrum of thiophosgene from 2 eV to 5.5 eV energy loss for 25 eV incident energy, $\theta = 10°$, and a resolution of 0.13 eV (FWHM).

Figure 80. Same as Figure 79 except $\theta = 50°$ and a resolution of 0.12 eV.

Figure 81. The 2 eV to 6 eV energy loss region in thiophosgene with an incident energy of 40 eV and a scattering angle of 10°.

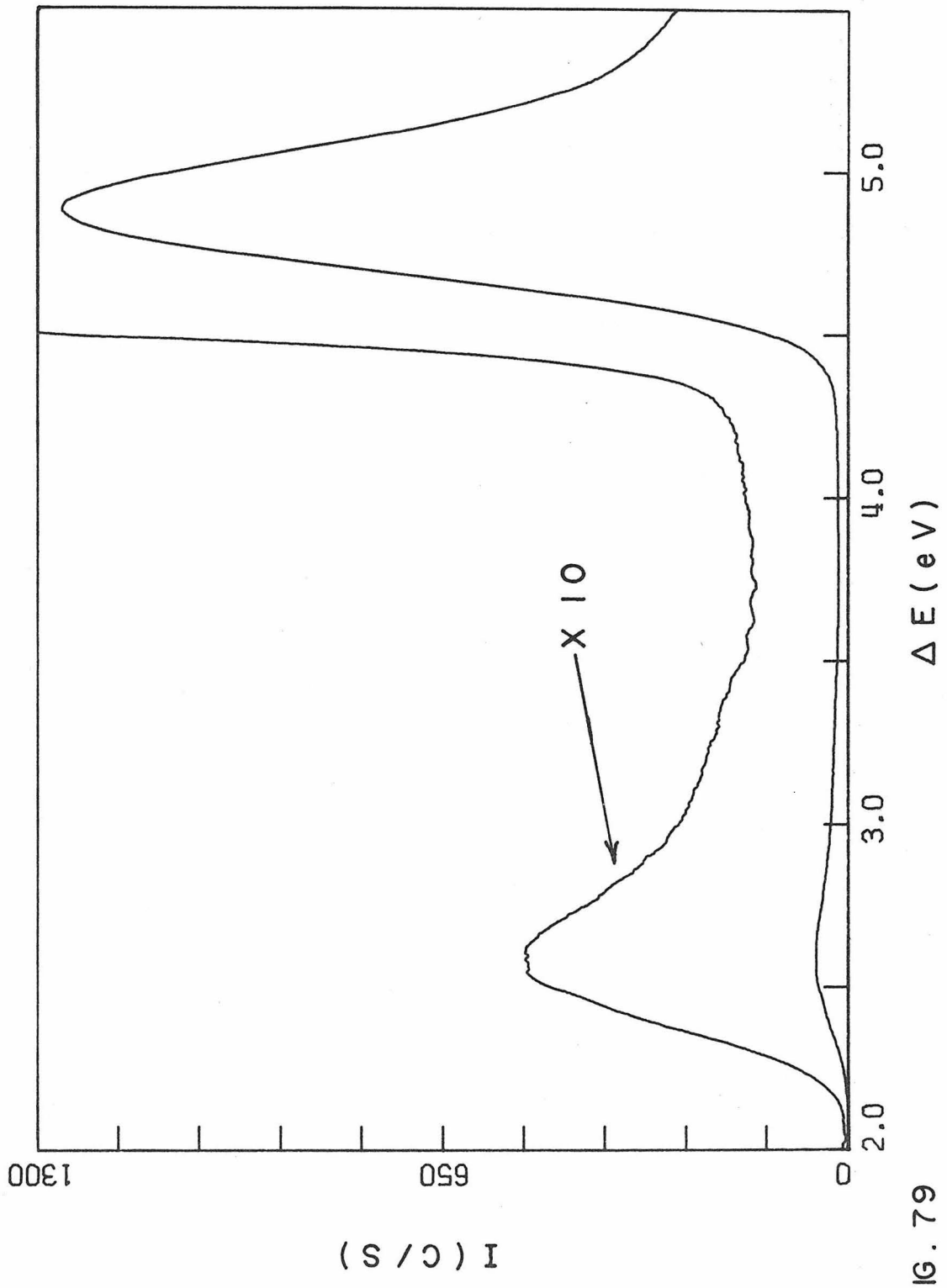

FIG. 79

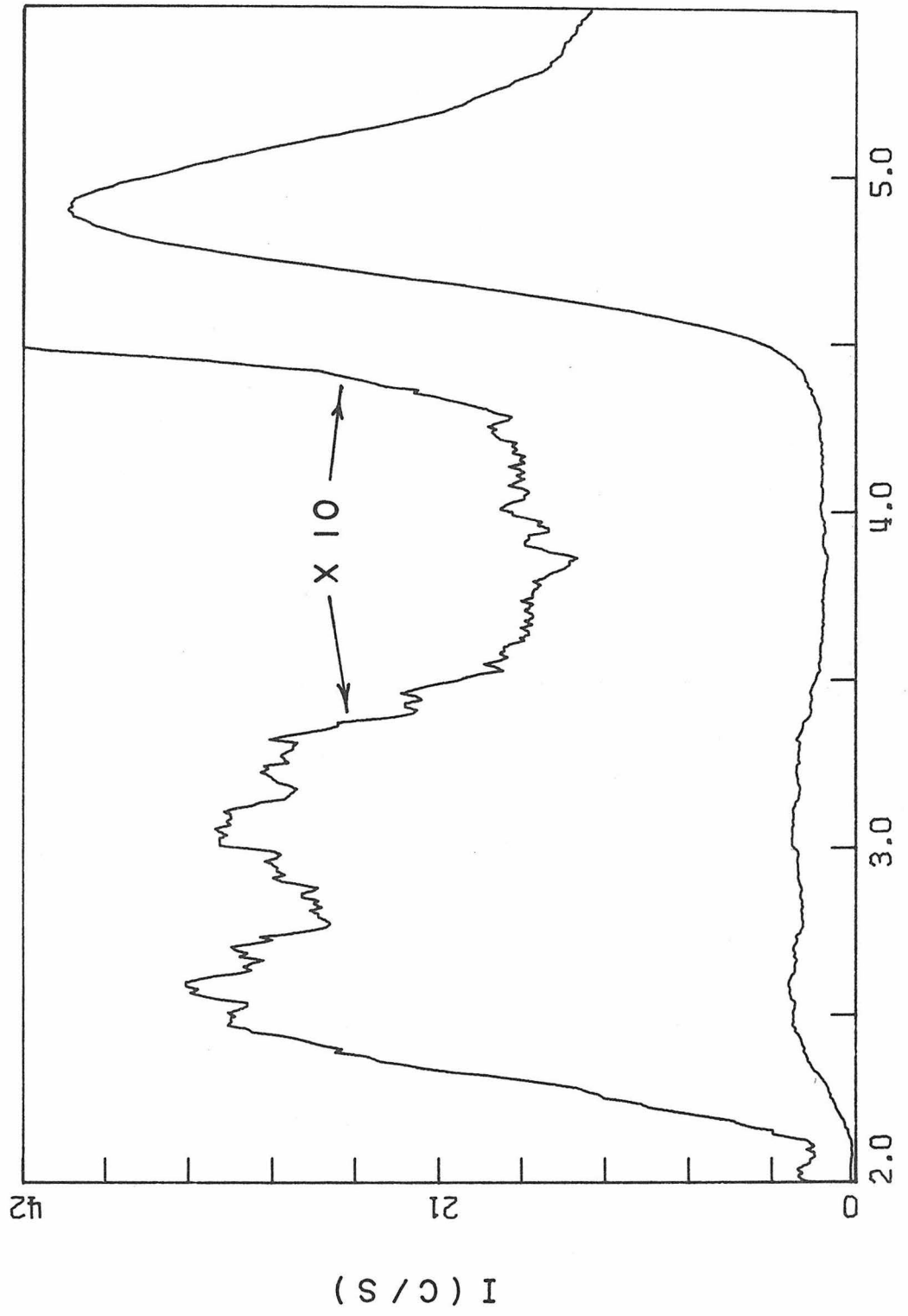

FIG. 80

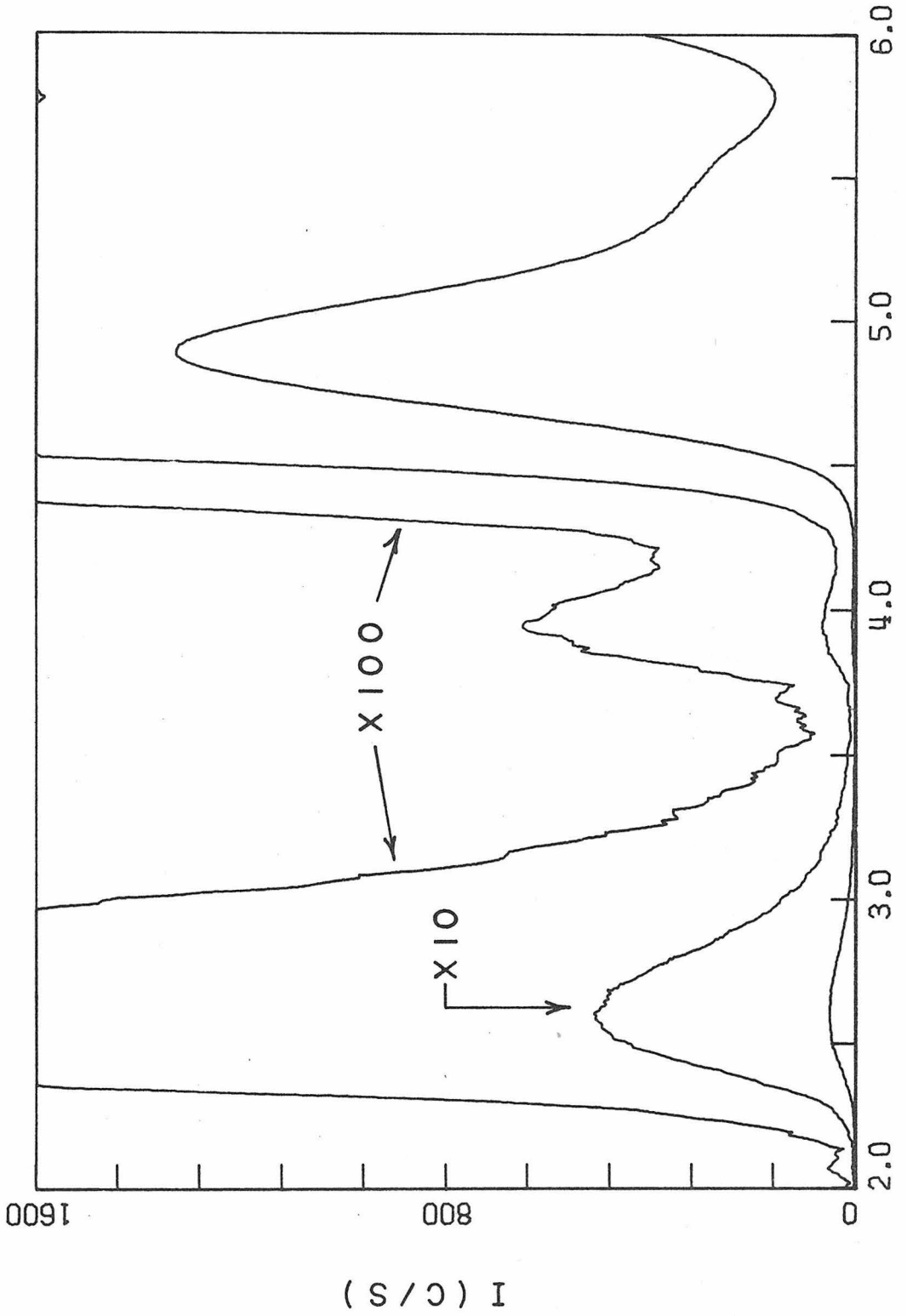

FIG. 81

References

1. T. Rosenfeld, A. Alchalel, and M. Ottolenghi, J. Phys. Chem., 78, 336 (1974).

2. R. Hubbard and A. Kropf, Proc. Nat. Acad. Sci. U.S., 44, 130 (1958).

3. R. A. Morton and G. Pitt, Biochem. J., 59, 128 (1955).

4. B. S. Hudson and B. E. Kohler, J. Chem. Phys., 59, 4984 (1973).

5. R. L. Christensen and B. E. Kohler, Photochem. Photobiol., 18, 293 (1973).

6. R. S. Mulliken, Chem. Phys. Lett., 25, 305 (1974).

7. R. Srinivasan, Advan. Photochem., 4, 113 (1966).

8. E. Havinga and J. L. M. A. Schlatmann, Tetrahedron, 16, 146 (1961).

9. S. Shih, R. J. Buenker, and S. D. Peyerimhoff, Chem. Phys. Lett., 16, 244 (1972).

10. T. H. Dunning, Jr., R. P. Hosteny, and I. Shavitt, J. Amer. Chem. Soc., 95, 5067 (1973).

11. R. P. Hosteny, T. H. Dunning, Jr., R. R. Gilman, A. Pipano, and I. Shavitt, Molec. Spec. Symposium, Ohio State University, June 1971.

12. O. A. Mosher, W. M. Flicker, and A. Kuppermann, Chem. Phys. Lett., 19, 332 (1973).

13. O. A. Mosher, W. M. Flicker, and A. Kuppermann, J. Chem. Phys., 59, 6502 (1973).

14. S. Trajmar, J. K. Rice, and A. Kuppermann, Adv. Chem. Phys., 18, 15 (1970).

15. D. F. Evans, J. Chem. Soc. (London), 1735 (1960).

16. G. S. Hammond, N. J. Turro, and A. Fischer, J. Amer. Chem. Soc., 83, 4674 (1961).

17. I. Haller and R. Srinivasan, J. Chem. Phys., 40, 1992 (1964).

18. J. Collin and F. P. Lossing, Can. J. Chem., 35, 778 (1957).

19. D. L. Dexter, J. Chem. Phys., 21, 836 (1953).

20. K. R. Naqvi and C. Steel, Chem. Phys. Lett., 6, 29 (1970).

21. M. W. Schmidt and E. K. C. Lee, J. Amer. Chem. Soc., 90, 5919 (1968).

22. M. W. Schmidt and E. K. C. Lee, J. Amer. Chem. Soc., 92, 3579 (1970).

23. R. S. Mulliken, J. Chem. Phys., 7, 121 (1939).

24. L. C. Jones, Jr., and L. W. Taylor, Anal. Chem., 27, 228 (1955).

25. W. C. Price and A. D. Walsh, Proc. Roy. Soc. (London), 174, 220 (1940).

26. E. P. Carr, L. W. Pickett, and H. Stücklen, Rev. Mod. Phys., 14, 260 (1942).

27. R. Pariser and R. G. Parr, J. Chem. Phys., 21, 767 (1953).

28. R. H. Pottier, G. P. Semeluk, and R. D. S. Stevens, Spectrosc. Lett., 2, 369 (1969).

29. C. Sandorfy, J. Molec. Struct., 19, 183 (1973).

30. W. Kauzmann, Quantum Chemistry, Academic Press, New York, 1957, p. 581.

31. N. L. Allinger, J. C. Tai, and T. W. Stuart, Theoret. Chim. Acta, 8, 101 (1967).

32. R. E. Kellog and W. T. Simpson, J. Amer. Chem. Soc., 87, 4230 (1965).

33. G. S. Hammond, J. Saltiel, A. A. Lamola, N. J. Turro, J. S. Bradshaw, D. O. Cowan, R. C. Counsell, V. Vogt, and C. Dalton, J. Amer. Chem. Soc., 86, 3197 (1964).

34. N. J. Turro, Photochem. Photobiol., 9, 555 (1969).

35. K. Inuzuka and R. S. Becker, Bull. Chem. Soc. Japan, 44, 3323 (1971).

36. S. Boué and R. Srinivasan, J. Amer. Chem. Soc., 92, 3226 (1970).

37. S. Boué and R. Srinivasan, Mol. Photochem., 4, 93 (1972).

38. R. Srinivasan and S. Boué, Tetrahedron Lett., 3, 203 (1970).

39. L. E. Jacobs and J. R. Platt, J. Chem. Phys., 16, 1137 (1948).

40. T. Fueno and K. Yamaguchi, J. Amer. Chem. Soc., 94, 1119 (1972).

41. See table in Reference 31.

42. G. O. Burr and E. S. Miller, Chem. Rev., 29, 419 (1941).

43. R. Srinivasan, J. Amer. Chem. Soc., 82, 5063 (1960).

44. R. Srinivasan, J. Amer. Chem. Soc., 83, 2806 (1961).

45. R. J. De Kock, N. G. Minnaard, and E. Havinga, Rec. Trav. Chim., 79, 922 (1960).

46. Y. L. Bahurel, D. J. MacGregor, T. L. Penner, and G. S. Hammond, J. Amer. Chem. Soc., 94, 637 (1972).

47. N. G. Minnaard and E. Havinga, Rec. Trav. Chim., 92, 1315 (1973).

48. N. G. Minnaard and E. Havinga, Rec. Trav. Chim., 92, 1179 (1973).

49. V. Henri and L. W. Pickett, J. Chem. Phys., 7, 439 (1939).

50. H. Schüler, E. Lutz, and G. Arnold, Spectrochimica Acta, 17, 1043 (1961).

51. G. R. De Maré, J. Chem. Phys., 55, 3057 (1971).

52. E. P. Carr and H. Stücklen, J. Chem. Phys., 6, 55 (1938).

53. E. P. Carr, Chem. Rev., 41, 293 (1947).

54. L. W. Pickett, M. Muntz, and E. M. McPherson, J. Amer. Chem. Soc., 73, 4862 (1951).

55. R. P. Frueholz, W. M. Flicker, O. A. Mosher, and A. Kuppermann, unpublished results.

56. B. S. Hudson and B. E. Kohler, Chem. Phys. Lett., 14, 299 (1972).

57. B. S. Hudson and B. E. Kohler, J. Chem. Phys., 59, 4984 (1973).

58. R. L. Swofford and W. M. McClain, J. Chem. Phys., 59, 5740 (1973).

59. R. L. Christensen and B. E. Kohler, Photochem. Photobiol., 18, 293 (1973).

60. K. Schulten and M. Karplus, Chem. Phys. Lett., 14, 305 (1972).

61. F. W. E. Knoop and L. J. Oosterhoff, Chem. Phys. Lett., 22, 247 (1973).

62. W. C. Price and A. D. Walsh, Proc. Roy. Soc. (London), A185, 182 (1945).

63. R. M. Gavin, Jr., S. Risemberg, and S. A. Rice, J. Chem. Phys., 58, 3160 (1973).

64. N. Boccara and P. Maitte, Bull. Chem. Soc. France, 3810 (1972).

65. J. G. Calvert and J. N. Pitts, Jr., Photochemistry, John Wiley, Inc., New York, 1966, p. 298.

66. A. Warshel and M. Karplus, Chem. Phys. Lett., 17, 7 (1972).

67. W. R. Roth and J. König, Ann. Chem., 688, 28 (1965).

68. W. M. Flicker, O. A. Mosher, and A. Kuppermann, unpublished results.

69. J. H. Moore, Jr., J. Phys. Chem., 76, 1130 (1972).

70. A. J. Merer and R. S. Mulliken, Chem. Rev., 69, 639 (1969).

71. S. Takamuku, M. Utsunomiya, and H. Sakurai, Chem. Commun., 1969, 173 (1969).

72. R. Hoffmann, Accts. Chem. Res., 4, 1 (1971).

73. R. Hoffmann, E. Heilbronner, and R. Gleiter, J. Amer. Chem. Soc., 92, 706 (1970).

74. K. G. Untch, J. Amer. Chem. Soc., 85, 345 (1963).

75. P. Bischof, J. A. Hashmall, E. Heilbronner, and V. Hornung, Helv. Chim. Acta, 52, 1745 (1969).

76. H. Oberhammer and S. H. Bauer, J. Amer. Chem. Soc., 91, 10 (1969).

77. R. C. Cookson, J. Henstock, and J. Hudec, J. Amer. Chem. Soc., 88, 1060 (1966).

78. H. H. Brongersma, Ph.D. Thesis, University of Leiden, Leiden, The Netherlands, 1968, pp. 52-54.

79. T. H. Dunning, Jr., W. J. Hunt, and W. A. Goddard III, Chem. Phys. Lett., 4, 147 (1969).

80. R. J. Buenker, S. D. Peyerimhoff, and W. E. Kammer, J. Chem. Phys., 55, 814 (1971).

81. J. A. Ryan and J. L. Whitten, Chem. Phys. Lett., 15, 119 (1972).

82. F. H. Watson, Jr. and S. P. McGlynn, Theor. Chim. Acta, 21, 309 (1971).

83. J. G. Calvert and J. N. Pitts, Jr., Photochemistry, John Wiley and Sons, Inc., New York, 1966, pp. 462-465.

84. S. S. Collier, D. H. Slater, and J. G. Calvert, Photochem. Photobiol., 7, 737 (1968).

85. P. S. Engel and C. Steel, Accts. Chem. Res., 6, 275 (1973).

86. P. S. Engel, J. Amer. Chem. Soc., 91, 6903 (1969).

87. M. B. Robin, R. R. Hart, and N. A. Kuebler, J. Amer. Chem. Soc., 89, 1564 (1967).

88. M. B. Robin and W. T. Simpson, J. Chem. Phys., 36, 580 (1962).

89. B. Tinland, Spectrosc. Lett., 3, 51 (1970).

90. G. Wagnière, Theor. Chim. Acta, 31, 269 (1973).

91. J. C. D. Brand, J. H. Calloman, D. C. Moule, J. Tyrrell, and T. H. Goodwin, Trans. Faraday Soc., 61, 2365 (1965).

92. J. C. D. Brand, J. H. Calloman, D. C. Moule, and J. Tyrrell, Proc. Chem. Soc. (London), 307 (1963).

93. V. Henri and J. Duchesne, Nature, 143, 28 (1939).

94. L. Burnelle, J. Chem. Phys., 24, 620 (1956).

95. D. C. Moule and C. R. Subramaniam, Chem. Commun., 1340 (1969).

96. E. R. Farnworth, G. W. King, and D. C. Moule, Chem. Phys., 1, 82 (1973).

97. J. W. Rabalais, J. M. McDonald, V. Scherr, and S. P. McGlynn, Chem. Rev., 71, 73 (1971).

98. V. Y. Foo, C. E. Brion, and J. B. Hasted, Proc. Roy. Soc. (London), A322, 535 (1971).

99. E. R. Farnworth and G. W. King, J. Molec. Spectrosc., 46, 419 (1973).

100. J. L. Whitten and M. Hackmeyer, J. Chem. Phys., 51, 5594 (1969).

101. R. J. Buenker and S. D. Peyerimhoff, J. Chem. Phys., 54, 4147 (1971).

Appendix I

Electronic spectroscopy of trans-azomethane by electron impact*

Oren A. Mosher,† Michael S. Foster,† Wayne M. Flicker, J. L. Beauchamp, and Aron Kuppermann

Arthur Amos Noyes Laboratory of Chemical Physics,‡ California Institute of Technology, Pasadena, California 91109

(Received)

The electron impact excitation of trans-azomethane (i.e., trans-dimethyl diazine $H_3C-N=N-CH_3$) has been studied by both trapped electron (TE) and differential electron scattering (DES) techniques. The nature of the excited state in each of several transitions has been identified by the energy and angular dependences of the excitation cross section. Two previously unreported singlet→triplet transitions are observed with maxima at 2.75 eV and 4.8_4 eV. Theoretical calculations on the parent compound, trans-diimide (H–N=N–H), suggest that these are the $\tilde{X}\,^1A_g \rightarrow 1\,^3B_g$ (produced by excitation of an

---

*Work supported in part by the United States Atomic Energy Commission under Grant Numbers AT(04-3)-767 PA No. 4 and AT(04-3)-767-8 awarded to A. Kuppermann and J. L. Beauchamp, respectively. Report Code CALT-767P4-131.

†Work performed in partial fulfillment of the requirements for the Ph.D. degree in Chemistry at the California Institute of Technology.

‡Contribution No. 4870.

electron from an n_+ molecular orbital to a π^* molecular orbital) and the $\tilde{X}\ ^1A_g \rightarrow 1\ ^3B_u$ ($\pi \rightarrow \pi^*$) transitions, respectively. The $\tilde{X}\ ^1A_g \rightarrow 1\ ^1B_g$ ($n_+ \rightarrow \pi^*$) transition is observed with a peak at 3.50 eV in the DES studies. A strong peak at 6.01 eV in the TE spectra appears as a weak shoulder in the DES studies and is interpreted as either a symmetry-forbidden or Rydberg-like singlet → singlet transition. Allowed singlet → singlet features overlap each other in the transition energy range from 6 eV to 10 eV. Peaks are seen in the DES spectra at 6.71 eV, 7.8 eV, and 9.5 eV and in the TE spectrum at 8.0 eV. Several significant differences between the TE and the DES spectra are analyzed on the basis of the different nature of the two experiments.

I. INTRODUCTION

Azomethane is the simplest acyclic azoalkane. The photochemistry of azoalkanes has been reviewed by Collier et al.[1] and by Engel and Steel.[2] These molecules decompose following light absorption in the near ultraviolet to produce N_2 and two alkyl radicals[1, 2] and thus are convenient sources of the latter species. The photochemical precursor state in each of several photochemical processes in the azoalkanes has not been clearly established. Elucidation of the nature of the precursor states has been hindered by a lack of any direct spectroscopic measurements of the energy of low-lying triplet excited states. In the present paper we describe studies employing both trapped electron (TE) and differential electron scattering (DES) techniques to locate these electronic states.

II. METHODS AND RESULTS

A. Sample preparation

Azomethane was prepared and handled as previously described.[3] Although the cis isomer can be generated photolytically[4] under certain conditions, azomethane exists only in the trans configuration[5] as commonly prepared, and we used this isomer throughout our studies. The mass spectrum was in good agreement with the published one.[6] The sample was subjected to several liquid nitrogen freeze-pump-thaw cycles prior to its use.

B. Trapped electron spectrum

The TE experiments were performed using an ion cyclotron resonance (ICR) spectrometer, as previously described.[7, 8] In one set of experiments, using the CCl_4 scavenging method,[7] the threshold excitation spectrum was obtained by monitoring Cl^- ions produced by the dissociative attachment reaction of thermal energy electrons with CCl_4. In a second series of experiments employing the total negative current method,[8] no electron scavenger is used. In the present study of azomethane, the negative current consists solely of trapped electrons since no negative ions were detected when the incident electron energy was varied from 0 to 70 eV. Identical results were obtained with both the CCl_4 scavenging technique and the total negative current method.

Figure 1a shows the TE spectrum obtained by the total negative current method using a trapping voltage of -0.40 V in a conventional "flat" ICR cell. This corresponds to a well depth of 0.36 V.[9] Spectra run at smaller well depths were identical except for a generally poorer signal-to-noise ratio. The incident electron current was 1×10^{-7} A and the pressure of azomethane was 6×10^{-5} torr, as measured by a Schulz-Phelps ionization gauge. The energy scale was calibrated by identifying the $E\ ^3\Sigma_g^+$ peak of nitrogen at 11.87 eV[10] in its TE spectrum and assuming the energy scale correction to be independent of electron accelerating voltage.

C. Differential electron scattering spectra

The variable angle electron impact spectrometer is the one described previously[11] except that the inner and outer radii of the energy analyzers have been increased from 2.22 cm and 2.86 cm to 3.49 cm and 4.13 cm, respectively, and the lens support system has been modified to facilitate assembly and insure accurate alignment. A Spiraltron electron multiplier has replaced the previous discrete dynode multiplier.

Electron spectra were taken at impact energies of 20 eV, 40 eV, and 60 eV and scattering angles ranging from 10° to 80°. The gas in the scattering chamber was maintained at a pressure of about 4×10^{-3} torr as indicated by an uncalibrated Schulz-Phelps ionization gauge. The incident electron current was about 6×10^{-8} A. The instrumental resolution, defined as the full width at half maximum of the elastic peak, was chosen typically in the range 0.10 eV to 0.15 eV, except for a few spectra run at 0.06 eV. Figures 1b, 2, and 3 show several DES spectra obtained under different conditions.[12]

Ratios of the differential cross section (DCS) of each spectral feature to that of the elastic peak or the singlet → singlet transition at 6.71 eV were determined from the areas under each peak as previously described.[13, 14] The ratios to the 6.71 eV transition are displayed in Figures 4 and 5.

The elastic DCS in arbitrary units shown in Figures 6 and 7 were determined by multiplying the observed count rates by the scattering volume correction[15] appropriate for each scattering angle (θ) and normalizing the results to an arbitrary value of

1.0 at $\theta = 40°$. The reproducibility of these elastic DCS measurements is about 10%.

The DCS for the 6.71 eV transition between 20° and 80° was obtained by multiplying the DCS ratio of this transition with respect to the elastic peak by the elastic DCS at each θ. In addition, for angles of 30° and below, the DCS of this transition was obtained without reference to the elastic peak using the same procedure as for the elastic DCS, except that the normalization procedure was to make the result at 20° agree with that obtained by the ratio method. These two methods agreed well for the 6.71 eV transition DCS value at $\theta = 30°$.

The DCS curves for the other inelastic transitions displayed in Figures 6 and 7 were determined by the ratio method using the elastic DCS as a reference for angles of 20° and above and the 6.71 eV transition DCS as a reference at $\theta = 10°$. The arbitrary units in Figures 6 and 7 are the same for all curves displayed. Due to contributions of elastic DCS irreproducibility (~10%), inaccuracies in the ratio measurements associated with band overlaps, energy-loss dependent background count rates, and other instrumental effects, the overall accuracy in these relative inelastic DCS measurements is estimated to be 35% at scattering angles of 30° and above. At smaller angles, uncertainty in the volume correction can increase this inaccuracy.

III. DISCUSSION

A. The molecular orbital scheme in azomethane and diimide

Azomethane is known to exist in a trans planar configuration in the gas phase and therefore possesses C_{2h} symmetry. The coordinate axes implied in the orbital designations used below are located as follows:

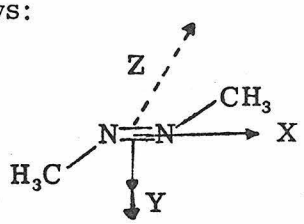

Only one calculation[16] of excited state energies has been performed on azomethane. This calculation used the zero-differential-overlap approximation and thus gave no estimate of the singlet-triplet splitting. Several studies[16-20] are available on the related molecule diimide. This molecule should provide a useful model for interpreting the lowest electronic states in azomethane provided that the appropriately localized orbitals involved in these states are relatively invariant[21, 22] to replacement of the H atom by CH_3. Such chemically invariant orbitals correspond to the intuitive idea of chemical bonds in the molecule.

The presence of two N atoms in the diimide molecule leads to two "formally nonbonding" MO's, the symmetric (n_+) and antisymmetric (n_-) linear combinations of the lone pair orbitals on the two nitrogen atoms. The interaction between such non-

bonding orbitals has recently been reviewed by Hoffmann.[23] Theoretical calculations for diimide[16-20] indicate that the highest filled orbital is the n_+ and that the energy splitting between it and n_- is large. The ground state has ^1A_g symmetry arising from a $1b_u^2 1a_g^2 2a_g^2 2b_u^2 3a_g^2 3b_u^2(n_-)\ 1a_u^2(\pi) 4a_g^2(n_+)$ configuration. The lowest excited states, the $1\ ^3B_g$ and the $1\ ^1B_g$, arise from an $n_+ \rightarrow \pi^*$ $[\cdots 4a_g^2(n_+) \rightarrow \cdots 4a_g^1(n_+)\ 1b_g^1(\pi^*)]$ excitation. The next state is the $1\ ^3B_u(\pi \rightarrow \pi^*)$. The results of the theoretical studies of diimide are summarized in Table I.

The ab initio calculation of Robin et al.[17a] employed a Gaussian basis set to obtain a self-consistent field (SCF) ground state. The excited states were obtained by performing a limited configuration interaction (CI) calculation involving configurations generated from the virtual orbitals of the ground state. Wagniére[16] also performed an ab initio calculation using a Gaussian basis set. The energies from his calculation listed in Table I are the differences between the open-shell SCF state energies and the lowest closed-shell SCF state energy. Wong, Fink, and Allen[18] calculated an ab initio SCF ground state using Gaussian lobe orbitals, and performed a separate calculation on the open shell $1\ ^3B_g$ state. The orbitals in the $1\ ^1B_g$ state were then assumed to be the same as in the $1\ ^3B_g$ state.[24] Tinland[19] used the modified CNDO/2 method, a semi-empirical approach, which involves an all-valence-electron CI. Winter and Pitzer[20] performed an SCF calculation in which they

carried out extensive calculations on the ground state, using a Gaussian basis set. They obtained the excited state energies by optimizing only the open-shell orbitals, taking the remaining orbitals from the ground state calculations.

B. Trapped electron spectrum

As shown in Figure 1a, three prominent features appear in the TE spectrum of trans-azomethane with peaks at 2.72 ± 0.05 eV, 6.01 ± 0.05 eV and 8.0 ± 0.1 eV. The optical absorption spectrum[1,17a] has also been shown in Figure 1c for comparison. The lowest optically observed transition is the $\tilde{X}\ ^1A_g \rightarrow 1\ ^1B_g$ ($n_+ \rightarrow \pi^*$) peaking at 3.64 eV. Therefore, the state at 2.72 eV above the ground state is presumably the $1\ ^3B_g$. The possibility that this transition was due to a temporary negative ion resonance was eliminated by making measurements with well depths of 1.2 eV and noticing that the peak was still present. This assignment is further discussed in section III.C.1. The nature of the states corresponding to the higher energy peaks cannot be determined by the TE method alone because threshold electron impact can produce both spin-allowed and spin-forbidden excitations with comparable effectiveness.[25] The factors which determine relative peak intensities in TE spectra are further discussed in section III.D.

C. Differential electron scattering spectra

Figure 1b shows the 2 eV to 10 eV energy-loss region at 40 eV impact energy and $\theta = 50°$, while Figure 2 displays the 2 eV to 10 eV energy-loss region at 20 eV impact energy and scattering

angles of 10° and 60°. Figure 3 shows the 5 eV to 8 eV energy-loss region at 20 eV incident electron energy and $\theta = 30°$. Peaks are seen at 2.75 ± 0.04, 3.50 ± 0.04, $4.8_4 \pm 0.1$, 6.71 ± 0.03, 7.8 ± 0.1, and 9.5 ± 0.1 eV in the DES spectra. Each feature is discussed in greater detail in the following sections, and the results are summarized in Table II.

1. The $1\ ^3B_g$ ($n_+ \rightarrow \pi^*$) state

A peak is observed with a maximum at 2.75 ± 0.04 eV and a Frank-Condon region from about 2.3 eV to 3.1 eV. The sharp increase with scattering angle of the ratio of the area under this peak to that of the strong singlet at 6.71 eV (see section III.C.6), as shown in Figures 4 and 5, is characteristic[11, 13, 14] of a spin-forbidden excitation. The magnitude and relative insensitivity to θ of the DCS for excitation of this state supports this conclusion. The position of this peak is in good agreement with the TE maximum occurring at 2.72 ± 0.05 eV.

Theoretical calculations[16-20] for diimide uniformly predict that the lowest triplet arises from an $n_+ \rightarrow \pi^*$ excitation and thus the 2.75 eV peak in azomethane most likely corresponds to the $\tilde{X}\ ^1A_g \rightarrow 1\ ^3B_g$ transition.

2. The $1\ ^1B_g$ ($n_+ \rightarrow \pi^*$) state.

The second inelastic feature has a maximum at 3.50 ± 0.04 eV with an approximate onset and end of 2.9 eV and 4.2 eV, respectively. This transition, which in the optical spectrum has a maximum at 3.64 eV in the gas phase[1,17a] and at 3.47 eV in hydrocarbon

solution,[26] has been assigned[17] to the $\tilde{X}\ ^1A_g \rightarrow 1\ ^1B_g$ ($n_+ \rightarrow \pi^*$) excitation. It is a spin-allowed but electric dipole-forbidden transition. The area ratio behavior shown in Figures 4 and 5 and the forward peaking behavior of the DCS shown in Figures 6 and 7 confirm the assignment to a spin-allowed transition. The absence of this transition in the TE spectrum is discussed in section III. D.

3. The 4.8_4 eV triplet state

A broad, weak feature is observed with an apparent onset of 4.0 eV, a maximum at $4.8_4 \pm 0.1$ eV and an end beyond 5.5 eV. The area ratio plots in Figures 4 and 5 and the DCS curves in Figures 6 and 7 are quite similar to the results obtained for the $\tilde{X}\ ^1A_g \rightarrow 1\ ^3B_g$ transition and confirm its singlet → triplet nature. This transition is not observed in the TE spectrum (see discussion in section III. D).

Theoretical calculations for diimide predict[16, 17, 19] that the second triplet state is the $1\ ^3B_u$ ($\pi \rightarrow \pi^*$), but this assignment may not be applicable to azomethane because diimide may not properly describe the higher energy states in azomethane.

The optical absorption spectrum (see Figure 1c) in this region[1] shows a horizontal inflection point at about 5.1 eV with an extinction coefficient of about 0.5 liter/mole cm. A rough estimate of the oscillator strength f for this region using a classical dispersion theory formula[27] gives $f = 4 \times 10^{-6}$, which is relatively large but still within the estimated range[28] of f values for $\pi \rightarrow \pi^*$ singlet → triplet excitations. However, this optical feature need not correspond to the

4.8_4 eV triplet; it could instead [29] be due to a 0.01% impurity having an extinction coefficient of $\epsilon = 5 \times 10^3$ liter/mole · cm. Such an ϵ is typical of many optically allowed transitions.

4. The 6.01 eV singlet state

The TE spectrum shows a strong peak at 6.01 eV, while many of the DES spectra show a weak shoulder around 6.0 eV energy loss. Figure 3 shows this feature in more detail. The slope break is noticeable in both low and high angle spectra. This suggests that it is due to a weak singlet → singlet transition which may either be symmetry-forbidden or of a Rydberg type. The strong intensity in the TE spectrum also establishes that it is not due to a singlet → singlet transition of an impurity in the sample. A discussion of the relative strength of this transition in the TE and DES spectra is given in section III. D.

Robin et al.[17a] have attributed a weak feature (extinction coefficient of about 1 to 5 ℓ/mole·cm)[30] peaking at 5.48 eV in their optical spectrum to the symmetry-forbidden $\tilde{X}\ ^1A_g \rightarrow 2\ ^1A_g$ transition. The DES spectra show an onset around 5.4 eV but do not have any observable peak at 5.5 eV energy loss. Thus the 6.0 eV feature appears to be unrelated to the state at 5.48 eV. Robin has since suggested[30] that the 5.48 eV optical peak may reflect the presence of a small amount of photochemically produced[4] cis-azomethane in the sample or that it may be due to a very minor impurity.

5. Higher singlet states

The first strong feature in the DES spectrum has a maximum at 6.71 ± 0.03 eV. The DCS curves shown in Figures 6 and 7 are characteristic of optically allowed singlet → singlet transitions.[11]

This is confirmed by the fact that such a transition appears in the optical spectrum at about 6.75 eV.[17a] Additional strong singlet → singlet transitions are seen at 7.8 ± 0.1 and 9.5 ± 0.1 eV. Our DES spectra as well as the optical one[17a] give some indication that an additional singlet state may exist in the neighborhood of 8.5 eV. The TE spectrum shows a peak at 8.0 eV superimposed on a background from the strongly overlapped singlet or triplet states in this energy region.

D. Comparison of differential electron scattering and trapped electron spectra

A comparison of the DES and TE spectra shows that several significant differences exist between these two types of electron impact spectra. The reason for these differences is that the spectra reflect different electron impact properties. In the DES spectra, the ordinate is proportional to the magnitude of the differential scattering cross section, at the impact energy and scattering angle being considered, corresponding to the energy loss given by the abscissa. In the TE spectra the ordinate is proportional to the derivative of the total cross section with respect to impact energy, in the neighborhood of the excitation energy threshold represented by the abscissa.[25, 31]

As mentioned in section III.C.2, the $\tilde{X}\ ^1A_g \rightarrow 1\ ^1B_g$ transition is not observed in the TE spectrum shown in Figure 1a. The absence of this transition in the TE spectrum indicates that, at threshold, its excitation cross section rises quite slowly compared to those of the

observed singlet → triplet and singlet → singlet transitions. A variety of TE studies have shown that singlet →singlet transitions may be absent or very weak in the TE spectrum. The $1\ ^1S \rightarrow 2\ ^1P$ transition in He is very strong in the DES spectrum[11] but shows up only as a small shoulder on the high energy side of the $1\ ^1S \rightarrow 2\ ^3P$ peak in the TE spectrum.[25, 31] As another example, the $\tilde{X}\ ^1\Sigma^+ \rightarrow\ ^1\Pi$ transition in CO appears very weakly in the TE spectrum[31] but is a strong feature in the DES spectra.[11]

In section III.C.3 it was noted that the 4.8_4 eV triplet feature appeared in the DES spectrum but not in the TE one. This suggests that its cross section increases slowly with increasing energy in the threshold region. Analogous behavior occurs in 1,3-butadiene, where the $\tilde{X}\ ^1A_g \rightarrow 1\ ^3A_g$ transition is easily seen by the DES method[13, 14] but is very weak in the TE spectrum.[32]

Section III.C.5 contains an example of an inverse behavior, in which the transition at 6.0 eV occurs strongly in the TE spectrum but very weakly in the DES spectrum. Further differences between the two methods are also seen in the energy-loss region from 6 eV to 10 eV as shown in Figure 1a and 1c.

Therefore, the absence of a transition from a TE spectrum and its presence in a DES or optical spectrum does not imply a disagreement between the different techniques. Furthermore the presence in the TE spectrum of an intense feature does not necessarily correlate with its optical absorption coefficient or DES strength. As a result, great caution should be exercised in interpreting TE spectra without comparing them with other kinds of electronic spectra.

IV. CONCLUSIONS

The results of the TE and DES spectral studies presented in this paper and an analysis of earlier work lead to several conclusions. The lowest excited electronic state is the $1\,^3B_g\,(n_+ \rightarrow \pi^*)$ peaking at 2.72 eV in the TE study and 2.75 eV in the DES spectra.

A second triplet state is observed at 4.8_4 eV. The analogy with diimide suggests that this is the $1\,^3B_u\,(\pi \rightarrow \pi^*)$ state. The lowest excited singlet state, the $1\,^1B_g\,(n_+ \rightarrow \pi^*)$ at 3.50 eV in the DES spectrum, is excited by an electric dipole-forbidden transition from the ground state. A prominent peak is seen at 6.01 eV in the TE spectrum, while it occurs as a weak shoulder in the DES spectra. The weakness of this transition in both the DES and optical spectra suggests that it is either a symmetry-forbidden or a Rydberg-type singlet → singlet transition with an excitation cross section which increases sharply with electron energy near threshold. Additional strongly allowed singlet → singlet transitions produce overlapped bands in the 6 eV to 10 eV transition energy region. The results of this study illustrate the importance of interpreting TE spectra in conjunction with other types of electronic spectra.

ACKNOWLEDGMENTS

We thank Drs. M. B. Robin, N. W. Winter, and W. A. Goddard III for several helpful discussions. We also thank Dr. Winter for communication of his theoretical results prior to their publication.

REFERENCES

[1] S. S. Collier, D. H. Slater, and J. G. Calvert, Photochem. Photobiol. 7, 737 (1968).

[2] P. S. Engel and C. Steel, Accts. Chem Res. 6, 275 (1973).

[3] M. S. Foster and J. L. Beauchamp, J. Am. Chem. Soc. 94, 2425 (1972).

[4] R. F. Hutton and C. Steel, J. Am. Chem. Soc. 86, 745 (1964).

[5] C. H. Chang, R. F. Porter, and S. H. Bauer, J. Am. Chem. Soc. 92, 5313 (1970).

[6] Z. Prásil and W. Forst, J. Am. Chem. Soc. 90, 3344 (1968).

[7] D. P. Ridge and J. L. Beauchamp, J. Chem. Phys. 51, 470 (1969).

[8] T. McAllister, Chem. Phys. Lett. 13, 602 (1972).

[9] T. B. McMahon and J. L. Beauchamp, Rev. Sci. Inst. 42, 1632 (1971).

[10] G. Herzberg, Molecular Spectra and Molecular Structure I (D. Van Nostrand, Princeton, 1950), p. 551.

[11] S. Trajmar, J. K. Rice, and A. Kuppermann, Adv. Chem. Phys. 18, 15 (1970).

[12] Count rates in spectra taken at different angles and impact energies can be compared only after changes in incident electron current, scattering volume, and sample gas pressure are taken into account.

[13] O. A. Mosher, W. M. Flicker, and A. Kuppermann, Chem. Phys. Lett. 19, 332 (1973).

[14] O. A. Mosher, W. M. Flicker, and A. Kuppermann, J. Chem. Phys. 59, 6502 (1973).

[15] S. Trajmar, D. C. Cartwright, J. K. Rice, R. T. Brinkmann, and A. Kuppermann, J. Chem. Phys. 49, 5464 (1968).

[16] G. Wagniére, Theor. Chim. Acta 31, 269 (1973).

[17] (a) M. B. Robin, R. R. Hart, and N. A. Kuebler, J. Am. Chem. Soc. 89, 1564 (1967); (b) M. B. Robin and W. T. Simpson, J. Chem. Phys. 36, 580 (1962).

[18] D. P. Wong, W. H. Fink, and L. C. Allen, J. Chem. Phys. 52, 6291 (1970).

[19] B. Tinland, Spectrosc. Lett. 3, 51 (1970).

[20] N. W. Winter and R. M. Pitzer, private communication.

[21] S. F. Boys, Rev. Mod. Phys. 32, 296 (1960).

[22] W. England, L. S. Salmon, and K. Ruedenberg, Fortschritte der chemischen Forschung 23, 31 (1971).

[23] R. Hoffmann, Acct. Chem. Res. 4, 1 (1971).

[24] As Wong et al. [18] note in their paper, the approximations involved in this open-shell calculation make the results somewhat suspect.

[25] G. J. Schulz, Phys. Rev. 112, 150 (1958).

[26] G. Kortuem and H. Rau, Ber. Buns. Physik. Chem. 68, 973 (1964).

[27] W. Kauzmann, Quantum Chemistry (Academic Press, New York, 1957) p. 581.

[28] S. P. McGlynn, T. Azumi, and M. Kinoshita, Molecular Spectroscopy of the Triplet State (Prentice-Hall Inc., New Jersey, 1969), p. 20.

[29] C. Steel reports in a private communication that the bump at 5.1 eV disappears when the azoalkane is rigorously purified.

[30]M. B. Robin, provate communication.

[31]H. H. Brongersma, A. J. H. Boerboom, and J. Kistemaker, Physica 44, 449 (1969).

[32]H. H. Brongersma, Ph. D. Thesis, University of Leiden, Leiden, The Netherlands (1969).

TABLE I. Calculated electronic state energies of trans-diimide

Orbitals Involved in the transition	Upper State	Calculated Transition Energy (eV)				
		Wagniére[a]	Robin et al.[b]	Tinland[c]	Wong et al.[d]	Winter and Pitzer[e]
$n_+ \rightarrow \pi^*$	$1\,^3B_g$	1.75	3.01	2.60	3.22	1.8
$n_+ \rightarrow \pi^*$	$1\,^1B_g$	3.08	3.92	2.60	3.84	3.1
$\pi \rightarrow \pi^*$	$1\,^3B_u$	3.69	6.53	4.50		

[a] Reference 16

[b] Reference 17a

[c] Reference 19

[d] Reference 18

[e] Reference 20

TABLE II. Excited electronic states of trans-azomethane

Excited State	Nature of Transition	Transition Energy (eV)		
		TE	DES	Optical[a]
$1\,^3B_g$	$n_+ \rightarrow \pi^*$	2.72 ± 0.05	2.75 ± 0.04	
$1\,^1B_g$	$n_+ \rightarrow \pi^*$	--	3.50 ± 0.04	3.64
Triplet ($1\,^3B_u$?)	$\pi \rightarrow \pi^*$ if ^3B_u	--	4.8_4	5.1?
Singlet	Symmetry forbidden or Rydberg-like	6.01 ± 0.05	6.01 ± 0.1	--
Singlet	Optically allowed		6.71 ± 0.03	6.75
		8.0 ± 0.1	7.8 ± 0.1	7.95
			9.5 ± 0.1	

[a]Reference 17a

Figure Captions

Figure 1. (a) Trapped electron spectrum of azomethane. The ordinate I_t is the trapped electron current, for the following conditions: 1×10^{-7} A incident beam current; 6×10^{-5} torr sample pressure as read on an uncalibrated Schulz-Phelps gauge; 0.4 V well depth.

(b) Electron energy-loss spectrum. The ordinate I is the scattered current at $\theta = 50°$; 40 eV incident electron energy; 7×10^{-8} A incident beam current; 3.6×10^{-3} torr uncalibrated Schulz-Phelps gauge sample pressure reading.

(c) Optical absorption spectrum taken from Figures in References 1 and 17a The ordinate ϵ is the molar extinction coefficient.

For all curves the abscissa ΔE is the excitation energy.

Figure 2. Electron energy-loss spectrum of azomethane at (a) $\theta = 60°$ and (b) $\theta = 10°$; 20 eV incident electron energy; 1×10^{-8} A incident beam current; 4.4×10^{-3} torr uncalibrated sample pressure reading; 0.15 eV resolution (full width at half maximum of elastic peak).

Figure 3. Electron energy-loss spectrum of azomethane in the 5.0 to 8.0 eV energy-loss region for $\theta = 30°$; 20 eV incident electron energy; 3.5×10^{-3} torr uncalibrated sample pressure reading.

Figure 4. Ratio of intensities I of several electronic transitions in azomethane to that of the 6.71 eV singlet → singlet transition ($I_{6.71\ eV}$) as a function of θ at an incident electron energy of 20 eV. The excited

states for the curves shown are $1\ ^3B_g$(○), $1\ ^1B_g$(△), and the 4.8_4 eV triplet (×).

Figure 5. Same as Figure 4 at an incident electron energy of 40 eV.

Figure 6. Differential cross sections as a function of θ at an incident electron energy of 20 eV for elastic scattering (+) and for transitions to the following excited states: $1\ ^3B_g$(○), $1\ ^1B_g$(△), 4.8_4 eV triplet (×) and the 6.71 eV singlet (□).

Figure 7. Same as Figure 6 for an incident electron energy of 40 eV.

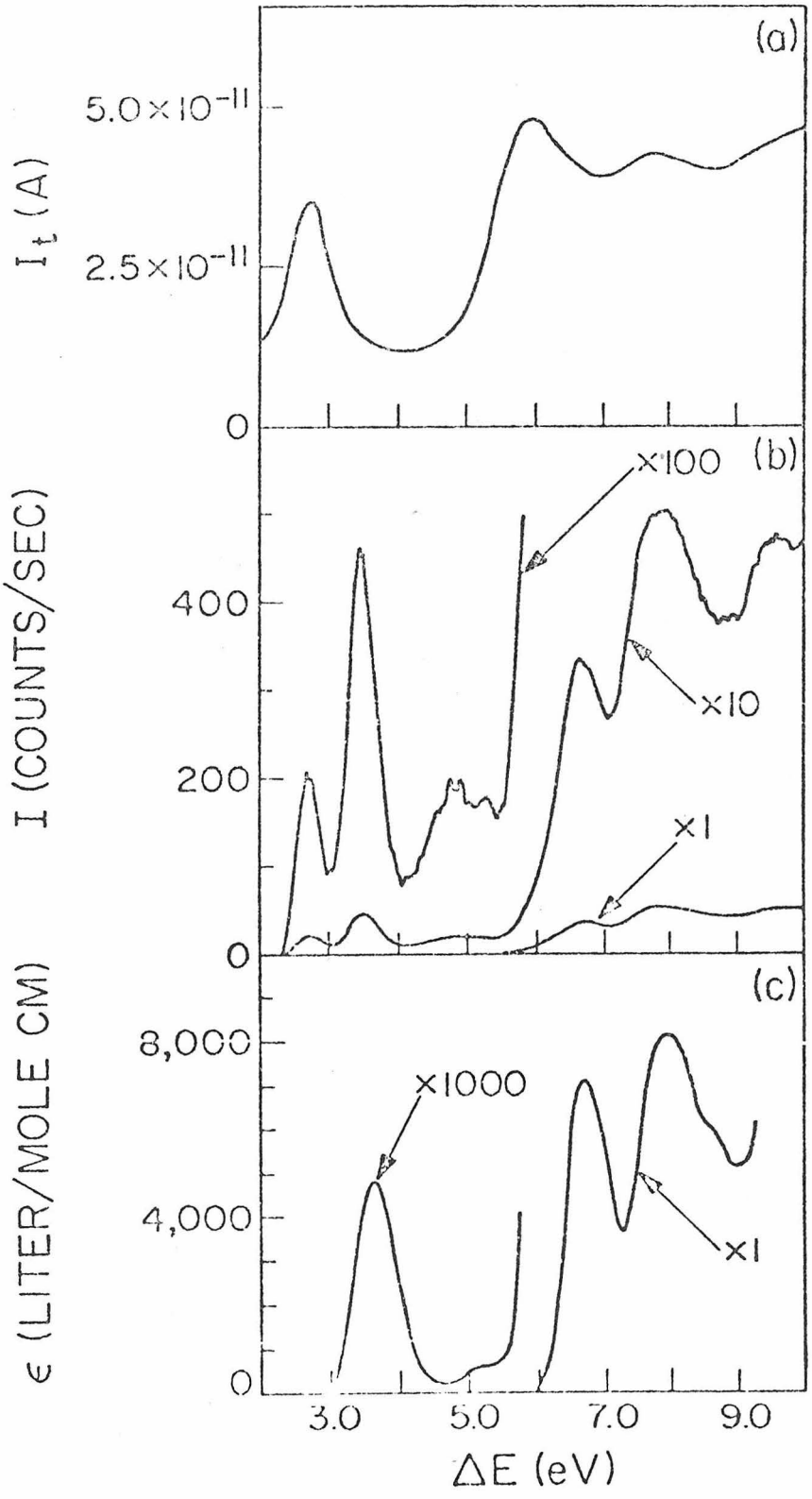
(a)
5.0×10⁻¹¹
2.5×10⁻¹¹
0
I_t (A)
(b)
×100
×10
×1
400
200
0
I (COUNTS/SEC)
(c)
×1000
×1
8,000
4,000
0
ϵ (LITER/MOLE CM)
3.0
5.0
7.0
9.0
ΔE (eV)

Figure 1

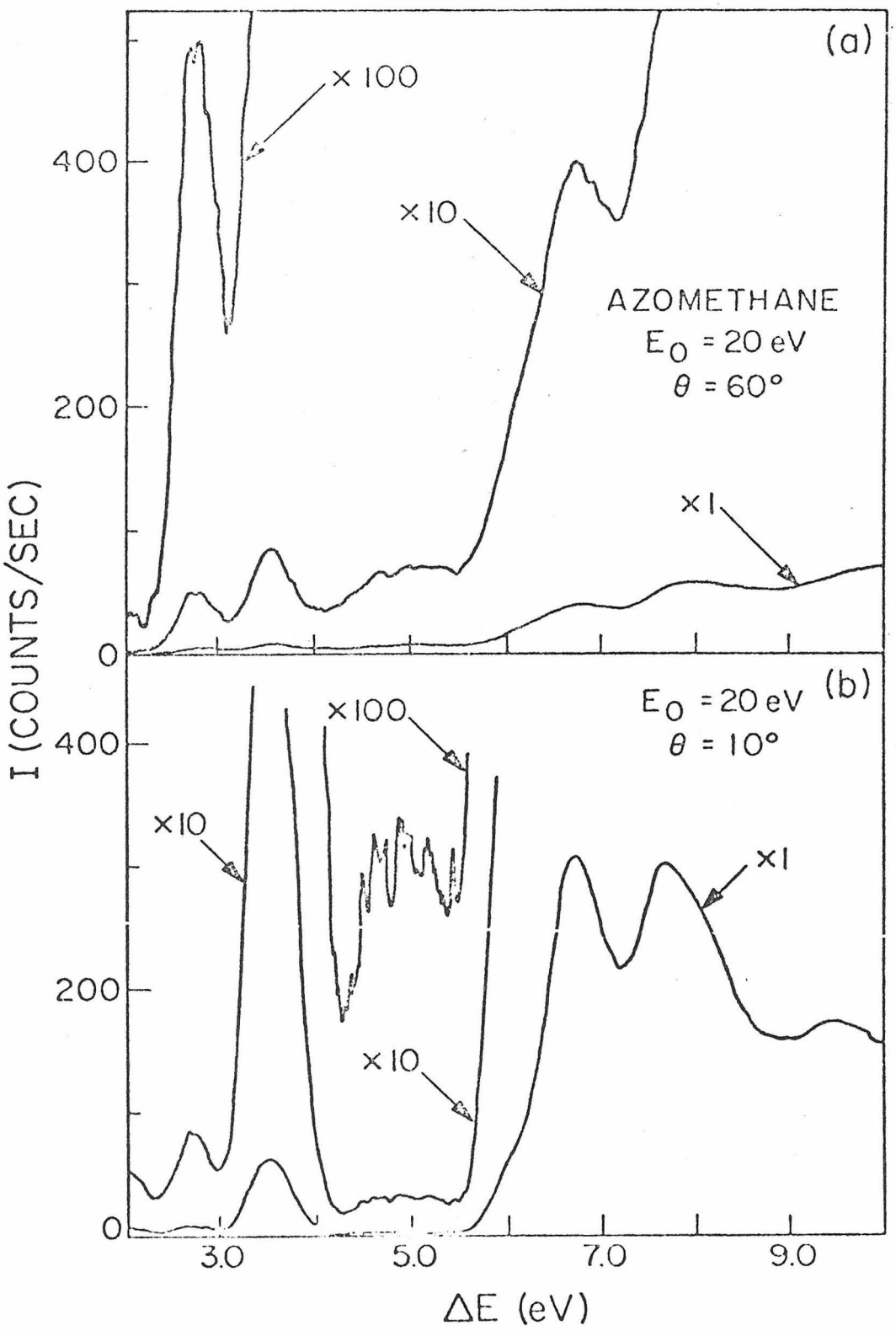
(a)
× 100
× 10
× 1
AZOMETHANE
E_0 = 20 eV
θ = 60°
400
200
0
I (COUNTS/SEC)
(b)
E_0 = 20 eV
θ = 10°
× 100
× 10
× 1
× 10
400
200
0
3.0
5.0
7.0
9.0
ΔE (eV)

Figure 2

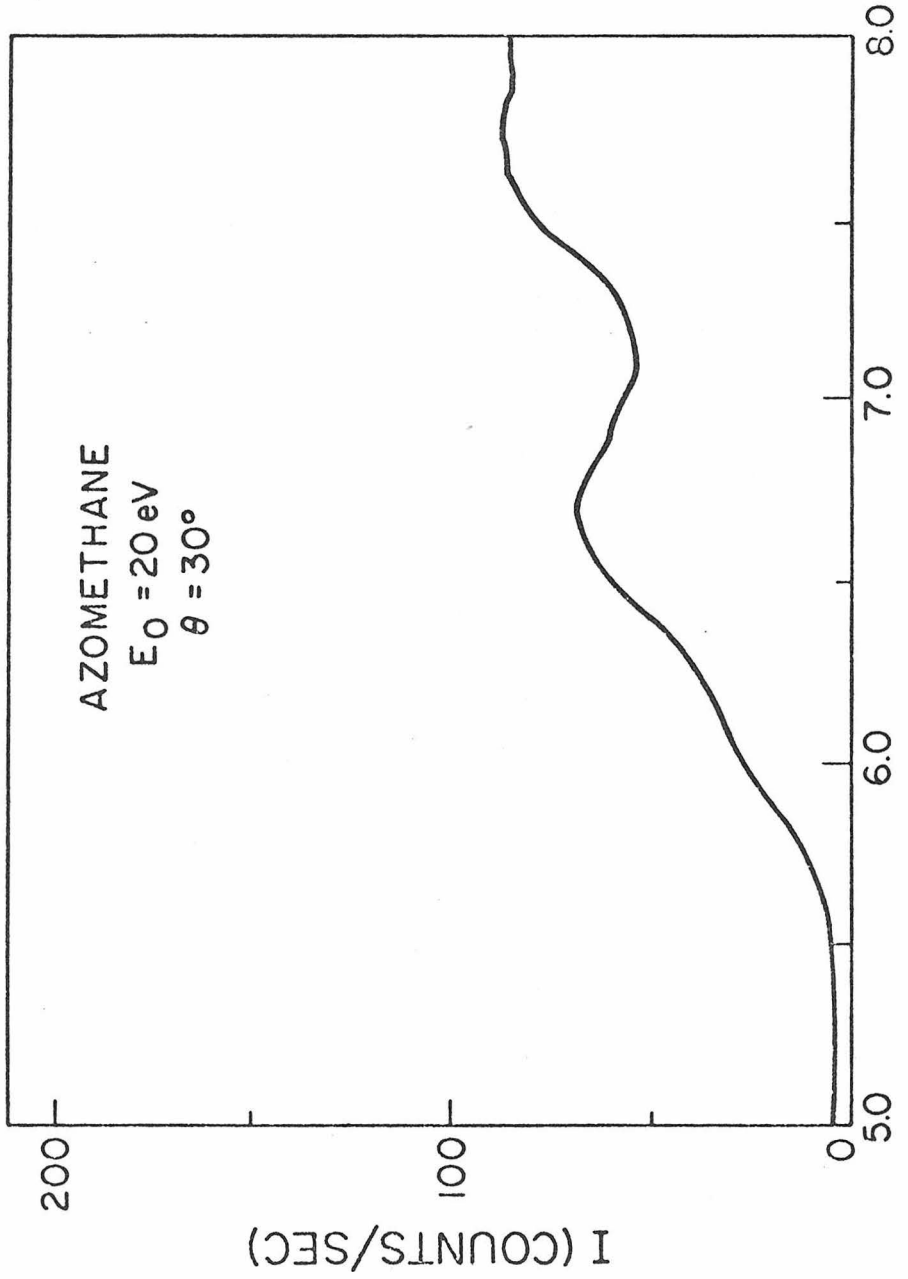
AZOMETHANE
E_0 = 20 eV
θ = 30°
I (COUNTS/SEC)
200
100
0
5.0
6.0
7.0
8.0
ΔE (eV)

Figure 3

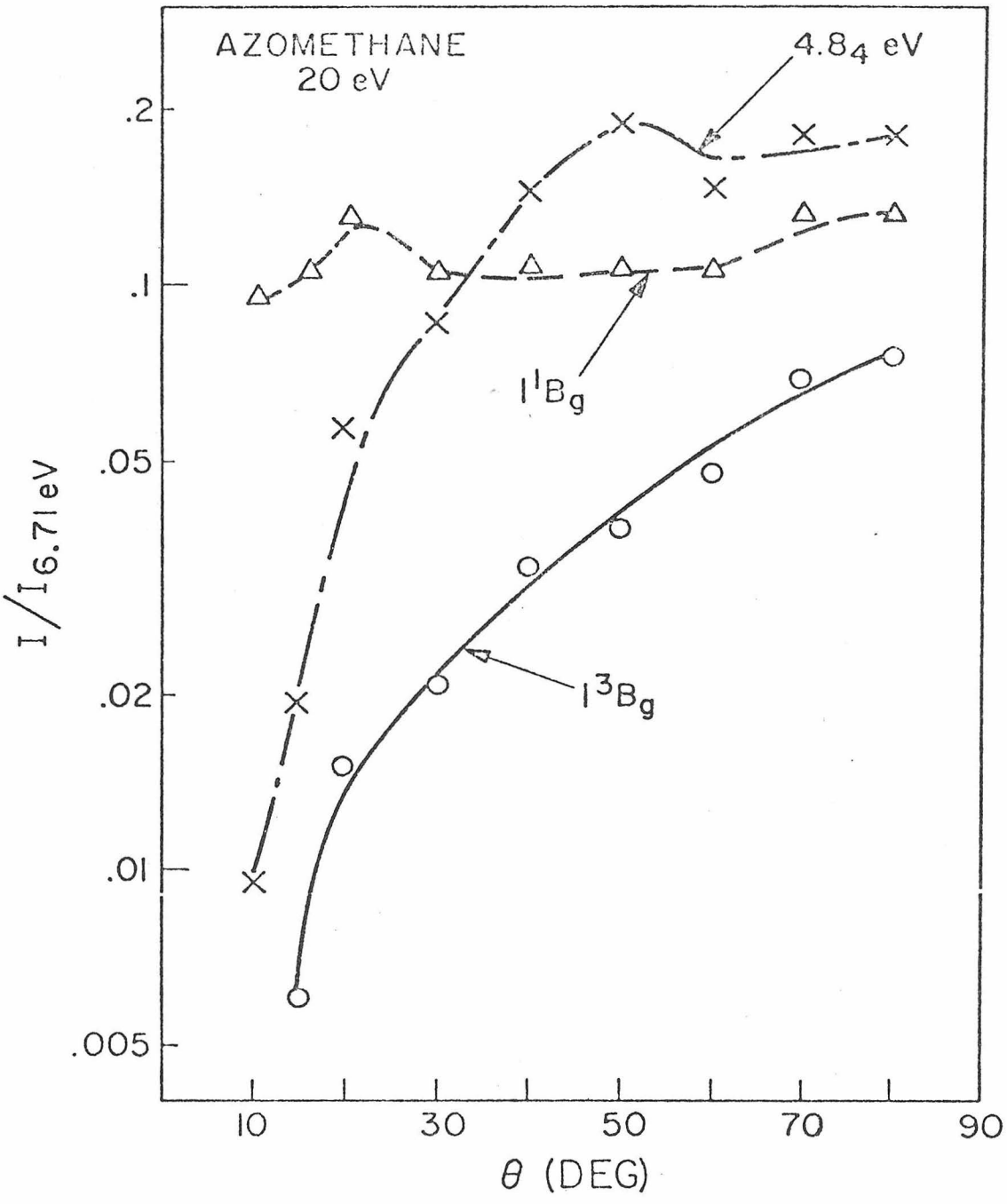
AZOMETHANE
20 eV
4.84 eV
1¹Bg
1³Bg
I/I6.71eV
.2
.1
.05
.02
.01
.005
10
30
50
70
90
θ (DEG)

Figure 4

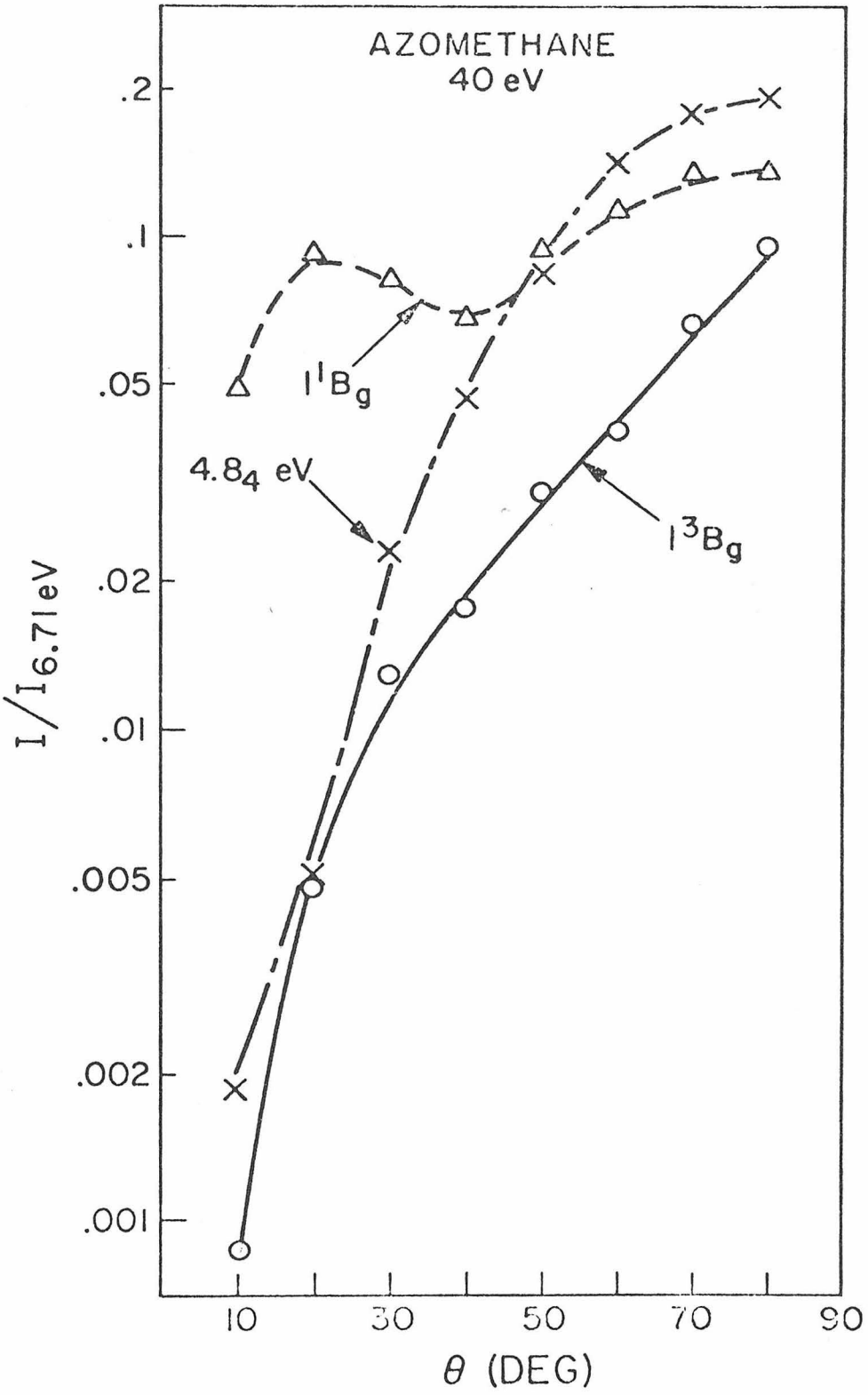
AZOMETHANE
40 eV
.2
.1
.05
.02
.01
.005
.002
.001
$I/I_{6.71\,eV}$
1^1B_g
4.8_4 eV
1^3B_g
10
30
50
70
90
θ (DEG)

Figure 5

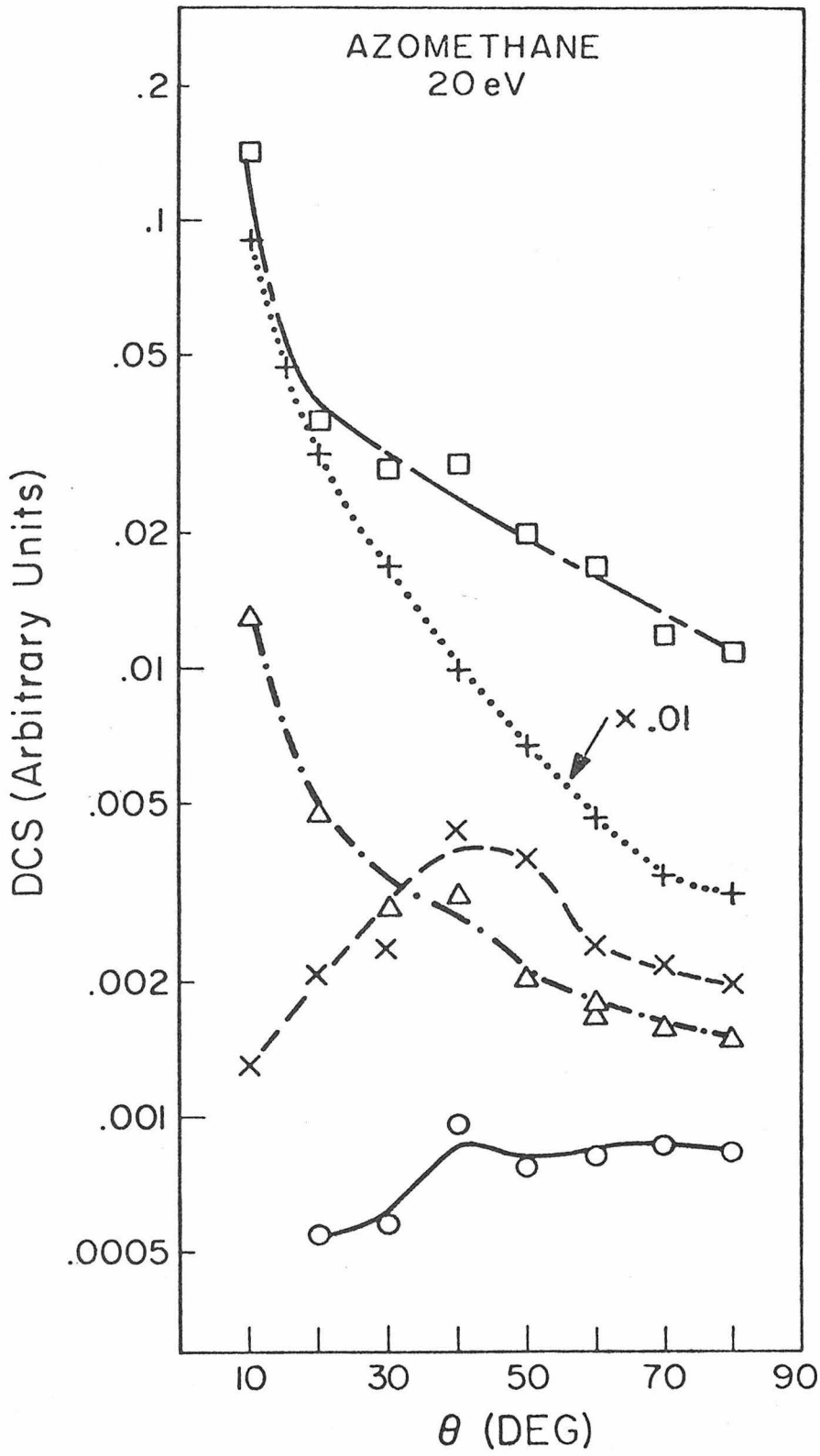
AZOMETHANE
20 eV
.2
.1
.05
.02
.01
.005
.002
.001
.0005
DCS (Arbitrary Units)
× .01
10
30
50
70
90
θ (DEG)

Figure 6

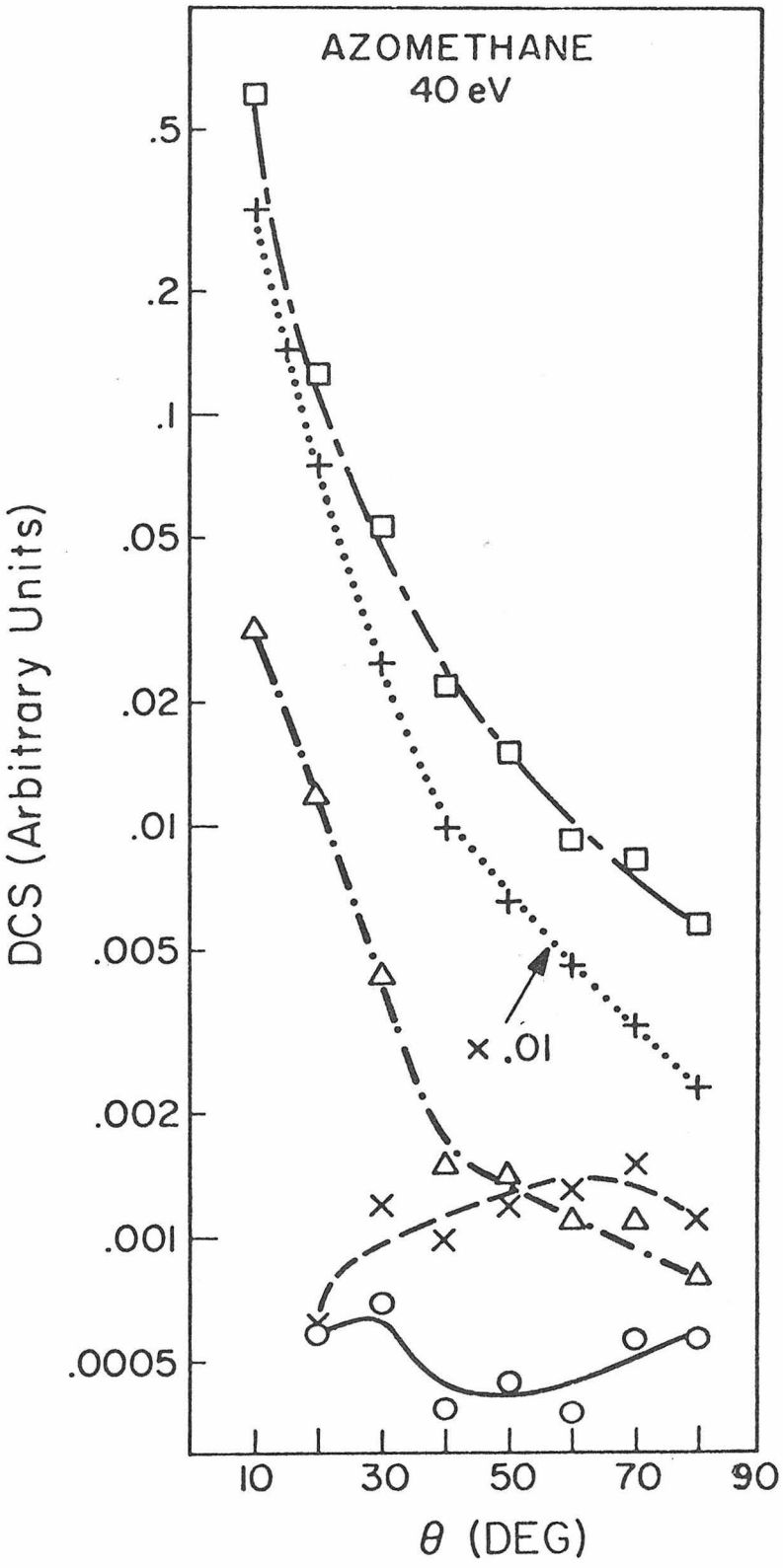
AZOMETHANE
40 eV
DCS (Arbitrary Units)
.5
.2
.1
.05
.02
.01
.005
.002
.001
.0005
× .01
10
30
50
70
90
θ (DEG)

Figure 7

Appendix II

ELECTRON IMPACT SPECTROSCOPY OF TRANS-AZOMETHANE*

Oren A. MOSHER,† Michael S. FOSTER,† Wayne M. FLICKER,
Aron KUPPERMANN** and J. L. BEAUCHAMP

Arthur Amos Noyes Laboratory of Chemical Physics,‡
California Institute of Technology, Pasadena, California 91109

Received

The electron impact excitation spectrum of trans-azomethane (i.e., trans-dimethyl diazine, $H_3C—N=N—CH_3$) has been studied by both trapped electron and differential electron scattering techniques. Two previously unreported singlet → triplet transitions are observed with maxima at 2.75 eV and 4.8_4 eV, as well as a singlet→ singlet transition at 6.01 eV.

An experimental study of the electron impact excitation of trans-azomethane, employing both trapped electron (TE) and differential electron scattering (DES) techniques, has contributed new information about

---

*Work supported in part by the United States Atomic Energy Commission under Grant Numbers AT(04-3)-767-4 and AT(04-3)-767-8.
Report Code CALT-767P4-133

†Work performed in partial fulfillment of the requirements for the Ph.D. degree in Chemistry at the California Institute of Technology.

**To whom correspondence on this paper should be addressed.

‡ Contribution No. 4903

its low-lying excited electronic states. These states are of interest because of their roles in the photochemical dissociation of both azomethane and larger azoalkanes ($R_1N{=}NR_2$) to give N_2 and alkyl radicals [1, 2]. Only a limited number of spectroscopic studies of azomethane have been reported [1, 3] and no direct measurements of the energy of triplet excited states exist. Low energy electron impact spectroscopy, which is a powerful method [4] for studying optically forbidden transitions, was applied to azomethane to detect such transitions.

The trapped electron experiments were performed using an ion cyclotron resonance spectrometer [5, 6] operating in the total negative current [6] and the $CC\ell_4$ electron scavenging modes [5]. Both methods gave identical results. Figure 1a shows a total negative current mode spectrum of azomethane. In the present case, this current consists solely of trapped electrons, since no negative ions were detected when the incident electron energy was varied from 0 eV to 70 eV. Typical experimental conditions in the TE negative current mode spectrum are a well depth of 0.36 V, an incident electron current of 1×10^{-7} A, and a sample pressure reading of 6×10^{-5} torr from an uncalibrated Schulz-Phelps ionization gauge. The energy scale was calibrated by identifying the E $^3\Sigma_g^+$ peak of nitrogen at 11.87 eV [7] in its TE spectrum and assuming the energy scale correction to be independent of electron accelerating voltage.

An example of the differential electron scattering (DES) spectrum of azomethane is given in fig. 1b at an incident electron energy (E_0) of

40 eV and a scattering angle (θ) of 80°. Other DES spectra were taken for E_0 = 20 eV, 40 eV, and 60 eV and θ from 10° to 80°. The apparatus used was basically that described by Kuppermann et al. [4] except that the inner and outer radii of the energy analyzers were both increased by 1.27 cm and the lens support system was considerably modified. Typical experimental conditions in the DES spectra are 6×10^{-8} A incident electron current; 4×10^{-3} torr sample pressure reading from an uncalibrated Schulz-Phelps ionization gauge; and 0.10 eV to 0.15 eV instrumental resolution, defined as the full width at half maximum of the elastic peak. The trans-azomethane used in the TE and DES studies was prepared as described previously [8], and was subjected to several liquid nitrogen freeze-pump-thaw cycles prior to its use.

Three prominent features appear in the TE spectrum of azomethane (fig. 1a) with peaks at 2.72 ± 0.05 eV, 6.01 ± 0.05 eV, and 8.0 ± 0.1 eV. The lowest energy peak in the optical absorption spectrum occurs at 3.64 eV [1, 3] and has been attributed to the $\tilde{X}\ ^1A_g \rightarrow 1\ ^1B_g$ ($n_+ \rightarrow \pi^*$) electric dipole-forbidden transition. The peak at 2.72 eV is presumably due to the corresponding $n_+ \rightarrow \pi^*$ singlet → triplet $\tilde{X}\ ^1A_g \rightarrow 1\ ^3B_g$ transition. The $\tilde{X}\ ^1A_g \rightarrow 1\ ^1B_g$ transition is not observed in the TE spectrum, although it is seen in both the optical and DES spectra (see later discussion).

The DES spectrum, shown in fig. 1b, has peaks at 2.75 ± 0.04 eV, 3.50 ± 0.04 eV, 4.8_4 ± 0.1 eV, 6.71 ± 0.03 eV and 7.8 ± 0.1 eV. Many of the DES spectra also show a weak shoulder around 6.0 ± 0.1 eV. The optical absorption spectra [1, 3] show peaks at 3.64 eV and 6.75 eV.

The differential cross section for excitation of the 3.50 eV and 6.71 eV transitions are both strongly forward peaked and confirm the earlier assignments, based on the optical spectra [1, 3], to singlet → singlet transitions.

The first observed inelastic feature of azomethane in the DES spectra has a Franck-Condon region from about 2.3 eV to about 3.1 eV. At 40 eV incident energy the ratio of the area under this feature to that of the strong singlet at 6.71 eV increases by a factor of about 100 as θ increases from 10° to 80°. A similar but less pronounced increase is observed for E_0 = 20 eV. In addition, for most scattering angles studied, the intensity of the 2.75 eV transition increased relative to that of the 6.71 eV singlet → singlet transition as the impact energy was lowered from 60 eV to 20 eV. Both characteristics are typical of spin-forbidden transitions [4] and confirm the assignment of the 2.75 eV feature to the lowest singlet → triplet transition in azomethane. The peak position is in good agreement with the TE maximum occurring at 2.72 eV.

The feature with a maximum at 4.8_4 eV and a Franck-Condon region from about 4.0 eV to beyond 5.5 eV has a scattering angle and impact energy dependence which is similar to that of the 2.75 eV transition and can also be assigned to a singlet → triplet excitation. It is not seen in the TE spectrum.

The strong peak at 6.01 eV in the TE spectrum appears as a weak shoulder in the DES spectra around 6.0 eV. The shoulder is observable in both low and high angle DES spectra with similar intensity, relative to the 6.71 eV transition, and this suggests that it is a singlet → singlet

excitation. In addition, the weakness of this feature in both DES and optical spectra [3] is indicative of either a symmetry-forbidden or Rydberg type singlet → singlet transition.

As noted earlier, there are several apparent discrepancies between the results for the TE and DES methods of determining the low-lying states of azomethane. The reason is that the TE and DES spectra reflect different electron impact properties so that significant differences may exist without implying a disagreement between the techniques. The ordinate in the TE spectrum measures the slope near threshold of the excitation cross section of a given transition with respect to impact energy, whereas the ordinate in the DES spectrum measures the differential excitation cross section at the impact energy considered. Therefore, the relative intensity of a transition in the TE spectrum does not necessarily correlate with its DES strength or optical absorption coefficient.

No theoretical calculations of the singlet → triplet splittings for the low-lying excited states of azomethane are available. Several studies [3, 10-13] on the related molecule trans-diimide (H—N=N—H) should provide a model for interpreting the lowest electronic states in the former molecule if these states are relatively invariant to the replacement of the H atom by CH_3. The diimide calculations suggest that the 2.75 eV triplet state is the $1\,^3B_g$ and that the 3.50 eV state is the $1\,^1B_g$ one. The 4.8_4 eV triplet may be the $1\,^3B_u$ state. Both B_g states are produced by excitation of an electron in the n_+ lone pair orbital to the lowest π^* orbital while the B_u state comes from a $\pi \rightarrow \pi^*$ excitation.

The results of this study have located several electronic transitions in trans-azomethane by both TE and DES techniques. They indicate the need to exercise caution in interpreting TE spectra without comparing them with other kinds of electronic spectra. A more detailed paper on this molecule will appear elsewhere [14].

References

[1] S. S. Collier, D. H. Slater, and J. G. Calvert, Photochem. Photobiol. 7 (1968) 737.

[2] P. S. Engel and C. Steel, Accts. Chem. Res. 6 (1973) 275.

[3] M. B. Robin, R. R. Hart, and N. A. Kuebler, J. Amer. Chem. Soc. 89 (1967) 1564.

[4] A. Kuppermann, J. K. Rice, and S. Trajmar, J. Phys. Chem. 72 (1968) 3094; S. Trajmar, J. K. Rice, and A. Kuppermann, Advan. Chem. Phys. 18 (1970) 15.

[5] D. P. Ridge and J. L. Beauchamp, J. Chem. Phys. 51 (1969) 470.

[6] T. McAllister, Chem. Phys. Lett. 13 (1972) 602.

[7] G. Herzberg, Molecular Spectra and Molecular Structure, I (D. Van Nostrand, Princeton, New Jersey, 1950) p. 551.

[8] M. S. Foster and J. L. Beauchamp, J. Amer. Chem. Soc. 94 (1972) 2425.

[9] O. A. Mosher, W. M. Flicker, and A. Kuppermann, J. Chem. Phys. 59 (1973) 6502.

[10] G. Wagniére, Theor. Chim. Acta 31 (1973) 269.

[11] D. P. Wong, W. H. Fink, and L. C. Allen, J. Chem. Phys. 52 (1970) 6291.

[12] B. Tinland, Spectros. Lett. 3 (1970) 51.

[13] N. W. Winter and R. M. Pitzer, private communication.

[14] O. A. Mosher, M. S. Foster, W. M. Flicker, J. L. Beauchamp, and A. Kuppermann, J. Chem. Phys., in press.

Figure Captions

Fig. 1 (a) Trapped electron spectrum of azomethane showing the trapped electron current, I_t, for the following conditions: 1×10^{-7} A incident beam current; 6×10^{-5} torr sample pressure as read on an uncalibrated Schulz-Phelps gauge; 0.36 eV well depth.

(b) Electron energy-loss spectrum. The scattered current is shown for a scattering angle $\theta = 80°$ and 40 eV incident electron energy.

For both curves the abscissa, ΔE, is the excitation energy.

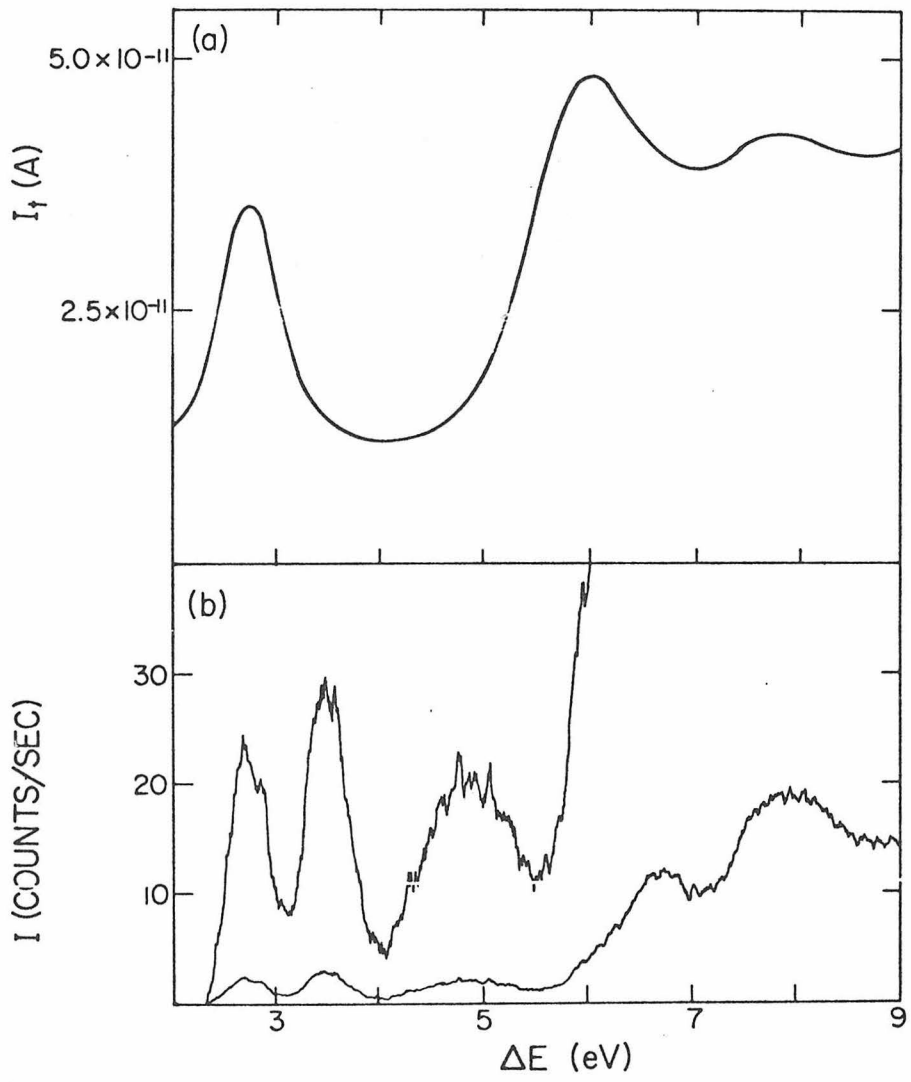
(a)
5.0×10⁻¹¹
2.5×10⁻¹¹
I_f (A)
(b)
30
20
10
I (COUNTS/SEC)
3
5
7
9
ΔE (eV)

Appendix III

Electronic Spectroscopy of Propadiene (Allene) by Electron Impact*

Oren A. Mosher, ** Wayne M. Flicker,
and Aron Kuppermann

Arthur Amos Noyes Laboratory of Chemical Physics†
California Institute of Technology
Pasadena, California 91109
(Received

ABSTRACT

The electron impact excitation of propadiene (allene) has been studied experimentally at impact energies of 20 eV, 40 eV, and 60 eV and scattering angles from 6° to 80°. Two transitions with maxima at 4.28 eV and 4.89 eV are identified as singlet → triplet excitations. The magnitude of the splitting between these transitions is a measure of the interaction between the two perpendicular π molecular orbitals. The significance of these triplet excited states in the interpretation of previous electronic energy transfer experiments and sensitized photochemical studies is briefly discussed. Two very weak transitions are observed between 5.0 eV and 6.5 eV. The angular dependence of the corresponding cross sections indicates that these are spin-allowed but symmetry-forbidden transitions. A weak singlet → singlet transition is seen with a maximum at 6.74 eV. This feature has also been observed optically and attributed to an electric dipole-allowed $\tilde{X}\,{}^1A_1 \rightarrow 1\,{}^1E$ transition. This assignment is discussed

in the light of the present results. The first strong transition, the $\tilde{X}\ ^1A_1 \rightarrow 1\ ^1B_2$ $\pi \rightarrow \pi^*$ transition appears with a maximum at 7.24 eV. Higher energy-loss features between 7.95 eV and 10 eV probably involve excitations to Rydberg states. A previously unreported transition to a superexcited state is observed with a maximum at 11.25 eV.

1. INTRODUCTION

Allene (propadiene) is the simplest example of a cumulene or adjacent carbon-carbon double bond system. The ground electronic state is probably nonplanar[1, 2] with the CH_2 planes at 90° to each other. The molecule then has D_{2d} symmetry with the following structure.[1]

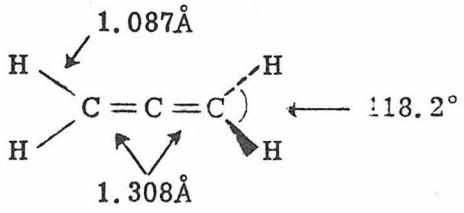

The π electron molecular orbitals (MOs) are at right angles and should have only limited interaction with each other. The observed $\pi \rightarrow \pi^*$ excitation energies may then be compared with those values in ethylene to furnish an estimate of the π MO interaction. An electron impact study of allene was undertaken to locate accurately the positions of the low-lying $\pi \rightarrow \pi^*$ forbidden transitions. Previous unpublished 90° electron scattering[3] and trapped electron studies[4] indicated the presence of one or more triplet excited states in the region from 4 eV to 5 eV and it was hoped that the present study would provide more detailed information and a better understanding of this energy-loss region. Semiempirical and ab initio theoretical calculations are available for comparison with experimental results.

2. SUMMARY OF THEORETICAL CALCULATIONS

There have been a number of studies[5-9] of allene using either Pariser-Parr-Pople or related methodologies. Table I summarizes the results of these studies. The ground state total energy and configuration has been the subject of an extensive ab initio calculation[10] using Gaussian type molecular orbitals as the basis set. The ground state configuration is $(1a_1)^2\ (1b_2)^2\ (2a_1)^2\ (3a_1)^2\ (2b_2)^2\ (4a_1)^2\ (3b_2)^2\ (1e)^4\ (2e)^4 = \tilde{X}\ ^1A_1$. In a separate ab initio calculation[11], both the ground and excited electronic states were studied. The excited states which are lowest in energy arise from promoting an electron from a 2e to a 3e orbital. This produces four singlet and four triplet states. The 2e and the 3e molecular orbitals are each composed of two accidentally degenerate π or π^* orbitals, respectively. Thus the 2e orbital may be thought of as two π orbitals, say π_a and π_b. The four pairs of excited states can then be thought of as arising from the $\pi_a \rightarrow \pi_a^*$, $\pi_a \rightarrow \pi_b^*$, $\pi_b \rightarrow \pi_a^*$, and $\pi_b \rightarrow \pi_b^*$ excitations. The ab initio calculations are also included in Table I. Although the energy values differ from study to study, the order of the triplet states remains the same. The lowest two triplets ($1\ ^3A_1$ and $1\ ^3B_2$) are predicted to have quite similar energies and to lie significantly below the $1\ ^3B_1$ and $1\ ^3A_2$ states. The order of the singlet states in all these calculations is the same except for the $2\ ^1A_1$ state. The lowest electric dipole-allowed transition is predicted[11] to be the $\tilde{X}\ ^1A_1 \rightarrow 1\ ^1B_2$. The calculations indicate that two or possibly three weak transitions should be observed below the first strong singlet $\rightarrow$ singlet transition.

3. SUMMARY OF PREVIOUS EXPERIMENTAL STUDIES

The results to be discussed below are summarized in Table II.

3.1 Optical Absorption

The optical spectrum has been studied by several authors[12-14] and some of the results have been listed by Herzberg[2]. Very weak continuous absorption starts around 4.8 eV and extends to about 6.5 eV. Rabalais et. al.[13] tentatively attributed an excitation in the region from 4.8 to 5.5 eV to the $\tilde{X}\ ^1A_1 \rightarrow 1\ ^1A_2$ transition and a very small inflection point at 5.76 eV to the $\tilde{X}\ ^1A_1 \rightarrow 2\ ^1A_1$ transition. The first transition which shows vibrational structure is a weak band system[13] ($f \approx 3 \times 10^{-2}$) between about 6.4 eV and 6.9 eV with a maximum at 6.70 eV. An $\tilde{X}\ ^1A_1 \rightarrow 1\ ^1E$ assignment has been suggested[13] for this excitation based on an analogy with linear triatomic groupings containing 16 valence electrons.

The first strong optical absorption occurs[12-14] between 6.9 eV and 7.9 eV with prominent peaks at 7.24 eV and 7.38 eV. This transition is optically allowed and has been assigned[13] as $\tilde{X}\ ^1A_1 \rightarrow 1\ ^1B_2$. Additional strong transitions with vibrational structure are seen in the region from 7.95 eV to 10 eV[12-14]. Some of the observed bands have been arranged[12-14] into Rydberg series but a number of the peaks are not yet assigned.

3.2 Electron Scattering Experiments

The 90° spectrum of allene[3] showed a weak feature at 4.5 ± 0.2 eV as well as stronger features at 7.6 eV, 8.7 eV, and 9.5 eV. The trapped

electron spectrum[4], which measures a quantity proportional to the integral cross section in a narrow energy band above the threshold energy, showed a broad peak from 3.5 eV to 5.5 eV with small maxima at 4.4 eV and 4.8 eV. Five stronger peaks were seen between 6.1 eV and 9.0 eV. The features observed from 4 eV to 5 eV were associated with triplet excited states in both studies.

4. RESULTS AND DISCUSSION

4.1 Experimental Procedure

The electron impact spectrum of allene was studied at impact energies of 20 eV, 40 eV, and 60 eV and at scattering angles θ ranging from 6° to 80° in a modified version of an apparatus previously described[15, 16]. The size of the energy analyzers has been increased from 5.08 cm to 7.62 cm diameter, and the lens support system has been modified to facilitate assembly and insure accurate alignment. Allene (97% minimum purity) from the Matheson Co. was subjected to several liquid nitrogen freeze-pump-thaw cycles before use in this study. The pressure in the scattering chamber was 5×10^{-3} torr as indicated by an uncalibrated Schulz-Phelps ionization gauge. The resolution (defined as the full width at half maximum of the elastic peak) was typically .13 eV to .15 eV. One spectrum was run at a resolution of .065 eV.

Figures 1 and 2 show the 20 eV impact energy spectra of allene at scattering angles of 8° and 60°, respectively. Figure 3 shows a higher resolution spectrum at 40 eV impact energy and $\theta = 0°$.

The differential cross section (DCS) ratios with respect to either the elastic peak or the $\tilde{X}\ ^1A_1 \rightarrow 1\ ^1B_2$ transition at 7.24 eV energy loss are taken from the areas under each peak in the energy-loss spectrum as previously described[16]. The peaks in allene overlapped strongly so that the measured

cross section ratios are accurate to no better than ± 25%. The ratio of the DCS of several transitions to that of the $\tilde{X}\ ^1A_1 \rightarrow 1\ ^1B_2$ at impact energies of 20 eV and 40 eV are displayed in Figures 4 and 5, respectively.

The elastic DCS in arbitrary units shown in Figures 6 and 7 at impact energies of 20 eV and 40 eV, respectively, were determined by multiplying the observed count rates by the scattering volume correction[17] appropriate to each scattering angle and normalizing the results to an arbitrary value of 1.0 at $\theta = 45°$. The precision of these measurements is about 10%.

The $\tilde{X}\ ^1A_1 \rightarrow 1\ ^1B_2$ DCS between 22.5° and 80° was obtained by multiplying the $\tilde{X}\ ^1A_1 \rightarrow 1^1B_2$ to elastic DCS ratio by the elastic DCS at each scattering angle. In addition, for angles of 30° and below, the $\tilde{X}\ ^1A_1 \rightarrow 1\ ^1B_2$ DCS was determined without reference to the elastic peak using the same procedure as for the elastic DCS, except that the normalization procedure was to make the result at 22.5° agree with the one obtained by the ratio method. These two methods agreed well at 30°.

The DCSs for the other inelastic transitions displayed in Figures 6 and 7 were determined by the ratio method using the elastic DCS as a reference for angles of 22.5° and above, and the $\tilde{X}\ ^1A_1 \rightarrow 1\ ^1B_2$ DCS below 22.5°. The estimated uncertainty in the inelastic DCSs is 35%. The arbitrary units in Figures 6 and 7 are the same for all curves displayed.

4.2 The Triplet States (T_1 and T_2)

4.2.1 Electron impact spectroscopy

Two weak features are observed with maxima at 4.28 ± .05 eV and 4.89 ± .05 eV (the uncertainty refers to the range of peak positions observed).

The apparent onset of the lowest excitation is below 3.6 eV. The DCS ratios (see Figures 4 and 5) of both these transitions are equal within experimental error. Each shows the sharp increase [15, 16, 18] with scattering angle characteristic of a spin-forbidden transition. The inelastic DCS values (see Figures 6 and 7) for both transitions do not vary by more than a factor of three over the angular range from 10° to 80°, which confirms [15 - 18] the triplet nature of the excited states. These transitions are designated as $S_0 \rightarrow T_1$ and $S_0 \rightarrow T_2$.[19]

All available theoretical calculations[5, 7, 11] suggest that the upper states of these transitions are the 1^3A_1 and 1^3B_2 states. Although these calculations indicate that the 1^3A_1 should be the lowest triplet state, they may not be sufficiently accurate to insure the correctness of this prediction.

The lowest triplet excited state in ethylene has a maximum intensity at a transition energy of 4.40 eV[18]. The average excitation energy of the two lowest triplet states in allene is 4.58 eV with an energy splitting of 0.61 eV. In s-trans 1, 3-butadiene the corresponding values[16] are 4.07 eV and 1.69 eV. The similarity of the $\pi \rightarrow \pi^*$ triplet excitation energy in ethylene with the average triplet excitation energies in both allene and butadiene supports a valence bond or "molecules-in-molecules" description of these systems[20] The magnitude of the energy splitting (0.61 eV) in allene is substantially less than in butadiene (1.69 eV). This result is in qualitative agreement with simple MO theory. The coplanar butadiene π MOs have considerable interaction with each other, even though they are physically separated by a C - C single bond, and this interaction produces the large energy splitting. The relatively small energy split in allene reflects the fact that although the π MOs are closer, they are perpendicular to each other and have a relatively small overlap.

4.2.2 Role in energy-transfer and sensitized-photochemical studies

The results of recent experiments[21] involving π-bonded molecules have led to the suggestion that the rate of triplet-triplet energy transfer in the gas phase is proportional to the energy overlap of the donor molecule phosphorescence spectrum with the $S_0 \rightarrow T$ optical absorption spectrum of the acceptor molecule. This finding is consistent with the theoretical prediction of Dexter,[22] developed for solid state systems, for triplet-triplet energy transfer rates due to exchange interactions. The shape and location of the low energy side of the T_1 electron impact excitation in allene is quite similar to that of ethylene[18] and, according to Dexter's theory, both molecules might be expected to have similar cross sections for quenching benzene in the $1\,^3B_{1u}$ state (T_{00} = 3.66 eV[23]). Indeed, the experimental quenching rate coefficients[21b] of these two systems are equal within experimental error. In contrast, a molecule such as acetylene, which has an $S_0 \rightarrow T_1$ electron impact excitation spectrum with an onset above 4.0 eV[24], has a benzene $1\,^3B_{1u}$ quenching rate coefficient[21b] which is more than fifty times smaller than that of allene. These observations support the suggestion of Schmidt and Lee[20b] that the shape and location of the acceptor $S_0 \rightarrow T_1$ electron impact excitation spectrum and of the donor phosphorescence spectrum may be useful for predicting relative quenching efficiencies of different acceptors.

The second triplet state may be the state which is initially excited in the Hg photosensitized decomposition of allene[25]. The decomposition[25] following photosensitization into propargyl radicals ($\cdot CH_2 - C{\equiv}CH + H \cdot$) may occur from T2, T1, or vibrationally excited levels of the ground state. Hg in the $^3P_1$ state is 4.89 eV above its ground state, and this energy appears to be insufficient to excite the lowest singlet state of allene.

4.3 S_1 and S_2

A weak feature in the electron impact excitation spectrum of allene is observed between about 5.0 eV and 6.5 eV. The cross section ratios and the shape[18, 26] and magnitude of the differential cross sections shown in Figures 4 through 7 are consistent with theoretical predictions that the transitions in this region are spin-allowed but symmetry-forbidden. This inference is also consistent with the weakness of the optical absorption[13] In the low resolution spectra (Figures 1 and 2), the region shows only one maximum, but its location is angle-dependent and varies from 5.93 eV to 6.10 eV. This behavior indicates that in this region there are at least two transitions occurring which have differential cross sections that vary differently with scattering angle. The high resolution spectrum (Fig. 3) shows a slope break at 5.79 ± .03 eV in agreement with optical results[13]. Fig. 3 shows that one state is located between about 5.0 eV and 6.2 eV while another has an onset around 5.5 eV and extends to about 6.5 eV. Several theoretical calculations[5, 6, 11] predict that the lowest excited singlet state is the $1\,^1A_2$ and that the second one is the $1\,^1B_1$ state. These assignments are consistent with our observation that the transitions to the first two excited singlet states are symmetry-forbidden.

4.4 The 6.74 eV Singlet (S_3)

Another transition is observed from 6.2 eV to beyond 7.0 eV with a maximum at 6.74 ± .02 eV, in agreement with optical observations[12-14]. Rabalais et. al.[13] assign this region to the optically allowed $\tilde{X}\,^1A_1 \rightarrow 1\,^1E$ transition. These authors[13] argue that it is a weak transition because it

is analogous to the symmetry forbidden $^1\Sigma_g^+ \rightarrow {}^1\Pi_g$ transition in linear triatomic molecules of $D_{\infty h}$ symmetry, like CO_2. However, the ab initio calculation of Schaad, Burnelle, and Dressler[11] places the 1 ^{1}E excited state 13.9 eV above the ground state. An alternate assignment of this transition in allene as spin-allowed but symmetry-forbidden is also consistent with the observed facts. Indeed, the observed ratio of the DCS for this transition to that of the optically allowed $\tilde{X}\ ^1A_1 \rightarrow 1\ ^1B_2$ transition oscillates weakly with scattering angle, as shown in Figures 4 and 5. Such behavior has been observed in the past[18] for spin-allowed, symmetry-forbidden transitions. Nevertheless, this oscillatory behavior is not inconsistent with the $\tilde{X}\ ^1A_1 \rightarrow 1\ ^1E$ assignment. An example[15] occurs in CO, in which the intensity ratios of two fully allowed transitions, the $\tilde{X}\ ^1\Sigma^+ \rightarrow B\ ^1\Sigma^+$ and the $\tilde{X}\ ^1\Sigma^+ \rightarrow C\ ^1\Sigma^+$, to that of the fully allowed $\tilde{X}\ ^1\Sigma^+ \rightarrow A\ ^1\Pi$ transition show oscillatory behavior with θ.

4.5 The 7.24 eV ($1\ ^1B_2$) State

A strong transition is observed from below 6.5 eV to about 8.0 eV, with a maximum at 7.24 ± .02 eV. The DCS for this transition (Figures 6 and 7) is consistent with its fully allowed nature. The peak location is in excellent agreement with optical studies[12-14] and the transition has been assigned[13] as the optically allowed $\tilde{X}\ ^1A_1 \rightarrow 1\ ^1B_2$ excitation.

4.6 Higher Transitions

Two features at higher energy loss are observed with peaks at 8.07 eV and 8.60 eV. These features are also observed optically[12-14], although the lack of resolution in this study masks many of the finer details of each band system.

A previously unreported transition to a superexcited state (i.e., above the first ionization potential) is seen with a peak at 11.25 eV. No further peaks were observed out to 16 eV energy loss.

5. CONCLUSIONS

The results of this study are summarized in the last column of Table II. Excitations to two low-lying triplet states have been observed at 4.28 eV and 4.89 eV. The region from 5.0 eV to 6.5 eV contains at least two singlet – singlet transitions which may be symmetry-forbidden.

A singlet→singlet transition from about 6.2 eV to 7.1 eV with a peak at 6.74 eV shows a behavior which suggests that it is either a symmetry-forbidden excitation or analogous to a transition which in the isoelectronic molecule CO_2 is symmetry-forbidden. A previously unreported superexcited state 11.25 eV above the ground state is observed.

REFERENCES

* Work supported in part by the United States Atomic Energy Commission Report Code CALT-767P4-128

** Work performed in partial fulfillment of the requirements for the Ph. D. degree in Chemistry at the California Institute of Technology

† Contribution No. 4842

1. A. G. Maki and R. A. Toth, J. Mol. Spect. 17, 136 (1965).
2. G. Herzberg, Molecular Spectra and Molecular Structure, III (D. Van Nostrand, Princeton, 1967), p. 640.
3. P. S. P. Wei, Ph. D. Thesis, California Institute of Technology, Pasadena, California (1968).
4. F. W. E. Knoop, Ph. D. Thesis, University of Leiden, Leiden, The Netherlands (1972).
5. R. G. Parr and G. R. Taylor, J. Chem. Phys. 19, 497 (1951).
6. J. Serre, J. Chimie Physique 53, 284 (1956).
7. W. T. Borden, J. Chem. Phys. 45, 2512 (1966).
8. A. Pellégatti, Theor. Chim. Acta 8,128 (1967).
9. J. C. Tai and N. L. Allinger, Theor. Chim. Acta 12, 261 (1968).
10. R. J. Buenker, J. Chem. Phys. 48, 1368 (1968).
11. L. J. Schaad, L. A. Burnelle, and K. P. Dressler, Theor. Chim. Acta 15, 91 (1969).
12. (a.) L. H. Sutcliffe and A. D. Walsh, J. Chem. Phys. 19, 1210 (1951). (b.) L. H. Sutcliffe and A. D. Walsh, J. Chem. Soc. (London) 1952, 899.
13. J. W. Rabalais, J. M. McDonald, V. Scherr, and S. P. McGlynn, Chem. Rev. 71, 73 (1971).

14. A. A. Iverson and B. R. Russell, Spectrochim. Acta 28A, 447 (1972).

15. A. Kuppermann, J. K. Rice, and S. Trajmar, J. Phys. Chem. 72, 3894 (1968).

16. O. A. Mosher, W. M. Flicker, and A. Kuppermann, J. Chem. Phys. 59, 6502 (1973).

17. S. Trajmar, D. C. Cartwright, J. K. Rice, R. T. Brinkman, and A. Kuppermann, J. Chem. Phys. 49, 5464 (1968).

18. S. Trajmar, J. K. Rice, and A. Kuppermann, Adv. Chem. Phys. 18, 15 (1970).

19. The notation used here does not indicate the spatial symmetry of the electronic state. Singlet spin states are designated S_0, S_1, ... where the state energy increases with increasing numerical subscript. In a similar manner the triplet electronic states are designated as T_1, T_2, ... This notation is commonly used in spectroscopic and photochemical studies of large molecules. For further discussion see S. P. McGlynn, T. A. Zumi and M. Kinoshita, Molecular Spectroscopy of the Triplet State (Prentice-Hall, Inc., Englewood Cliffs, New Jersey, 1969), pp. 1-3.

20. (a.) W. T. Simpson, J. Am. Chem. Soc. 73, 5363 (1951).
(b.) W. T. Simpson, J. Am. Chem. Soc. 77, 6164 (1955).

21. (a.) M. W. Schmidt and E. K. C. Lee, J. Am. Chem. Soc. 90, 5919 (1968).
(b.) M. W. Schmidt and E. K. C. Lee, J. Am. Chem. Soc. 92, 3579 (1970).

22. D. L. Dexter, J. Chem. Phys. 21, 836 (1953).

23. T. V. Ivanova and B. Ya. Sveshnikov, Optics &Spectrosc. 11, 322 (1961).

24. S. Trajmar, J. K. Rice, P. S. P. Wei, and A. Kuppermann, Chem. Phys. Lett. 1, 703 (1968).

25. J. Collin and F. B. Lossing, Can. J. Chem., 35, 778 (1957).

26. D. C. Cartwright, W. J. Hunt, W. Williams, S. Trajmar, and W. A. Goddard, III, Phys. Rev. A 8, 2436 (1973)

Table I

Summary of Theoretical Calculations

Electronic State	Orbital Transition	Calculated Energy (eV)							
		Ab Initio		Semiempirical					
		Schaad et. al.[a]	Buenker[c]	Parr & Taylor[d]	Serre[e]	Borden[f, g]	Pellégatti[h]	Tai & Allinger[i]	
$\tilde{X}\ ^1A_1$	None	-114.8392[b]	-115.6979[b]						
$1\ ^3A_1$	$2e \rightarrow 3e$	4.887eV		0.9		4.39			
$1\ ^3B_2$	$2e \rightarrow 3e$	5.078		1.4		4.61			
$1\ ^3B_1$	$2e \rightarrow 3e$	6.522		4.5		6.39			
$1\ ^3A_2$	$2e \rightarrow 3e$	6.713		5.0		6.69			
$1\ ^1A_2$	$2e \rightarrow 3e$	6.865		5.1	5.44	6.77	4.64	6.03	[j]
$1\ ^1B_1$	$2e \rightarrow 3e$	7.263		5.5	5.76	7.15	4.86	6.55	[j]
$2\ ^1A_1$	$2e \rightarrow 3e$	9.633		11.1	6.87	6.46	4.73	7.62	[j]
$1\ ^1B_2$	$2e \rightarrow 3e$	10.792		8.9	7.05	7.85	7.40	7.84	
$1\ ^1E$	$2e \rightarrow 5a_1$	13.908							

a. Reference 11
b. This is the total energy of the ground electronic state in hartrees.
c. Reference 10
d. Reference 5
e. Reference 6
f. Reference 7
g. As measured from graph in Reference 7
h. Reference 8
i. Reference 9
j. These states were identified as forbidden singlets, but not specifically identified by symmetry.

Table II

Summary of Experimental Observations on Allene

Nature of Transition	Possible Upper State[a]	Optical Studies		Electron Scattering		
		Iverson & Russel[c]	Rabalais et. al.[d]	90° Scatt.[e]	Trapped Electron[f]	Present Study
Singlet-Triplet	$1\,^3A_1$ and $1\,^3B_2$			4.5 (±.2)	4.4	4.28 ± .05 (3.6 → 4.8)[g]
Single-Triplet					4.8	4.89 ± .05 (4.3 → 5.6)
Symmetry-Forbidden or Weak Allowed Singlet-Singlet	1^1A_2, $1\,^1B_1$, $2\,^1A_1$, or 1^1E[b]		4.8 → 5.5		6.1	5.0 → 6.2
			5.76			5.5 → 6.5
		6.71	6.70		6.6	6.74 ± .02 (6.2 → 7.1)
Electric Dipole-Allowed Singlet-Singlet	$1\,B_2$	7.25	7.23	7.6	7.2	7.24 ± .02 (6.5 → 7.9)
Rydberg Bands						
Π → 3p		8.05	8.02		8.1	8.07 ± .03 (7.95 → 8.48)
Π → 4s		8.58	8.57	8.7	9.0	8.60 ± .03 (8.48 → 10)
				9.5		
Superexcited State						11.25 eV

a. None of these identifications are certain. They represent an assignment based on an analysis of experiments and theoretical calculations.
b. For a discussion of the ordering of these states, see Sections 4.3 and 4.4.
c. Reference 14
d. Reference 13
e. Reference 3
f. Reference 4
g. The onsets and ends of the transitions are estimates based on band shapes in this study.

FIGURE CAPTIONS

Figure 1 — Electron energy-loss spectrum of allene at $\theta = 8°$; 20 eV incident electron energy; 3×10^{-8} A incident beam current; 3.7×10^{-3} torr sample pressure reading from an uncalibrated Schulz-Phelps gauge; resolution approximately 0.12 eV.

Figure 2 — Same as Figure 2 at $\theta = 60°$.

Figure 3 — Electron energy-loss spectrum of allene in the 5.0 to 12.0 eV energy-loss region for $\theta = 0°$; 40 eV incident beam energy; 2×10^{-9} A incident beam current; 7.0×10^{-3} torr sample pressure reading from an uncalibrated Schulz-Phelps gauge; resolution approximately 0.06 eV.

Figure 4 — Intensities of several electronic transitions in allene divided by the intensity of the $\tilde{X}\ ^1A_1 \rightarrow 1\ ^1B_2$ transition as a function of θ at an incident electron energy of 20 eV; the excited states for the curves shown are T1 (o), T2 (Δ), $S_1 + S_2$ ($\square$) and the 6.74 eV singlet ($\times$).

Figure 5 — Same as Figure 4 at an incident electron energy of 40 eV.

Figure 6 — Differential cross sections as a function of θ at an incident electron energy of 20 eV for elastic scattering (+) and for transitions to the following excited states: T1 (o), T2 (Δ), S1 + S2 ($\square$), 6.74 eV singlet ($\times$), $1\ ^1B_2$ (∇).

Figure 7 — Same as Figure 6 for an incident electron energy of 40 eV.

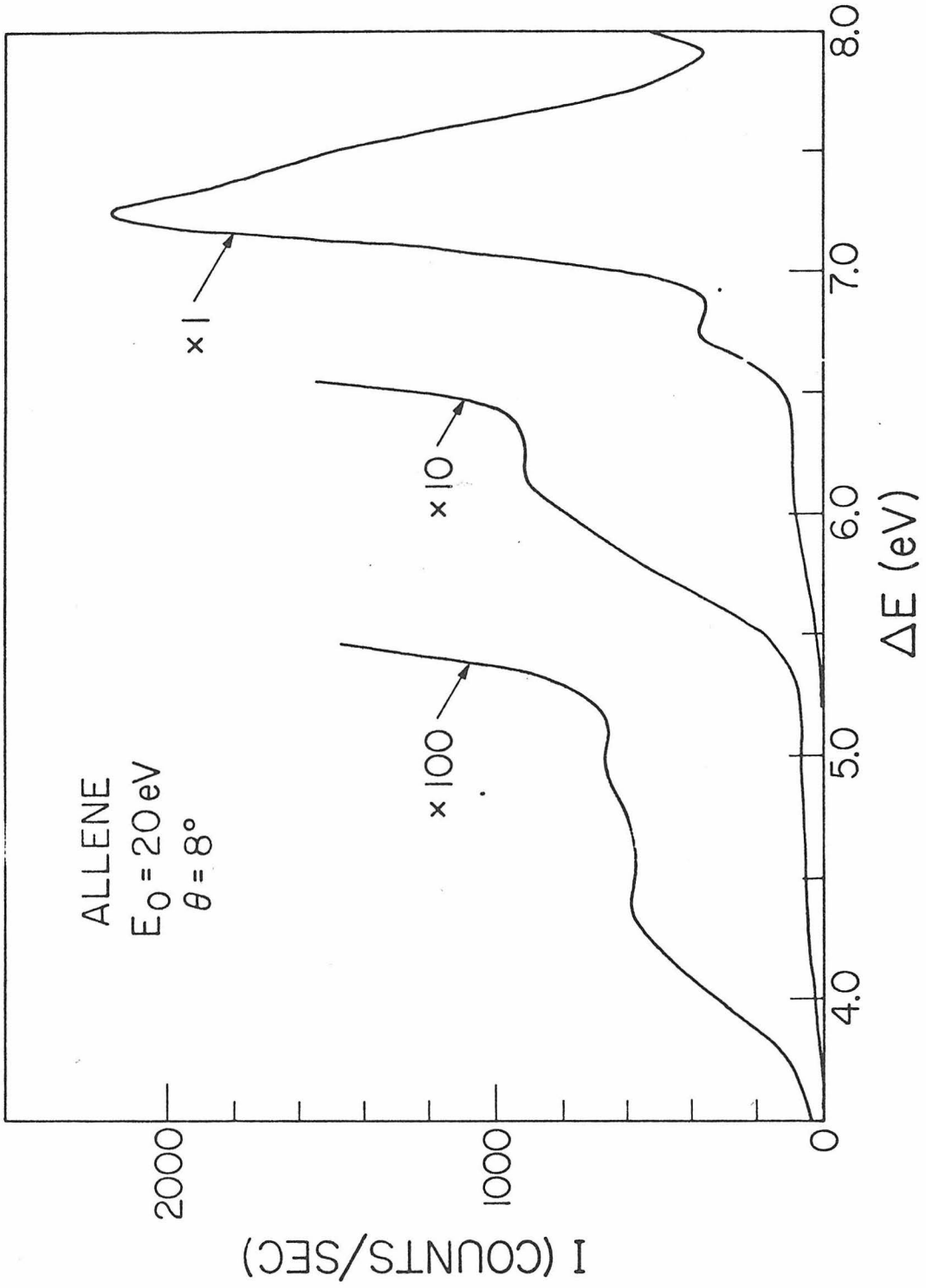
ALLENE
$E_0 = 20$ eV
$\theta = 8°$
×1
×10
×100
I (COUNTS/SEC)
2000
1000
0
4.0
5.0
6.0
7.0
8.0
ΔE (eV)

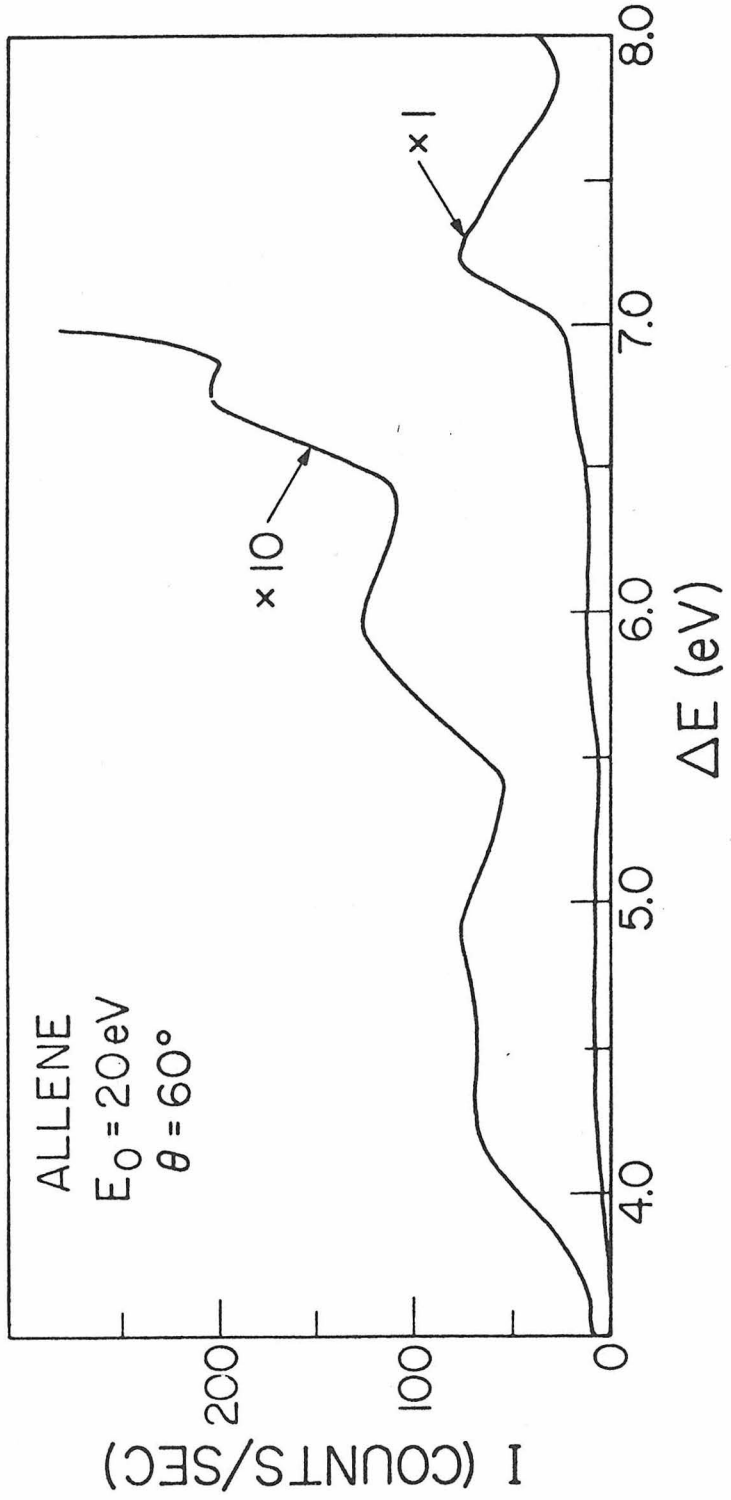
ALLENE
E_0 = 20 eV
θ = 60°
× 10
× 1
I (COUNTS/SEC)
0
100
200
4.0
5.0
6.0
7.0
8.0
ΔE (eV)

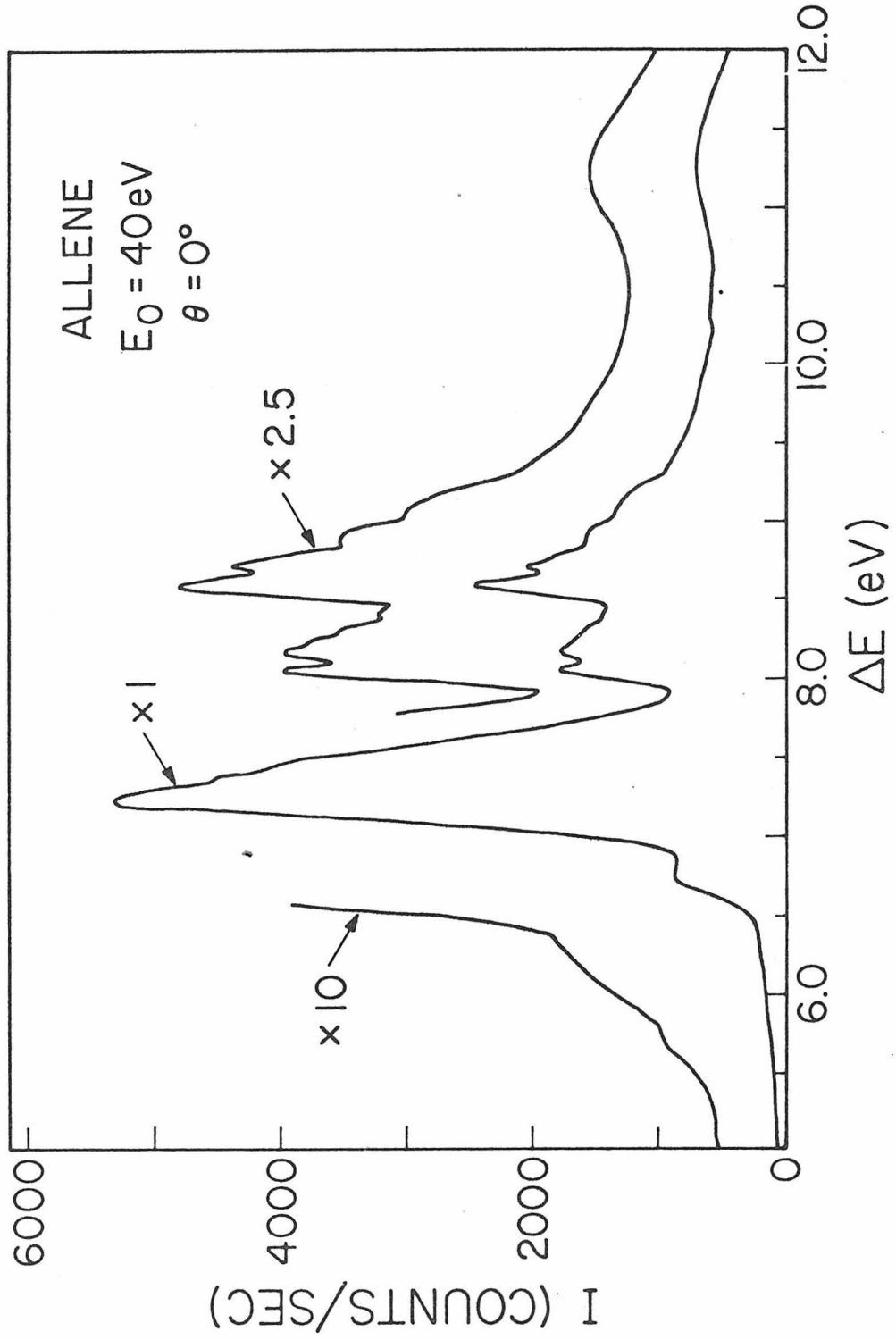
ALLENE
$E_0 = 40eV$
$\theta = 0°$
×1
×2.5
×10
I (COUNTS/SEC)
6000
4000
2000
0
6.0
8.0
10.0
12.0
ΔE (eV)

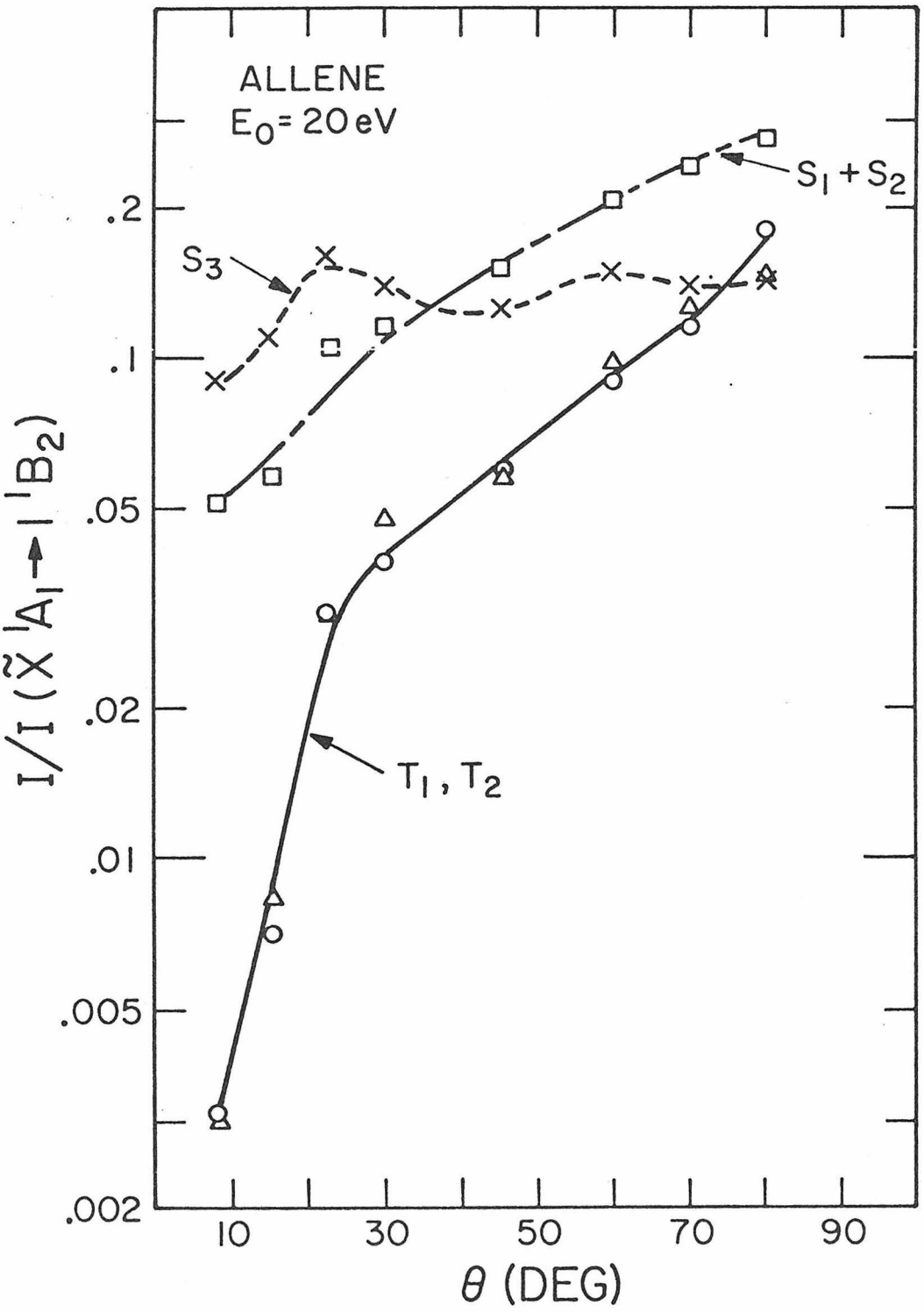
ALLENE
E_0 = 20 eV
$S_1 + S_2$
S_3
T_1, T_2
$I/I(\tilde{X}\,{}^1A_1 \rightarrow 1\,{}^1B_2)$
.2
.1
.05
.02
.01
.005
.002
10
30
50
70
90
θ (DEG)

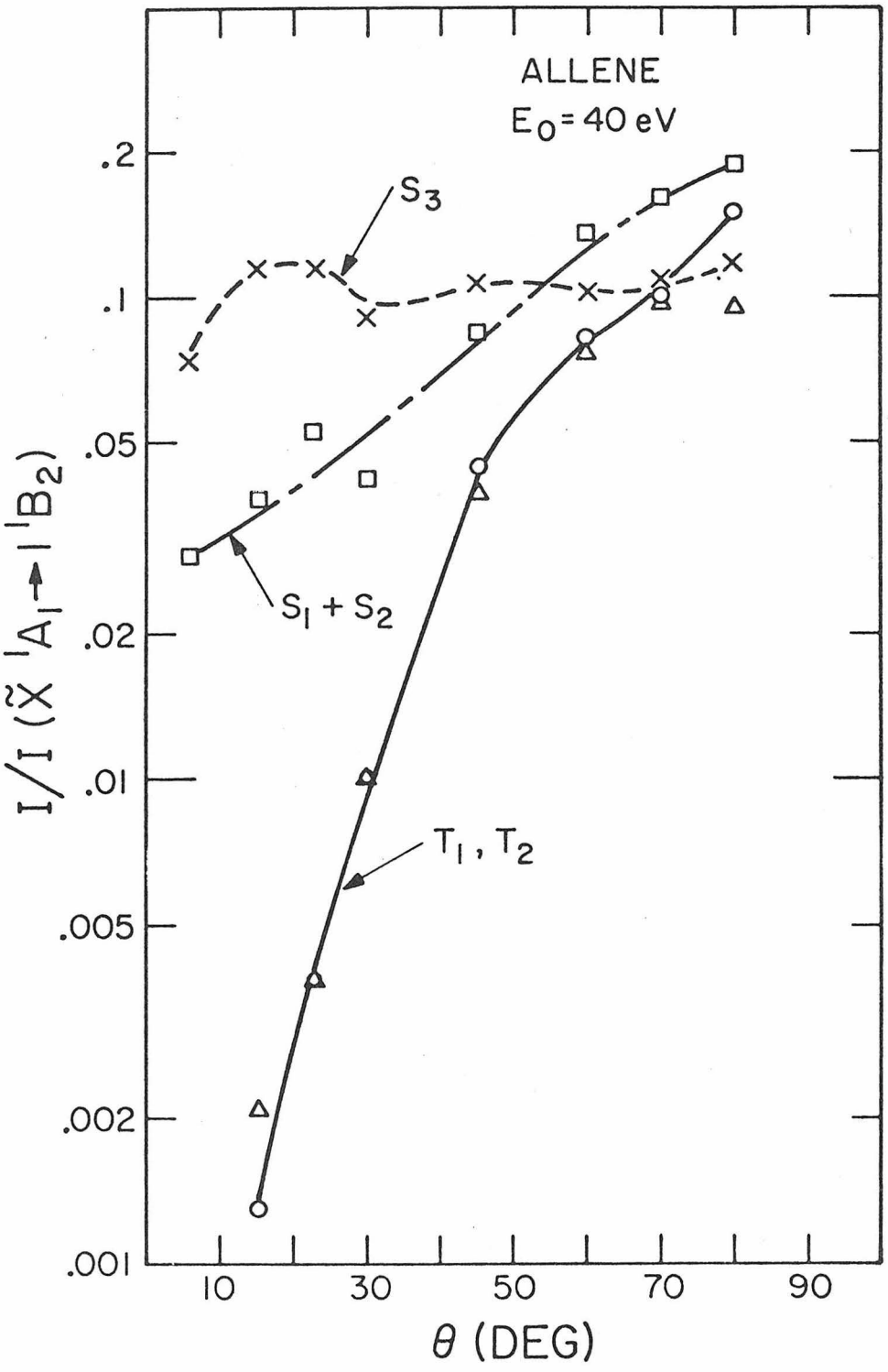
ALLENE
$E_0 = 40$ eV
S_3
$S_1 + S_2$
T_1, T_2
$I/I(\tilde{X}\ ^1A_1 \rightarrow 1\ ^1B_2)$
.2
.1
.05
.02
.01
.005
.002
.001
10
30
50
70
90
θ (DEG)

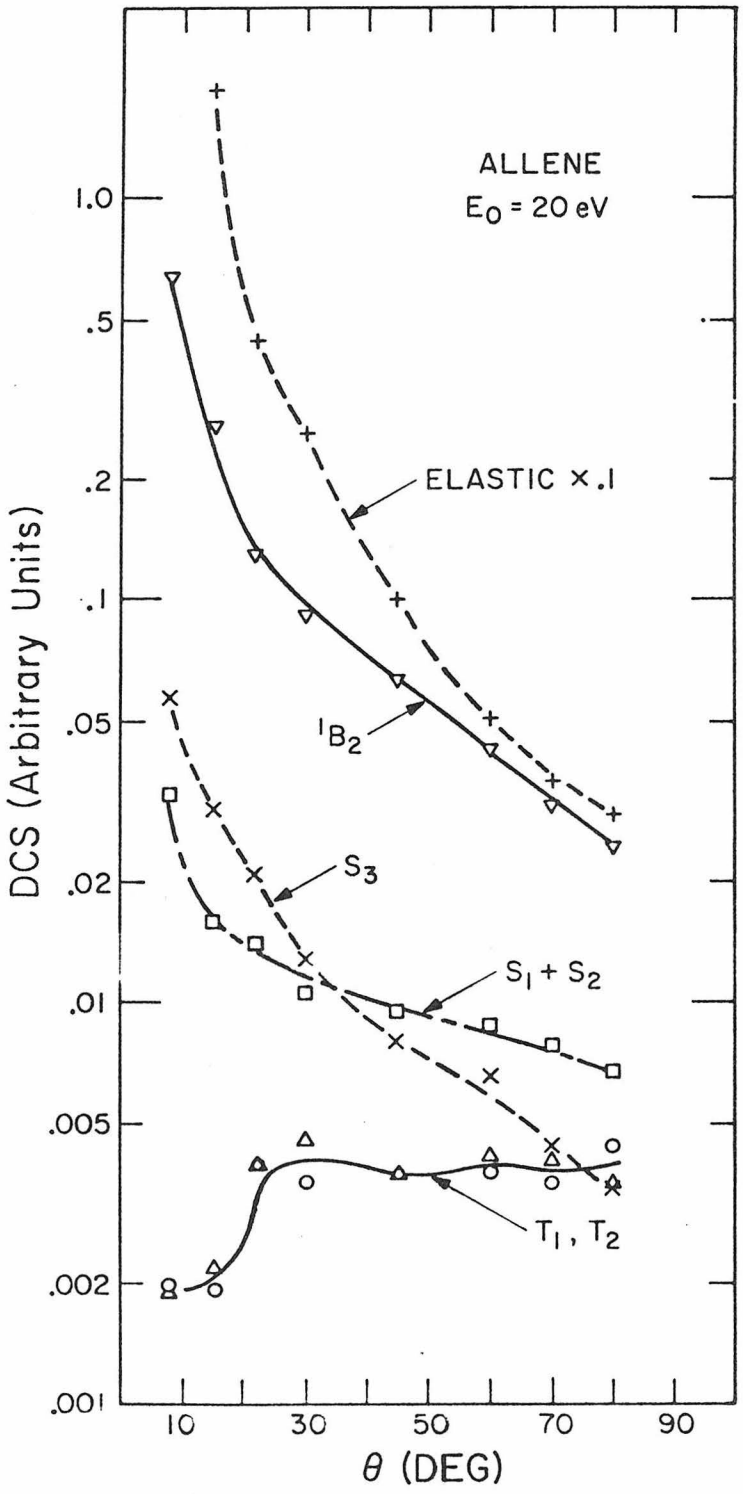
ALLENE
E_0 = 20 eV
ELASTIC × .1
$^1B_2$
S_3
$S_1 + S_2$
T_1, T_2
DCS (Arbitrary Units)
1.0
.5
.2
.1
.05
.02
.01
.005
.002
.001
10
30
50
70
90
θ (DEG)

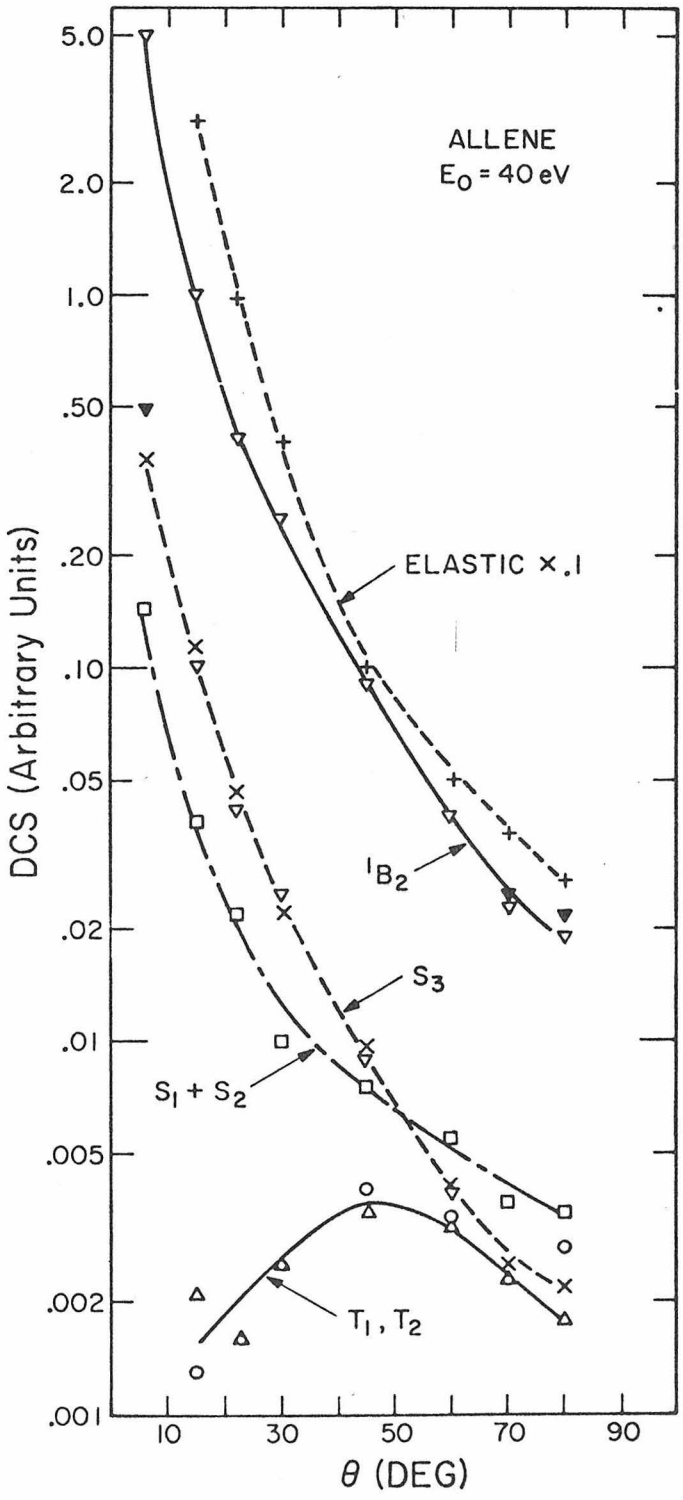
ALLENE
E_0 = 40 eV
ELASTIC × .1
$^1B_2$
S_3
$S_1 + S_2$
T_1, T_2
DCS (Arbitrary Units)
θ (DEG)
5.0
2.0
1.0
.50
.20
.10
.05
.02
.01
.005
.002
.001
10
30
50
70
90

Propositions

PROPOSITION I

A matrix isolation experiment is suggested in order to prepare XeF and KrF and then observe their ultraviolet, visible and infrared absorption spectra. The results can be used to confirm earlier gas phase emission studies which attributed certain bands to electronic transitions of XeF.

In 1933 Yost and Kaye [1] made what was to be one of the last attempts for several decades to prepare a chloride or fluoride of xenon. Pauling had suggested to them that these types of compounds might exist even though xenon was a noble gas. The "rule" of eight valence electrons can be broken, and SF_6 is a common example of a compound with more than eight valence electrons. Yost and Kaye were unsuccessful in their efforts, and attempts at synthesizing these compounds were discontinued in most laboratories.

Interest in noble gas compounds was stimulated again in 1962 by Bartletts [2] preparation of $Xe(PtF_6)_x$ where x ranges from 1 to 2.[3,4] Other authors reported the preparation of several binary rare gas fluorides during the next three years. XeF_2,[5] XeF_4,[6] XeF_6,[7] and KrF_2[8,9] have all been made and are found to be relatively stable compounds in the absence of water and oxygen at temperatures below 0°C.

It is apparent that stable compounds exist only for even numbers of fluorine atoms. Coulson has discussed the nature of bonding in xenon fluorides[10] in terms of both molecular-orbital theory and valence bond resonance theory. Using the valence bond resonance theory for XeF_2, for example, gives

$$F-Xe^{+}-F^{-}, \qquad F^{-}-Xe^{+}-F, \qquad F^{-}-Xe^{2+}-F^{-},$$

and $\overline{\lceil F-Xe-F \rceil}$ as resonance structures. The energy necessary to create the $Xe^{+}-F^{-}$ structure is the ionization potential (xenon)–electron affinity (fluorine)–e^2/R where R is the average distance separating the charges. Coulson estimates that this term is 6.8 eV and thus the energy necessary to form $Xe^{+}-F^{-}$ is 12.1-3.6-6.8 = 1.7 eV. If the $F-Xe^{+}$ bond is now formed the energy is likely to be recovered and a stable molecule should exist. Even numbers of ligand groups should be attached to produce stable structures. For XeF, however, the only resonance structure is $Xe^{+}-F^{-}$ and this is at a high energy relative to the dissociated atoms. Thus simple valence bond arguments predict that XeF and KrF are not stable compounds. This conclusion is also supported by extensive ab initio self-consistent field calculations on KrF.[11] These studies indicated that in the Hartree-Fock approximation the molecule is not bound and dissociates smoothly to Kr + F.

However, there are several reports in the literature in which it is claimed that either XeF or KrF has been produced and studied under non-equilibrium conditions. The most reliable reports appear to be those of

an electron spin resonance spectrum of a radical produced by γ irradiation of crystals of either XeF_2,[12] XeF_4,[13,14] or KrF_2[15] at 77°K. The observed hyperfine structure is interpreted as that of XeF or KrF. Other identifications of XeF electronic transitions in the gas phase are much less certain.

Weeks and Matheson[16] irradiated xenon and fluorine gas mixtures with near ultraviolet light. Flash photolysis of a mixture of 185 torr of xenon and 185 torr of fluorine produced a transient species with a 20 microsecond half life. The species produced bands at about 3300 Å and 2500 Å and it was suggested that the transient species was XeF.

L. A. Kuznetsova et al.[17] have reported the results of passing a high frequency discharge through the vapors of XeF_2. They observed 3 band systems. The lowest energy system started at 3536 Å and ran to about 2800 Å. A second similar system started at about 2650 Å and went to below 2500 Å. A third diffuse system was observed at 2350 Å and this is where XeF_2 was previously reported to absorb.[11] Kuznetsova suggests that the lower energy bands are produced by XeF radical.

Emission bands are also found when a high frequency discharge is passed through a mixture of xenon and LiF, NaF, or BF_3.[18] These bands can be correlated with the bands reported by Kuznetsova et al.[17]

Matrix isolation techniques[19] could be employed to prepre XeF or KrF and then study their infrared (IR) and electronic transitions in order to verify the results of the earlier studies.[16,17] The experiment is performed in the following way. Free radicals, like XeF or KrF, are produced in small concentrations as a solute in a rare gas solvent stream.

The carrier gas enters a region of high vacuum and strikes a liquid helium cooled window. Some of the stream freezes on the window producing a frozen deposit of rare gas with some of the radical species dissolved in it. Migration of large molecules in the lattice at 4.2°K is almost impossible, so the radicals are isolated from each other, and it is then possible to make spectroscopic investigations of the radical.

For the XeF experiment xenon could be used as the carrier gas and XeF_2 could be the source of the XeF molecule. The solvent and solute for the KrF experiment could be krypton and KrF_2. Just before entering the deposit region, the solvent stream would pass through a high frequency discharge, which would presumably produce the radicals. Spectra (IR and UV) can be taken of the deposit of KrF_2 or XeF_2 without the discharge running in order to determine the transition energies of these molecules in solution. A second experiment could be performed with the discharge running and the new lines and bands should be those of XeF or KrF. If for some reason XeF_3 or KrF_3 were formed then it should[20] add 3 [D_{3h} symmetry] or 4 [C_{3V} symmetry] or more IR active fundamentals to the known XeF_2[21] or KrF_2[22] IR spectrum. In contrast, however, XeF or KrF should add only one new IR line. Therefore the matrix isolation method should permit the identification of the electronic transitions associated with both XeF and KrF in solution.

References

1. D. M. Yost and A. L. Kaye, J. Amer. Chem. Soc., 55, 3890 (1933).

2. N. Bartlett, Proc. Chem. Soc. (London), 218 (1962).

3. N. Bartlett, Chem. Can., 15, 33 (1963).

4. N. Bartlett and N. K. Jha in Noble Gas Compounds, University of Chicago Press, Chicago, 1963, p. 23.

5. R. Hoppe, W. Dahne, H. Mattauch, and K. M. Rodder, Angew. Chem., 74, 903 (1962).

6. H. H. Claassen, H. Selig, and J. G. Malm, J. Amer. Chem. Soc., 84, 3593 (1962).

7. J. G. Malm, I. Sheft, and C. L. Chernick, J. Amer. Chem. Soc., 85, 110 (1963).

8. A. V. Grosse, A. D. Kirshenbaum, A. G. Streng, and L. V. Streng, Science, 139, 1047 (1963). These authors incorrectly identified KrF_2 as KrF_4.

9. F. Schreiner, J. G. Malm, and J. C. Hindman, J. Amer. Chem. Soc., 87, 25 (1965).

10. C. A. Coulson, J. Chem. Soc., 1442 (1964).

11. B. Liu and H. F. Schaeffer III, J. Chem. Phys., 55, 2369 (1971).

12. R. S. Eachus and M. C. R. Symons, J. Chem. Soc. A, 304 (1971).

13. W. E. Falconer and J. R. Morton, Proc. Chem. Soc., 95 (1963).

14. J. R. Morton and W. E. Falconer, J. Chem. Phys., 39, 427 (1963).

15. W. E. Falconer, J. R. Morton, and A. G. Streng, J. Chem. Phys., 41, 902 (1964).

16. J. L. Weeks and M. S. Mattheson in Noble Gas Compounds, University of Chicago Press, Chicago, 1963, p. 89.

17. L. A. Kuznetsova, Yu Ya Kuzyakov, V. A. Shpanski, and V. M. Khutoretski, Vestn. Mosk. Univ. Ser. II Khim, 19, 19 (1964). See also C. A. 61, 9060d (1964).

18. S. L. N. G. Krischnamachari, N. A. Narashimham, and M. Singh, Current Science India, 34, 75 (1965).

19. R. P. Frosch, Ph. D. Thesis, California Institute of Technology, 1965, pp. 1-20; G. W. Robinson and M. McCarty, J. Chem. Phys., 28, 349 (1958); H. W. Brown and G. C. Pimentel, J. Chem. Phys., 29, 883 (1958); D. E. Milligan and G. C. Pimentel, J. Chem. Phys., 29, 1405 (1958).

20. G. Herzberg, Infrared and Raman Spectra, D. Van Nostrand Company, Inc., Princeton, 1968, p. 298.

21. J. J. Turner and G. C. Pimentel in Noble Gas Compounds, University of Chicago Press, Chicago, 1963, p. 101.

22. J. J. Turner and G. C. Pimentel, Science, 140, 974 (1963).

PROPOSITION II

It is proposed that the variable angle electron impact method be applied to the aromatic amino acids phenylalanine, tyrosine and tryptophan.

Phenylalanine, tyrosine, and tryptophan are the building blocks for the globular proteins which are an essential part of most biological systems. Weber [1] first pointed out in 1953 that the fluorescence of biological materials originates in these aromatic amino acids. The spectral characteristics of the proteins and their amino acids have been the subject of several review articles [2-4] where the discussion was based solely on the results of condensed phase studies. An electron impact study of the amino acids would help explain the protein spectra and would help in understanding certain energy transfer phenomena in proteins and in the isolated amino acids in liquid or solid solutions. This experiment would provide the first gas phase energy level spacings.

Optical absorption experiments are often done with sample pressures exceeding 1 torr. In contrast, the electron impact experiment only requires sample pressures of about 1×10^{-3} torr. The vapor pressure of the aromatic amino acids is not known. Their high melting points (above 280°C) [5] indicate that the room temperature vapor pressure is very small. A heated inlet system would be required and is available on the electron

impact spectrometer. This system would permit operation of the instrument with the inlet lines and scattering chamber at temperatures of up to 200°C. Two experiments in the literature [6-8] suggest that amino acid vapor pressures in the 10^{-3} torr range are achievable by heating to 200°C without significant pyrolysis. Sinsheimer and co-workers [6] were able to prepare homogeneous films of the amino acids on a quartz slide by vacuum sublimation of the sample at temperatures ranging from 50°C to 150°C. Spectra of the resulting deposits were similar to those of the amino acids in solution indicating that significant pyrolysis had not occurred. Additional evidence is available from photoionization mass spectral studies [7, 8] which also used a heated sample source. The intensity of the mass spectrum increased as the source temperature was raised from 50°C to 250°C but no new lines appeared. A change in the spectrum would have indicated that pyrolysis was occurring prior to ionization. Thus the use of the heated inlet system would permit a study of gas phase electronic spectra of these amino acids. The details of the experiment have been described earlier in this thesis (see Sections 4 and 5). The amino acid singlet → triplet states have not been observed in absorption but should be seen easily in the proposed study. In addition, a number of other interesting problems in the interpretation of the spectra of these compounds exist and are discussed below.

The absorption spectrum of tyrosine in neutral solution [4] shows peaks at 2750 Å (ϵ = 1500 ℓ/mole cm) and 2275 Å (ϵ = 8000). Both transitions

are $\pi \rightarrow \pi^*$ transitions and the lower peak shows some vibronic structure. Tyrosine should be strongly effected by changes in the pH of the solvent. At low pH values the CO_2H group is protonated[9] while at high pH values the H atoms are removed[9] from both the phenyl OH group and the CO_2H group. Fayette and Wahl[9] have studied the pH dependence of the fluorescence quantum yield and provided a theoretical analysis of the spectral effect of each of the ions formed. A similar study[10] has been made for the phosphorescence intensity of tyrosine and it was suggested that for the neutral molecule the energy of the $^3n, \pi^*$ state is just above that of the $^1\pi, \pi^*$ (presumably the 2750 Å) state while in the negative ion this energy ordering is reversed. The reason for this suggestion was the fact that phosphorescence was greatly increased at high pH values. This suggests that intersystem crossing (ISC) efficiencies increase in alkaline solution. As the pH is increased ionization may cause the energy of the $^3(n, \pi^*)$ state to move from just above to just below that of the $^1(n, \pi^*)$ state. The results of the electron impact study may be useful in deciding if this explanation is correct. The lowest triplet state (presumably the $^3(\pi, \pi^*)$) should appear in the range from 4000 Å to 3300 Å. If a second singlet → triplet transitions occurs in the region between 3500 Å and the onset of the singlet (2900 Å) then the above argument about a triplet state moving to just below the singlet state to produce enhanced ISC may not be correct. A second question that the electron impact spectrum may answer is whether the 2750 Å transition is actually a combination of two $\pi \rightarrow \pi^*$ transitions as has been suggested for tryptophan (see discussion below). One additional

question is suggested by the previous results for tyrosine. The ratio of phosphorescence to fluorescence is wavelength dependent [11] at low pH values. Most previous experiments which had measured the ratio (P/F) of phosphorescence to fluorescence had shown that P/F was independent of exciting wavelength. This had been interpreted to mean that there is very rapid ($k \approx 10^{12}$ sec^{-1}) internal conversion by vibrational relaxation from higher excited electronic states to the first excited state. Only this state has a long enough lifetime to permit competition between radiative and non-radiative transitions to the ground state and intersystem crossing to the spin forbidden manifold of states. A recent study has shown, however, that the P/F ratio in tyrosine can increase when the excitation wavelength decreases from 2750 Å. Some authors suggest [12] that this is because of increased intersystem crossing efficiency at higher levels in the singlet manifold. R. S. Becker [13] believes that this is observed only because of photochemical or impurity effects. If the electron impact study indicated that there were triplet states on the low energy side of the 2275 Å state this would support the enhanced ISC explanation of the results.

Phenylalanine has the highest onset energy for singlet → singlet transitions of any of the amino acids. The lowest energy transition peaks at 2570 Å (ϵ = 200) and then shows additional transitions at 2100 Å (ϵ = 10,000) and below 1900 Å (ϵ = 44000). [4] The intensity and location of these transitions are similar to those of benzene where maxima [14] are located at 2550 Å (ϵ = 200), 2000 Å (ϵ = 6300), and 1800 Å (ϵ = 100,000). The molecule

should also have similar triplet state energies and these should be observable by electron impact. Benzene triplet states are seen by electron impact[15] at 3178 Å, 2640 Å and 2213 Å.

Tryptophan has two peaks in neutral solution[4] with maxima at 2800 Å (ϵ = 5000) and at 2200 Å (ϵ = 30,000). These were both thought to be $\pi \rightarrow \pi^*$ transitions with each one representing one electronic transition. Studies on the 2800 Å peak have shown, however, that it actually is a combination of two transitions. Evidence is available from tryptophan fluorescence polarization studies,[16] circular dichroism studies of tryptophan containing proteins,[17] and from semiempirical SCF calculations on tryptophan.[18] The SCF studies suggest that all 3 transitions in the 2000 Å → 3000 Å region are $\pi \rightarrow \pi^*$ and that the lowest two singlet → singlet transitions are almost degenerate. Electron impact studies should reveal whether such a degeneracy exists for the corresponding two lowest singlet → triplet transitions.

Evidence for still another singlet → singlet transition around 3500 Å is found in the work of Fujimori.[19] Emission from tryptophan frozen in glucose solution at 77°K shows two distinct sets of emission bands depending on λ_{ex}. Excitation at 2800 Å leads to the usual fluorescence and phosphorescence bands at 3250 Å and 4200 Å, respectively, while 3500 Å excitation leads to short and long-lived bands at 4500 Å and 5000 Å. Other workers[20, 21] have also observed these bands but have postulated that the 4500 Å emission is produced by "interacting" tryptophan molecules

because the emission intensity increase as the concentration of tryptophan in the solid is increased is slightly more than linear. Fujimori believed that these bands were produced by tryptophan. The electron impact study may resolve this problem by showing whether or not there is an electronic state around 3500 Å.

The problems discussed above in interpreting and understanding the results of previous experiments on the amino acids provide a number of reasons for making the attempt to observe the electron impact spectra of these molecules.

References

1. G. Weber, Advan. Protein Chem., 8, 415 (1953).

2. G. H. Beaven and E. R. Holiday, Advan. Protein Chem., 7, 319 (1952).

3. G. H. Beaven, Advan. Spectroscopy II, 331 (1961).

4. D. B. Wetlaufer, Advan. Protein Chem., 17, 303 (1962).

5. Handbook of Chemistry and Physics, 46, Chemical Rubber Co., Cleveland, 1965, pp. C-472, C-587, C-588.

6. R. L. Sinsheimer, J. F. Scott, and J. R. Loofburrow, J. Biol. Chem., 187, 299 (1950).

7. M. E. Akopyan and Y. V. Loginov, High Energy Chem., 1, 83 (1967).

8. M. E. Akopyan and Y. V. Loginov, Khim. Vys. Energ., 1, 97 (1967).

9. M. Fayette and P. Wahl, Biochim. Biophys. Acta, 229, 102 (1971).

10. T. Truong, R. Bersohn, P. Brumer, C. K. Kuk, and T. Tao, J. Biol. Chem., 242, 2979 (1967).

11. H. Rau and L. Augenstein, J. Chem. Phys., 46, 1773 (1967).

12. E. Yeargers, F. R. Bishai, and L. Augenstein, Biochem. Biophys. Res. Commun., 23, 570 (1966).

13. R. S. Becker, Theory and Interpretation of Fluorescence and Phosphorescence, Wiley Interscience, New York, 1969, p. 187.

14. J. G. Calvert and J. N. Pitts, Jr., Photochemistry, John Wiley and Sons, Inc., New York, 1966, p. 265.

15. J. P. Doering, J. Chem. Phys., 51, 2866 (1969).

16. G. Weber, Biochem. J., 75, 335 (1960).

17. E. H. Strickland, J. Horwitz, and C. Billups, Biochemistry, 8, 3205 (1969).

18. E. Yeargers, Biophys. J., 8, 1505 (1968).

19. E. Fujimori, Biochim. Biophys. Acta, 40, 251 (1960).

20. I. Isenberg and A. Szent-Györgyi, Proc. Nat. Acad. Sci. U.S., 44, 519 (1958).

21. I. R. Steele and A. Szent-Györgyi, Proc. Nat. Acad. Sci. U.S., 44, 540 (1958).

PROPOSITION III

It is proposed that the technique of resonance Raman spectroscopy be applied to 1, 3-butadiene, 1, 3, 5-hexatriene, and 1, 8-diphenyloctatetraene in an attempt to observe the $2\,^1A_g$ excited electronic state.

The vision process in humans is initiated by photochemically induced cis → trans isomerization of 11-cis retinal.[1] The excited electronic states in this polyene are presumably similar to those of the smaller polyenes-like butadiene or hexatriene. The excited state of retinal through which the isomerization process occurs is not known for certain but it has often been presumed to be the $1\,^1B_u$ state. The strong absorption band in the polyenes is produced by the transition to the $1\,^1B_u$ state. Recent experimental studies have suggested that a transition to the $2\,^1A_g$ state in some polyenes occurs at an energy below or near that of the $\tilde{X}\,^1A_g \rightarrow 1\,^1B_u$ transition. If such a state does exist then it may play an important role in the visual process because internal conversion of the initially formed $1\,^1B_u$ state to the $2\,^1A_g$ state below it should occur[2] in less than 10^{-11} seconds. Evidence in support of a low-lying $2\,^1A_g$ state is available from optical absorption and emission studies of 1, 8-diphenyl octatetraene[3, 4] and 2, 10-dimethylundecapentaene[5] and from two photon absorption studies of 1, 4-diphenylbutadiene.[6] Some theoretical calculations on butadiene[7-9] and

hexatriene[8-10] also place the $2\,^1A_g$ state below the $1\,^1B_u$ state. In contrast to these results, optical absorption studies of butadiene,[11] hexatriene,[12] and all trans-retinal[5] did not show such a state. The results of threshold electron impact[10,13] and intermediate energy electron impact on butadiene and hexatriene (see Sections 6.1.1 and 6.1.6 of Thesis) were also negative. Thus some doubt still exists as to whether the $2\,^1A_g$ state is present below the $1\,^1B_u$ state in all polyenes.

Raman spectroscopy is one of the two common methods of studying the vibrational frequencies of a molecule. In normal infrared vibrational spectroscopy where a photon is absorbed a fundamental frequency will be seen only if its symmetry species is the same as that of at least one of the components of the electric dipole moment.[14] In the Raman spectrum, which is produced by inelastic photon scattering, a fundamental frequency will appear only if its symmetry species is the same as that of at least one of the components of the molecular polarizability.[14] The two methods often provide complementary information about the fundamental frequencies of a specific molecule.

The intensity of a Raman transition assuming random orientations of the target molecules is given by the following expression[15]

$$I_{mn} = \frac{8\pi}{9c^4} I_0 \omega^4 \sum_{ij} \left|(\alpha_{ij})\right|^2 \qquad (1)$$

where I_0 is the incident light intensity, ω is 2π times the scattered light frequency ν and α_{ij} is the i, jth component of the polarizability tensor.

The polarizability tensor is related to the Raman tensor R_{ij} by the following equation[16] where Stokes scattering (vibrational excitation of the molecule rather than de-excitation) is assumed.

$$\alpha_{ij} = \nu + 2\rho(n_2 + 1)^{1/2} R_{ij} \tag{2}$$

ν is the vibrational quantum number, ρ is the density of states of the incoming photons, n_2 is the number of outgoing photons in the field, and R_{ij} is the Raman tensor. An expression for the Raman tensor itself is available from the work of Peticolas and co-workers.[17] The expression is derived using third order time-dependent perturbation theory where the three quanta involved are: the destruction of an incident photon of energy $\hbar\omega_1$, the creation of a vibrational quanta $\hbar\Omega$, and the creation of a photon of energy $\hbar\omega_2$. The general expression for R_{ij} is quite complicated (6 terms) when the incident photon energy is not equal to the energy of an electronic transition in the molecule. In energy ranges where there is such an energy degeneracy the expression simplifies to[16,18]

$$R_{ij} = \sum_{\alpha\beta} \frac{\langle f^1 | e_2 \cdot \mu | B^1 \rangle \langle \beta^1 | (\frac{\partial H}{\partial Q_{a\,0}}) | \alpha^1 \rangle \langle \alpha^1 | e_1 \cdot \mu | g^1 \rangle}{(E^0_{\beta g} - \hbar\omega_2)(E^0_{\alpha g} - \hbar\omega_1)} \tag{3}$$

where g^1 is the initial ground state vibrational level, α^1 and β^1 are vibronic levels of two intermediate electronic states and f^1 is the final ground state vibrational level. $E^0_{\beta g}$ and $E^0_{\alpha g}$ are the energy differences between the various states. The study of molecular Raman spectra in energy regions

where the incident photon energy is degenerate with energy of molecular electronic transitions is known as resonance Raman spectroscopy. Because the intensity of a line depends on matrix elements coupling the intermediate electronic states a study of the intensity of a Raman line as a function of incident photon energy may show the energies where different electronic transitions occur. The electronic transitions do not need to be spin or symmetry allowed by optical dipole selection rules to affect the Raman line intensity. Rimai and co-workers [19] have used this method to "observe" singlet → triplet transitions in retinal and naphthalene. Lewis [20] has studied bovine rhodopsin's Raman spectrum on the low energy side of the $1\,^1B_u$ state and interpreted an intensity anomaly as evidence in support of a low-lying $2\,^1A_g$ state. Thus the resonance Raman spectroscopic method may be of use in observing the $2\,^1A_g$ state in the smaller polyenes where they cannot be seen by other methods.

Details of the Raman experiment and instrumentation are discussed by Schrötter. [21] The third-order nature of the process requires the use of laser light sources for good signal-to-noise ratios. 1, 3-Butadiene could be studied in the gas phase at about 1 atm pressure while 1, 3, 5-hexatriene and 1, 8-diphenyloctatetraene (DPO) are good candidates for crystal studies. DPO is included in the experiment because its $2\,^1A_g$ state has been observed by optical methods [3, 4] and provides a good test of the ability of the method to detect this state. For observations on butadiene a tunable laser in the 5 eV to 6 eV range should be used while for hexatriene the incident

photon energy range is from 4 eV to 5.2 eV. Tunable lasers have been recently developed in these energy ranges.[21, 22] DPO should be studied between 2.5 eV and 3.5 eV.

References

1. R. Hubbard and A. Kropf, Proc. Nat. Acad. Sci. U.S., 44, 130 (1958).

2. M. Kasha, Disc. Faraday Soc., 9, 14 (1950).

3. B. S. Hudson and B. E. Kohler, Chem. Phys. Lett., 14, 299 (1972).

4. B. S. Hudson and B. E. Kohler, J. Chem. Phys., 59, 4984 (1973).

5. R. L. Christensen and B. E. Kohler, Photochem. Photobiol., 18, 293 (1973).

6. R. L. Swofford and W. M. McClain, J. Chem. Phys., 59, 5740 (1973).

7. T. H. Dunning, Jr., R. Hosteny, and I. Shavitt, J. Amer. Chem. Soc., 95, 5067 (1973).

8. N. L. Allinger, J. C. Tai, and T. W. Stuart, Theoret. Chim. Acta, 8, 101 (1967).

9. K. Schulten and M. Karplus, Chem. Phys. Lett., 14, 305 (1972).

10. F. W. E. Knoop and L. J. Oosterhoff, Chem. Phys. Lett., 22, 247 (1973).

11. R. H. Pottier, G. P. Semeluk, and R. D. S. Stevens, Spectrosc. Lett., 2, 369 (1969).

12. R. M. Gavin, Jr., S. Risemberg, and S. A. Rice, J. Chem. Phys., 58, 3160 (1973).

13. H. H. Brongersma, J. A. van der Hart, and L. J. Oosterhoff, in Fast Reactions and Primary Processes in Chemical Kinetics, Interscience, New York, 1967, p. 211.

14. L. A. Woodward in Raman Spectroscopy II, Plenum Press, New York, 1970, p. 2.

15. J. Tang and A. C. Albrecht in Raman Spectroscopy II, Plenum Press, New York, 1970, p. 33.

16. A. Lewis and J. Spoonhower to be published in Neutron, X-ray, and Laser Spectroscopy in Biophysics and Chemistry, Academic Press, New York, 1974.

17. W. L. Peticolas, L. Nafie, P. Stein, and B. Fanconi, J. Chem. Phys., 52, 1576 (1970).

18. A. C. Albrecht and M C. Hutley, J. Chem. Phys., 55, 4438 (1971).

19. L. Rimai, M. E. Heyde, H. C. Heller, and D. Gill., Chem. Phys. Lett., 10, 207 (1971).

20. Aaron Lewis, to be published.

21. G. A. Massey, Appl. Physics Lett., 24, 371 (1974).

22. F. B. Dunning, F. K. Tittel, and R. F. Stebbings, Optics Comm., 7, 181 (1973).

PROPOSITION IV

It is proposed that photochemistry of the linear 1, 3-conjugated dienes be studied following direct excitation at 2537 Å as a function of diene pressure in order to determine the role of the triplet electronic state manifold in the reactions which occur.

The photochemistry of the conjugated dienes has been studied previously and the results have been reviewed by Srinivasan.[1] The aim of most previous studies was identification of the products rather than the identification of the diene electronic states which led to these products. In the gas phase, reactions of 1, 3-butadiene have been studied by both direct irradiation and Hg photosensitization at 2537 Å.[1-4] Direct irradiation populates the $1\,^1B_u$ state (see Section 6.1.1 of Thesis) while energy transfer from Hg^* ($^3P_0$) places the butadiene molecule in the $1\,^3A_g$ state. The observed reactions are as follows:

$$\text{1, 3-butadiene} \longrightarrow CH{\equiv}C{-}CH{=}CH_2 + H_2 \quad (1)$$

$$\longrightarrow (CH_2{=}C{=}CH{-}CH_3)^* \quad (2)$$

$$\longrightarrow \text{2 methylcyclopropene} \quad (3)$$

$$\longrightarrow C_2H_2 + C_2H_4 \quad (4)$$

Reactions 1 to 3 are seen in both direct and sensitized studies while 4 is only found in the direct studies. Reactions 1, 2, and 4 are observed with diene pressures around 4 torr while reaction 3 is seen at diene pressures of 194 torr. Haller and Srinivasan[4] have argued that the low pressure reactions (1, 2, 4) proceed via the vibrationally excited ground state of butadiene. These reactions are subject to collisional quenching by additive gases and this indicates that the lifetime of the precursor excited state is comparable to or longer than the time between collisions at 4 torr ($\approx 10^{-7}$ sec). This observation eliminates the singlet state as the precursor because its lifetime is shorter than 10^{-9} seconds. The remaining choices are the vibrationally excited ground state or a triplet state. The participation of a triplet state was ruled out because the energy gap between the highest triplet state known at that time (Evans[5,6] spurious triplet at 3.9 eV) and the $1\,^1B_u$ was thought to be too large. The only remaining choice for the precursor state is the vibrationally excited ground state.

The results of the present study on the dienes (see Section 6.1) have shown, however, that these molecules have a triplet state (the $1\,^3A_g$) on the low energy side of the $\tilde{X}\,^1A_g \rightarrow 1\,^1B_u$ transition at 4.9 ± 0.1 eV. The similarity of the products seen in the low pressure reactions (1 and 2) in both the direct and photosensitized study suggests that the triplet manifold may be involved in the direct photolysis reactions. A similar suggestion was made for the photochemical reactions of cyclooctatetraene.[7] The $1\,^3A_g$ could be populated by intersystem crossing (ISC) from the $1\,^1B_u$ state.

The low pressure reaction which leads to ethylene and acetylene is not seen in the Hg photosensitized study and appears to proceed via the vibrationally excited ground state. The vibrationally excited ground state is reached via internal conversion (IC) from the low lying levels of the $1\,^1B_u$ state. The possible significance of the triplet manifold in the direct excitation photochemistry of molecules is not always considered because it is usually assumed that IC is much faster than ISC in the gas phase. A number of authors have pointed out that IC may be much slower from $S_1 \rightarrow S_0$ than from the higher singlets to S_1 because of the increased energy gap[8] and therefore ISC may compete successfully with IC in some molecules.

A general theory of radiationless processes has been developed by Jortner and co-workers.[9,10] They specifically point out that ISC from S_1 to a higher triplet state may be a fast process because of a decreased energy gap. It is difficult to predict the rate of a given radiationless process for a specific molecule but the theory permits a number of important generalizations to be made. Bixon and Jortner[9] have classified molecules into three groups. Molecules in the "statistical limit" have such a density of vibronic states that coupling between the initial state (a single vibronic level of the initial singlet state in a zero-order approximation) and the background manifold of vibronic states (from lower zero-order approximation singlet or triplet electronic states) occurs entirely as an intramolecular phenomenon. Molecules in this class undergo electronic

relaxation which is independent of external perturbations and do not require collisions with other molecules. Large organic molecules like naphthalene belong to this group. Pressure changes in the gas or a change to condensed phases should not significantly effect ISC and IC rates in these molecules. A second class of molecules are those in the "resonance limit" in which the zero-order states are widely spaced. Any accidental degeneracies will be split but relaxation cannot occur in the isolated molecule. Collisions with other molecules in the gas or coupling with lattice vibrations in the solid state are necessary to produce ISC or IC and thus the rates of these processes are pressure or solvent dependent. Molecules in the "resonance limit" are usually small (less than 4 or 5 atoms) and thus have only a limited number of fundamental vibrational frequencies. Many molecules fall into the third case which is called the "intermediate case" where the transition rates have some pressure dependence but are not as sensitive as the molecules in the "resonance limit". Molecules like the dienes probably fall under this category although the larger ones (say, 1, 3 hexadiene) may approach the statistical limit.

If the dienes fall into the intermediate case, a study of their direct photochemistry as a function of diene pressure may provide further information about the role of the triplet states. There is no reason to believe that changes in pressure will effect both ISC and IC rates in a similar manner. The rates depend on Franck-Condon factors between the $1\,^1B_u$ and the $1\,^3A_g$ or the $\tilde{\chi}^1A_g$ states and also the effective vibronic density of

the two lower states. Thus in some pressure regions IC may dominate over ISC while in other regions the reverse may occur. The direct photolysis experiment can be performed over the pressure range from .1 mm to at least 250 mm and compared with the results of the sensitized experiment at the same pressure. In addition to 1,3-butadiene the study could be applied to 1,3-pentadiene, 1,3-hexadiene and the methyl substituted 1,3-butadienes. There has been little previous study of the gas phase direct photolysis except for butadiene[1-3] but most of these molecules have been studied over limited pressure ranges in the Hg sensitized reactions.[3,11,12] These studies could be repeated for comparison over a wider range of pressures. The correlation of products and yields in both types of studies may permit the identification of pressure ranges where ISC is significant with respect to IC and thus where the triplet states participate in the direct photochemical reactions.

References

1. R. Srinivasan, Adv. Photochem., 4, 113 (1966).

2. R. Srinivasan, J. Amer. Chem.Soc., 82, 5063 (1960).

3. R. Srinivasan and S. Boué, Tetrahedron Lett., 3, 206 (1970).

4. I. Haller and R. Srinivasan, J. Chem. Phys., 40, 1992 (1964).

5. D. F. Evans, J Chem.Soc. (London), 1735 (1960).

6. D. F. Evans and J. N. Tucker, J. Chem. Soc. Faraday Trans. II, 68, 174 (1972).

7. H. Yamazaki and S. Shida, J. Chem. Phys., 24, 1278 (1956).

8. See S. P. McGlynn, T. Azumi, and M. Kinoshita, Molecular Spectroscopy of the Triplet State, Prentice Hall, Inc., Englewood Cliffs, New Jersey, 1969, p. 10 and references therein.

9. M. Bixon and J. Jortner, J. Chem. Phys., 48, 715 (1968).

10. J. Jortner, S. A. Rice, and R. M. Hochstrasser, Adv. Photochem., 7, 149 (1969).

11. R. Srinivasan and S. Boué, J. Amer. Chem. Soc., 93, 5606 (1971).

12. S. Boué and R. Srinivasan, Mol. Photochem., 4, 93 (1972).

PROPOSITION V

It is proposed that a matrix isolation study of NO^- be undertaken by codepositing NO and cesium atoms in a rare gas matrix. The Cs atoms provide a convenient photoelectron source in the solid and the experiment will permit a study of band systems in NO^-, some of which may have been previously attributed to NO itself.

Recent studies have shown that if an electron source, such as cesium atoms, is codeposited with a rare gas and solute molecules in a low temperature solid, then transitions of the molecular negative ion can be studied following irradiation of the Cs atoms to produce electrons in the solid deposit. The method can be applied to many molecules and provides a unique source of information about electronic transition energies in negative ions. The results could be compared with the energies of negative ion states as indicated by the impact energies at which resonances are observed in electron impact studies of the neutral molecule.

In the following discussion a specific application of this technique is suggested for NO where the M bands ($^4\Pi \rightarrow {}^2\Pi$) are observed in low temperature matrices but are not seen in gas phase optical or electron impact studies. The experiment could determine if these bands are those of NO or NO^-.

Early gas phase absorption studies of NO were performed by Bernstein and Herzberg [1] in an effort to find the $a\,^4\Pi \leftarrow \tilde{X}\,^2\Pi$ transition predicted by Mulliken. [2] Extreme care was taken in preparing the NO to prevent impurity transitions from masking the $^4\Pi \leftarrow {}^2\Pi$ transition. No bands were found which could be ascribed to the $^4\Pi \leftarrow {}^2\Pi$ transition in the energy range from 3.5 eV to 5.6 eV although path lengths of up to 28 meter atmospheres were employed.

Broida and Peyron [3, 4] condensed the products from an argon discharge containing traces of N_2 and 1% O_2 onto a liquid helium cooled surface and observed a series of emission bands which they called the M bands. This band system has also been seen by Vegard [5] following electron impact excitation of frozen N_2 and O_2 although the bands were attributed to N_2. Broida and Peyron [3] have shown by isotopic substitution studies that the emitter contains one oxygen atom and one nitrogen atom. The final state vibrational frequency is close to the value measured for the $\tilde{X}\,^2\Pi$ state of NO in the gas phase [6] and it was therefore suggested that the M bands are the $a\,^4\Pi \rightarrow \tilde{X}\,^2\Pi$ transition.

Frosch and Robinson [7, 8] have also measured the M bands in emission from NO molecules trapped in solid argon and krypton following excitation by 50 KeV x-rays. Lifetime measurements were made and the results suggested that a spin-forbidden transition was involved in support of a $^4\Pi \rightarrow {}^2\Pi$ assignment. Frosch and Robinson also suggested that the transition might be seen in absorption between 4.71 eV and 5.4 eV. The easiest

features to observe should be the (4-0), (5-0), and (6-0) bands whose Franck-Condon (F-C) factors are 0.08, 0.14, and 0.2, respectively, and which occur between 5.19 eV and 5.40 eV. The onset of the first allowed transition occurs at 5.464 eV (ν_{00}) and is identified as the γ band system ($A^2\Sigma \leftarrow \tilde{X}^2\Pi_{3/2}$).[6]

The $^4\Pi \leftarrow {}^2\Pi$ transition in NO appeared to be an attractive candidate for observation by the electron impact method. Earlier studies[9] at 50 eV and 0° scattering angle had not revealed the transition but this was not surprising because spectra taken under these conditions are usually similar to optical spectra. Electron impact studies[10] were made on the Caltech instrument at impact energies as low as 20 eV and scattering angles of up to 60° but there was still no evidence of this transition. The spectra showed a slowly rising background count rate between 4 eV and 5.4 eV but no peak was observed. This was surprising because electron impact spectra under these conditions usually permit observation of spin-forbidden transitions. It is possible, of course, that the F-C distribution is so broad and peaks so close to the onset of the ν bands that the transition cannot be seen above the slowly rising background. An alternate explanation is that this transition is not occurring in NO but rather in NO^-. This possibility was suggested by the fact that emission bands obtained from either trapping the products of a microwave rare gas discharge containing hydrocarbons[11] or by subjecting acetylene frozen in a rare gas matrix to 50 KeV x rays[12] had been identified as the Swan bands in C_2 but were later shown[13] to be a transition in C_2^-.

Only limited information is available about the ground and excited states of NO^-. The ground state is presumed to be a $^3\Sigma^-$ state in analogy with O_2.[14] The electron affinity of NO is small but positive (0.024 eV $^{+.01}_{-.005}$).[15] The gas phase collisional detachment rates for $NO^- + M \rightarrow NO + M + e^-$ where M is a rare gas indicate that the process has an activation energy (E_a) of about 0.1 eV.[16] If the process in the rare gas matrix at 4.2°K has a similar E_a then once NO^- is formed the electron is not likely to detach subsequently unless NO^- is excited by light absorption.

Information about the NO^- ground state is available in various electron impact studies where it appears[17-19] as a resonance in elastic and vibrationally inelastic scattering off NO. Spence and Schulz[18] have analyzed the spacing of the resonances in the elastic scattering cross section to get a value of ω_e of 1371 cm^{-1} for the $^3\Sigma^-$ state of NO^-.

There is apparently only one reference in the literature to NO^- excited states. Sanche and Schulz[20] observed resonances in the scattering of electrons off NO in the region from 5.0 eV to 7.4 eV. At least four separate band series are present and they are attributed to Rydberg series in NO^-. The lowest starts at 5.04 eV.

The limited information about NO^- excited states does suggest that there may be states in the 5 eV to 6 eV region which could produce the M bands. The most serious objection to this proposal is that the vibrational spacing of the M band ground state is approximately that of NO (1904 cm^{-1})[6] while it should be closer to the calculated 1371 cm^{-1} vibrational spacing of

the NO^- ground state [18] if the final state is the $^3\Sigma^-$ ground state of NO^-. In spite of this objection it would be useful to repeat the matrix isolation studies of NO using Cs atoms in the matrix as a photoelectron source.[13] The experiment could be done using rare gas resonance lamps, the hydrogen discharge lamp or mercury arc lamps to photolyze the deposit instead of using 50 KeV x rays. The results would provide further information about the M bands and should indicate whether they belong to NO or NO^-. In addition, information about other electronic transitions in NO^- would be available for comparison with the electron impact resonance results on NO and the optical studies on O_2.

References

1. H. J. Bernstein and G. Herzberg, J. Chem. Phys., 15, 77 (1947).

2. R. S. Mulliken, Rev. Mod. Phys., 4, 1 (1932).

3. H. P. Broida and M. Peyron, J. Chem. Phys., 32, 1068 (1960).

4. M. Peyron and H. P. Broida, J. Chem. Phys., 30, 139 (1959).

5. L. Vegard, Ann. Physik., 79, 377 (1926).

6. G. Herzberg, Molecular Spectra and Molecular Structure I, D. Van Nostrand Co., Inc., Princeton, 1966, p. 559.

7. R. P. Frosch and G. W. Robinson, J. Chem. Phys., 41, 367 (1964).

8. R. P. Frosch, Ph.D. Thesis, California Institute of Technology, 1965, p. 21.

9. E. N. Lassettre, A. Skerbele, M. A. Dillon, and K. J. Ross, J. Chem. Phys., 48, 5066 (1968).

10. O. A. Mosher, W. M. Flicker, and A. Kuppermann, unpublished results.

11. M. McCarty and G. W. Robinson, J. Chim. Phys., 56, 723 (1959).

12. Reference 8, page 50.

13. D. E. Milligan and M. E. Jacox, J. Chem. Phys., 51, 1952 (1969).

14. F. R. Gilmore, J. Quant. Spectrosc. Radiat. Transfer, 5, 369 (1965).

15. M. W. Siegel, R. J. Celotta, J. L. Hall, J. Levine, and R. A. Bennett, Phys. Rev. A, 6, 607 (1972).

16. M. McFarland, D. B. Dunkin, F. C. Fehsenfeld, A. L. Schmeltekopf, and E. B. Ferguson, J. Chem. Phys., 56, 2358 (1972).

17. M.J.W. Boness, J. B. Hasted, and I. W. Larkin, Proc. Roy. Soc. A, 305, 493 (1968).

18. D. Spence and G. J. Schulz, Phys. Rev. A, 3, 1968 (1971).

19. I. W. Larkin and J. B. Hasted, J. Phys. B, 5, 95 (1972).

20. L. Sanche and G. J. Schulz, Phys. Rev. Lett., 27, 1333 (1971).